FireFly
DSE Group 13
Final Report

Flying Carpet for Fire Departments

AE3200: Design Synthesis Exercise

Delft University of Technology

TU Delft

This page is intentionally left blank.

FireFly
DSE Group 13
Final Report

Flying Carpet for Fire Departments

by

Student Name	Student Number
Marnix van den Berg	4558405
Egor Goz	4676459
Mees de Graaf	4867246
Alune Greeve	4820738
Arvis Jomerts	4840917
Jason Liang	4846222
Silvio Peressini	4847156
Mateo Rodriguez	4793137
Wouter van der Sluis	4783476
Chloë Van Droogenbroeck	4649591

Instructor:	Ronald van Gent
Teaching Assistant:	Livio Carzana, Alessandro Mancinelli & Tristan Hamers
Institution:	Delft University of Technology
Place:	Faculty of Aerospace Engineering, Delft
Project Duration:	April, 2021 - July, 2021

Cover Image: Royalty-free image of a street in Chicago by *Josh Hild* at
`https://unsplash.com/photos/SJDMYFfsD7c`

TU Delft

Preface

This is the final report in a series of three reports [1, 2] for the Design Synthesis Exercise (DSE). This final report encapsulates the detailed design phase of the `FireFly`, previously known as `Flying Carpet for Fire Departments`. It was once again written by ten bachelor student from the Faculty of Aerospace Engineering at the Technical University of Delft.

This report was written for the examination board of the DSE which includes the professors, coaches and tutors. It was also written for the Project Management & Systems Engineering teaching assistants. Therefore it is assumed that the reader is knowledgeable in project management, system engineering and aerospace engineering. It should be noted that specific pages (e.g. the Gantt chart) should be printed on at least A3 paper for readability.

We would like to thank our tutor Ronald van Gent, coaches Livio Carzana and Alessandro Mancinelli and teaching assistant Tristan Hamers for their continuous and greatly helpful assistance throughout the project, as well as the Aerospace Engineering faculty and staff for organising and managing our graduation project.

Also a special thanks goes out to Marlon Bovelander of the Haaglanden fire department for the valuable insight into firefighter procedures and standards and Dr. Daniele Ragni for his expertise and feedback on propeller sizing.

A hyperlink to the now open-source code used for the project can be found on `https://github.com/mateorodfr/DSE-13-Flying-Carpet`.

Delft, June 2021

Executive Overview

As population density keeps increasing around the globe, high rise buildings are becoming increasingly common. These buildings, however, pose several challenges related to evacuation during disaster situations. Existing evacuation methods are unsuitable for high rise applications. Consequently there is a need to develop a solution for these situations. Is it possible to design an aerial vehicle for urban high-rise fire evacuations?

This DSE demonstrates the feasibility of designing and operating a vehicle able to evacuate people from high rise disaster situations. This was done by first setting up a framework to tackle the project, and then producing a report outlining such a vehicle. This vehicle operates by carrying a cabin up to altitude, loading the payload, and transporting the people down in powered flight. The mission profile is divided into four main phases: 1) Deployment, 2) Operation , 3) Recovery & Disengagement and 4) Maintenance.

The main stakeholder need that the project is tackling is that ”Mankind must be protected from high-rise building disasters conditions.” Then the stakeholder needs were transferred into a set of user requirements. Additionally, the identification of constraints to the design put in place by either airworthiness, municipal or national authorities as well as physical or cultural limitations was performed. The mission requirements were then drafted and translated into system requirements, which were then used for to create the subsystem requirements and design.

The preliminary design selected from the past reports was chosen to be the release and pickup concept, which has the advantage of shorter turnover time between operations. The operational and logistics aspect of the long term project are focused on both correct operation and low environmental impact in production, maintenance and end of life. Production is done on an order by order basis, such that the demand is met exactly and storage is limited. In operations and logistics the boarding mechanism is considered and different options are laid out and compared. It is ultimately decided to use an extendable bridge stored below the floor of the cabin.

Information and Data handling is then addressed, and the communication is then discussed. It is ensured that communication can be maintained online for the duration of the mission. The aerodynamic characteristics of the craft are then determined. The propellers are then sized using blade element momentum theory. The performance of this propeller is quantified and off the shelf vs custom designs are compared for this solution. The cabin was then selected in order to have attractive aerodynamic performance. Motors are then compared between in order to find the most optimal outcome. Ultimately AC induction motors are selected for this purpose. The power supply is then sized for operation.

A state space matrix is then implemented to analyse the stability and controllability characteristics. A feedback matrix is then added in order to control the unstable system. The resultant system is highly controllable. The structure of the system was analysed with the objective of sizing a weight optimized structure able to interface the different subsystems and withstand operation loads.

An analysis is then performed on the crash landing. This is done by identifying a crush zone and then analysing the accelerations experienced by the payload during hard landing. Based on this analysis, no mitigation methods are identified. The heat caused by the batteries is addressed and a thermal management system is sized for the purpose of keeping the craft at operational temperature.

The configuration of the subsystems is laid out within the craft. This consists of the relative placement of all components investigated, as well as a proposed internal layout for payload seating arrangement. Geometric issues arose during this process which pointed out the unsuitability of the length of the bridge. A new bridge is modelled to mitigate this and the design is proposed. Verification and validation plan is then presented with some of the results already obtained. Methods to further validate the results are also discussed. A compliance matrix is then created and filled in to reflect the status of the requirements. A Market analysis is conducted estimating market parameters and possible returns based on investment. After, the final design is analysed in comparison to the the concept from the

previous report, and the changes are discussed. RAMS characteristics of the product are then outlined. The post DSE plan is then shown, with the workflow laid out in a gantt chart for clarity.

The structure of the cabin is a cube with sides of 1.65 *m* surrounded by an aerodynamic skin in the shape of a pill. The thrust will be provided by eight electrical motors in four pairs placed above the cabin. Two cabins will be used together with one propulsion system which switches cabins which decreases the turnaround time on the ground. To attach and detach the propulsion system to and from the cabin a twist and lock system is in place.

The total mass of the system, that is one cabin with the propulsion system on top, is 731 *kg*. One mission duration will take 778 *s* or approximately 13 *min* of which 11 *min* is in the air. This includes: ascent, hover, descent and turnaround time. On average, for normal operations, the required power is 86.25 *kW*.

Despite proving that the design and solution are feasible, steps still need to be taken to provide a final design that is ready for production. Therefore a few recommendations can be made for further actions. First, all requirements of which compliance is at this stage uncertain should be analysed and verified completely in the future. Second, a detailed study of the non-critical subsystems must be performed. At this stage in the design the feasibility of all subsystems has been addressed but not been sized yet. If all these recommendations are followed up it is advised to proceed with the post-DSE phase and raise funding for manufacturing a prototype. This should then be tested and validated before production of the actual product can begin.

At this stage the final vehicle design meets 94% of all requirements and is expected to exceed all after the post-DSE phase. This demonstrates that the design and operation of a high rise fire evacuation system is feasible. At this stage of the project the design has met all critical requirements and is able to perform the mission. The system is very robust and is able to operate in a variety of operational environments while performing the mission efficiently. Overall, the aim of the project has been met and the feasibility of the design has been proven. This means that using current technology it is possible to make a vehicle that is both powerful and stable enough to perform evacuation missions in dense urban centers.

Contents

Nomenclature

Abbreviations

Abbreviation	Definition	Abbreviation	Definition
AC	Alternating current	MC	Motor controller
AMS	Accumulator management system	MCU	Micro-controller unit
BEMT	Blade Element Momentum Theory	MMOI	Mass Moment of Inertia
BIL	Basic insulation level	MOSFET	Metal-oxide-semiconductor field effect transistor
CAN	Controller area network	OEAI	One Engine Arm Inoperative
CCM	Continuous conduction mode	OEI	One engine inoperative
CG	Centre of Gravity	PCB	Printed circuit board
CUL	Culture	PF	Power factor
DC	Direct current	PS	Propulsion system
DCM	Discontinuous conduction mode	PVB	Polyvinyl butyral
DSE	Design Synthesis Exercise	RMS	Root mean square
DoD	Depth of Discharge	RPM	Rounds per minute
ENV	Environment	SD	Secure digital
EVA	Ethylene–vinyl acetate	SNR	Signal to noise ratio
EXT	External	SPI	Serial peripheral interface
FBD	Free Body Diagram	SRAM	Static random access memory
FBS	Functional Breakdown Structure	TCH	Technical
FC	Flight computer	TLR	Technology Readiness Level
FEA	Finite Element Analysis	TV	Transport vehicle
FEM	Finite Element Method	U	User
FFD	Functional Flow Diagram	UART	Universal asynchronous receiver/transmitter
GPS	Global positioning system	USB	Universal serial bus
HPBW	Half power beamwidth	UHF	Ultra high frequency
HV	High voltage	VCU	Vehicle control unit
IC	Integrated circuit	VHF	Very high frequency
IGBT	Insulated gate bipolar transistor	V0	Version zero
ISA	International Standard Atmosphere		
I^2C	Inter integrated circuit		
LAW	Law and regulations		
LED	Light emitting diode		
LF	Loss factor		
LV	Low voltage		

Symbols

Symbol	Definition	Unit
a	Axial induction factor; Acceleration	[-]; [m/s^2]
a'	Tangential induction factor	[-]
a_i	Acceleration in ith direction	[m/s^2]
b	Flange width	[m]
B	Channel Bandwidth	[Hz]

Symbol	Definition	Unit
$\bar{c}$	Average chord length	[m]
C	Channel capacity	[Mbit/s]
C_T	Thrust coefficient	[-]
C_Q	Torque coefficient	[-]
C_P	Power coefficient	[-]
C_d	2-D Drag coefficient	[-]
C_D	3-D Drag coefficient	[-]
C_l	2-D Lift coefficient	[-]
C_{rotor}	Rotor constant	[-]
d	Distance; Drag force; Duty cycle; Antenna diameter	[m]; [N]; [-]; [m]
e_t	Pointing offset	[°]
F	Force; Prandtl's Tip Loss Factor; Noise factor	[N]; [-]; [-]
F_g	Flight alleviation factor	[-]
F_{gz}	Flight factor height	[-]
F_{gm}	Flight factor mass	[-]
f_s	Switching frequency	[Hz]
f_{wi}	Wind force in ith direction	[N]
g	Gravitational constant	[m/s^2]
G_x	X's gain	[-]
h	Web height	[m]
$I_{C_{RMS}}$	Capacitor's RMS current	[A]
I_{In}	Input current	[A]
$I_{L_{RMS}}$	Inductor's RMS current	[A]
I_{Out}	Output current	[A]
$I_{S_{RMS}}$	MOSFET's RMS current	[A]
I_{xx}	Principal MMOI in x axis	[kgm^2]
I_{yy}	Principal MMOI in y axis	[kgm^2]
I_{zz}	Principal MMOI in z axis	[kgm^2]
k	Boltzmann's constant	[m^{2}kg/(Ks^2)]
k_c	Compression buckling coefficient	[-]
K	Feedback matrix	[-]
K_s	Shear buckling coefficient	[-]
$K_{i,j}$	Gain at position i,j of K	[-]
l	Wire length	[m]
L	Inductance	[H]
L_X	X's loss factor	[-]
m	Mass	[kg]
$m_{landing}$	Landing Mass	[kg]
m_{mhw}	Maximum hover mass	[kg]
m_{tow}	Take off mass	[kg]
m_{zfw}	Zero fuel mass	[kg]
M_h	Moment around horizontal internal axis	[Nm]
M_v	Moment around vertical internal axis	[Nm]
N_B	Number of blades	[-]
N_0	Noise power density	[dB/Hz]
P	Power	[W]
P_{Out}	Output power	[W]
P_t	Transmitted power	[W]
Q	Torque	[Nm]
Q_{GS2}	Gate to source charge	[C]
Q_{GD}	Ground to drain charge	[C]
R	Resistance	[Ω]
R_B	Propeller blade radius	[m]
S	Frontal surface area	[m^2]

Symbol	Definition	Unit
S	Wire's cross sectional area	[m^2]
$\frac{S}{N}$	Signal to noise ratio	[-]
t_X	Time of X	[s]
T	Thrust force; Simulation time;	Characteristic period [N]; [s]; [s]
t	time	[s]
T_s	Switching time	[s]
T_{sys}	Systems noise temperature	[K]
T_x	X's noise temperature	[K]
T_0	Standard atmosphere temperature	[K]
U	Gust speed	[ms^{-1}]
U_{ds}	Design gust speed	[m/s]
U_{max}	Maximum gust speed	[m/s]
U_0	Ground gust speed	[m/s]
u	Input vector	[-]
V	Velocity	[m/s]
V_{In}	Input voltage	[V]
V_{Out}	Output voltage	[V]
V_{term}	Terminal Velocity	[m/s]
$V_{+\infty}$	Free-stream velocity far front	[m/s]
$V_{-\infty}$	Free-stream velocity far aft	[m/s]
V_{0^+}	Velocity front of rotor blade	[m/s]
V_{0^-}	Velocity aft of rotor blade	[m/s]
V_Ω	Tangential velocity	[m/s]
W	Weight	[N]
x	x-position; State vector	[m]; [-]
x'	Internal cross-section x-coordinate	[m]
$\dot{x}$	x velocity	[m/s]
$\ddot{x}$	x acceleration	[m/s^2]
x_{cg}	X location of centre of gravity	[m]
y	y-position; Output vector	[m]; [-]
y'	Internal cross-section y-coordinate	[m]
$\dot{y}$	y velocity	[m/s]
$\ddot{y}$	y acceleration	[m/s^2]
y_{cg}	y location of centre of gravity	[m]
z	z-position; Altitude	[m]; [m]
$\dot{z}$	z velocity	[m/s]
$\ddot{z}$	z acceleration	[m/s^2]
z_0	Ground sensor altitude	[m]
z_{mo}	Maximum operation altitude	[m]
z_s	Surface roughness constant	[m]
α	Attenuation exponent	[-]
$\alpha_{\frac{1}{2}}$	Half power beamwidth	[°]
Δ_{I_L}	Current ripple	[A]
Δ_L	Max to zero inductor current time fraction	[-]
η_s	Shear plasticity factor	[-]
η_c	Compression plasticity factor	[-]
η_X	Efficiency of X	[-]
ρ	Density	[kg/m^3]
ρ_R	Specific density	[Ωm]
θ	Pitch angle	[deg]
$\dot{\theta}$	Pitch rate	[deg/s]
$\ddot{\theta}$	Pitch angular acceleration	[deg/s^2]

Symbol	Definition	Unit
λ	Wavelength	[m]
μ	Poisson's ratio	[-]
τ	Shear stress	[Pa]
τ_f	Shear stress in flange	[Pa]
τ_i	Torque around ith axis	[Nm]
$\tau_{s,cr}$	Critical shear buckling stress	[Pa]
τ_w	Shear force in web	[Pa]
τ_{wi}	Wind torque around ith axis	[Nm]
σ	Rotor density; Normal stress	[-]; [Pa]
$\sigma_{c,cr}$	Critical buckling stress	[Pa]
σ_f	Flange normal stress	[Pa]
σ_{vM}	von Mises stress	[Pa]
ϕ	Roll angle	[deg]
$\dot{\phi}$	Roll rate	[deg/s]
$\ddot{\phi}$	Roll angular acceleration	[deg/s^2]
ψ	Yaw angle	[deg]
$\dot{\psi}$	Yaw rate	[deg/s]
$\ddot{\psi}$	Yaw angular acceleration	[deg/s^2]
Ω	Rotor radial velocity	[1/s]

List of Figures

List of Tables

1. Introduction

In the last few decades the world has become more and more densely populated. This has prompted a rise in the development of high rise buildings to accommodate for the large amounts of people living in urban areas. High rise buildings are buildings that exceed 21.3 *m* in height [3], but currently these can reach as high as 828 *m* [4]. This provides a challenge for evacuation procedures in case of high rise building fires or disasters. Since regular fire trucks can only reach limited heights with their ladders, the taller a buildings becomes, the harder it becomes to evacuate to ground before occupants are engulfed by smoke or fire or are trapped with no escape possibility. This creates the demand for a specialised airborne vehicle able to evacuate people from high rise buildings in disaster scenarios.

This DSE project aims to design such an airborne vehicle to provide a solution for evacuating people from high rise buildings. This is done in several steps. So far the project organisation was set up, a baseline report was created to identify all requirements for the vehicle and establish different design solutions and a midterm report was written to select the optimal design solution. This report, the final report, aims to present the final design of the system. This is done by describing the detailed design phase and stating the results of different analyses on the aerodynamics, structures and stability of the system. From this, all subsystems are designed and the final configuration is described. From this, the system can be verified and validated. Additionally, the post DSE-phase is laid out and detailed.

The report is structured as follows. Firstly, the project objectives are defined in Chapter 2. Afterwards, the functionalities of the system are laid out in Chapter 3 and from this the user requirements and constraints are determined in Chapter 4. Then Chapter 6 details the sustainability approach for the entire system design and production. Then the preliminary design phase is summarised in Chapter 5 before the analysis of the final design are done in the subsequent chapters. The operations and logistics of the system and the mission are given in Chapter 7. Next, Chapter 12, Chapter 8, Chapter 9 give an analysis of the info handling, aerodynamic characteristics and the power and propulsion system of the craft respectively. With this in place, the stability and controllability of the system is analysed in Chapter 10 before having an analysis on the structure of the system in Chapter 11. After all of these analyses, the possibility of a crash landing in case of an emergency is investigated in Chapter 13. Some systems characteristics are explained in Chapter 14 before the configuration is given in Chapter 15. With the entire system designed, the system is verified and validated in Chapter 16. Chapter 17 determines the return on investment and the market analysis and subsequently the final analysis is performed in Chapter 18. Finally the future steps of the post-DSE phase are detailed in Chapter 19 and the final results are presented in Chapter 20.

2. Project Objectives

When starting a project, it is important do define its goals. This ensures an efficient flow of the project as well as a guarantee that all objectives are met. The project objectives therefore have to be defined during each subsequent stage of the project.

In this phase, the final report was the upcoming project deliverable. This report mainly aims to describe the detailed design phase and present the final design. Below a more elaborate list of project objectives is given:

- Introduce the project
- Define the functionality of the vehicle
- Detail requirements of the vehicle
- Identify sustainability approach
- Summarize the preliminary design phases
- Determine operational specifications
- Determine communication flow of vehicle
- Determine aerodynamic characteristics of the vehicle
- Design a propulsion vehicle
- Determine stability characteristics of the vehicle
- Design a power vehicle
- Determine controllability characteristics of the vehicle
- Determine configuration of the vehicle
- Verify the vehicle
- Validate the vehicle
- Identify compliance of the vehicle with the requirements
- Identify the market
- Analyse performance of the vehicle
- Determine resource and budget allocation
- Lay out the post-DSE phase

Meeting all these objectives builds towards the end goal of the DSE project. In the next chapter a functional analysis will be performed on the mission in order to know all the necessary functions of the vehicle in order to perform the mission successfully.

3. System Functional Analysis

This chapter focuses on a key step in designing a product: performing a functional analysis. It takes a look at the necessary functions to perform the missions successfully. A functional flow diagram, shown in Section 3.1, shows the time sequence of the functions. Thereafter, the system can be functionally broken down into a functional breakdown structure which can be seen in Section 3.2.

3.1. Functional Flow Diagram

This section will describe the sequence of functions necessary to perform the mission successfully. This sequence is summarised in a functional flow diagram (FFD) which can be seen in Figure 3.2.

In global terms the sequence of functions for this case is: production, deployment, operations, disengagement, maintenance and end-of-life. The first and last one were considered because they are useful with respect to sustainability and requirement generation. The decision was made that one level of detail was enough as this is outside the main goal of performing the mission.

A top level of the FFD is shown in Figure 3.2. A more detailed breakdown of deployment, operations, disengagement and maintenance are shown in Figure 3.4, Figure 3.3, Figure 3.5 and Figure 3.6 respectively.

Note that the FFD has been slightly adapted to match the design chosen based on the trade-off which is shown in Chapter 5. This concept consists of two cabins and one propulsion system where if one cabin has landed, the propulsion system switches to the cabin that was on standby and then takes off with that cabin. The differences this concept made in the functional flow diagram are the following:

- In F:1.3 Unload system, one of the cabins (cabin 1) immediately takes off from the transport vehicle (TV) on which it was loaded after the truck is in the correct position. The other cabin (cabin 2) is removed from the transport vehicle while cabin 1 is already in the air.
- F:2.11 Switch cabin was added. When one cabin lands, the propulsion system (PS) moves to the standby cabin and takes off with that one. The cabin switch and the unloading of the payload happen simultaneously. Ground maintenance of one cabin is done while the other one is in the air.

3.2. Functional Breakdown Structure

The functional breakdown structure (FBS) provides an overview of all the functions a system needs to perform to succeed in its mission. The FBS for this system is show in Figure 3.7 and Figure 3.8. It is split into two for legibility. The FBS is divided in four levels. Firstly, the mission phases were defined as functions the system must execute in the orange boxes, this is the top level. After that, these functions were split up into lower level functions in the blue boxes. However, these lower level functions are

not specific enough to detail any actions and therefore the sub-functions were specified in the green boxes. Most of these sub-functions are stand alone and specified. However, some needed more detail which was done in the purple boxes. Together all the boxes provide all the necessary functions for the mission. It should be noted that the phase of production and end-of-life operations are only included at a top level as was also done in the FFD.

3.3. Mission Profile

The mission profile is detailed in Figure 3.1. The mission phases are identified from the functional flow diagram and the functional breakdown structure.

- 1. Deployment
  - 1.1 Transportation
  - 1.2 Secure Operational Area
  - 1.3 Unloading
  - 1.4 Initialization
- 2. Operations
  - 2.1 Take-off
  - 2.2 Ascent
  - 2.3 Approach
  - 2.4 Docking
  - 2.5 Load payload
  - 2.6 Un-docking
  - 2.7 Hovering
  - 2.8 Descent
  - 2.9 Landing
  - 2.10 Unload payload
  - 2.11 Ground maintenance
  - 2.12 Repeat
- 3. Recovery & Disengagement
  - 3.1 De-activation
  - 3.2 Loading for transport
- 4. Maintenance
  - 4.1 Damage inspection
  - 4.2 Diagnosis
  - 4.3 Repeat
  - 4.4 Pre-operation setup.

Figure 3.1: Mission profile and phases

The mission profile is broken up in 4 main phases: deployment, operations, recovery & disengagement and maintenance. The deployment phases refers to all the steps necessary for the system to be ready to take off in operational conditions. The operations phase is repeated until the mission is done, it represents all the operational steps necessary to execute the evacuation. The recovery & disengagement phase refers to the work necessary to de-activate the system and load it for transport once the evacuation is done. Finally the maintenance phase refers to the necessary steps to ensure the system is ready to be used again. Each phase is broken down in sub-phases, which clearly indicates which functions need to be performed. This concludes the functional analysis which permits the start of requirement generation from the mission profile, FBS and FFD. Now that it is know what the system should be able to do, requirements can be set up based on the functionality and what was asked in the project guide [5] as well as any constraints.

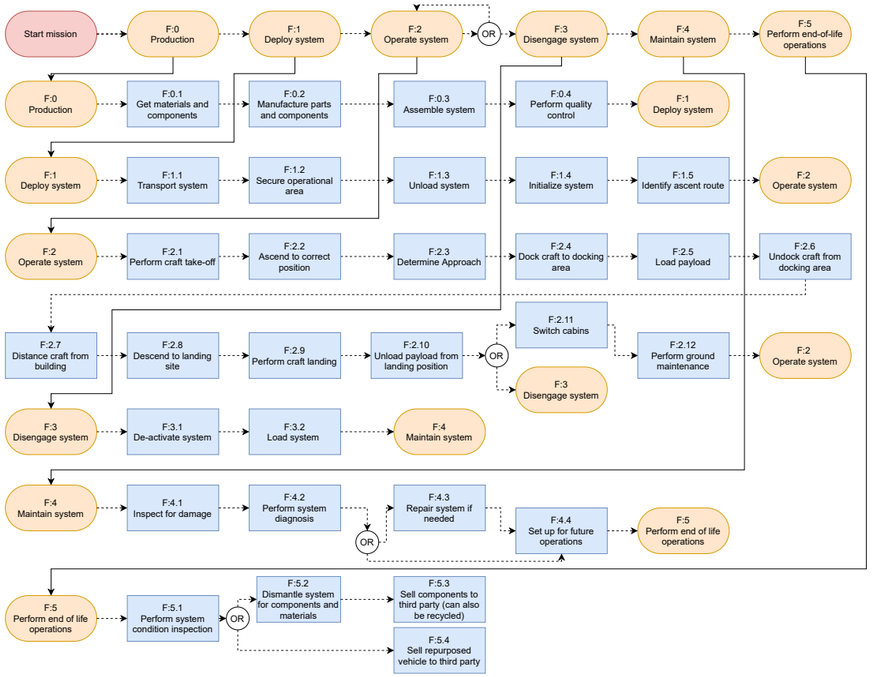

Figure 3.2: Functional flow diagram top level

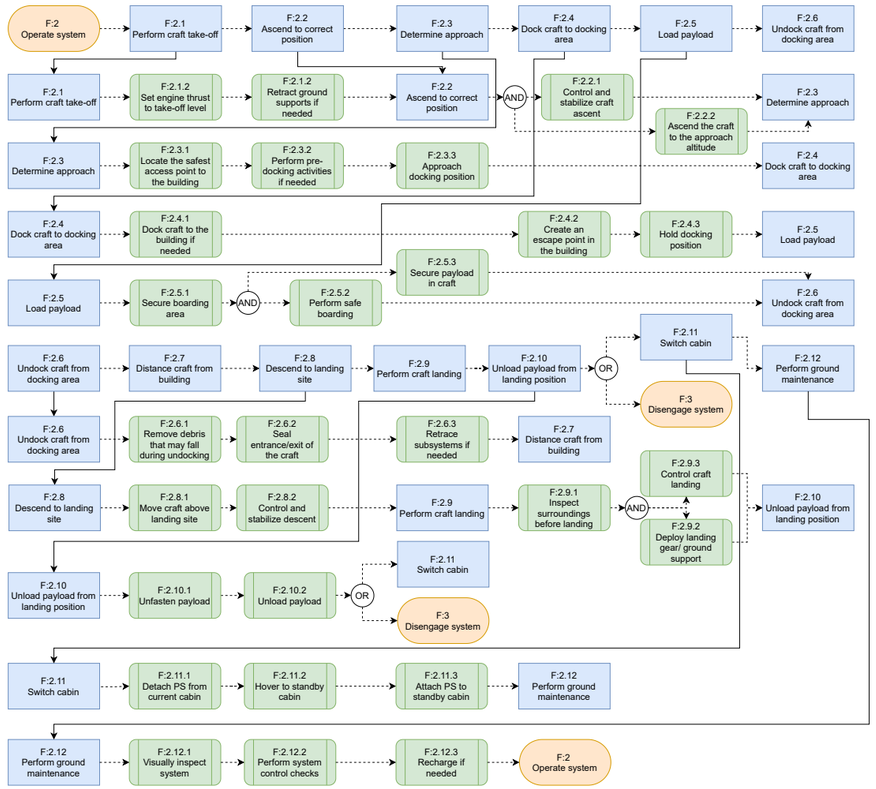

Figure 3.3: Functional flow diagram F:2 Operate system

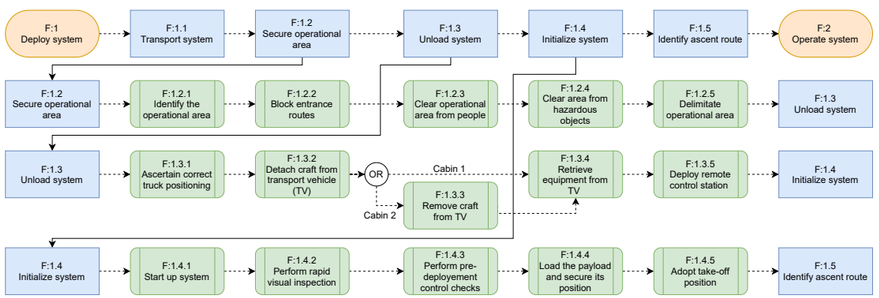

Figure 3.4: Functional flow diagram F:1 Deploy system

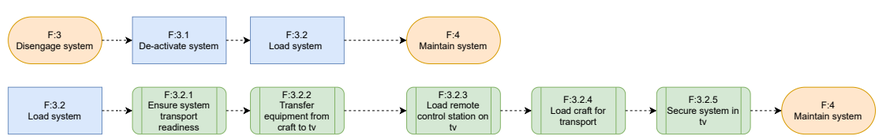

Figure 3.5: Functional flow diagram F:3 Disengage system

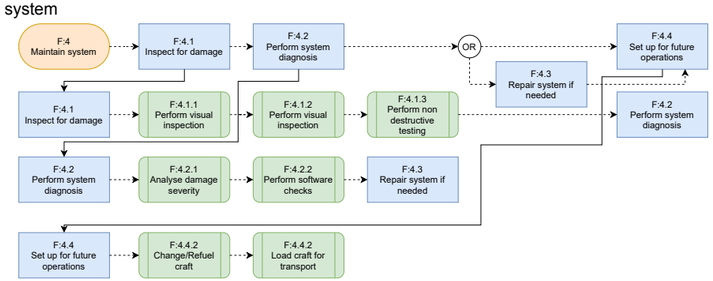

Figure 3.6: Functional flow diagram F:4 Maintain system

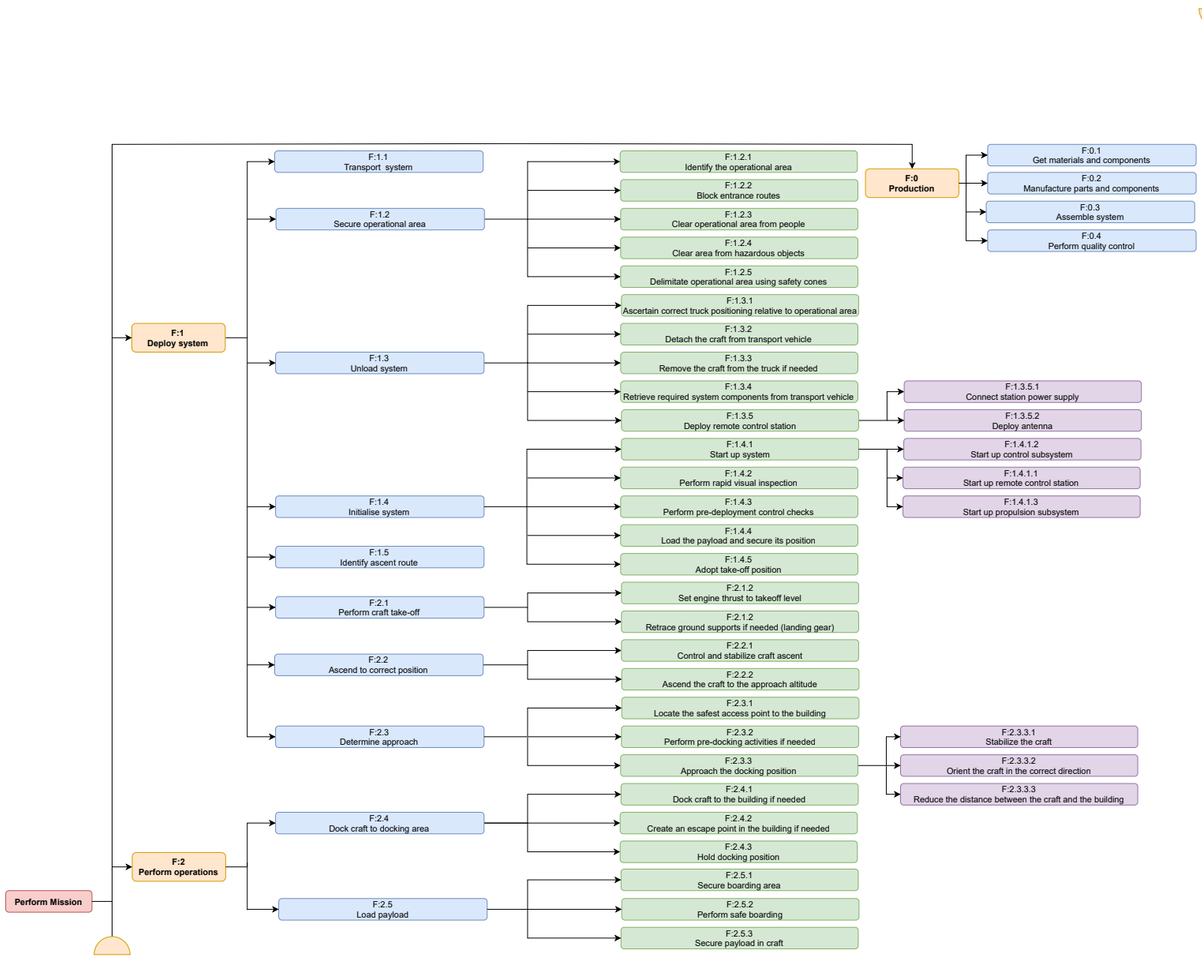

Figure 3.7: Functional breakdown structure part 1/2

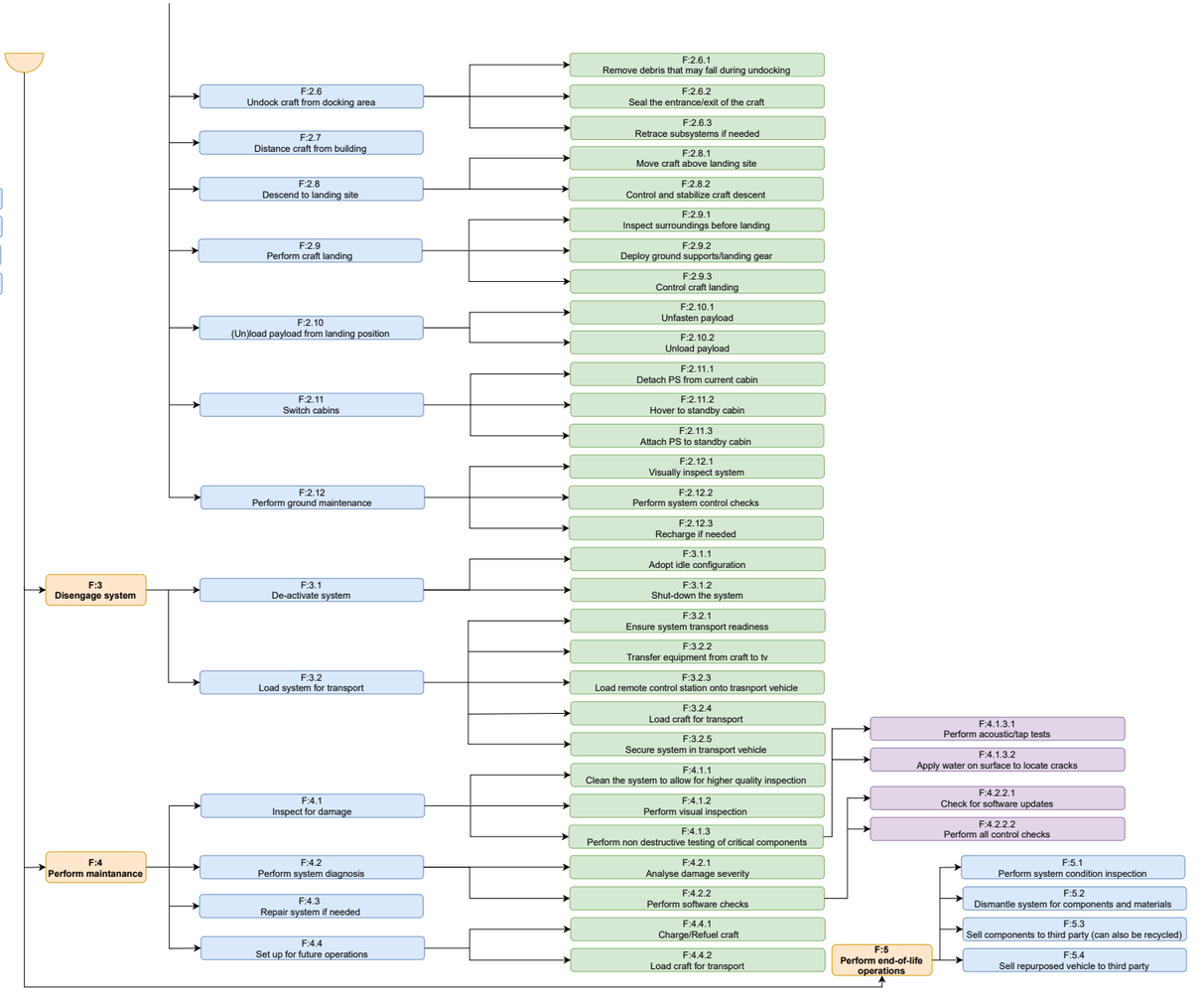

Figure 3.8: Functional breakdown structure part 2/2

4. Requirements & Constraints

Up until now the project objectives and system functionality have been described. It is now time to state the requirements and constraints as these will have a large influence on the design of the system and are later used to verify the product. The need statement of this project is *"Mankind must be protected from high-rise building disasters conditions"*. This statement will be used to generate requirements. Section 4.1 shows the user requirements drafted during the project plan. Section 4.2 takes a look at the design constraints, these constraints are then worded as requirements. Lastly, the mission requirements are given in Section 4.3. Only the system requirements that were not completed but contained <TBD> are given in Section 4.4.

4.1. User Requirements

The first step in requirement generation is to translate the stakeholder needs into a set of unambiguous stakeholder requirements. These stakeholders include but are not limited to municipalities, airworthiness authorities, investors, and TU Delft in the form of the DSE Organisational Committee. Using the mission need statement and the project guide, the user requirements have been drafted and presented in the midterm report's appendix [2].

4.2. Constraints

Design constraints manifest as restrictions on the degree of freedom to provide a solution to a given problem. They often stem from physical and psychological limits such as: laws & regulations, environmental considerations, technical limits and cultural barriers. The constraints have been translated into a set of unambiguous requirements, also presented the midterm report's appendix [2]

4.3. Mission Requirements

The top level mission requirement highlight the requirements of the mission as a whole. The mission objectives are summarised in Table 4.1 as a set of mission requirements

Table 4.1: Mission requirements

ID	Requirement
MIS-E-01	The system shall safely evacuate people from high-rise disaster conditions.
MIS-F-01	The system shall safely transport a firefighter and his equipment where necessary in the event of a high-rise disaster.

4.4. System Requirements

The system requirements remain the same in their essence compared to previous report [2]. However, some of them that had "TBD" marks instead of numerical values have now been updated appropriately according to the new insights gained over the design process. The updated requirements are presented below, along with explanations of the changes that have been made. The general table containing all the requirements together is presented further in the report in Chapter 16, along with verification & validation procedure, in order to avoid confusion and self-repeating.

~~***SYS-GEN-04:** The system shall provide means to create an exit through a conventional glass window with a glass thickness of <TBD> [mm]*~~ This requirement has been removed due to a more thorough study of the glass types used in high-rise building facades. Essentially, there are so many possible thicknesses and manufacturing ways to create reinforced glass, that the requirement on its own becomes useless for future design. The topic is further elaborated on in Section 7.5.

***SYS-GEN-05:** The system shall be able to land and take off in 0 m distance.* This is due to a secured

area around emergency sight where special agencies operate, along with possible debris on ground, so runway cannot be guaranteed.

SYS-PAYL-03: *The system shall accommodate 20 kg of firefighter equipment.* It is expected that only handheld tools are taken on board. The equipment mass is approximated by taking a heavy-duty crowbar (weight $\sim$ 10 *kg*) and assuming two tools of the same weight type are to be taken.

~~***SYS-COM-02:*** *The system shall have a signal strength of at least <TBD> W* when operational.~~
~~***SYS-COM-03:*** *The system shall be operational with noise levels of <TBD> dB* present.~~
SYS-COM-02.2: *The system shall have Signal-to-Noise ratio of at least 25 dB.* The *SYS-COM-03* and *SYS-COM-03* requirements have been added with a mistake, as they are interdependent. Furthermore, the SNR is found to be the main parameter that ensures a good communication link [1]

SYS-COM-04: *The system shall have a maximum delay of <0.1> ms from the control input.* The value is based on the fact that past that value unacceptable airplane handling qualities arise in UAVs. [2]

SYS-DEV-03: *A single craft shall be manufactured and assembled in no more than <TBD> days.* Remains in TBD state because a more detailed market/production analysis is needed to get a viable value.

SYS-STRUC-06: *The system shall be equipped with means of providing ground support for a minimum load bearing capability of 2640 kg.* The value is derived from the first estimate of maximum craft landing weight of 2200 *kg* with a safety factor of 1.2.

~~***SYS-STRUC-07:*** *The system shall be able to deliver the payload to the ground intact after a one-sided impact of <TBD> N minimum*~~
SYS-STRUC-07.1: *The system shall be able to deliver the payload to the ground intact after a ground impact with a peak acceleration of 26 G.* The requirement value comes from Chapter 13 in which the human G limits are used to calculate the maximum acceleration.

Additionally, **SYS-DEV-01** has been identified with red color as killer requirement for the design. It is not achievable for multiple reasons. The design has been done in a minimalist way, with cheapest solutions possible, and already does not satisfy the requirement (as is explained in Chapter 16), while the costs tend to grow over the whole development process, and only preliminary design has been done at this point. Additionally, the development is not a quick process, taking years, so considering a 5% yearly inflation rate for a dollar the nominal cost will grow on its own as well.

5. Preliminary Design

As it is now clear how the system needs to function and what requirements and constraints it needs to adhere to, it is time to design a system. First, concepts need to come up with which which was done in the baseline [1] after which one had to be chosen based on a trade-off.

This chapter will summarise the trade-off performed in the midterm report [2] (see Section 5.1) and the characteristics that will still be used in the detailed design phase of the chosen design in Section 5.2.

5.1. Summary of Design Concept Trade-off

From the design option tree, four different concepts were chosen to analyse. These were, note all of them are electrical propulsion rotorcraft with VTOL capability:

- **Concept 1 Rotorcopter**: Vehicle which has twelve tiltable electric rotor engines which uses suction cups or a robot arm as docking mechanism. It makes use of auto-rotation to reduce the power needed during descent.
- **Concept 2 Falling cabin drawbridge**: This vehicle has four moveable electric rotor engines which can vary their angle of attack. It attaches to the building using a drawbridge and hooks.

[1] URL `https://resources.pcb.cadence.com/blog/2020-what-is-signal-to-noise-ratio-and-how-to-calculate-it` [cited 22 June 2021]
[2] URL `https://www.researchgate.net/publication/235120515_UAVs_and_Control_Delays` [cited 22 June 2021]

The closed cabin is released from the craft and is slowed down during its descent using measures such as a parachute or airbags.

- **Concept 3 Release & pick up**: The Release & Pick up has eight potentially movable electric motors and hovers next to the building, making use of a drawbridge to load people in. It descends using its engines. When on the ground, the closed cabin is detached and a new cabin is mounted to reduce turnover time.
- **Concept 4 Walk over the engines**: The vehicle has four ducted electric engines. One of the engines has a grid above it over which people can walk to get to the closed cabin in the center of the vehicle. A railing is present to support the evacuees when leaving the building and crossing the engine.

Seven trade-off criteria determined and weights using the AHP method. Each member of the group individually assesses the relative importance of each criterion over the other. This was done using an online tool [6], and happened for all 21 pairs of criteria. This tool also calculates the standard deviation of the weight. The individual weight distributions are then averaged. The final criteria, the system requirements they are linked to, the weight distribution, weight importance ranking and their standard deviations are summarised in Table 5.1

Table 5.1: Criteria requirement coverage and weight summary

#	Criteria	System Requirements	Weight	Rank	Std dev.
1	Safety	SYS-OPS-08, SYS-LAW-03, SYS-STRUC-08, SYS-SAFE-01, SYS-SAFE-02, SYS-SAFE-03	39.41%	1	6.53%
2	Reliability	SYS-SAFE-04	6.99%	5	1.93%
3	Weight	SYS-LAW-07, CTR-TCH-03	23.15%	2	4.11%
4	Relative Cost	SYS-DEV-01	3.86%	7	1.63%
5	Turn around time	SYS-OPS-01	15.00%	3	5.00%
6	Technology Readiness Level (TRL)	SYS-LAW-03	6.31%	4	1.91%
7	Simplicity	SYS-COM-06, SYS-OPS-04, SYS-OPS-05, SYS-GEN-02	5.28%	6	1.86%

At this point, all four concepts received performance scores for each criterion after being preliminary assessed on the criteria. This assessment was done only relatively between concepts and any quantitative analyses were also performed very preliminary. The performance scores were from 1 to 5. As has been stated, the score did *not* represent individual performance in a category, but indicated (under)performance with respect to other concepts in the trade-off, i.e. when none of the designs received a 5, it means that all have considerable drawbacks and none was able to significantly out-stand among others. After all this, a trade-off was able to be performed.

The resulting trade-off can be seen in Table 5.2. The columns are widened to represent the relative weights of the criteria, and the colors represent the overall performance for that concept in that criterion.

Table 5.2: Trade-off matrix

Weights	0.395	0.23	0.07	0.039	0.15	0.053	0.063	1
Concept	**Safety**	**Reliability**	**Weight**	**Cost**	**Turnover time**	**Sim-pli-city**	**TRL**	**Results**
Rotor-copter	5	2	4	2	1	2	2	3.175
Falling cabin draw-bridge	2	1	1	1	4	1	1	1.845
Release and pickup	4	4	5	3	5	3	3	4.065
Walk over the engines	3	5	3	4	1	4	5	3.378

The trade-off indicated that Concept 3 was the best. To verify this three different sensitivity analyses were performed: solution sensitivity to the weights, to input parameters and parameter combinations. After these analyses it became clear that Concept 3 was still the winner.

5.2. Chosen Concept Description

The following characteristics, which were determined in [2] will be used in the rest of the report:

- The cabin will be a cube with sides of 1.65 *m*. The seating configuration will be two rows of three people shoulder by shoulder facing each other. 1.5 *m* was taken as the height, 0.5 *m* for shoulder width and 0.75 *m* for leg room [3]. To provide minor clearances between the people a safety factor of 1.1 is added.
- Eight electrical motors in four pairs placed above the cabin.
- Two cabins and one propulsion system which switches cabins.

6. Sustainable Development Strategy

The chosen concept needs to adhere to certain requirements regarding sustainability. The sustainability development approach from the baseline report [1] thus needs to be slightly adapted to the chosen concept. In this chapter, adjustments to the sustainable development strategy are discussed. Numerous design decisions have been made up to the current stage, many of which trace back to the four main sustainability directions, in the form of environmental, technical, social, and economic aspects. These are described in Section 6.1, Section 6.2, Section 6.3 and Section 6.4 respectively. It should be noted, however, that the goal of the system is rescue, and thus that the safety of the evacuees is the absolute priority. Some trades may therefore have to be made in disfavour of sustainability for the sake of achieving this mission goal.

6.1. Environmental Sustainability

The Cradle-to-Cradle principle is based on minimization of product waste from production to end-of-life. It encompasses three principles; the use of recyclable materials, minimization of the use of non-recyclable materials, and the use of bio-degradable materials.

The use of recyclable materials will become a large part of the production of the system. Materials that can be reused at end-of-life shall be used as much as possible. Some metals or metal alloys

are suitable for this and are also strong enough for an aircraft structure to carry six people. However, other strong and light materials like many composites are difficult to recycle at end-of-life, which should therefore be avoided. Not only are recyclable materials of interest, recyclable parts or subsystems can also reduce the end-of-life waste. If the craft itself reaches an unreliable stage and is decommissioned, some of its subsystems may still be of high quality. These could then be reused in other systems. This is called ”direct” or ”as is” recycling [7].

This direct recycling is also a partial solution to the use of non-recyclable materials when their use is absolutely necessary. It does however remain temporary as the material will inescapably become waste after multiple product life cycles, although this waste may become relatively minimal. The use of non-recyclable materials should therefore still be limited. This is more attainable for non-critical, non-load-bearing parts than for parts integral to the structure. For these parts, better performance may have a more significant impact on its sustainability.

Bio-degradable materials should also be considered. Components constructed from these materials do not add to the end-of-life waste as they degrade over time to natural products. However, many bio-degradable materials are made of natural fibres. This is a problem for a load bearing structure as natural fibres have several drawbacks. Firstly, they do not have consistent properties as these depend on, for example, the harvest. Next to that, natural fibres have limited thermal stability. Permitted temperatures go up to 200 $^{\circ}$ *C* and may therefore be too low for high rise fire conditions [8].

Lastly, it should be considered that if a recyclable or bio-degradable materials are chosen over non-recyclable materials, this might increase the mass of the vehicle. In the long term this may actually be more resource intensive as this increases the power required. This should be considered and a trade-off should be done for the material choice and sustainability.

6.2. Technical Sustainability

Technical properties for the system can be selected as to make the system more sustainable. The most important design choice for this is the choice of the power and propulsion systems. The most operationally polluting types of conventional engines are those that rely on fossil fuels. Electrical engines on the other hand have zero emissions during operation, and were therefore selected for the concepts. However, the production of batteries is currently very energy and material intensive. Next to this, both their production and decommissioning can often be dangerous and polluting [9]. It is therefore first of all vital to produce batteries with a long life-cycle for this system. Next to this it must be verified that the benefits of their operation outweigh their production- and disposal-associated problems, and that this net effect is better than fossil fuel alternatives.

6.3. Social Sustainability

Much attention has also been paid to social sustainability aspects during the conceptual design process and the design trade-off. Safety aspects especially, as a subset of social sustainability, have been critical. So far in the design stage the following considerations have been made that can be (partially) traced back to social sustainability:

- Safety criteria during the trade-off are weighed most heavily, to increase the certitude that the final option satisfies considerations related to risk minimization, safe evacuation and safe transportation procedures for both the evacuees and firefighter on board, while maintaining feasible design solutions.
- Consequently the design concepts feature closed cabin designs, with securing mechanisms for boarding. When entering the craft, the evacuees step directly into the cabin, while bridge systems close gaps between cabins and building facades. Passengers will also be transported to the ground via powered descent, which would offer the operator more freedom during problematic scenarios and emergencies. Detachable cabins provides passengers with sufficient time to safely and calmly leave the cabin.
- In addition, an electric propulsion method with rotors decreases the endangerment of people in direct vicinity of the system in operation when compared to combustion engines with their exhausts. It also removes the noise contribution of combustion methods. For the same reasons

radioactive and other hazardous propulsion types were eliminated as viable options.

6.4. Economic Sustainability

At this stage, little can be determined about the economic sustainability aspects that add to the general guidelines discussed in the baseline report [1]. Most design elements are still under question, which means many cost aspects are still unknown. However, some additional notes can be made:

- Production cost heavily depends on the structural design of the vehicle. During the trade-off, Technology Readiness Level (TRL) is considered as a criterion. This helps reduce the implementation of underdeveloped tech, pushing in favour of certified and tested equipment, which reduces potential development and production costs. It allows safer exploration of new technologies, which may aid future use of these.
- The TRL criterion also works in aid of operational and maintenance costs. The use of proven and existing technology increases the availability of replacement parts and simplifies the design. Next to increased reliability, off-the-shelf components often offer cheaper solutions than the development, design and production of technologically new solutions. This would allow fire departments and municipalities to save on maintenance costs.
- It is also becoming clear that the design requires unique engineering solutions and perhaps new technology. This opens patenting opportunities which can provide a financial and marketing edge to startups centred on this solution.
- The high-risk nature of the design problem may allow for the exploration of new technologies that may not typically be ready enough for widespread commercial use. This favours the development of these new technologies into a stage acceptable for commercial use.

7. Operations & Logistics Description

Requirements and constraints have been set, a concept has been chosen and a sustainability approach has been set up so it it now time to begin a detailed design of this chosen concept in such a way that it meets the requirements starting with operations and logistics as this has a large influence on the rest of the design. This chapter aims to describe the operation the system will perform and the logistics around it.
Firstly, the operations and logistics diagram will be shown in Section 7.1. The operational duration is given in Section 7.2. How the propulsion system will attach to and detach from the cabin is illustrated in Section 7.3. A very important part of the mission is getting people on board thus a boarding mechanism is needed, various options were gathered and their (dis)advantages listed to in the end find a solution. This is given in Section 7.4. Some operational details about the concept will then be explained in Section 7.5.

7.1. Operations & Logistics Diagram

This section contains the operations and logistics diagram. This is a visual tool to show the operation of the product from start to finish, from the initial order to the end-of-life phase. It can be seen in Figure 7.1. Below the diagram each phase will be specified further.

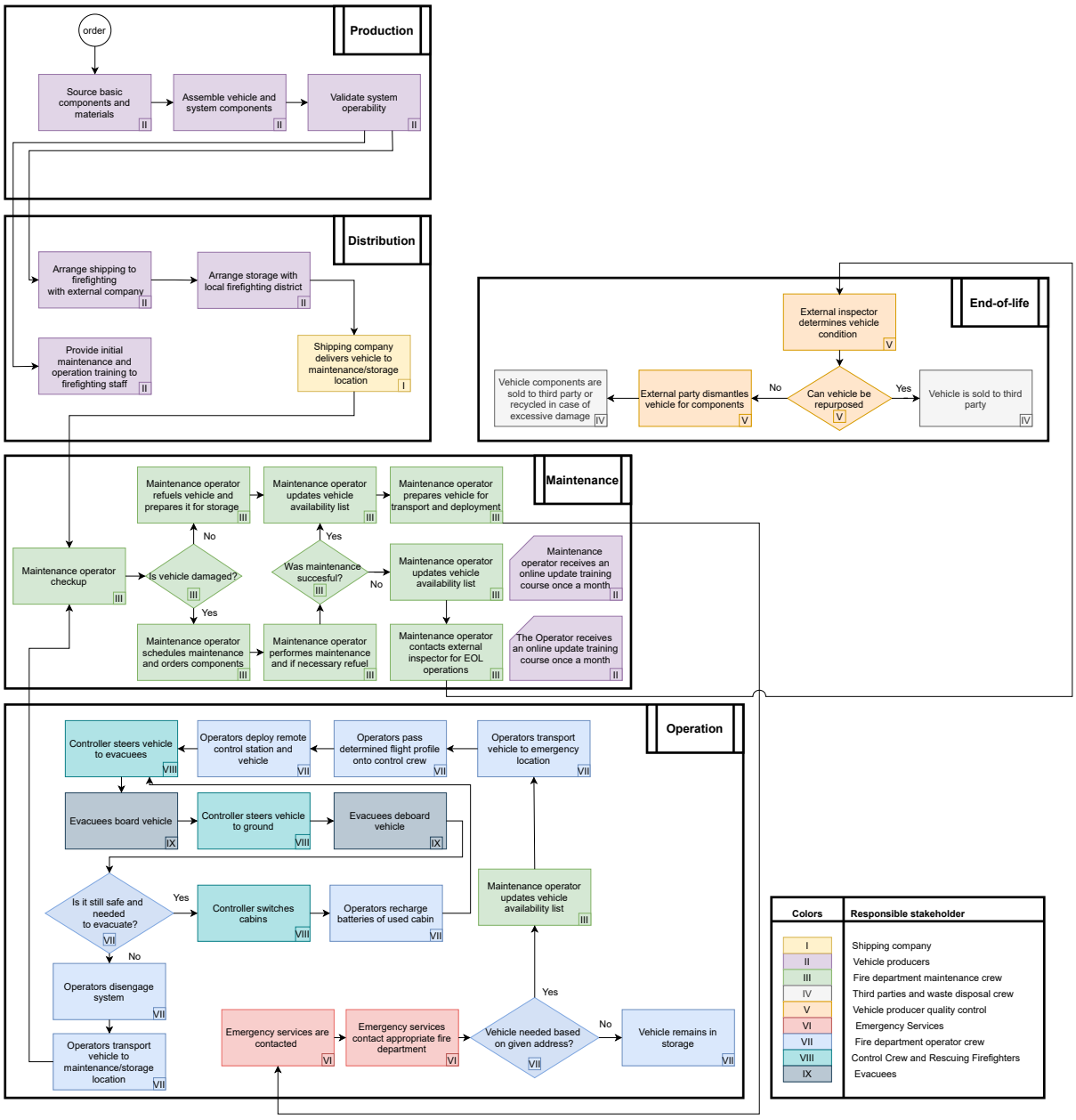

Figure 7.1: Operations and logistics concept block diagram

Order

The process begins at receiving an order from a fire department after which the vehicle is specifically produced for that particular fire department. This approach was deemed appropriate since the production cost of the system will be fairly high and the demand relatively low. Especially since, most likely, not every fire department will request a vehicle and rather one or a few per region. Losses due to overproduction by first producing and then selling a vehicle, must thus be minimised.

Production

The production phase is completely overseen vehicle producing firm and is depicted as the top block of Figure 7.1. During production the firm must source components, either through vertical integration or outsourcing after which these will be assembled by a production crew. Due to the complexity and specificity of the system, the focus should lie on lean manufacturing and in-line production during assembly. Since the estimated demand of the product will not be sufficient to justify continuous production, in-line

assembly is deemed to be ideal. However, batch production would still be convenient even in case of low demand in order to take some advantage of the economies of scale it provides. Lean production is also beneficial as it typically results in lower error rate, faster error identification and mitigation practices, more precise production and higher efficiency. This is judged to be worth the additional assembly worker payment and required training. Using lean production also helps meet the sustainability quotas. After the vehicle has been assembled, the system is tested to determine functionality and operability. If the system is determined to be produced to its specification, the distribution phase takes place. [10, 11]

Distribution

After the production of the vehicle it should be distributed to the customers, in this case the fire departments. This distribution phase is depicted in Figure 7.1 as the second block from the top. The firm responsible for the production of the system will have responsibility for the distribution phase as well. It will have to interact with third party shipping companies to get the product to the correct places. Firstly, the responsible firm estimates the the delivery time for the product. After this, the firm contacts the fire department to provide information on storage and maintenance requirements of the system. After this, the firm will add the fire departments to a list of active system operators. This is done to provide them with digital training courses and maintenance information as well as provide updates. After all this is done, the product is ready for transport and delivery. This is handled by a third party which is experienced in delivery. However, the responsibility for contacting this third party, the fire department and possible damage during transport still lies with the firm. This is because the firm will have the most knowledge about the product and is therefore more likely to find a suitable transporter. This decreases the delivery time and the likelihood of pre-operation damage, which is beneficial for the economical and environmental sustainability of the product.

Maintenance

After distribution, the vehicle immediately goes into the maintenance phase which is outlined as the third block from the top of Figure 7.1. This summarises all routine activities not related to operation or dismantling. The maintenance is mainly carried out by the fire department maintenance crew who have received appropriate maintenance training provided by the production firm. A prominent feature of the maintenance and operations phases is that they require the maintenance operator to keep an updated list of all available and serviced vehicles. Each time a vehicle arrives at the maintenance location, a check-up is performed. When a vehicle is new, this is to verify that it respects design specifications and was not damaged during transport. If the vehicle has been operated, it is checked for operational maintenance. The maintenance operator must then determine if the vehicle was damaged or not. If it has been, it will follow a process of maintenance where it is attempted to restore the system. If this is not possible, the maintenance operator defines the vehicle as decommissioned and updates the vehicle availability list. The maintenance operator is then required to contact the production firm to coordinate an external inspection. When no damage is revealed in the initial inspection, the vehicle is simply recharged and prepared for operation. Once this is done, the vehicle availability list is updated and the vehicle is considered serviced which is also the outcome of a successful maintenance. The vehicle is then loaded for transport ans placed on standby. Two notable responsibilities of the production form are to provide and update courses for both vehicle operators and maintenance operators. This will allow the system users to train additional operators depending on necessity.

Operation

When the system can finally be used for its intended purpose it enters the operation phase. This phase is depicted in Figure 7.1 as the bottom block. There are three principal stakeholders in this phase: the emergency services, the fire department and the evacuees. The fire department can be subdivided into the maintenance crew, the operation crew and the control crew. The flow of actions is as follows. Firstly, the emergency services will be contacted by individuals in danger, who will later be referred to as evacuees, or by people witnessing them. After this, the fire department is contacted. The fire department can then determine if the vehicle is needed for the specific emergency. A maintenance operator will then set up one of the service vehicles in the region and update the vehicle availability list to indicate the number of vehicles available. Now the fire department operation crew can transport the vehicle to the emergency location. There it will be deployed and the control crew will set up to be ready

for take off. In the mean time the fire department operational crew will determine the flight profile based on the amount of evacuees at each location, which is passed on to the control crew for the operation. The controller will steer the vehicle up, containing one fire fighter, and there the evacuees will board the vehicle before being brought back to the ground. In the mean time it will be examined by the fire department operations crew if another cycle is needed. If so, the controller will switch cabins and the batteries will be recharged by the operational crew. If not, the system will be disengaged and loaded back onto the transport vehicle to be brought back for maintenance and storage.

End-of-life

The end-of-life phase is entered when vehicle maintenance and repair are not possible anymore or is conducted unsuccessfully. This phase is shown in Figure 7.1 as the top right block. The principal stakeholders in this phase are the fire department, as they are losing their product, the responsible firm and third party like a waste disposal company. After the vehicle has been deemed unserviceable, the responsible firm is contacted. They will determine is the vehicle should be repurposed and if the fire department can sell it. Then it will be used as a heavy lifting autonomous vehicle, which is possible if it is safe, but not safe anymore for human rescue operations. If the inspector determines the vehicle to not be reliable anymore it will be dismantled. The fire department can then sell individual components or bring them to a waste disposal company to be recycled or processed. This is done to minimise waste on an economical and environmental level.

7.2. Operational Duration

The operation exists of multiple parts and phases. All the parts will take a different amount of time. However, it should be estimated how long they will take as this needs to be accounted for in several subsystems of the vehicle such as the power and propulsion subsystems. This was calculated in four phases: ascend, hover, descend and turnaround. A visual representation of the mission in those four phases can be seen in Figure 7.2.

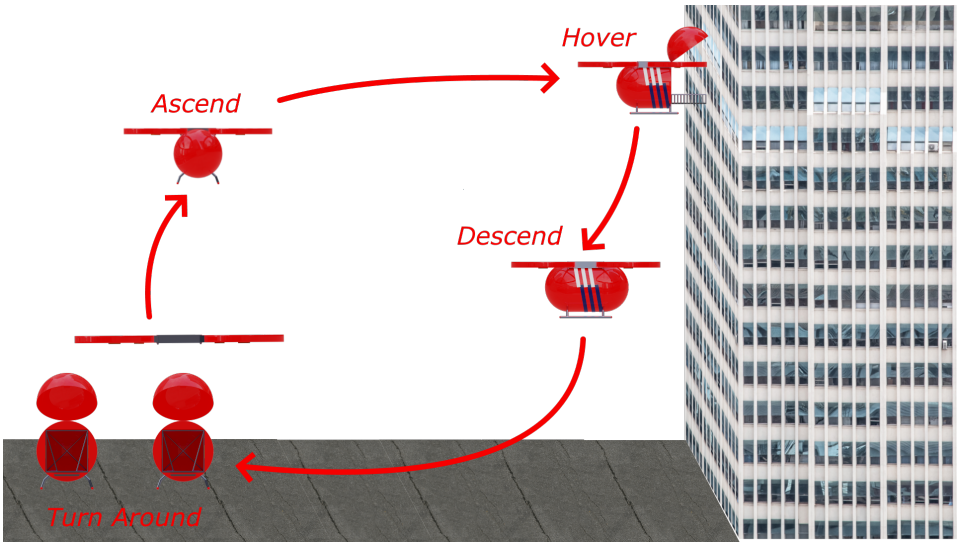

Figure 7.2: Four phases of the mission profile

Subsequently, the required duration of all four phases was analysed to further estimate the time of one mission cycle. Every phase was broken down into the parts and the time for those parts was estimated in Table 7.1. The time to load evacuees was multiplied by six to account for every individual evacuee. The time of 20 *s* was taken as this account for the extra time needed to evacuate incapacitated people. As can be seen in Table 7.1 a safety margin was applied to all phases. An extra large safety margin was applied to the hover face as it is largely dependant on unpredictable factors which can greatly differ in time. For example making the entry point might take long if a window needs to be broken, but can also be short if a balcony is already available. Next to that, evacuees might be hesitant to board the

craft and therefore take longer than expected. In total, the complete time, including safety margins, for one mission cycle is 778 *s* or 13 *min*.

Table 7.1: Mission duration breakdown

Mission phase							
Ascent		**Hover**		**Descent**		**Turnaround**	
Part	*Time [s]*	*Part*	*Time [s]*	*Part*	*Time [s]*	*Part*	*Time [s]*
Motor spin up	2	Extend bridge	12	Acceleration	6	Detach	15
Acceleration	6	Make entry point	90	Constant velocity	68	Hover and lineup	60
Constant speed	66	Load evacuees	20*6 = 120	Decelleration	6	Attach	15
Decceleration	6	Retract bridge	15				
		Maneuvering	60				
Total time	80	**Total time**	297	**Total time**	80	**Total time**	90
Safety margin	1.33	*Safety margin*	1.5	*Safety margin*	1.33	*Safety margin*	1.33
Total time inc. safety margin	106.4	Total time inc. safety margin	445.5	Total time inc. safety margin	106.4	Total time inc. safety margin	119.7

7.3. Attachment Mechanism

As can be seen in Chapter 5, the concept relies on the propulsion system being able to switch cabins. It is therefore vital to come up with a system that easily and quickly connects the centrepiece with the propulsion system to the cabin. This system is shown in Figure 7.3-Figure 7.5. This figures show the steps taken to attach the centrepiece. For detachment the steps need to be carried out in reverse.

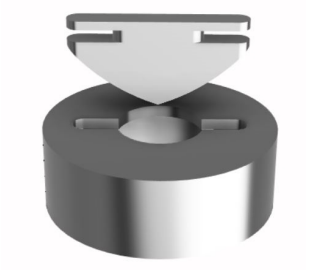

Figure 7.3: Attachment system step 1

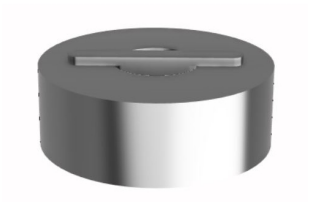

Figure 7.4: Attachment system step 2

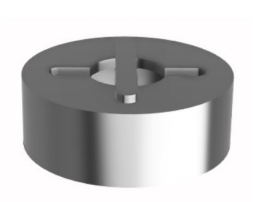

Figure 7.5: Attachment system step 3

The top part will be attached to the centre part connecting the rotor arms and the bottom part will be inside the cabin. The top part will contain a small electrical motor that twists once it is lowered inside the bottom one. Multiples of this system will be present. Their weight and how much power and energy will need to be analysed in the post-DSE phase as well as an analysis on if the system will still work when the skin and cabin deform due to a hard landing. For the power and energy it is possible to say that it will not have a big influence as it is negligible compared to the power and energy needed for the engines of the propulsion system.

7.4. Boarding Mechanism

A critical part of the mission is getting the evacuees on board. It is thus essential to come up with a solution for this. Several ideas were gathered after which these will be compared based on their (dis)advantages and how well they meet the criteria. Ultimately, the best one will be chosen.

7.4.1. Essential criteria of boarding mechanism

When coming up with a boarding mechanism, the following essential criteria need to be taken into account:

A. The boarding mechanism needs to be reusable for the next operational cycle.

B. Safety of the evacuees and firefighter needs be guaranteed.

C. Hover time of evacuation procedure must be within an acceptable time limit.

D. Evacuation of incapacitated people needs to be possible.

E. Suitable for most buildings.

The goal is to meet these conditions as closely as possible. For a boarding mechanism to be considered viable, a certain level of compliance to these conditions is required. The second criterion has a big influence on the attachment of the connection between the cabin and the building. The cabin can suddenly move during operations due to gusts causing an unforeseen gap between the building and the connection. If an evacuee was about to step onto the connection, this sudden gap could be disastrous.

7.4.2. Possible options

Two main categories of boarding mechanisms were considered: a bridge and alternative solutions. For the bridge option, different types of bridges will analyzed as well as how the bridge will attach to the building. Different combinations of the bridge type and attachment can be made for the final boarding mechanism.

Types of bridges

1. Pseudo-elastic bridge: This bridge is made of pseudo-elastic material, also called superelastic material. This will allow for a large deformation, but will also revert back to its previous shape after removing the stress, like after a gust [12].
2. Gimbal cabin: A gimbal is a support which allows an object to rotate around all three axes. In the case of the bridge it will be attached to the cabin in such a way that if the cabin moves, the bridge will stay in the exact same place it was.
3. Self-stabilizing bridge:The bridge will have a system that can sense the horizon and will ensure that the bridge is always horizontal. Even if the cabin rotates, the sensors and the support will make it possible such that the bridge can rotate relative to the cabin.
4. Enclosed cage: This cage will be made of a rigid material enclosing a rigid bridge. This cage will thus prevent anyone from falling of the bridge.
5. Pulling bridge: This bridge will be suspended on two ropes. It will be more like a floating raft that does not stretch all the way between the cabin and the building. By pulling on the rope, which can be done manually or automatically, the raft is moved from the building to cabin and back to evacuate people in danger.
6. Folded, extendable bridge: This bridge is folded into the cabin and can unfold upon docking. It is then automatically extendable such that is can reach the building perfectly.

Bridge attachment

7. Spikes: Bridge end contains sharp spikes at the bottom. This end will be slammed into the floor inside the building.
8. Double sided adhesive: The end of the bridge sticks to the floor inside the building using double sided duct tape.
9. Inflation device: At the end of the bridge, an inflatable ring is attached. The bridge enters the building and the ring inflates such that it is larger than the opening through which the bridge entered.
10. Clamps: The bridge end is equipped with clamps which can clamp onto balconies and window frames. Clamps can also be at the end of extendable arms which are installed on the cabin.

11. Drilling/screwing: The bridge end is armed with drills/screws. Either holes are drilled first and then the bridge is screwed in or the bridge is immediately attached to the building by drilling. The drills/screws can also be on extendable arms mounted to the cabin.
12. Suction cups: Suctions cups at the end of the bridge attached it to the building. The cups can also be at the end of extendable arms which are mounted to the cabin.

Alternatives

13. Zip line with harness: A zip line is attached to the building. Evacuees are attached to this zip line with a harness and then glide into the cabin. A stretcher can also be attached to the zip line to evacuate incapacitated people.
14. Slide: One end of the slide is attached to the building and the other ends in the cabin. The cabin hovers below the floor on which the evacuees are standing, the evacuees enter the cabin by sliding down.
15. Flexible extending cage: Think of rope play equipment in a children's play park. A flexible tunnel structure through which people can crawl is attached to the building, connecting it to the cabin.

7.4.3. Advantages and disadvantages

To be able to compare the different ideas for the bridge type, attachment and alternatives, all of their respective advantages and disadvantages need to be listed.

1. **Pseudo-elastic bridge**
   - + Decreases loads introduced into the cabin.
   - + Decreases loads introduced into the building.
   - − Unstable when a person walks on the bridge.
   - − Complex
2. **Gimbal cabin**
   - + Keeps cabin and bridge stable
   - − Complex system
   - − All loads are concentrated into one point
3. **Self-stabilizing bridge**
   - + Bridge will be stable
   - − Complex system
   - − All load are concentrated in a single point
4. **Enclosed cage**
   - + Evacuees cannot fall off the bridge
   - − Large structure which will be hard to fold into the cabin
   - − Adds more mass
5. **Pulling bridge**
   - + Rope can be flexible while bridge is rigid
   - + Decreases loads introduced into the cabin.
   - + Decreases loads introduced into the building.
   - − The rope needs to be attached rigidly into a potentially unstable building
   - − The firefighter might need to aid people but there is no permanent connection between cabin and building
   - − Rope needs to be held under tension at all times
6. **Folded, extendable bridge**
   - + A translation in x-direction will not result in a gap
   - + Decreases loads introduced into the cabin due to gusts in x-direction
   - − The extendable part is failure prone
7. **Spikes**
   - + Prevents translation in x- and y-direction
   - + Reusable
   - − Bridge needs to enter building, windows might be too small and not possible when bridge cannot reach the floor (windows higher than floor or balcony railing in the way)
   - − A lot of force needed to slam the spikes into the floor
   - − Peeling force needed to release
8. **Double sided adhesive**
   - + Very lightweight

+ Prevents translation in x- and y-direction
+ Non-destructive
− Won't properly stick to the floor if it is not clean
− Not reusable, loses its sticking power after each use
− Bridge needs to enter building, windows might be too small and not possible when bridge cannot reach the floor (windows higher than floor or balcony railing in the way
− Pressure needed to make it stick
− Peeling force needed to detach

9. Inflation device

+ Non-destructive
+ Prevents translation in x-direction (in y- and z-direction depends on the size)
+ Bridge does not need to enter building so, depending on the size of the deflated inflatable part, it fits through most to all windows.
− Needs to be made out of non-flammable material
− Material used needs to be puncture proof
− Gas used to inflate needs to be non-flammable
− Strong airflow needed to inflate rapidly
− Pressurised deflation needed to deflate quickly
− Pressurised gas needed

10. Clamps

+ Non-destructive
+ Reusable
+ Prevents translations in x-, y- and z-direction
+ Bridge does not need to enter building so suitable for any size window or balcony
− Depends on structural integrity of building (window/balconies)
− Opening of clamps needs to be adjustable in order to properly clamp a balcony or window sill
− Distance between clamps needs to be adjustable in order to properly clamp a balcony or window sill

11. Drilling/screwing

+ Prevents translation in x-, y- and z-direction
− First drilling and then screwing takes a lot of time
− Different drills/screws needed for different facade materials
− New holes need to be drilled every time
− Unscrewing takes time

12. Suction cups

+ Reusable
+ Prevents translation in x-, y- and z-direction
− Suction cups do not work on porous materials

13. Zip line with harness

+ Not impacted by gusts
+ Secure, evacuee cannot fall when harness is properly attached
− People need to put on a harness in a stressful situation, takes a long time and might be incorrectly attached
− Very hard to attach to building
− Special stretcher needed for incapacitated people
− Adaptable or large variety of harnesses needed (for children, small child plus parent, pregnant people etc)

14. Slide

+ Easy for injured people
+ Quick evacuation procedure
− Very difficult to attach to building since it is flexible

15. Flexible extending cage

+ Cannot fall when on it
+ Not influenced by gust since wind blows through it
+ Does not put forces on building due to flexibility
− Not suitable for incapacitated people, very difficult for firefighter to help
− Very difficult for a parent to bring their small child with them
− Difficult to attach to building

7.4.4. Determining final boarding mechanism

As can be seen from Section 7.4.3 many of the options have similar disadvantages. These problems re-occur in many concepts because it is vital to the design to have a solution for them. Therefore some additional systems have been considered to eliminate the drawbacks of several concepts. Firstly, the pulling bridge, zip line, slide and flexible extending cage need a system that can attach to the building, before they can attach to the building itself. Therefore a harpoon could be used from the cabin to the building for the pulling bridge and the zip line to span a rope between the two. However, this is not an option as a harpoon is not always able to grab onto a building in case of a glass or concrete facade and next to that it is not reusable for multiple rescue cycles. This is because a harpoon is made to go into something, but not get out of it anymore. For the slide and the flexible extending cage the situation is different. It is also a non-rigid object that should be attached, but it is larger than a rope. Therefore something sturdier must be used to attach it. This could be an extending robot arm or ladder from the cabin. However, a robot arm will add an extra complex system and a lot of mass. A ladder would cause a concentrated load on the cabin and the firefighter will have to carefully balance on it while carrying the system that needs to be attached and then attach it making it very unsafe and thus not an option. Since all of these 'solutions' are not actually working solutions these boarding mechanisms are considered nonviable.

The pseudo-elastic bridge, the gimbal cabin and the self-stabilizing bridge were considered too complex to be analysed in the given time constraint. They could be viable options but would need to be analysed in more detail in the post-DSE phase.

At this point only bridge types 4 and 6 and all attachments are still left. There is little difference between bridge type 4 and type 6. Both are rigid bridges, however, type 4 is enclosed in a cage while type 6 is not. This is beneficial for the safety of the evacuees as they cannot fall off of it. Type 6 might not have this safety benefit but that can be overcome by adding railings on the side that are high enough to keep people from falling off. Type 6 is not just a rigid bridge but will also be extendable. Two parts of the bridge can slide over each other to make it longer or shorter. This is beneficial because it reduces the loads on the cabin when gusts occur in the x-direction, as the bridge can just move with it. This property, together with the fact that type 6 will be smaller and lower in mass and therefore easier to stow in the cabin, makes type 6 the most suitable bridge for the boarding of the rescue vehicle.

Table 7.2 compares the different types of attachments by checking how well they meet the criteria based on their (dis)advantages. Because only a bridge is left, the time it takes for the evacuees to board by walking across the bridge will be the same. Thus, criterion C "Hover time of evacuation procedure must be within an acceptable time limit." is now only applicable to the time it takes to attach and detach to and from the building. Criterion D "Evacuation of incapacitated people needs to be possible" was left for completeness but is only influenced by the bridge and was thus fulfilled by every attachment type.

Table 7.2: Comparison of attachment types

	Criteria				
Attachment	A	B	C	D	E
7	+/-	+	-	+	-
8	+/-	-	+/-	+	-
9	+	+/-	+	+	+
10	+	+/-	+	+	+
11	+/-	+	-	+	+/-
12	+	-	+	+	-

It can be seen that attachment type 9 and 10 score the same. This is based on the five most important, overarching criteria. However, as can be seen in Section 7.4.3 both concepts have several drawbacks. The main issue with the inflation device (type 9) is its feasibility. Alongside a tank to deflate the device, pressurised gas is needed to inflate it quickly meaning a tank of this gas needs to be on board. Several of these tanks will need to be taken to site and swapped out after one is not full enough anymore in order to keep being able to use the inflation device. Besides this, bringing pressurised gas into a

building is not very safe. If the inflatable part would be punctured and explodes, it would create a lot of airflow or even worse if the gas inside is flammable. The material would thus need to be puncture proof. This combined with the fact that a large area of this material is needed, would make this option heavy. Even though, based on the criteria, attachment type 9 scores well it is more complicated and thus less feasible than type 10 as well as more dangerous in case something goes wrong. Considering this danger type 10 will be used as the final concept for the boarding mechanism.

The option of using a reaction control system (RCS) in the form of small propellers on the side of the cabin to alleviate the loads on the building when a gust moves the cabin, was considered. However, these will not be able to react fast enough to gusts and are thus not useful.

7.4.5. Final boarding mechanism

Summarising, the final concept will consist of a rigid bridge with an extendable part. This part may extend when the cabin is translating in the x-direction to reduce the loads on the cabin and the building. How much this translation needs to be will depend on how much gusts will push the cabin back. The unextended length of the bridge will have to be 1.5 times the thickness of a standard wall, which is about 50 *cm* on average, in order for the clamps to be able to function properly. Some deflection in the z-direction is allowed. This value will be put on 5%. A wheelchair ramp has an acceptable slope of 8.3%[4] but since the craft has no space to take in a wheelchair, the firefighter will need to carry these people inside as well as incapacitated people thus a deflection of 5% was chosen. Some twist is also allowed but is preferably kept to 5 degrees. By adding slip-resistant material to the bridge, covering the walking path, the risk of having an evacuee fall off due to a twisting bridge is reduced. This non-skid material is often used in other high-risk areas like on boats. The bridge will be attached to the building by clamps. These clamps have a range and can thus clamp to differently sized walls, window sills, balconies or door posts. This modular design is important to be able to evacuate people from all sorts of all buildings. The clamps will make sure that the bridge cannot detach from the building in case of a gust, thus preventing evacuees from falling while boarding cabin via the bridge. The average width of a person is around 46 *cm* so this will have be the minimum width of the bridge but a safety margin will be included as a wider bridge might be needed when the firefighter has to drag an incapacitated person in to the cabin. In the end it was decided to go for a width of 0.75 *m*. The bridge itself will be stowed between the the cabin and the aerodynamic skin on the bottom part. So depending on the shape of the aerodynamic skin a certain amount of space is available for the bridge and railings.

7.5. Operational Additions to the Concept

The general concept of two cabins and one propulsion system that switches cabins was generated and the main operations and logistics regarding this concept have been generated in Section 7.1. Some smaller but still important points still need to be addressed. These include the storage of the system, the transport and (un)loading, how the steering of the vehicle will take place, the safety for the firefighters and evacuees, how the evacuation exit will be created and how the evacuation will take place.

Storage

The storage of the vehicle seems simple. However, it is of the utmost importance that when it is stored it is ready for use at anytime. Therefore a set of regulations is defined. Firstly, the rescue vehicle will be stored on the transport trailer attached to the fire truck at all times. This way it is ready for use and can be taken to the rescue site immediately in case of an emergency. The only time the vehicle will not be on this trailer is when it is in maintenance. This will be the case for the regular weekly maintenance and the maintenance after each use. When the vehicle is in maintenance this is noted in the vehicle availability list. This ensures that the emergency services know it cannot be used at that time. Next to this availability list there will also be a list detailing how many rescue vehicles there are in every region with high rise buildings and where these are located. As the vehicle will be large, expensive and its use will be sporadic not every fire department needs one of these vehicles in its facility. A map will detail which vehicle should be used at which location and how many vehicles there should be in a region to make sure that all locations are covered.

[4] URL `https://www.un.org/esa/socdev/enable/designm/AD2-01.htm` [cited 16 June 2021]

Transport and (un)loading

Since time is of the essence when handling an emergency situation, a quick and efficient way of loading and unloading the vehicle is vital. Two cabins and one propulsion system will need to be transported but constraints exist on the dimensions of vehicles on the road and these need to be taken into account. The constraints are of no issue for the cabins but the propulsion system is too large, hence it will need to be folded. The rotor arms will be turned in such a way that their rotors overlap in a scissor-like way aligned to the structure connecting the rotors after which these can be folded inwards. The trailers on which the cabins and propulsion system will be fastened and transported, will be adapted with a automated conveyor belt of which a part is able to become a ramp. The slope of this ramp needs to be such that the parts of the vehicle don't slide off. Once on sight, the trucks on which the trailers are attached needs to drive to a location where the vehicle can take off and land and the cabins and propulsion system can be unfastened. The propulsion system will now have to be unfolded and the engines can be turned on. The engine setting should be such that enough lift is created to be able to fly on top of one of the cabins. The propeller system is then lowered onto the cabin and attached. This cabin then takes off to rescue people while the other cabin is unloaded from the trailer using the conveyor belt system.

Steering

The vehicle will be remotely controlled by a ground operator. This operator will steer the vehicle towards the evacuees, ensures safe boarding and brings them back down to the ground. All of this will be done by using cameras on board which provide an overview to the operator to be able to steer the craft. In addition to this it will have sensors to keep an acceptable distance from the building. The ground operator and the fire fighter on board of the vehicle will have a communication system to give information to the the ground operator if vision of the cameras is impaired or there is an unexpected situation. The ground operator will have full control, however the fire fighter will also have the option to open and close the cabin and bridge or to extend the bridge. This bridge will have sensors to detect the building and will be able to extend out. This is beneficial because it means the vehicle will not have to move during hover to get the bridge centimeters closer to the building. The bridge will have clamps as well to hook to the building, which the fire fighter will be able to control as well as the ground operator. To ensure that the ground operator will be able to safely control the vehicle a stability system is implemented. The vehicle will be more stable than controllable, thus it will have low agility. This means that a small input mistake from the ground operator does not have a big influence on the vehicle.

Firefighter safety

The safety of the firefighters who are rescuing the evacuees is of utmost importance hence extra safety measures are taken to provide a safe working environment. Inside the cabin, close to the door, a winch system will be present to which the firefighter can attach themselves to the harness they will be wearing using a carabiner. The winch system's rope will elongate as the firefighter is moving but if it senses a high acceleration, it will block. Similar to a seat belt. The firefighter will come down with the evacuees every time. This is also done for safety reasons: if something were to happen with the craft causing it to not be able to go up anymore or something happens within the building making it too dangerous for the craft to still go up, the firefighter would be stuck in the building. This is not acceptable and thus the firefighter will need to come down every time.

Safety for evacuees

In case of an emergency, evacuees will be in a dangerous situation and there is a high chance they will panic. Therefore it is important to make the evacuation procedure safe for the evacuees and get them to the ground. Safe does not just mean the physical aspect, but also to calm them and reduce their panic to reduce the likeliness of somebody getting hurt. Therefore three things have to be considered: the boarding of the evacuees over the bridge, the descending with the evacuees in the cabin and the safety of any evacuees left in the building when the vehicle is at maximum capacity. Therefore multiple measures are taken to ensure safety:

- The bridge will have a railing on the side with a minimum height[5] of 1.30 m.
- Railings on the bridge slide along with the bridge when it extends.

- Cabin contains chairs with a seat belt to keep people in place.
- All chairs have a head rest with an adjustable height which prevents people from hitting their heads against the wall or other evacuees.
- To prevent or decrease the chances of injuries during a hard landing, dampers will be present underneath the seats.
- A small fire extinguisher will be present in the cabin that can be used to extinguish fire close to the entry point, fire approaching the cabin or any person that might be on fire.
- Fire blankets will be present in the cabin to wrap around evacuees who are on fire or for the fire fighter to give to evacuees left in the building. This can protect them until the vehicle will go up again to rescue the people left.
- All of these additional items will be stowed between the aerodynamic skin and the cabin to have easy access.
- The cabin will contain windows. Although it might seem better to prevent people from seeing what is happening outside to keep them from panicking, some people might get motion sick, claustrophobic or scared because of the darkness. By being able to look outside, they can also prepare themselves for landing which is especially important when the landing is quite hard. Through the windows, the firefighter can also see if something is out of the ordinary and warn the controller on ground.
- The cabin will contain one 6 Watt LED light to light up the cabin when it is dark outside and the windows will not let any light through. This will prevent panic due to darkness in the cabin.
- The centrepiece will contain a warning beacon light such that it is easily recognizable as being part of the fire department and being a rescue vehicle. A suitable one is the 78092 Permanent Mount, Short Lens.[6]

Building evacuation exit

To rescue people trapped in a building through its facade an exit should be available. This can either be an existing exit, like a balcony or a window or a temporary exit, which can be made by breaking glass or other structures. The exit would be the entry point for the firefighter, as well as the evacuation spot for the evacuees. It should be accessible with the rescue vehicle and the boarding point should be able to attach. This is a possibility with an existing point like a balcony, fully opening window, rooftop, heli-pad, and a damaged opening in the bulding's facade. However, difficulties arise when that is not the case.

When the building is of "closed" type, meaning it is prevented for a human body to leave the building by means other than ground exit, evacuation becomes problematic. As of now, absolute majority of high rise buildings have windows (though there are other instances, such as AT&T Long Lines Building - windowless skyscraper in NYC), and that is the weakest point in the facade. Thus, the glass is what needs to be targeted when creating an open exit.

Normally, a glass window which is not possible to open can be broken with a crowbar. In that case a firefighter would stand at the tip of the bridge and strike the glass with a few hits. A typical glass window would break, creating an evacuation exit. However, a large portion of high rise buildings have reinforced glass - purposely used so that it is not possible to break out in the open air. Typically, laminated glass is used in such cases. There are three types of it: annealed laminated glass, heat-strengthened glass, and toughened laminated glass. The first has the least load-bearing capability, but keeps most of its structural integrity after breakage. The last is the strongest, but once broken it shreds into small pieces. For these reasons, the heat-strengthened version is used in most buildings with safety glass windows. It maintains its structure after breakage, while being strong enough to withstand forces $\tilde{7}0$ N/mm^2 [13]. Also very frequently, laminated glass is made out of two or more layers of glass stuck together by an interlayer. It can be made of different materials, such as polyvinyl butyral (PVB) or ethylene–vinyl

[5]URL https://www.bouwbesluitonline.nl/docs/wet/bb2012_nvt/artikelsgewijs/hfd2/afd2-3/par2-3-1/art2-18 [cited 14 June 2021]

[6]URL https://www.grote.com/warning-hazard/beacons/material-handling-led-beacons/78092/ [cited 21 June 2021]

acetate (EVA) [14]. This interlayer keeps the glass together to prevent injury of people when the glass breaks, this is however not beneficial when one tries to break the glass to make an entry way [15]. It is therefore highly problematic to break through it by means of hand tools. It takes an effort to break, and even after a hole appears, it does not propagate easily, requiring more destruction work, as can be seen in Figure 7.6.

Figure 7.6: Laminated glass break test. [13]

Thus, it is already an issue requiring a firefighter to be steadily placed right next to a window for a period of time. Even more problems arise when glass is used as a facade skin - meaning it is part of a load bearing structure. In that case, it is practically unfeasible to break through it without heavy machinery, meaning there is no possibility to create an exit in any way easily. A facade with glass used as load-bearing structure is shown in Figure 7.7

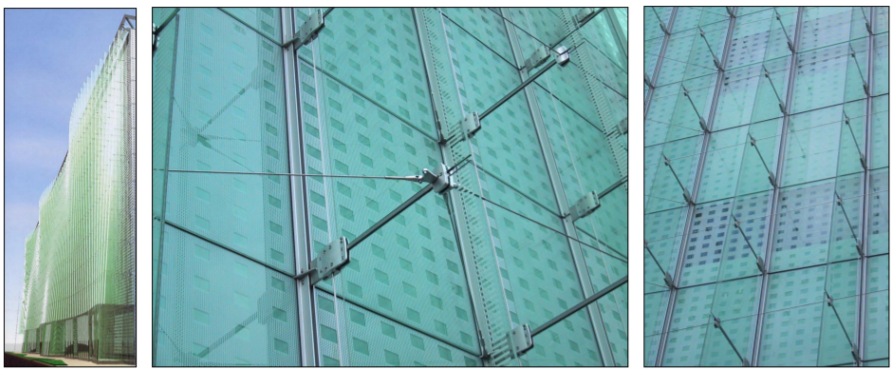

Figure 7.7: Load-bearing glass facade [13]

Explosive means are a potential tool in this case. However, it is deemed to be dangerous for the people on the inside, and the people on ground as they can be hit by falling glass. Additionally, it is not per se safe to break a load bearing structure in a building during its cataclysm, risking a loss of (partial) structural integrity.

Lastly, there are electromagnetically exploding wires. The process involves sending a high current through a conductive wire, the heating resistance of which causes the wire to vaporize, thus creating a shock wave. Normally, they are used as high intensity light sources, participate in a production of metal nanoparticles, and as explosive detonators, especially for nuclear weapons. However, there have been experiments where these wires are used as means to break through a material. B.M. Novac, I.R. Smithx, P.R. Downs, P. Marston and D. Fahey conducted an experiment where the explosive wire was used to open-cut a jet plane plastic windshield for pilot emergency ejection [16]. While it was a success, with a semi-clean cut through the shield and with the necessary power source compact enough to carry on board, the experiment only concerned a plastic material, which is not brittle in nature. Since the laminated glass can maintain its structural integrity after breakage, it makes the electromagnetically explosive wire to be the only potential solution to the building entrance problem. However, this requires

thorough experimentation, as of now no information has been found of such practical implementations. If the method were to deem successful, it would be quite easily implementable in the current design.

As a last measure possible to take, the architects and constructors of high-rise building should take into account the possibility of aerial evacuation in the future, and take appropriate design choices. These could be, for example, evacuation doors on every floor of the building, so that it is possible to exit the structure through means of aerial rescue. Existing buildings could also be modified by potentially replacing multiple closed-type windows with emergency doors. Alternatively, the buildings could be equipped with some means of breaking their glass facades from the inside in an emergency situation. Nowadays, aerospace technology is continuously developing, and architecture sphere should take that into account.

As a result, although the rescue vehicle is able to evacuate people from high floors externally, it will not be suitable for high rise buildings with windows that are made up entirely of thick multi-layer laminated glass. A lot of current high rise building designs simply do not allow it. For that case, if there is no existing exit point, people will have to be evacuated via the inner structure of the building.

This introduces a problem with satisfying requirement *SYS-STRUC-02: The system shall be operable in at least 90% of high-rise disaster conditions/environments*, as this is highly dependent on the building facade type and window glass structure. As has been stated before, large number of high-rise buildings have reinforced closed windows, with no balconies whatsoever. It therefore cannot be guaranteed that 90% of conditions are suitable for vehicle operations, as it cannot be guaranteed that the exit point is present or can be created.

Evacuation procedure

The evacuation procedure starting at the firefighter reaching the evacuees and ending at the evacuees leaving the vehicle will be done in the following way:

1. Firefighter picks a number of people in such a way that the payload mass does not exceed 600 *kg*, of which the firefighter's mass is assumed to be 100 *kg*. Usually this would be six people but in case someone is heavier than 83 *kg*, this might reduce to five people. Small children plus a parent might be seen as one person although that will depend on what the firefighter decides.
2. Boarding the evacuees will be done from back to front. If a person is incapacitated, the firefighter will help with boarding.
3. People are strapped to their seat with a seat belt and the height of their head protection is adjusted. Evacuees who are not incapacitated should be able to do this themselves but the firefighter will help if needed.
4. Firefighter goes down with the evacuees and performs first aid on an injured person if needed.
5. Once the craft has landed, people can unbuckle their seat belts and leave the cabin with aid of the firefighter and medical personnel on ground.
6. Evacuees are handed off to medical services for a check up.

7.6. Conclusion

All in all, it is now clear which parties are doing what in each stage of the entire operation. A boarding mechanism was created to get evacuees from the building to the rescue vehicle while keeping their safety and the safety of the firefighter in mind. Next to this it was determined which buildings are suitable for evacuation through this vehicle.

8. Aerodynamic Characteristics

With the aim to be able to perform the mission at hand the system's aerodynamic properties has to be established by analysis of favourable conditions. This process consists of analysing the propeller that will be used for the system as well as an analysis on the cabin exterior design.

Firstly the Diameter and design thrust coefficient C_T will be determined. This is outlined in Section 8.1. Then the propeller(s) will be designed and analysed to match the requirements of the system and its subsystems. This is done by first determining the approach in Section 8.2 that is most efficient and suits the needs of the product. After the approach is established the theory behind the chosen approach is explained in Section 8.3. Following this section, in Section 8.4, will be a justification of the chosen characteristics. Next, in Section 8.5 the performance from the previous section's characteristics will be presented. These results for the custom design will then be compared with off-the-shelf propellers within Section 8.6.

After the propeller(s) have been properly sized the cabin geometry has to be analysed in Section 8.7. This mainly consists of analysing its favourable characteristics with regards to translational and rotational stability when disturbed by external forces. The respective performances of the various cabin designs can also be found here. More in-depth analyses on how these parameters influence the system can be found in Chapter 10.

8.1. Disk Loading

In order to design the propeller, first a value for the rotor diameter was chosen by analysing the disk loading of the propeller. The disk loading is the thrust per square meter and is the main parameter used to determine the rotor diameter. From a purely aerodynamic standpoint, to have an efficient hover, the disk loading should be as low as possible [17]. However that means that to achieve a low value, the rotor diameter has to be large to ensure the thrust requirement is met. Having a large rotor diameter is not desirable because the rotor tips will go trans-sonic at a lower RPM and long slender rotor blades are less rigid so more structural weight is required. This balance between aerodynamics and structures is summarised in Figure 8.1. The calculations were done for a quadcopter configuration with coaxial rotors as described in Chapter 15.

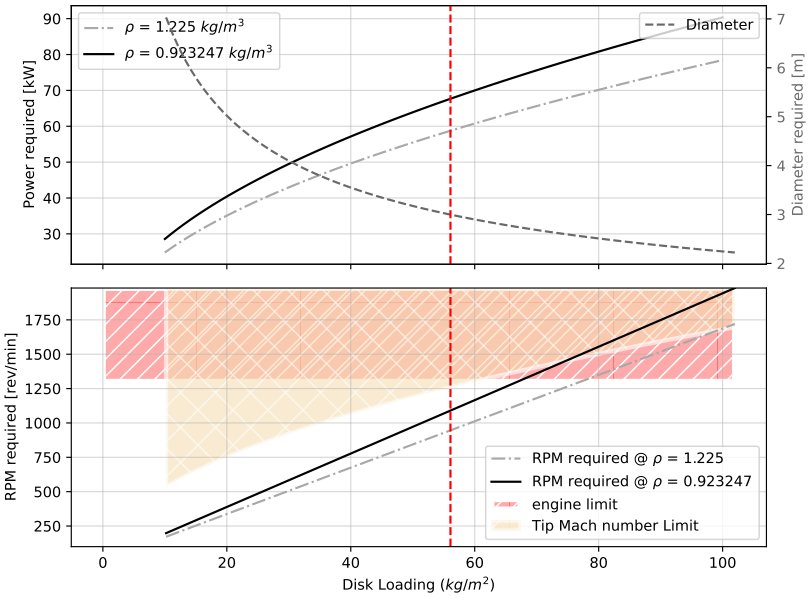

Figure 8.1: Propeller design space as a function of disk loading

It can be seen that required power and RPM increase with disk loading but the required diameter decreases. All calculations were performed at sea level and at an altitude of 3000 m. The maximum RPM that the motor can provide is another limiting parameter for the rotor design. As mentioned in Section 9.1, the maximum RPM of the motor is 1300. All things considered, a design disk loading of 56 kg/m^2 was chosen giving the rotor a diameter of 3 m. This results in a design C_T of at least 0.11 average of both rotors on one arm.

8.2. Propeller Design & Approach

Arguably one of the most important features of the system is the propulsion system. The method of propulsion was previously [1, 2] chosen to be by means of propellers driven by electrical motors. An explanation of the chosen motor design and its specifications can be found in the next chapter in Section 9.1. Since the system is an eVTOL rotorcraft which will have a mission profile that consists of mostly hovering and thus low airspeeds propellers are a very suitable solution.

A suitable propeller for the system can be found through statistical analysis and scaling according to the systems needs or a complete custom design can be made by utilising existing theories. It was chosen to design the propeller in a custom manner, however the value of the statistical data was not ignored and the usage of which can be found in Section 8.6.

For the custom design of such a propeller the blade element momentum theory (BEMT) was used in order to determine multiple parameters such as the thrust force created by the blades, the torque required in order to spin the blade at its required rotational speed, and the power required to achieve the previously mentioned torque. These parameters are most critical for the system at hand since these drive the sizing of other subsystems most critically. BEMT additionally allows for coaxial rotor sizing which the system will be equipped with.

8.3. Blade Element Momentum Theory

The theory that is employed in order to create a custom propeller is the blade element momentum theory which is a theory that merges the momentum theory and the blade element theory. Blade element theory allows for the discrete quantisation along the radial length of a propeller blade such that each individual component can be seen as an extruded airfoil with constant chord of which a straight-forward wing-element analysis can be done. Combining all component forces gives the total force characteristics of the blade disregarding any losses.

Most of the written out theory following was acquired from *Aerodynamics of Wind Turbines* [18] and *Elements of Airplane Performance* [19]. BEMT begins with the assumption of a 1-Dimensional wind stream tube flowing from far away front ($+\infty$) to far away aft ($-\infty$).

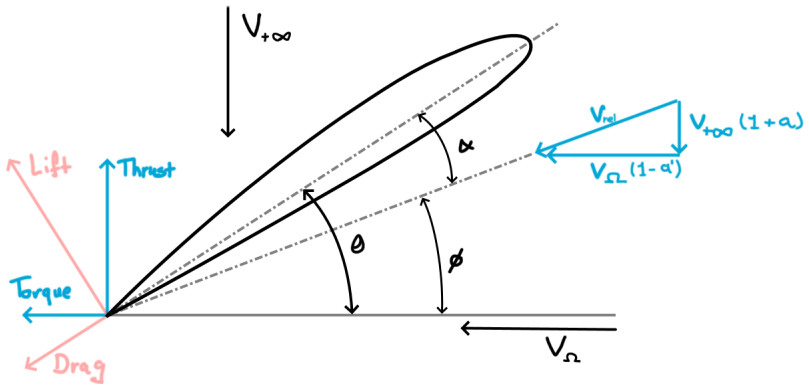

Figure 8.2: Rotor blade cross-section free-body diagram

Figure 8.2 shows the cross-section of a radial station of the blade that is being examined. What can be seen is that the thrust force and the torque are components of the lift and drag force of the profile due to the angle deviation from the true angle of attack (ϕ). Subsequently this deviation is created by the rotational motion of the blade and leads to differing local velocities from the free-stream velocity. A set of induction factors has to be synthesised in order to more accurately define the fluid velocity near the rotor as opposed to an undisturbed flow. The axial induction factor increases the local flow velocity

and the tangential induction factor decreases the local flow velocity for a propeller blade.

$$V_{0^+} = V_{+\infty}(1 + C_{rotor} \cdot a) \tag{8.1}$$
$$V_{\Omega} = \Omega R_B(1 - C_{rotor} \cdot a') \tag{8.2}$$
$$V_{\text{eff}} = \sqrt{{V_{0^+}}^2 + {V_{\Omega}}^2} \tag{8.3}$$

In which V_{0^+} is the axial velocity in *m/s*, V_{Ω} the tangential velocity in *m/s*, and V_{eff} the effective velocity in *m/s* seen by the profile. C_{rotor} is the constant which is set to +1 for rotors turning potential energy into kinetic energy and -1 for rotors turning kinetic energy into potential energy.

With this knowledge the following two equations can be formulated with the effective velocity term.

$$V_{\text{eff}} \sin(\phi) = V_{0^+} = V_{+\infty}(1 + C_{rotor} \cdot a) \tag{8.4}$$
$$V_{\text{eff}} \cos(\phi) = V_{\Omega} = \Omega R_B(1 - C_{rotor} \cdot a') \tag{8.5}$$

Then dividing (8.4) by (8.5) results in the following relation.

$$\tan(\phi) = \frac{V_{\text{eff}} \sin(\phi)}{V_{\text{eff}} \cos(\phi)} = \frac{V_{+\infty}(1 + C_{rotor} \cdot a)}{\Omega R_B(1 - C_{rotor} \cdot a)} \tag{8.6}$$

Coming back to Figure 8.2 once more an additional set of equations can be formulated straightforwardly, namely Equation 8.7 and Equation 8.8.

$$C_T = C_l(\alpha)\cos(\phi) - C_{rotor} \cdot C_d(\alpha)\sin(\phi) \tag{8.7}$$
$$C_Q = C_l(\alpha)\sin(\phi) + C_{rotor} \cdot C_d(\alpha)\cos(\phi) \tag{8.8}$$

In which C_T is the thrust coefficient, C_Q is the torque coefficient, C_l is the two-dimensional lift coefficient, C_d is the two-dimensional drag coefficient. Equation 8.7 and Equation 8.8 are both used for the two-dimensional analysis of the thrust and torque coefficients. The angle of attack is determined as follows:

$$\alpha = C_{rotor} \cdot (\theta - \phi) \tag{8.9}$$

From literature[18] the equations for the segmented thrust force and torque can be acquired.

$$\Delta T = C_T \sigma_{prop} \pi \rho {V_{\text{eff}}}^2 r \Delta r \tag{8.10}$$
$$\Delta T = 4\pi\rho {V_{+\infty}}^2 (1 + C_{rotor} \cdot a) a r \Delta r \tag{8.11}$$
$$\Delta Q = C_Q \sigma_{prop} \pi \rho {V_{\text{eff}}}^2 r^2 \Delta r \tag{8.12}$$
$$\Delta Q = 4\pi\rho V_{+\infty} \Omega R_B (1 + C_{rotor} \cdot a) a' r^2 \Delta r \tag{8.13}$$

ΔT and ΔQ are defined as the thrust force and torque provided in *N* and *Nm* respectively by the segment of blade analysed. Δr is the radial width of the segment. Equating Equation 8.10 and Equation 8.11, as well as Equation 8.12 and Equation 8.13 the following relations can be found for the induction factors.

$$a = \left[\left(\frac{4F \sin^2(\phi)}{\sigma_{prop} \cdot C_T} \right) - C_{rotor} \right]^{-1} \tag{8.14}$$
$$a' = \left[\left(\frac{4F \sin(\phi)\cos(\phi)}{\sigma_{prop} \cdot C_Q} \right) + C_{rotor} \right]^{-1} \tag{8.15}$$

$$\sigma_{prop} = \frac{N_B \cdot \bar{c}}{2\pi R} \tag{8.16}$$
$$F = \frac{2}{\pi} \cos^{-1}(e^{-f}) \tag{8.17}$$
$$f = \frac{N_B}{2} \frac{R - r}{r \sin(\phi)} \tag{8.18}$$

σ_{prop}, the rotor solidity, is used in which N_B is the number of blades, $\bar{c}$ is the mean aerodynamic chord in *m*, and R is the radial length of the blade in *m*. F is the Prandtl's Tip Loss Factor a dimensionless variable dependent on (8.18).

Now that the equations are established the penultimate step to be taken is iterating through the various dependent equations with the steps described next.

(`Step 1`) Set $a = 0$ & Set $a' = 0$ as first estimate;

(`Step 2`) Compute ϕ from (8.6);

(`Step 3`) Compute α from (8.9);

(`Step 4`) Get $C_l(\alpha)$ and $C_d(\alpha)$;

(`Step 5`) Compute C_T and C_Q from (8.7) and (8.8);

(`Step 6`) Compute a and a' from (8.14) and (8.15);

(`Step 7`) If $da > \epsilon$ and $da' > \epsilon$ GOTO `Step 2` Else `Step 8`;

(`Step 8`) Compute ΔT and ΔQ from (8.11) and (8.13);

Adding the segmented thrust forces and torques results in the total reactions on blades. From these the thrust, torque, and power coefficients can be acquired.

$$C_T = \frac{T}{\rho n^2 D^4} \quad (8.19) \qquad C_Q = \frac{Q}{\rho n^2 D^5} \quad (8.20) \qquad C_P = \Omega \cdot C_Q \quad (8.21)$$

In which n is equal to the amount of revolutions per second, and D is defined as the propeller diameter in *m*.

8.4. Propeller Characteristics

This section outlines the blade and propeller characteristics that were established and acquired. These properties are mainly summarised in Table 8.1.

Per engine arm a configuration of two co-axial propellers exists. It needs to be noted is that these are counter-rotating at different RPMs as to create a net-zero torque on the engine arm. The chord distribution follows a linear relationship with respect to the radius. Three blades was chosen as to generate enough thrust. The hub radius was chosen in such a way as to maintain enough spacing for the motor width. A different less-performant, though thicker, airfoil was considered for the blade sections near the root of the propeller blade since this is commonly standard practice[7] since this provides more stiffness. This was however deemed unnecessary for the system in question.

For the mission a maximum payload weight of 600 *kg* is used. This together with the empty weight, more about this in Chapter 18, totals to a weight of 1331 *kg*.

Figure 8.3 displays a render of the blade geometry. From Table 8.1 and empirical Equation 8.22 [20] together with the inverse-square law Figure 8.4. This figure shows an estimate of the noise generated by the top propellers and the bottom propeller with respect to distance.

$$\text{SPL}_{1,max} = 83.4 + 15.3 \log(P_{br}) - 20 \log(D) + 38.5 M_{tip} - 3(N_B - 2) + 10 \log(N_{Prop}) \quad (8.22)$$

$$M_{tip} = \frac{\pi D}{a} \cdot \frac{\text{RPM}}{60} \quad (8.23)$$

[7] URL `http://avstop.com/ac/flighttrainghandbook/basicpropellerprinciples.html` [cited 21 June 2021]

Table 8.1: Propeller characteristics for $V_{+\infty} = 0\ m/s$ and $\rho = 1.225\ kg/m^3$

	Top propeller			Bottom Propeller		
Property	**Symbol**	**Value**	**Unit**	**Symbol**	**Value**	**Unit**
Chord length function	$c(r)$	$\frac{13.70-r}{70}$	[m]	$c(r)$	$\frac{13.70-r}{70}$	[m]
Number of Blades	N_B	3	[-]	N_{B2}	3	[-]
Diameter	D	3.0	[m]	D	3.0	[m]
Hub radius	R_{hub}	0.126	[m]	R_{hub}	0.126	[m]
Propeller RPM	RPM	726	[1/min]	RPM2	754	[1/min]
Thrust coefficient	C_T	1.282×10^{-1}	[-]	C_{T2}	8.801×10^{-2}	[-]
Torque coefficient	C_Q	5.267×10^{-4}	[-]	C_{Q2}	4.714×10^{-4}	[-]
Power coefficient	C_P	4.005×10^{-2}	[-]	C_{P2}	3.676×10^{-2}	[-]
Thrust-to-Power ratio	C_T/C_P	3.202 : 1.000	[-]	C_{T2}/C_{P2}	2.394 : 1.000	[-]
Airfoil $0 \leq r \leq 1.5m$		s8037	[-]		s8037	[-]

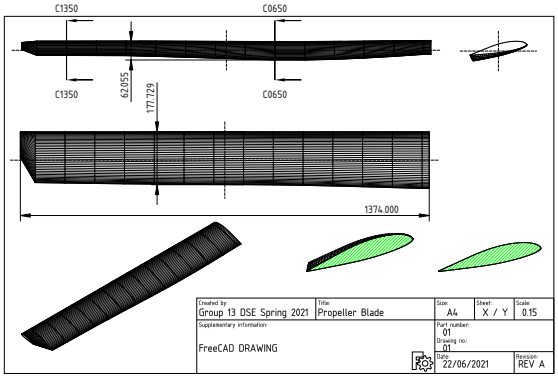

Figure 8.3: Custom blade geometry

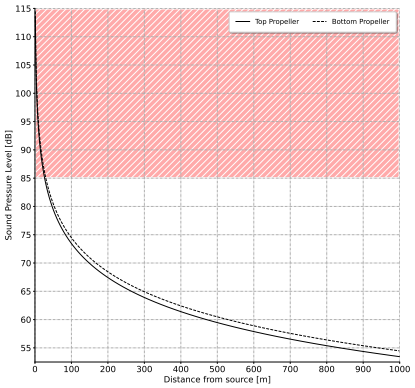

Figure 8.4: Custom propeller noise

8.5. Performance Results

Using the methods laid out in Section 8.3, with the utilisation of an external automation module[8] [78], and the parameters used in the Section 8.4 a set of performance figures can be acquired. The first figure, Figure 8.5, shows the performance of the propellers for the leading part of the mission. The hover stage, thus an inlet velocity of $V_{+\infty} = 0\ m/s$.

[8] URL `https://github.com/kegiljarhus/pyBEMT` [cited 18 June 2021]
[78] URL `https://pybemt.readthedocs.io/en/latest/validation.html` [cited 18 June 2021]

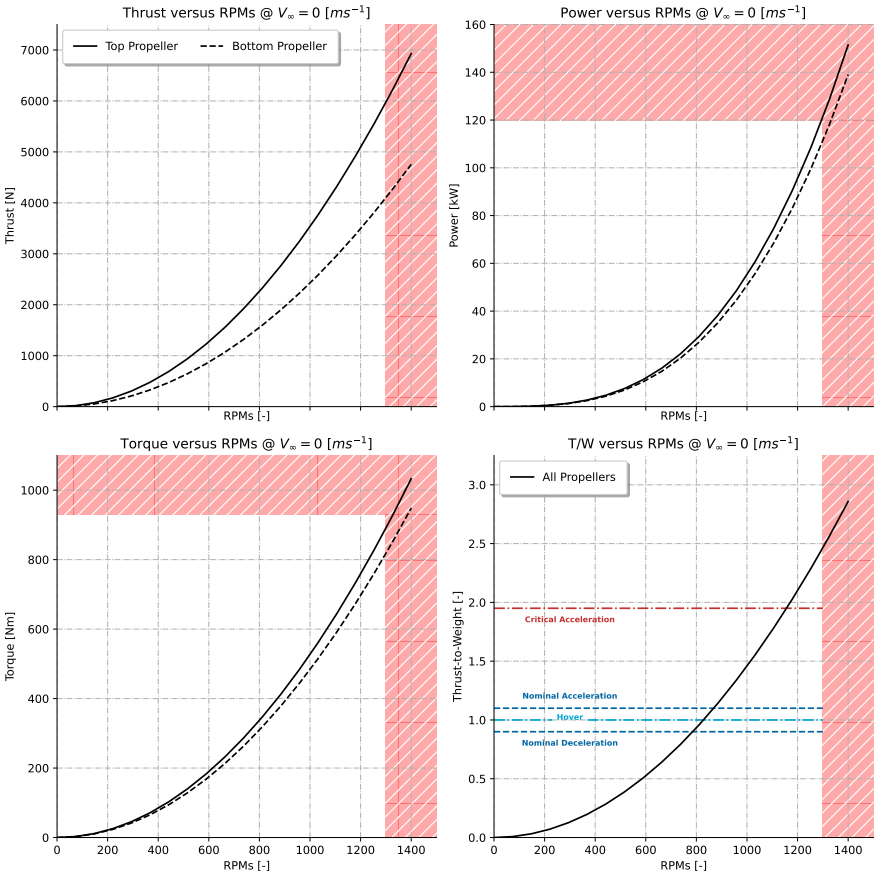

Figure 8.5: Propeller performance at $V_\infty = 0\ m/s$

The red vertical hashed sections indicate the motor performance limitations. The motor used, which can be read about in Section 9.1, has an upper limit of 1300 RPM. For the bottom-left subfigure, the torque versus the RPMs, also shows an upper-limit for the torque that the motor can provide. Since the power is dependent on the torque this previous upper limit on the y-axis directly translates also to the subfigure on the top-right. Finally the bottom-right subfigure shows the thrust-over-weight ratio with their corresponding RPMs.

8.6. Off-the-shelf vs. Custom Design

In order to justify the choice for the creation of a fully custom propeller design it has to be traded-off against already existing off-the-shelf propeller designs. A database of 528 drone propellers[10] was used for the trade-off. The blade angle at 75% of the radial length of the blade $\beta_{0.75}$ was chosen as one of the comparable properties for the differing propellers. The previously mentioned blade angle together with the ratio of the thrust coefficient versus the power coefficient were used for the comparison. The results of which can be found below.

[10] URL `https://www.apcprop.com/` [cited 16 June 2021]

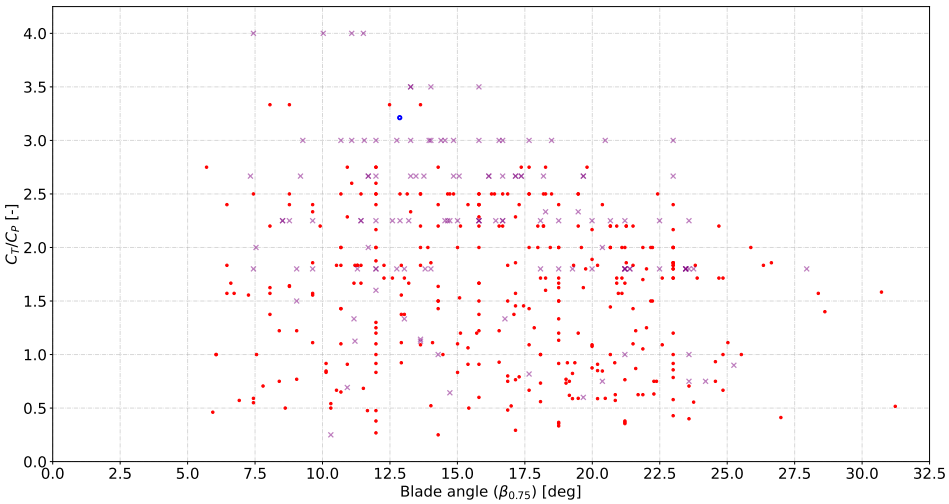

Figure 8.6: Statistical data on existing propeller designs

In Figure 8.6 the blue circle represents the custom propeller design designed by the team, the purple crosses represent the propellers from the database that yield a thrust coefficient below the required thrust coefficient for the mission profile, and the red dots represent the propellers from the database that yield a thrust coefficient above the required thrust coefficient for the mission profile.

From Figure 8.6, and further analysis of the raw data, it can be seen that only 4 propellers yield a thrust-over-power ratio higher than the custom propeller design. However these designs are not necessarily better since their design includes a high twist angle near the root, thus is not suitable for hover situations.

8.7. Cabin Design Selection

The additional analysis with regards to the aerodynamic properties of the system was done on the design of the cabin. The cabin exterior is a non-load bearing shell which serves two main purposes. The first purpose is providing minimal drag with regard to lateral gusts as to minimise translation and/or rotation thus increasing stability and controllability. The second purpose is to provide storage spaces for the different subsystems of the product.

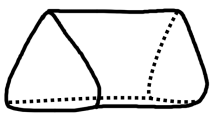

Figure 8.7: Cabin c0

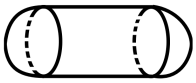

Figure 8.8: Cabin c1

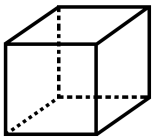

Figure 8.9: Cabin c2

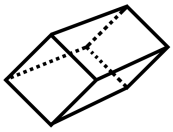

Figure 8.10: Cabin c3

Cabin c0 has a frontal C_d of 0.2 and a lateral C_d of 1.14, cabin c1 has a frontal C_d of 0.2 and a lateral C_d of 0.6, cabin c2 has a frontal and lateral C_d of 1.05, and finally for cabin c3 the frontal C_d is equal to 1.05 and lateral C_d is equal to 0.8.[11] [12] [13] It was decided that cabin c1 was the most suitable for the mission since this design yield the most favourable drag coefficients.

[11] URL `https://www.simscale.com/` [cited 22 June 2021]
[12] URL `https://www.engineersedge.com/fluid_flow/cube_flow_perpendicular_14042.htm` [cited 22 June 2021]
[13] URL `https://www.engineersedge.com/fluid_flow/cube_flow_perpendicular_edge_14043.htm` [cited 22 June 2021]

8.8. Conclusions and Recommendations

In conclusion a propeller was designed in such a way to be optimal for the mission profile. It has a low twist angle change with respect to the blade radius and consist of three blades to generate enough thrust to perform within the mission profile, but also for one engine-arm inoperative.

As for the cabin a pill-shaped exterior was chosen such that the stability has as favourable a drag coefficient as possible.

For future analysis a more extensive analysis with CFDs should be done on the exterior design.

9. Power & Propulsion

The craft's power & propulsion systems design revolves around the high voltage (HV) and low voltage (LV) grids of the vehicle. The HV side consists of the motors, inverters and the high voltage batteries, while the LV side is made up from the processing units (PCBs - printed circuit boards), the power converters and the low voltage battery. All the aforementioned components are sized and their fit as well as connection in the system is analysed using trade-off methodology.

9.1. Motor Selection

One of the most important components of the power & propulsion system is the motor. As discussed in Chapter 15, pure electricity is used as power source of the craft, meaning that an electric motor has to be chosen. Thereafter, the various motors running on electricity have to be analysed and the best one has to be selected with the help of a trade-off. In the following list, main electric motor types are displayed:

AC motors:

- Synchronous
- Induction

DC motors:

- Permanent magnet
- Series
- Shunt
- Compound

A distinction between single and three phase motors can be done for the AC grid, while both motors can be split in brushless and brushed engines. However, the specifics are analysed only after the trade-off winner has been determined. Before the trade-off can be made, the criteria taken into consideration have to be defined. The parameters used in scaling are weight, simplicity, torque, efficiency, power. The weight of the motor is defined as a criteria due the fact that lighter engines result in less thrust required. Simplicity of the system allows for easier maintenance and is hence included in the list of criteria. The torque of the motor is set to be one of the more important criteria as the motor must provide enough of it to be able to turn the rotors. The efficiency is crucial for the fact that higher efficiency systems dissipate less power and will in turn reduce the battery size and operating costs.

Table 9.1: Weight criteria

Criteria	Weight	Reason for the weight
Weight	15%	The mass of the motor affects the total weight of the craft. Since 8 motors are used in the design the motor contribution to the weight is significant.
Simplicity	5%	The simplicity is only of importance for maintenance, which in itself is a very small part of the mission. Moreover, simplicity does not directly relate to the performance of the motor hence it has been given such a low weight.
Torque	25%	The craft needs to provide enough torque to be able to rotate the propeller. In addition, the torque, together with the power, affects the rounds per minute (RPM) of the motor. Hence, the motor needs to have enough torque such that the RPM necessary for every mission phase can be reached.
Efficiency	25%	The efficiency of the engines have a great effect on the power consumption of the craft. A more efficient motor will lead to less power being consumed during the mission and thus a smaller battery size, which positively influences the weight of the craft.
Power	30%	Power is the most important aspect of the motor. The motor must provide enough power to generate sufficient thrust for the craft to operate in any conditions.

With the criteria set, the importance of them has to be assigned by a weight. The weights and their respective motivation are displayed in Table 9.1.

The next step in the trade-off is to assign scores to every motor. This is done qualitatively based on literature. Since some of the motors are not applicable for the mission the motors are omitted from the analysis to reduce the trade-off size. The motors neglected are the AC synchronous and DC (shunt and permanent magnet). The AC synchronous motor is complex and is built for the purpose of constant speed application which does not fit the mission profile of the craft. Additionally, it is not generally self-starting. The DC shunt motor cannot produce a high starting torque which means that the loads at the start need to be low for the shunt motor to function, which is not the case for the current design. The DC permanent-magnet is out of the picture due the fact that it high load carrying designs become unfeasibly heavy. In addition, the magnets themselves degrade over time which decreases the motor's reliability.

Remaining motors which are implemented in the trade-off are the AC induction, DC series and DC compound motors. The first criteria is weight. The DC motors that are currently out on the market are not designed for aviation. Hence, these motors are much heavier compared to the AC-induction motor which has been used in aviation [21].

Secondly, the simplicity of the motors is scored. AC induction motors are very simple and are easy to maintain. DC series motors require a bit more complexity but are not as complex as DC compound motors which use both shunt windings and series windings.

The third criteria is the torque performance of the motors. The starting torque of all motors are high. However, with increased speed the torque increases for AC induction whereas for the DC motors the torque decreases. The decrease is more significant for DC series motors compared to DC compound.

Efficiency is the fourth criteria that is assessed. In general, DC motors are more efficient compared to AC motors. The efficiency among DC motors is considered to be about the same as no information on this can be found in literature.

The last criteria is the power criteria. If the same power levels are assumed, AC motors are able to generate higher torques but lower RPMs compared to DC motors and are therefore considered more powerful for the particular application. When comparing the series and compound motor, the compound motor is able to provide higher torque at higher speeds whilst having the same starting torque. Thus, the compound motor is considered to be more powerful and suitable for the design.

The score assignment can be seen in the trade-off table depicted inTable 9.2. Each criteria is weighted

in the scale of 1-5 with 5 being the best score. The scoring methodology applies to all the consequent trade-offs in this chapter.

Table 9.2: Trade-off table motor type

Weights	0.15	0.05	0.25	0.25	0.3	1
Motor type	**Weight**	**Simplicity**	**Torque**	**Efficiency**	**Power**	**Result**
AC induction	5	5	5	3	5	4.5
DC series	3	3	1	5	1	2.4
DC compound	1	1	3	5	3	3.1

From these results it is found that the AC induction motors are best fit for the mission. It scored full points in all but one criteria. With the motor type now known, a final trade-off needs to be done between brushed and brushless motor.

Brushed motors have the advantage of being cheaper to construct. To add on to that, the motors are often more efficient compared to brushless motors. However, brushed motors have the downside that they are more expensive to maintain and most importantly have overall worse performance compared to brushless motors[14], mainly a lower RPM[15]. For these reasons it is opted to make us of brushless AC induction motors rather than brushed AC induction motors.

For the final choice of the motor two suitable candidates were found, which have been tested in aerospace appliances. As first the CityAirbus engine SP200D manufactured by Siemens [16] is selected due its relatively high torque and power to mass ratio. As second, P50S4 engine twin configuration by Saluqi is investigated due the all inclusive concept of inbuilt electronics. Analysing the first motor, it was determined that the maximum power available is exceeding the required margin, thus, a scaled version of SP200D is created, such that the RPM of the motor stays the same, while the maximum continuous power is reduced by 62.5% of the initial value. Assuming that the scaling is not fully linear since there is no product available in the market meeting the exact power and angular velocity requirements, the mass and the radius of the motor was reduced by 30% only to allow for a wider range of potential fits. It has to be noted that SP200D is scaled almost linearly because it does not have any subsystems included in its design except an inbuilt cooling network. It has to be noted that SP70D engine could have been chosen, nevertheless, its maximum continuous torque was deemed insufficient to spin the propeller.

By analysing the twin P50S4 configuration it was determined that the maximum power and the torque is sufficient for the critical case scenario of OEI. Nevertheless, the two P50S4 engine configuration is larger volumetrically than the scaled SP200D engine which is not preferred, as the stacking of engines becomes less efficient due the airflow degradation caused by obtrusion in proximity. In order to mitigate the efficiency losses, the P50S4 engine can be scaled such that a single engine responsible for driving a single rotor shaft is created. However, as the information of the electronics size and mass is confidential, the scaling cannot be performed explicitly. Thus it is chosen that a safety factor of 1.3 is implemented. In combination of the required scaling factor of 1.2, the motor satisfying all but torque requirement was found. If the maximum continuous torque of the motor was increased, it would be a viable option to be used for the design. However, as the inverter and the electronics are non-detachable from the motor itself, the length of the motor becomes larger, leading to an increase of the engine separation and larger structural supports carrying the engines.

Due the limitations of the volume and torque, it is opted to use scaled SP200D version (75 *kW*, 21 *kg*, 1300*RPM*) rather than the twin configuration of Saluqi motors. However, with a new motor released

[15] URL `https://cordlessdrillzone.com/drill-wars/brushless-vs-brushed-motor/` [cited 14 June 2021]
[14] URL `https://rozum.com/brushless-motor/` [cited 14 June 2021]

by Saluqi, which can be configured in lay-out, the craft's design could be reiterated as the all system inclusion concept is more efficient and lightweight overall.

9.2. Power Supply Sizing and Trade-off

The power and propulsion was chosen to be electrical, meaning that the two governing power supply methods are direct power line and/or energy storage in batteries. To determine the optimal design choice, a trade-off for the power supplies is performed.

9.2.1. Power supply trade-off

In order to acquire the most useful trade-off certain initial parameters for the concepts are defined, such that quantitative data can be compared. However, first the criteria is defined for which the initial estimations are performed.

The safety in operations is set as the main criteria for the power supply trade-off due the mission being a rescue operation. The weight follows as second, since there are mass limitations to successfully lift the vehicle with the current technology. As last, the simplicity of implementation is considered to ensure eased maintenance of the system. The criteria and their characteristic weights are given in Table 9.3.

Table 9.3: Weight criteria

Criteria	Weight	Reason for the weight
Safety	55%	To ensure that the people stuck in disastrous event are evacuated without losing any lives, the craft has to be made as safe as possible. Thus, it is set to be the driving force of the design.
Weight	35%	The weight of the craft has to be minimised in order to attain ability to lift-off from the ground and hover at altitude. Thereafter, is the secondary level criteria, as it has to be continuously checked to determine whether the mission is viable. However, there will always be a more powerful alternative which is most likely less safe or sustainable, thus, it is less important than the safety requirement.
Simplicity	10%	The simplicity of the craft implies the time it takes to maintain the craft is minimised, meaning that, it only considers a small part of the mission, thus, the low importance. It has to be noted, that reliability is not defined as a subpart of simplicity as complex systems can be made almost completely reliable.

To analyse the weights the concepts are achieving the combined qualitative and quantitative analysis has to be performed as previously mentioned. As first, the safety of each concept is discussed.

Regarding the safety of battery concept, it can be said that the battery systems are hazardous in general, thus requiring a lot of active control, especially if not fully developed batteries are used. The main safety consideration of the batteries is the immense heat dissipated caused by the power losses on the internal battery resistance. For certain battery types short circuits and malfunction can originate if the excess heat is not extracted. Applying an efficient cooling system to the batteries may mitigate the issue, however cooling system adds a lot of mass in turn. As a secondary safety issue running out of power mid-flight can be mentioned. Nevertheless, the severity and likelihood of power outage can be reduced by increasing the battery reserve capacity. However, again, additional mass is added. Another option is to perform a crash landing once in a while, however, in such a case the structure would need to be reinforced and changed more often, making this a more costly alternative. Lastly, the connectivity with the rest of the circuit can be investigated, however, this is an issue with both the battery and power line concepts thus omitted from the analysis.

[16]URL https://www.ie-net.be/sites/default/files/Siemens%20eAircraft%20-%20Disrupting%20Aircraft%20Propulsion%20-%2000%20JH%20THO%20-%2020180427.cleaned.pdf [cited 14 June 2021]

[0]URL https://nag.aero/wp-content/uploads/2020/12/Hybrid-Electric-Flying-Matthijs-de-Haan.pdf [cited 14 June 2021]

As for the direct power line, more potential safety threats were discovered compared to the battery concept. As first, heat accumulation in the wires can be mentioned. This means that the wires have to be kept in a layed-out configuration to allow for heat dissipation in the air and prevent melting of the wire protective coating. Additionally, a transformer can be used on both ends of the power line to reduce the current flowing in the wires, thus reducing the power dissipation which is accountable for heat generation in the wires. However, using powerful transformers[17] increases the craft weight tremendously. Another potential threat to the safety is the power lines' capability to tangle around the infrastructure of the operational area. For instance, due a gust disturbance, the wire could get stuck around a lamp post, thus exerting tension on the connection points, meaning that the connectors could unplug and power outage would occur. This risk could be mitigated by creating a permanent joint for the connectors, however, then the craft could not be operated by other power generators as the set-up would have to be changed. Moreover, the ground power station has to be made transportable during the mission, or excess cable has to be stored in order to allow the craft to have full accessibility of the building. Lastly, disturbances caused by over-tensed power line could potentially lead to loss of crafts level if the wire is attached to the craft in an angle. This could lead to controllability issues as no sudden manoeuvres can be made to level the craft, as potential wire tears or connection losses caused by connector failures.

Having decided that the safety risks for the power line cannot be mitigated as simply as it can be done for the battery concept, the scores in the safety category were given accordingly as seen in Table 9.4. In the table, the scores correspond to a fully risk mitigated concept.

The scoring for the weight of the craft is obtained by determining the preliminary mass of the craft for each possible design choice. More specifically, the mass of the concept different components is determined and then compared. Moreover, only the energy provision to the motors is analysed, as the LV side of the craft requires negligible amount of energy compared to HV side. For the battery concept to get a complete circuitry an inverter, HV battery and cooling system is needed while for the power line only the transformers and the lines themselves are needed. The high voltage battery mass required to have an operational vehicle estimation is based on two main parameters: the energy and power density. In the analysis only one of the aforementioned characteristics is the driving one as is elaborated in Section 9.3. The numerical values and the sizing methodology for the battery, inverter and the cooling mechanism mass can be found in Section 9.3, Section 9.5 and Section 14.1 respectively. Summing all the contributions leads to a total mass of 854 *kg*.

To be able to perform a weight trade-off between the weights of the power supplies, the mass of the power line concept has to be determined. For the calculations several assumptions are made. First of all, the mass of the cable is assumed to consist of the conductive part and the isolation part where the isolation is assumed to be 40% of the total wire filament weight. Second of all, the length of the wire exerting force on the craft is assumed to be equal to the hovering altitude. Lastly, it is assumed that only the weight of the wire exerts force on the craft, and any additional forces attributable to gusts or manoeuvres are neglected. If a supplementary assumption is added, which entails that infinite power source is used and the cooling of the wires is not necessary, the power line can be designed without using transformers. However, knowing that the power losses would be a concern as more power would be wasted as used usefully, only a power line with the transformers at each end is analysed.

To perform the mass estimation of the power line, the allowable power losses on the cable have to be defined. If the efficiency is set to be at least 95% and the conductor cross sectional area is chosen to be 10 mm^2, the voltage can be determined by Ohm's law as depicted in Equation 9.1.

$$V = IR \tag{9.1}$$

The current I in the equation above can be found by inspecting the wires to be used for the power line, and is taken to be 74 *A*[18], while the resistance R can be straight-forwardly computed by the formula:

$$R = \rho_R \frac{l}{S} \tag{9.2}$$

[17] URL `https://trafo-schneider.de/pdf/Katalog_en_komplett.pdf` [cited 7 June 2021]

where ρ_R is the specific resistance, l the length and S the cross sectional area of the wire. If the conductor material is selected to be copper and the maximum operational altitude with respect to the ground below is set to be 400 *m* and thus the wire length is chosen taken to be 600 *m* to have sufficient redundancy, the total resistance of a single strand is approximately 1 Ω. Thereafter, the voltage of the wire has to be 1454 *V*, if a single engine's hovering power is assumed to be 21.8 *kW* (at 650 *V*) as determined in Chapter 8. The voltage determined implies that instead of a single powerful transformer, several smaller ones have to be chosen to reduce both the global mass and the power loading of the system. Four transformers are applied such that greatest similarity between both the power concepts is acquired. Nevertheless, there is no of-the-shelf transformer tailored for aerospace applications meeting all the aforementioned requirements, thus exact mass estimations cannot be performed. Using an equation applied in general electrics industry, the transformer mass can be approximated by multiplying the size of the transformer in *kVA* with the basic insulation level (BIL) [19]. Basic insulation level is an entity that describes the voltage at a power surge in the engine initializing stage which, in the particular case, is taken to be 1.2 times the continuous voltage [20]. The multiplication of the givens provides mass well beyond the desired levels as the functions return for the high voltage transformer is 570 *kg*[21] for a single transformer. The mass of the wire can simply be estimated by multiplying the volume of the 3-phase wire filament by the density of copper and then by the safety factor of 1.4 which was mentioned previously. The total mass of the power line concept HV part becomes 2330 *kg* where the wire mass is only 50 *kg*. If a way of reducing the mass of the transformers was found such that the transformers weigh no more than 66 *kg* each, the power line concept is going to be less heavy than the battery concept.

Regarding the simplicity it can be said that both concepts are almost equally complex in their own way, however, the battery concept requires more internal check-ups and thus becomes harder to maintain. All the weights for the trade-off can be found in Table 9.4.

Table 9.4: Trade-off table power supply

Weights	0.55	0.35	0.1	1
Power supply	**Safety**	**Weight**	**Simplicity**	**Result**
Battery	4	3	3	3.55
Power line	1	1	4	1.3

The weights provided in Table 9.4 are mainly based on the explanation given in this subsection. However, to acquire a more accurate trade-off and have a greater amount of comparisons, alternative power supplies such as fossil fuel are included in the trade-off. Nevertheless, the other propulsion types were omitted due the choice of using electrical propulsion. From the trade-off table it can be seen that the battery concept is a clear winner and no sensitivity analysis is required as the margin of the total score is high. Thereafter, the next subsections only consider the design of craft concept with on-board energy storage system.

9.3. High Voltage Battery Sizing and Trade-off

A variety of batteries are available on the market and even more in development. To choose the optimal battery for the mission, a trade-off between batteries must be made. However, before a trade-off can be made the criteria need to be set-up. First of all, it is advantageous that the battery is as light as possible. This means that the battery should have as high energy and power density as practically is achievable. Nevertheless, it is known that energy and power density are negatively correlated due the influence of time, thus, the critical criteria has to be determined when sizing. Optimum ratio range, however, for energy versus power is determined to be 1:(3-5) as the mission for a single cabin from

[18] URL https://www.cse-distributors.co.uk/cable/technical-tables-useful-info/table-4e1a/ [cited 8 June 2021]
[19] URL https://sciencing.com/facts-8355405-can-estimate-weight-transformer.html [cited 8 June 2021]
[20] URL https://www.electrical4u.com/basic-insulation-level-definition-table-and-calculation/ [cited 8 June 2021]
[21] URL https://www.fujielectric.com/products/oil-immersed_transformer/specifications.html [cited 8 June 2021]

start to recharge lasts only 10-20 minutes. Thereafter, the criteria is named energy and power density range as only further analysis can provide a clear winner. Also, one has to keep in mind that the best energy density specified for the batteries is used in the analysis. Secondly, since the energy of the battery gets depleted every cycle, the charge rate whilst on the ground should be high to allow for a full recharging when switching cabins have been implemented. Likewise, the discharge rate should be variable and sufficiently high to allow for high power applications as the motors require immense amount of power. The ratio between energy and power is highly dependant on the discharge rate of the battery, thus, the discharge rate criteria considers only the available range of the depletion times. Lastly, the number of cycles the battery can be applied for is of high importance as being able to reuse the same battery repeatedly leads to savings in costs and increased reliability throughout the lifetime because of the delayed degradation process.

For each of these trade-off criteria a weight must be assigned. These weights are assigned by the subsystem engineers themselves. All weights combined will sum up to 100 percent in total. In Table 9.5 the weight per criteria is given as well as the reason for the weight.

Table 9.5: Criteria weights

Criteria	Weight	Reason for the weight
Energy to power density ratio	60%	The energy to power ratio is the main sizing parameter as both the parameters have to be balanced such that the optimum ratio is reached and the batteries are not over-designed.
Charge rate	10%	The battery needs to be able to be fully charged while its counterpart cabin is in operation. However, bigger batteries can be taken when the charge rate is not high enough or the batteries can be be made swapable. Nevertheless, additional battery mass triggers the snowball effect of mass increase.
Discharge rate	5%	The discharge rate has to be sufficiently high and alterable, such that power provision throughout the mission can be matched. The rate itself is mainly influenced in the power density, however, it has to be made sure that the discharge rate change range is wide enough.
Number of cycles	25%	The amount of charge-discharge cycles a battery can last is the secondary parameter after the power and energy provision, as having a battery with a short time span drives up the total costs of the product and can be a potential threat when nearing the end of life stage as power outages could occur.

Since there is vast amount of different battery types, only the most promising batteries are selected for the trade-off. The selected batteries are under the category of Li-based batteries due their high magnitudes of power or energy density in combination with the discharge rates. Moreover, Lithium metal which is still in development, but promises good specifications is also selected. Only the Li-Sulfur batteries are not selected for the analysis due their instability at elevated temperatures and highly limited number of cycles caused by sulfur degradation[22]. The number of missions required to be performed by a single craft in a single year can reach up to 50[22] times, thus, to have a reliable system for 5 years to fulfil SHR-U-16, the HV batteries would have to have a life span of approximately 2500 cycles if 10 cycles are performed per mission. Nevertheless, if the cycle time of the sulfur batteries gets prolonged in the future, the design of the craft can be re-iterated to allow for the changes to implement the sulfur batteries as they have the highest energy and power densities in the market at the current time. The specifications of the batteries are displayed in Table 9.6. It has to be noted that the charging/discharging times are expressed in C-rates which is defined as the number of times the battery could get emptied in a single hour.

Table 9.6: Specifications table

Battery	**Energy and power density range**	**Charge rate**	**Discharge rate**	**Number of cycles**
Li-Manganese Oxide	150:(150-1500)	1C	1-10C	300-700
Lithium Titanate Oxide	80:(80-800)	1-5C	1-10C	3000-7000
Lithium Nickel Manganese Oxide	220:(150-220)	0.7-1C	1-2C	1000-2000
Lithium Metal	350:(350-1750) [23]	1-5C [24]	1-5C	2500 [25, 26]

With the battery specifications determined, a trade-off table can be made. The trade-off is shown in Table 9.7.

Table 9.7: Trade-off table batteries

Weights	0.6	0.1	0.05	0.25	1
Battery	**Energy and power density range**	**Charge rate**	**Discharge rate**	**Number of cycles**	**Result**
Li-Manganese Oxide	2	2	5	1	1.9
Lithium Titanate Oxide	1	5	5	5	2.6
Lithium Nickel Manganese Oxide	3	2	1	4	3.05
Lithium Metal	5	5	4	4	4.7

From the trade-off it is concluded that the Lithium metal batteries are the best fit for the craft even without a sensitivity analysis. Do note however, that this type of battery is still in development and only limited amount of these have successfully been used in real life applications [23]. It has to be noted that high energy density ($\approx$ 500 *Wh/kg*) lithium metal battery tests have been performed [27], however, the information about the power specifications is still limited and classified. Thereafter, a lower energy density battery is selected for the design.

As the battery type and the corresponding specifications have been determined, the battery sizing can be performed. The battery size is estimated by breaking down the mission profile of the craft and then computing the characteristic parameters for each phase individually. First, the required thrust is calculated for each instance of the mission using Equation 9.3. The calculations are made iterative such that with any weight input which is lower than rapid estimations performed in the preliminary sizing the mass value is converging to the optimum.

$$F = m \cdot a \tag{9.3}$$

The mission profile is split into 3 main phases, ascent, descent and hovering. For the ascent and descent, the craft is expected to accelerate and decelerate for 5.5 *s* each and keep constant velocity for the rest of the time. The maximum operational height is taken to be 400 *m* with respect to the ground level to meet the requirement on 95% of the building reachability. The acceleration and deceleration is

[22] URL `https://batteryuniversity.com/learn/article/bu_218_summary_table_of_future_batteries` [cited 8 June 2021]

performed at a thrust to weight ratio of 1$\pm$0.1 to acquire a total ascent and descent time of 80 *s* to/from the maximum operational height. As the design contains the concept of switching cabins, the hover time of a single cycle is 445 *s* as stated in Chapter 7. The thrust needed to perform the manoeuvres is computed by applying the lift theory to the propellers of the craft as discussed in Chapter 8.

Having determined the power required to both hover and manoeuvre, the battery mass can be determined straight forwardly by dividing the total energy and maximum power by the respective densities and choosing the highest one. Nevertheless, the efficiencies of different components and the battery degradation and depletion factors have to be included in the computations to have the total mass of the batteries. The efficiencies directly influencing the size of HV battery are inverter efficiency (η_{inv} =98%) which is discussed in Section 9.5, battery efficiency (η_{bat} = 90%) which is equivalent to the power lost on the internal resistance of the battery and the wiring loss factor (LF = 15%) due the wire resistances and connection issues. Reduction of battery efficiency caused by elevated temperatures is assumed to be negligible as the temperature variation range is assumed to be optimal as discussed in Section 14.1. To increase the life span of the batteries, the depth of discharge (DoD) is selected to be 70% of the full initial capacity. With the defined *DoD* and discharge rate of 3.62C, the degradation rate of batteries is estimated to be constant and equal to 0.0238% per cycle [28]. The lifetime of the batteries is determined by assuming an exponential degradation as shown in Equation 9.4.

$$nr_{cycles} = \frac{\ln DoD}{\ln 1 - r_{deg}} \tag{9.4}$$

Using the given parameters it is determined that the batteries will last for 1500 cycles until the capacity will reach 70% of the initial magnitude, which might be insufficient to last for 5 years. The battery cycles are equivalent to the number of times a single cabin can be used repeatedly before either the batteries or the whole cabin has to be changed. It has to be noted that energy used for manoeuvring during the mission is not analysed separately as operational times are over-estimated as discussed in Chapter 7. Thus the energy needed to control the craft is assumed to be included in the estimations of the battery mass. Moreover, one engine arm inoperative (OEAI) case is not included in the analysis of continuous power usage as the craft would become over-designed as OEAI shall not occur more than once of the craft's lifetime. It was determined that necessary energy is the battery mass driving requirement, thereafter, the equation for the total HV battery mass becomes as follows:

$$M_{bat} = \frac{P_{hover} \cdot t_{cycle} \cdot (1 + LF)}{\rho_{Energy} \cdot \eta_{bat} \cdot \eta_{inv} \cdot DoD_{HV}} \tag{9.5}$$

where P_{hover} is the power required for hovering at maximum payload. Note that increasing the discharge rate by 0.1C leads to the energy becoming the driving requirement for the battery mass. Plugging the values defined earlier in Equation 9.5 the formula returns battery mass of 167.5 *kg* required to ensure that all the operations during the mission can be performed with the specified payloads. However, to increase cooling efficiency and the overall reliability of the system, the total mass of the HV battery is split into four high voltage batteries of the same size where a single battery is responsible of powering a total engine arm. It has to be noted that the batteries do include additional energy caused by the operational time safety factors, thus, OEAI scenario if not occurring during end of hover can be fully controlled.

Lastly, the volumetric density of the battery has to be discussed. Assuming that a value of 750 *Wh/l* [29] of volumetric density is taken, it can be concluded that the batteries will take up a total volume of 0.084 m^3.

9.4. Low Voltage Battery Sizing

In order to size the batteries completely, the low voltage grid consumption has to be determined. It has to be noted that majority of the electronics units (PCBs) running on low voltage are not designed during any stage of the project, thus the power losses can be characterized as educated guesses made by the engineers. Moreover, PCBs available in the market are not implemented in the product as adjusting hard-wired electrical connections with software tools requires more effort than creating a PCB from

scratch. Additionally, the efficiency parameters for the LV battery are assumed to be equal to those of the HV one except the DoD which is taken to be 85% for the LV battery.

The entire list of components requiring low voltage for operations can be found in Figure 12.1. The power consumption for the large scale PCBs as VCU, AMS and flight computer is assumed to be equal to that of medium scale gaming computers [23] and larger than the power consumption of autonomous Tesla car drive computer [24]. Thereafter, it is assumed that the VCU consumes 350 *W*, while the AMS consumes 150 *W* per PCB and the power loss on the flight computer is around 200 *W*. The motor controllers are assumed to be combined with the inverter and thus mainly running on the high voltage grid. However, the low voltage side which drives the micro controller and the comparators is assumed to be low and equal to 30 *W* per unit. Regarding the sensors, the total power consumption of them is approximately 50 *W*. The sensor node PCBs are assumed to consume 25 *W* per instance. Additionally, antennas required for the communications and the transciever on the craft are assumed to consume 250 *W*. Lastly the cooling pumps are determined to require 130 *W* of power per pump[25]. It has to be noted that the power of electrical mechanisms is neglected as it is applied for short time duration only and the limiting factor is the energy not the power. The power consumption of the lights and the sensors can be found in Chapter 7 and Section 12.1 respectively. Adding all of the contributions together, it is acquired that the total consumption reaches 2775 *W*. However, since the electronics components contain large quantities of capacitors, inductors and integrated circuits (IC's) an additional power factor (PF) of 0.9 is assumed, meaning that 10% of the power is the reactive or useless power. The mass of the battery cannot be directly determined from the total power consumption scaled by the power factor of as the power is split through different converters as described in Section 12.1. An average of the converter efficiency has to be taken as depicted in Equation 9.6:

$$\eta_{conv_{tot}} = \sum_{n=0}^{3} \frac{\eta_{conv_n} \cdot P_{conv_n}}{P_{cons}} \tag{9.6}$$

where P_{cons} is the total consumed power. The total converter efficiency is determined to be approximately 83.7%. Having determined all the factors influencing the total mass, the LV battery mass value can be computed as follows:

$$M_{bat_{LV}} = \frac{P_{cons} \cdot t_{cycle} \cdot n_{cycles}}{PF \cdot DoD_{LV} \cdot \eta_{conv_{tot}} \cdot \eta_{bat}} \tag{9.7}$$

with n_{cycles} being the total amount of cycles in a mission which is set to be 20. As there are 50 missions assumed per year, at least 250 cycles for the battery life span have to be ensured. Thereafter, the lithium metal concept is chosen for the LV battery. The configuration assumes the LV batteries attached on the detachable propulsion side to have continuous power feed to the electronics, such that the software does not have to be restarted at every change of the cabin. If mission has to be prolonged, the battery has to be recharged at the highest rate possible, being 5C, meaning that 12 minutes would be necessary before it was possible to repeat 20 more cycles. Executing Equation 9.7 returns a battery mass of 65 *kg*.

9.5. Inverter Sizing

To have AC motors working when applied to a DC supply, an inverter has to be placed in between to bridge the two. The exact inverter size cannot be determined at this stage of the product development, thereafter, statistical relationships are used to evaluate the approximate dimensions of the component. For the sizing, the specific active power density is used which is determined to be 26 *kVA/kg* [30]. Thus, the total required power has to be found, which can be done by dividing the maximum engine power by the motor efficiency. It is opted to have eight inverters (one inverter per engine) to increase the reliability of the design. Therefore, the inverter mass becomes approximately 2.9 *kg*.

[23] URL `https://computerinfobits.com/how-much-energy-do-gaming-computers-use/` [cited June 9, 2021]

[24] URL `https://chargedevs.com/newswire/lots-of-news-to-digest-as-tesla-demos-latest-autopilot-system/` [cited June 9, 2021]

[25] URL `https://races-shop.com/water-pumps/88340-universal-electric-water-pump-80l-min-75a.html` [cited 9 June 2021]

[26] URL `https://www.sunpower-uk.com/glossary/what-is-switching-frequency/` [cited June 10, 2021]

To determine the efficiency of the inverter, the power losses across the circuitry have to be determined. The inverter consists of mainly high energy volume capacitors used for filtering and smoothing of the incoming DC signal and MOSFETs or IGBTs (insulated-gate bipolar transistor) which are repeatedly turned on and off to generate the sine wave voltage profile. The power dissipation of the full circuitry can be computed by summing up the individual component power losses. Knowing that the capacitors are power efficient, it is assumed that all the power is dissipated through the transistors. Even though IGBTs are better for high power applications [31], for simplicity reasons it is assumed that high power MOSFETs are used to ensure higher frequency shifting and the transistors are configured such that six complementary transistor pairs are put to generate three level configuration to allow for high power operations [32]. The used MOSFETs would have to have maximum voltage characteristics of approximately 600 *V* and the drain-to-source current of around 100 *A* maximum. As the operational frequency of the inverter is high, the losses for the MOSFETs are mostly caused by the rapid switching [26]. Thereafter, the losses on the MOSFETs can be approximated with Equation 9.8[33].

$$P_{cons} = V_{in} \cdot I_{out} \cdot f_{sw} \cdot \frac{Q_{GS2} + Q_{GD}}{I_G} \tag{9.8}$$

In Equation 9.8 V_{in} is defined as drain to source voltage of the transistor, I_{out} is equal to the drain current Q_{GS2} is defined as the gate to source charge, Q_{GD} is the gate to drain charge and lastly, I_G is the gate current. As the gate current is absent from the datasheet for the transistors, it is approximated by the Ohm's law of dividing the gate plateau voltage by the gate resistance at the test conditions. For safety reasons, the gate current is divided by a factor of 1.5 as the test conditions do not apply. Additionally, the maximum values for all the parameters are taken to ensure that the worst case scenario is established. If MOSFET CoolMOS™ C7[27] is selected and the switching frequency is assumed to be approximately 100 *kHz*, the power loss on a single transistor becomes 78 *W*. As two of the transistors are switched on simultaneously, the continuous loss factor becomes approximately 160 *W*, thus the efficiency is determined to be more than 99%. However, the actual efficiency is likely lower, which cannot be estimated without a complete design and testing of the circuitry. Thereafter, to include a slight safety factor, the efficiency of an inverter is taken to be 98%. It has to be noted that using three level adaptation of the AC voltage eliminates the need for a small scale transformer to adjust the output voltage to the one of correct motor operations. Lastly, passive filtering (RLC circuitry) can be a applied to smoothen the output current and remove the unwanted noise of the voltage signal.

9.6. Conclusion

All in all, it was determined that the design can be powered by electrics as enough energy and power can be provided to the craft by the batteries. The claim was verified by iterating the motor parameters with the mass of the craft, such that all critical operational conditions (OEAI included) are sufficed. The batteries were chosen to be the experimental lithium metal as they have the most desirable charge rate, power and energy density characteristics available on the market. Lastly, the inverters needed to create the connections between the motors and the HV batteries were designed. Having sized all the power & propulsion parameters of the craft, the control and stability characteristics can be analysed.

10. Stability & Control Characteristics

In order to satisfy the design requirements and provide a safe, reliable and efficient system, an in depth analysis of the system's stability and control characteristics must be performed.

This starts by first determining the stability and control approach. Then a detailed study of operational disturbances will be performed. The various disturbances will be identified and models will be constructed to evaluate disturbances and quantify their impact on the system. Next, a model of the system will be derived in the form of a system of non-linear dynamic differential equations. This model will then be further simplified and linearised such that its behaviour can be analysed. Using the linearised

[27] URL https://www.infineon.com/dgdl/Infineon-IPW60R017C7-DS-v02_00-EN.pdf?fileId=5546d46253a864fe0153cc8319e77eb8 [cited 10 June 2021]

model, the system's response to disturbances will be analysed in order to study the natural stability of the system. Due to the system's instability a control method will be applied and the system's response to disturbances will once again be tested. Moreover, an analysis of one engine inoperative conditions for both the natural and controlled system will be performed. The results of the natural stability behaviour and the proposed control behaviour will then be discussed and evaluated. Finally, the model's limitations will be discussed and possible recommendations will be proposed.

10.1. Stability & Control Approach

In order to define the approach it is necessary to define the system properties and characteristics. The concept that will be evaluated is a quadcopter configuration with four counter rotating motor-propeller pairs (eight motors total). The engines are distributed symmetrically around the longitudinal and lateral axis of the craft and the centre of thrust lies on the centre of gravity (See Figure 10.1).

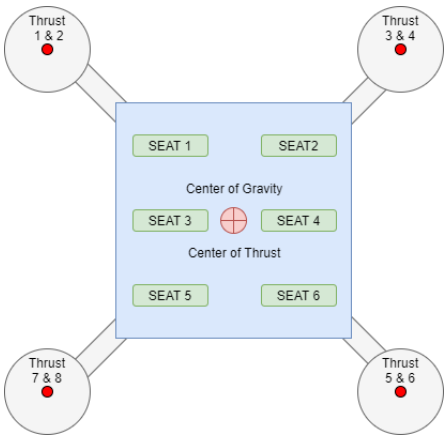

Figure 10.1: Simplified quadcopter concept

The chosen control approach will be to use differential thrust in the motors while keeping their position fixed to counteract all disturbances. This means the rotors cannot be tilted for control and there are no extra control parameters. The impact of this design choice will be discussed when evaluating the results and limitations.

In order to evaluate the stability and control characteristics of the system the critical operational phases must first be identified which will be the subject of the next section.

10.2. Critical Operational Phases

The system must be able to perform under a lot of different operational conditions. The mission profile details each phase of the mission and breaks them down into distinct phases. When looking at the mission profile (See Section 3.3) from a stability and control perspective it is clear that the most critical phases are: landing, hovering and approach (docking). Note that descent and ascent are not included as the craft requires more power to hover at full cargo. This means the available power to control the craft is lower while hovering at full cargo than when ascending without cargo or descending at full cargo.

The hovering phase is considered the most critical phase, this is because the system must be able to hover near a burning skyscraper while handling passengers who might be incapacitated, inability to control the craft during hovering will result in catastrophic failure. An example of this would be that the craft impacts the building while carrying the payload. This is also the case where the most thrust is required and therefore the least engine power is available for control.

The next most critical phase is considered to be the landing, this is because the craft is loaded with passengers and must be able to safely land such that the passengers can be rescued which is especially important if there are injured passengers. Given that the rotors cannot tilt the system must be perfectly horizontal when landing, any disturbance must be quickly counter acted. Once again inability to control the craft can lead to catastrophic failure.

The approach phase is considered least critical since the system is not loaded with cargo, this means the amount of power available for controls is higher. However, the approach phase requires a high degree of precision and low turn-over time, this can only be achieved through rigorous control of the system. Inability to approach can once again lead to catastrophic failure. An example of this would be failure to load the payload in a safe interval of time.

Finally, an additional critical phase is considered, this is not a part of the mission profile as it assumes partial component failure. This phase is the case where one engine arm is inoperative (OEAI), this means one of the rotor arms suddenly stops providing thrust but there is no net torque on the system. Once again OEAI can lead to catastrophic failure. This phase is unlikely to occur but the ability to control the craft during OEAI increases the reliability of the system and can save system complexity.

Only these phases are considered critical as all other phases can be controlled if the critical phases are controllable. The other phases are less limiting either due to the amount of payload, required power or required accuracy. After identifying the critical mission phases it is necessary to take a look at the disturbances on the system. This is the subject of the next section.

10.3. Operational Disturbances

When studying stability and control characteristics of a system an important property is the system's response to disturbances. A system is considered stable when it return to its initial equilibrium position after a disturbance. If a system is unstable or neutrally stable it will not counter act disturbances and must therefore be controlled.

It is not possible to analyze the system's stability characteristics without properly identifying and modelling the various operational disturbances. In the previous parts of the project a detailed study of the operational environment was performed and the main disturbances were identified. Those are disturbances due to gusts and disturbances due to a shift in centre of gravity and those will be analyzed separately.

10.3.1. Disturbances due to gusts

In urban environments the flow of air is obstructed by high rise buildings, this leads to increased gust velocities near buildings right within the operational environment of the system. These gusts apply disturbances on the craft which depend on the dimensions of the craft but also the altitude and the earth surface roughness. This means that a thorough analysis of the impact of gusts on the system must be performed which will be done via a model. However, before the model is constructed some assumptions are made and these are listed below.

- A1: The maximum gust velocity is in vertical direction.
- A2: The maximum gust velocity is equal in all directions.
- A3: Gust loads are applied as point loads on the centre of gravity (CG).
- A4: Gust loads are applied as triangular distributions on the surface of the craft.

Note that assumption A3 and A4 will be used for two separate analyses and are not contradicting.

The first step of the analysis is to build a model which determines the variation in gust speed as a function of altitude and local environmental conditions. The model is constructed using the logarithmic profile where wind speed is assumed to vary logarithmically with height[30]. The governing equation of this model can be seen in Equation 10.1.

$$U(z) = U_0 \cdot \left[\frac{\ln\left(\frac{z}{z_s}\right)}{\ln\left(\frac{z_0}{z_s}\right)} \right] \tag{10.1}$$

Where $U(z)$ is the gust speed as a function of height, U_0 the ground wind speed, z the altitude, z_0 the ground sensor altitude, and z_s the ground surface roughness constant. The overview of all the

[30] *URL*https://www.homerenergy.com/products/pro/docs/latest/wind_resource_variation_with_height.html [cited 17 May 2021]

parameters can be found in Table 10.1

Table 10.1: Gust speed model parameters

Parameter	U_0 [m/s]	z_0[m]	z_s [m]
Value	5.14	10	3

The ground wind speed was recorded in New York City for several days using a wind tracking website[29], the average value was then computed and doubled to account for seasonal variations. Furthermore, the sensor height is assumed to be 10 *m*, finally the ground surface roughness constant was taken to be 3 *m* for dense urban centres[30].

Using this model and the systems maximum operational height of 400 *m* a visualization of the gust speed over the height can be constructed and an estimate for the maximum gust speed can be derived. The plot in Figure 10.2 shows the gust speed distribution from the model. The maximum gust speed at an operational height of 400 *m* is equal to 20.32 *m/s*.

Using this model and the general drag equation a first level estimate of the various disturbances forces and moments can be estimated. In order to compute the disturbances due to gusts assumptions A1 and A2 are used. When looking at translational accelerations due to gust the loading is assumed to behave like in assumption A3. This means that the gust load does not generate any moments, the load is applied on the CG and is equal to the drag force over the cross section. By studying different faces and assuming the wind speed is equal in all directions preliminary values for translational accelerations due to gusts can be derived.

Assumption A3 assumes that the gust is a point load on CG, meaning there are no control torques required due to gusts, which is incorrect. Therefore assumption A4 is assumed where the gust is linearly distributed around the face of the craft in a triangular distribution, leading to a disturbance torque where the moment arm is equal to 1/6 the cabin width on that face. The results of the gust analysis using the model can be seen in Table 10.2.

Table 10.2: Disturbances due to gust

Parameter	**x-dir**	**y-dir**	**z-dir**
Gust force [N]	76.24	152.5	152.5
Translational accelerations [m/s^2]	0.104	0.208	0.208
Gust torque [Nm]	20.9	41.9	41.9
Angular accelerations[1/rads^2]	0.0073	0.0142	0.0074

These parameters detail the magnitude of the forces and torques experienced by the craft due to disturbances, however, more information must be derived on the application of those disturbances. During operations the craft will be subjected to disturbances over a certain period of time, assuming that the disturbances are applied as impulses would be incorrect. This is where the second part of the model is relevant.

After computing the maximum gust velocity and corresponding disturbances, the evolution of the gust load and intensity over time must be derived. In order to do this the aircraft CS25 gust certification method will be applied [34]. The CS25 certification method assumes that the gust load varies in intensity over the distance travelled. This method must first be adapted to function with the system, this is where the assumption that the gust intensity varies with time instead of distance travelled is made. The governing equations for the gust intensity as a function of time can be seen below.

[29] *URL* `https://www.windy.com/` [cited 18 May 2021]

$$F_g = 0.5 \cdot (F_{gz} + F_{gm}) \tag{10.2}$$

$$F_{gz} = 1 - \frac{z_{mo}}{76200} \tag{10.3}$$

$$F_{gm} = \sqrt{\left(\frac{m_{landing}}{m_{tow}}\right) \cdot \tan\left[\frac{\pi\left(\frac{m_{zfw}}{m_{tow}}\right)}{4}\right]} \tag{10.4}$$

$$U_{ds} = U_{max} \cdot F_g \cdot \left(\frac{T}{107}\right)^{\frac{1}{6}} \tag{10.5}$$

$$U(t) = \frac{U_{ds}}{2} \cdot \left[1 - \cos\left(\frac{\pi t}{T}\right)\right] \quad 0 \leq t \leq 2T \tag{10.6}$$

Where z_{mo} is the maximum operational height, $m_{landing}$ is the maximum landing weight, m_{tow} is the maximum takeoff weight, m_{zfw} is the maximum zero fuel weight, U_{max} is the maximum gust speed, U_{ds} is the design gust speed. The other variables are flight factors necessary for computations

The main difference between these equations and the CS25 certification model is that the gust characteristic distance H has been replaced by the gust characteristic period T. Furthermore, the distance penetrated s has been replaced by time t. The CS25 model is for airplanes which travel at a certain cruise velocity however the quadcopter may stay at 0 velocity for certain periods of time. Hence replacing distance by time means that the model can be applied to hovering crafts.

Given that the CS25 certification model is for aircraft the characteristic period T is hard to define for a quadcopter concept. Therefore, the model computes all possible gust intensity distribution for $T \leq 2z_{mo}$. All the distributions are plotted and this results in the gust envelope (See Figure 10.3). The gust envelope shows all possible gust intensity and disturbances that the system can encounter. At a later stage the left most and right most distribution will be used as disturbance inputs to the control model. For $T = 2z_{mo}$ the maximum design gust speed is encountered and is equal to 10.5 *m/s*.

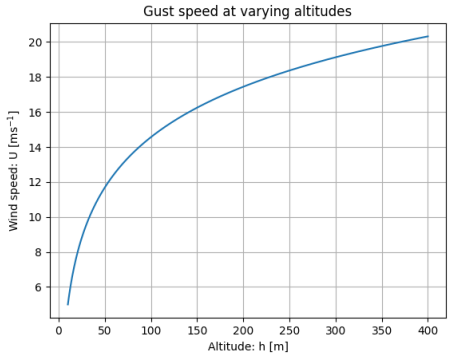

Figure 10.2: Plot of Gust speed as a function of altitude

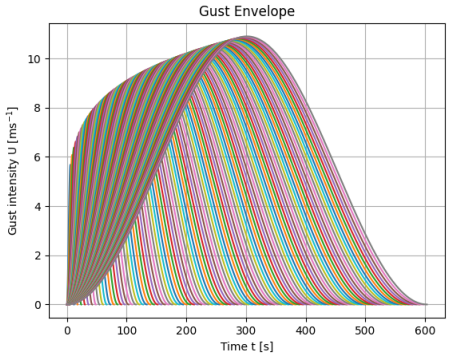

Figure 10.3: Operational gust envelope

At this stage, the gust disturbances have been fully characterised, the model results in a series of disturbance characteristics such as the disturbance forces and torques. Furthermore the model is able to construct the operational gust envelope which describes the way the craft experiences gusts over time. This information will be used as inputs to test the stability and controllability of the craft. The operational disturbances are not limited to gust loads but also include disturbances due to a shift in craft centre of gravity and these disturbances will be characterised next.

10.3.2. CG shift disturbances

Due to the nature of the payload, it is expected that the centre of gravity (CG) of the craft will shift throughout operations, this is especially relevant when boarding the payload. A shift in CG will lead to a moment unbalance around the centre of gravity, hence a differential thrust will be needed to compensate

for the shift. In order to perform this analysis a seating configuration has been assumed as can be seen in Figure 10.1.

The seating arrangement is such that when the craft is empty or at full cargo the centre of gravity lies in the middle of the craft. Two critical boarding situations have been determined, the first happens when the front-most seats (1 & 2) are loaded and the rest are empty, the second happens when the left most seats (1, 3 & 5) are loaded and the other are empty. Note that there are two other but exactly opposite critical situations due to cabin symmetry, this means only the two aforementioned critical situations must be analyzed.

The goal of this analysis is to construct a range of all possible CG positions for the craft, due to unsymmetrical payload boarding. In other to construct a model that can characterise the shifts in CG a series of assumptions must be made, these are listed below.

- A5: The payload boarding happens instantaneously.
- A6: The centre of gravity of all subsystems besides payload is in the centre of the craft.
- A7: Vertical shifts in centre of gravity are neglected.

Using these assumptions a simple model can be constructed, the model will perform a weighted mass average of the local centre of gravity of each subsystem and compute the location of the global centre of gravity of the system. The equations used for this model are shown below.

$$x_{cg} = \frac{\sum_{i=1}^{n} x_{cg_i} \cdot m_i}{\sum_{i=1}^{n} m_i} \qquad y_{cg} = \frac{\sum_{i=1}^{n} y_{cg_i} \cdot m_i}{\sum_{i=1}^{n} m_i} \tag{10.7}$$

Where x_{cg} is the x coordinate of the centre of gravity, y_{cg} is the y coordinate of the centre of gravity, and m_i is the mass of the ith subsystem.

Assumption A6 simplifies this weighted average if the origin is taken to be the centre as all terms, besides the payload, reduce to 0 in the numerator. By knowing the individual weight of the payload and the location of their seat with respect to the origin a range of CG values can be computed.

The next step is to translate the shift in CG to a certain disturbance torque due to the thrust unbalance. This can easily be computed by multiplying the thrust of the engines in by the shift in CG. This is because the centre of thrust (CT) lies in the middle of the craft, if the CG shifts from the centre the amount of shift is equal to the moment arm from the CT to the CG. This results in a net torque applied on the system which must be counteracted via differential thrust in the rotor arms. This differential thrust can be computed by dividing the disturbance torque by the distance from the rotor to the CG. The results of the CG analysis are shown in Table 10.3.

Table 10.3: CG shift stability and control characteristics

Parameter	CG shift [%]	Disturbance torque [Nm]	Differential thrust required [N]
Longitudinal axis x	6.57	1054	409
Lateral axis y	7.5	2353	996

Finally, given assumption A5 it can be assumed that the disturbance acts like a step input at a certain point in time. The disturbance torque due to CG shift is applied instantaneously for a period of time until all the payload has boarded.

This concludes the section about disturbances, at this stage two models have been constructed which characterize the operational disturbances experienced by the craft. These models have been verified and validated with physical data and can be used as disturbance inputs for the control model.

10.4. Dynamic Model of Quadcopter Concept

In order to further define the system stability and control characteristics a detailed understanding of the model and its dynamic behaviour is necessary. This will allow modelling of the quadcopter in an accurate and precise way such that the system can be analysed. The first step is to derive the Equations of Motion (EOM) of the quadcopter. This was derived from the Free Body Diagram (FBD) shown below (See Figure 10.4) [35].

Taking positive directions as indicated by the red arrows the force and moment equations around each axis can be computed via the equations shown below.

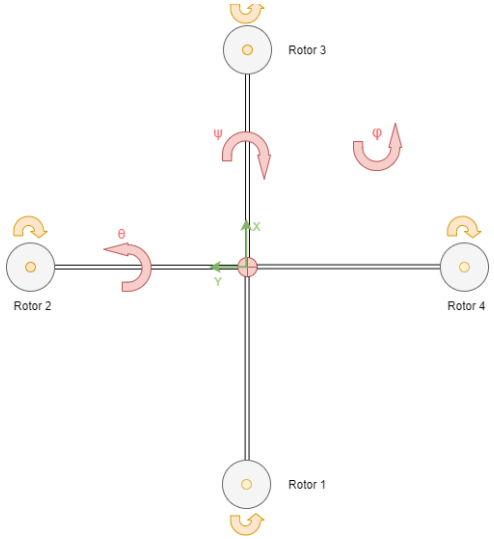

$$a_x = \frac{-T\sin\theta}{m} \tag{10.8}$$

$$a_y = \frac{T\sin\phi}{m} \tag{10.9}$$

$$a_z = \frac{T - mg}{m} \tag{10.10}$$

$$\tau_x = y_1T_1 + y_2T_2 + y_3T_3 + y_4T_4 \tag{10.11}$$

$$\tau_y = x_1T_1 + x_2T_2 + x_3T_3 + x_4T_4 \tag{10.12}$$

$$\tau_z = c\left(-T_1 + T_2 - T_3 + T_4\right) \tag{10.13}$$

Figure 10.4: Free body diagram of quadcopter

These equations are clearly not linear and in order to construct a control model of the drone, these equations must be simplified. The first assumption is that the roll and pitch angle are very small and therefore $\sin\theta \approx \theta$, furthermore $T \approx mg$. By plugging in the respective x and y distances to the origin and substituting the simplification mentioned previously the EOMs can be linearised and simplified. Furthermore, including the contribution of the wind force and torque makes the model complete. The results of this can be seen in the equations below.

$$a_x = -g\theta + \frac{f_{wx}}{m} \tag{10.14}$$

$$a_y = g\phi + \frac{f_{wy}}{m} \tag{10.15}$$

$$a_z = \frac{T - mg}{m} + \frac{f_{wz}}{m} \tag{10.16}$$

$$\tau_x = r\left(T_2 - T_4\right) + \tau_{wx} \tag{10.17}$$

$$\tau_y = r\left(T_1 - T_3\right) + \tau_{wy} \tag{10.18}$$

$$\tau_z = c\left(-T_1 + T_2 - T_3 + T_4\right) + \tau_{wz} \tag{10.19}$$

These are the EOM that govern the dynamic behaviour of the craft in all six degrees of freedom (DOF), given that all these equations are linear, it is now possible to construct a state-space model of the quadcopter to study the behaviour of the craft due to control or disturbance input. This will be the subject of the next section.

10.5. State Space Model of Quadcopter

To study the stability and control characteristics of the quadcopter, a state space model will be constructed. A state space model is a model which solves the state and output equations over time (See 10.20). A state space model can be constructed for a set of linearised differential equations with a given number of states, inputs and outputs.

$$\dot{x}(t) = Ax(t) + Bu(t) \qquad y(t) = Cx(t) + Du(t) \tag{10.20}$$

The first step when constructing the model is to identify the state vector x, the state vector contains all the parameters of the system which are not controllable but vary in time. In the case of a 6 DOF system the state vector is shown below. It contains all the information about position, velocity, angular position and angular rate of the craft in time.

$$x = \left[x, y, z, x', y', z', \phi, \theta, \psi, \dot{\phi}, \dot{\theta}, \dot{\psi}\right]^T \tag{10.21}$$

Where x, y, z are the respective coordinates in each axis, x', y', z', are the respective velocities in each axis, ϕ is the roll angle, θ is the pitch angle and ψ is the yaw angle. Similarly the last three states are the roll, pitch and yaw rate.

The second step when constructing a state space model is to identify the control inputs and therefore input vector u. The input vector contains all the parameters which can be controlled as well as the disturbance inputs, this is to make the state equation more simple. In the case of a quadcopter with 6 DOF the input vector is shown below.

$$u = \left[T - mg, f_{wx}, f_{wy}, f_{wz}, \tau_x, \tau_y, \tau_z, \tau_{wx}, \tau_{wy}, \tau_{wz}\right]^T \tag{10.22}$$

Where $T - mg$ is the net force in z direction, f_{wi} is the wind force in ith direction, τ_i is the engine torque around the ith axis and τ_{wi} is the wind torque around the ith axis.

In this model the only control inputs are the torques around each axis due to the engine and the net vertical force, the disturbances are included in the input vector for simplicity but they are not controllable.

After defining the state and input vector it is now necessary to derive the output vector. The output vector contains 10 parameters and not 12 such that its length is equal to the input vector, this is to make the system simpler to control and will be discussed later in the report. The output vector for this model is shown below. Note that all variables have previously been defined.

$$y = \left[x, y, z, \phi, \theta, \psi, x', y', \dot{\phi}, \dot{\theta}\right]^T \tag{10.23}$$

Having determined what the input, state and output vector are it is now possible to build the matrices such that the state equation is satisfied. By taking the time derivative of the state vector and expressing each parameter using the EOMs, control inputs and disturbances matrix A and B can be constructed. The equations below show how to express the derivative of the state vector as a function of the states, inputs and disturbances.

$$\begin{aligned}
x' &= x' & y' &= y' & z' &= z' \\
x" &= -g\theta + \frac{f_x}{m} & y" &= g\phi + \frac{f_y}{m} & z" &= \frac{T - mg}{m} + \frac{f_z}{m} \\
\dot{\phi} &= \dot{\phi} & \dot{\theta} &= \dot{\theta} & \dot{\psi} &= \dot{\psi} \\
\ddot{\phi} &= \frac{\tau_x + \tau_{wx}}{I_{xx}} & \ddot{\theta} &= \frac{\tau_y + \tau_{wy}}{I_{yy}} & \ddot{\psi} &= \frac{\tau_z + \tau_{wz}}{I_{zz}}
\end{aligned}$$

For clarity the time derivative of the state vector is shown below.

$$\dot{x} = \left[x', y', z', x", y", z", \dot{\phi}, \dot{\theta}, \dot{\psi}, \ddot{\phi}, \ddot{\theta}, \ddot{\psi}\right]^T \tag{10.24}$$

These equations can be written in matrix form (See Equation 10.20). The corresponding A and B matrices can be seen below.

$$A = \begin{bmatrix} 0 & 0 & 0 & 1 & 0 & 0 & 0 & 0 & 0 & 0 & 0 & 0 \\ 0 & 0 & 0 & 0 & 1 & 0 & 0 & 0 & 0 & 0 & 0 & 0 \\ 0 & 0 & 0 & 0 & 0 & 1 & 0 & 0 & 0 & 0 & 0 & 0 \\ 0 & 0 & 0 & 0 & 0 & 0 & 0 & -g & 0 & 0 & 0 & 0 \\ 0 & 0 & 0 & 0 & 0 & 0 & g & 0 & 0 & 0 & 0 & 0 \\ 0 & 0 & 0 & 0 & 0 & 0 & 0 & 0 & 0 & 0 & 0 & 0 \\ 0 & 0 & 0 & 0 & 0 & 0 & 0 & 0 & 0 & 1 & 0 & 0 \\ 0 & 0 & 0 & 0 & 0 & 0 & 0 & 0 & 0 & 0 & 1 & 0 \\ 0 & 0 & 0 & 0 & 0 & 0 & 0 & 0 & 0 & 0 & 0 & 1 \\ 0 & 0 & 0 & 0 & 0 & 0 & 0 & 0 & 0 & 0 & 0 & 0 \\ 0 & 0 & 0 & 0 & 0 & 0 & 0 & 0 & 0 & 0 & 0 & 0 \\ 0 & 0 & 0 & 0 & 0 & 0 & 0 & 0 & 0 & 0 & 0 & 0 \end{bmatrix} \quad B = \begin{bmatrix} 0 & 0 & 0 & 0 & 0 & 0 & 0 & 0 & 0 & 0 \\ 0 & 0 & 0 & 0 & 0 & 0 & 0 & 0 & 0 & 0 \\ 0 & 0 & 0 & 0 & 0 & 0 & 0 & 0 & 0 & 0 \\ 0 & \frac{1}{m} & 0 & 0 & 0 & 0 & 0 & 0 & 0 & 0 \\ 0 & 0 & \frac{1}{m} & 0 & 0 & 0 & 0 & 0 & 0 & 0 \\ \frac{1}{m} & 0 & 0 & \frac{1}{m} & 0 & 0 & 0 & 0 & 0 & 0 \\ 0 & 0 & 0 & 0 & 0 & 0 & 0 & 0 & 0 & 0 \\ 0 & 0 & 0 & 0 & 0 & 0 & 0 & 0 & 0 & 0 \\ 0 & 0 & 0 & 0 & 0 & 0 & 0 & 0 & 0 & 0 \\ 0 & 0 & 0 & 0 & \frac{1}{I_x} & 0 & 0 & \frac{1}{I_x} & 0 & 0 \\ 0 & 0 & 0 & 0 & 0 & \frac{1}{I_y} & 0 & 0 & \frac{1}{I_y} & 0 \\ 0 & 0 & 0 & 0 & 0 & 0 & \frac{1}{I_z} & 0 & 0 & \frac{1}{I_z} \end{bmatrix}$$

Similarly the output matrix C can be derived by simply selecting the chosen outputs, note that matrix D is a 10x10 null matrix. The output matrix is shown below.

$$C = \begin{bmatrix} 1 & 0 & 0 & 0 & 0 & 0 & 0 & 0 & 0 & 0 & 0 & 0 \\ 0 & 1 & 0 & 0 & 0 & 0 & 0 & 0 & 0 & 0 & 0 & 0 \\ 0 & 0 & 1 & 0 & 0 & 0 & 0 & 0 & 0 & 0 & 0 & 0 \\ 0 & 0 & 0 & 0 & 0 & 0 & 1 & 0 & 0 & 0 & 0 & 0 \\ 0 & 0 & 0 & 0 & 0 & 0 & 0 & 1 & 0 & 0 & 0 & 0 \\ 0 & 0 & 0 & 0 & 0 & 0 & 0 & 0 & 1 & 0 & 0 & 0 \\ 0 & 0 & 0 & 1 & 0 & 0 & 0 & 0 & 0 & 0 & 0 & 0 \\ 0 & 0 & 0 & 0 & 1 & 0 & 0 & 0 & 0 & 0 & 0 & 0 \\ 0 & 0 & 0 & 0 & 0 & 0 & 0 & 0 & 0 & 1 & 0 & 0 \\ 0 & 0 & 0 & 0 & 0 & 0 & 0 & 0 & 0 & 0 & 1 & 0 \end{bmatrix}$$

After deriving matrices A, B and C the state space model has been constructed. In order to study the systems stability and control characteristics the control module for python will be used. Multiple input and disturbance inputs will be tested as to study the system's stability.

10.6. Stability of Quadcopter Model

Now that the state space model has been constructed, an analysis of the stability for the system can be performed. Stability is the behaviour of a system to a disturbance input, a system is considered stable when it returns to its initial undisturbed state after a disturbance.

The stability of the model will be evaluated in terms of its outputs. This will be done in multiple steps, the first will be study the system's behaviour to an initial condition where the states are not zero. Then, the system's response to a given control input will be analysed. Finally, the system's response to a given disturbance input will be evaluated. The three cases mentioned previously will provide information on the system stability and the need to actively control the system.

The first case study will be to study the system's response to non-zero initial conditions but no disturbance or control inputs (See Figure 10.5). The initial conditions are taken to be 1 for each state at $t = 0$, the system's behaviour is then simulated over 10 *s*.

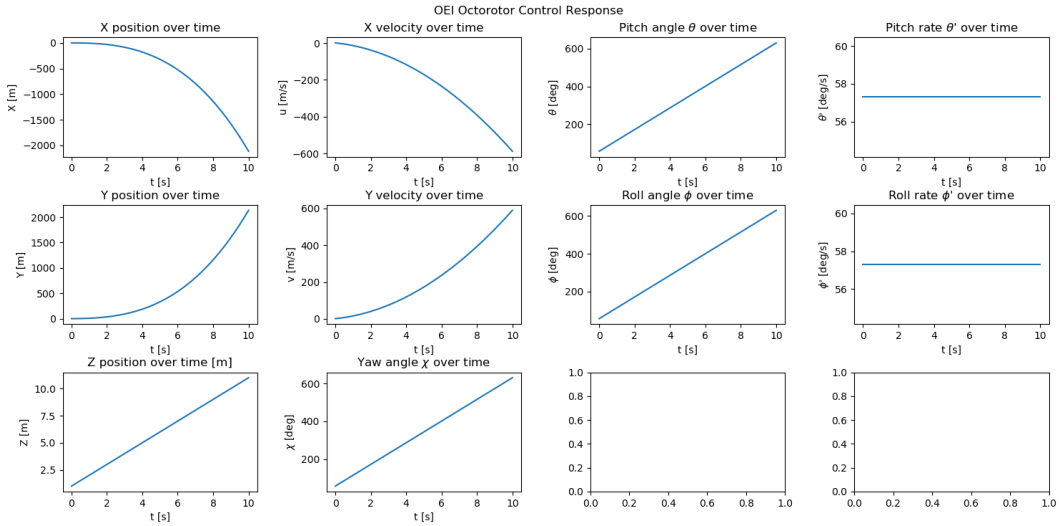

Figure 10.5: Quadcopter undisturbed behaviour for non zero initial conditions

The response of the system to non-zero initial conditions provides a lot of information about the system. It is clear that for non-zero initial conditions the craft is unstable and most states tend to infinity over time. This makes sense when considering the various states, by setting a value of 1 for the roll, pitch and yaw rate leads to a constant increase in roll, pitch and yaw angle, this leads to a quadratic increase of x, y, z velocities and finally a cubic increase of x, y, z coordinates. This is because each state is the integral of another state and will affect its rate of change. From this case study it is clear that the states depend on the respective roll, pitch and yaw rates and for non zero angular rates the system's outputs tend to infinity.

The next case study necessary to determine the system's stability is the behaviour of the system under zero initial conditions for a certain control input. In this case study, the four control inputs ($T - mg$, τ_x, τ_y, τ_z) are input as impulses with strength 1, the impulse is applied at $t = T/2$. The corresponding input functions can be seen in Figure 10.6. Note that all the input and disturbance functions are plotted on top of each other.

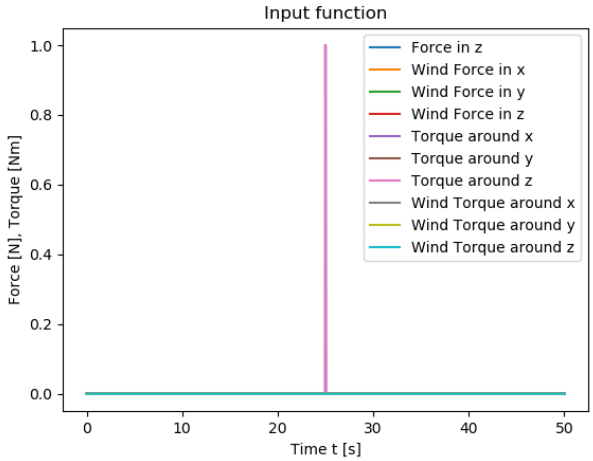

Figure 10.6: Quadcopter impulsive control input

For the given control inputs, the systems behaviour can be simulated using the state space model, the result of this can be seen in Figure 10.7.

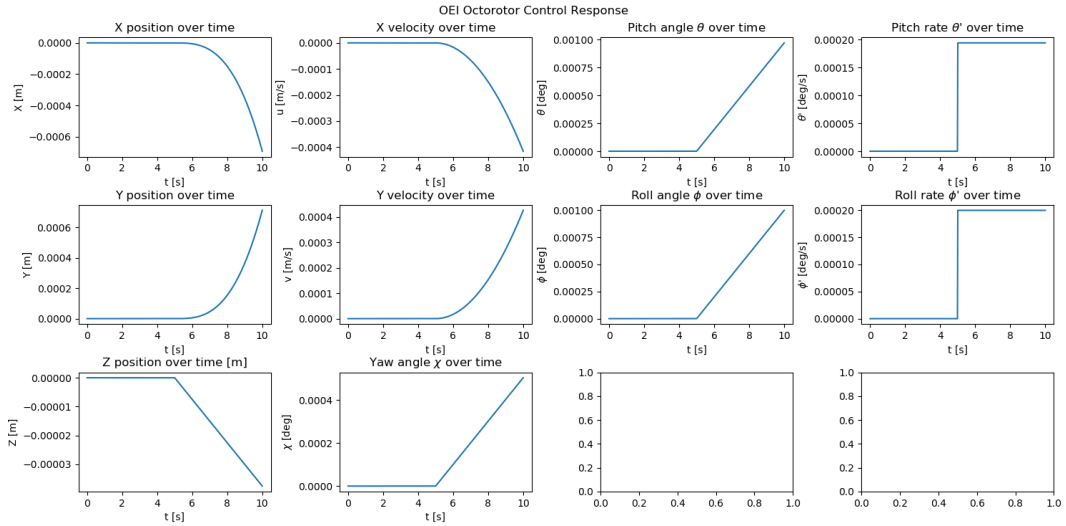

Figure 10.7: Quadcopter disturbed response due to an impulsive control input

A similar response can be derived when looking at the system response due to an impulsive disturbance input. Here the disturbances (f_{wx}, f_{wy}, f_{wz},τ_{wx}, τ_{wy}, τ_{wz}) are all set to be equal to 1 at $t = T/2$, they are 0 for the rest of time. Once again the system response due to impulsive disturbance input can be seen in Figure 10.8. Note that the input function is very similar to the one in Figure 10.6.

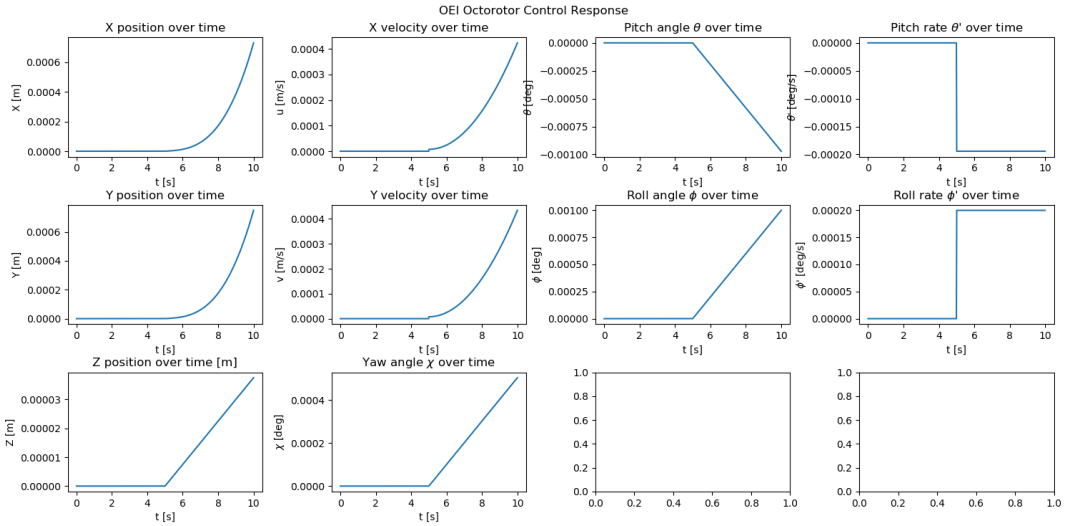

Figure 10.8: Quadcopter disturbed response due to an impulsive disturbance input

From both case studies it is once again obvious that the states tend to infinity due to a disturbance or certain non-zero initial conditions. Having looked at these three case studies the stability of each state can be determined. A neutral equilibrium implies that the system stays disturbed when disturbed but the disturbance does not increase or decrease over time, this is the case of the roll, pitch and yaw rate. An unstable equilibrium means that the state tends to infinity for a given disturbance, this is the case for all other states. Overall, it can be said that the system is unstable as all states are either neutral or unstable, this is obvious when looking at Figure 10.5, 10.7 and 10.8. This means that the system must be controlled in order to ensure safe operations. The system stability is summarized in the list below.

- x : Unstable equilibrium
- y : Unstable equilibrium
- z : Unstable equilibrium
- x': Unstable equilibrium
- y': Unstable equilibrium
- z': Unstable equilibrium
- ϕ : Unstable equilibrium
- θ : Unstable equilibrium
- ψ : Unstable equilibrium
- $\dot{\phi}$: Neutral equilibrium
- $\dot{\theta}$: Neutral equilibrium
- $\dot{\psi}$: Neutral equilibrium

10.7. State Space Control Approach

It was previously derived that the system was unstable, this means that the system has to be controlled in order to operate the craft. There are multiple control methods that can be implemented, for this system it was chosen to use a feedback loop where the output vector is used to correct the input vector. The control system must try to make the error vector e as small as possible. This is achieved by choosing a specific gain matrix, by tuning the gain matrix an unstable system can be controlled.

The state space model can be simplified as a single transfer function H where the inputs are transformed into the outputs. The block diagram and transfer function of the uncontrolled system can be seen in Figure 10.9. By adding a feedback matrix to the system a feedback loop can be created, in order to control the craft the feedback matrix must be such that the states dampen over time. The block diagram and transfer function of the proposed controlled system can be in Figure 10.10 where K is the feedback gain matrix.

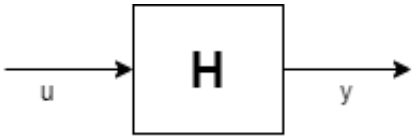

Figure 10.9: Block diagram and transfer function of state space model

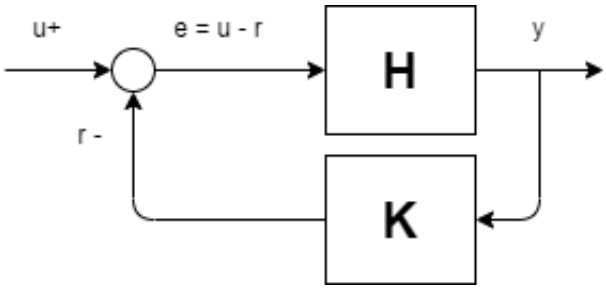

Figure 10.10: Block diagram and transfer function of controlled state space model

In order to control the system a feedback gain matrix K must be derived. The aim is to dampen the response to a disturbance for all states and eventually return to the initial state. The process of deriving the correct gain matrix is called gain tuning and will be the subject of the next subsection.

10.8. Gain Matrix Tuning: Root-locus Method

To tune the gain matrix for the state-space feedback model the root-locus method will be used. The transfer function H can be factorised into a set of poles, due to the nature of the system all these poles are complex poles. By plotting the poles on the complex plane the behaviour of the states can be analysed and the feedback matrix can be chosen such that the states are stable. Since the system has 12 states the number of poles is also 12. Figure 10.11 shows how the location of the poles of a system impacts state stability.

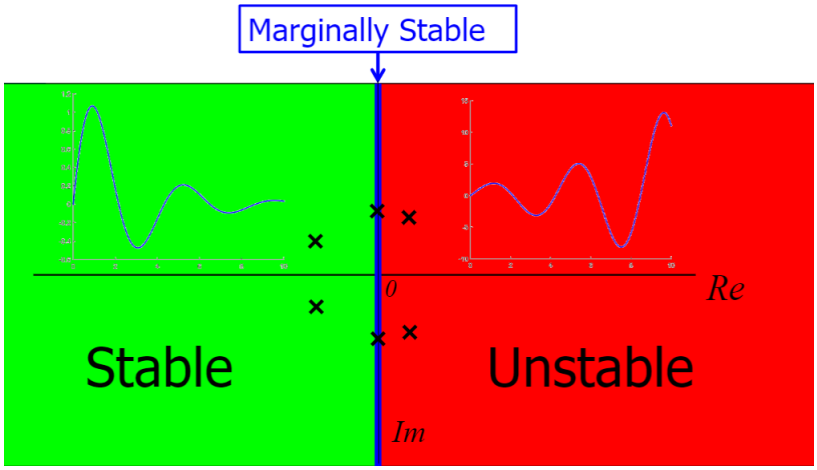

Figure 10.11: Root-locus pole stability

When looking at Figure 10.11 it is clear that in order for the system to be stable all poles must lie in the negative real plane. If poles only have an imaginary part the corresponding states are marginally stable. Another behaviour of the states that can be derived from the pole placement is the amount of oscillation during the response, this is because the imaginary part of the pole determines the frequency of the oscillation. Large imaginary parts lead to high frequency oscillation. Furthermore, the real part of the pole determines the dampening of the response, where positive dampening factor amplify the response. This is why the poles of the quadcopter model must have negative or zero real parts and low relatively low imaginary parts.

The feedback gain matrix must be chosen such that the poles are stable. This is because the feedback matrix changes the transfer function and moves the pole. In order to tune the root locus the relationship between the outputs and the control inputs must be defined. It is clear that some outputs can provide direct information about the required control input in order to stabilise the craft. The equations below show the dependencies between the outputs and the control inputs.

$$T - mg \propto z \qquad \tau_x \propto \phi, \dot{\phi}, y, y' \tag{10.25}$$

$$\tau_z \propto \psi \qquad \tau_y \propto \theta, \dot{\theta}, x, x' \tag{10.26}$$

The torques in x- and y-direction directly impact the roll and pitch rate, this in turn affects the angles, velocities and positions in x- and y-direction. Furthermore the force in z impacts the acceleration in z which through integration impacts the z-position. Finally, the torque around z impacts the yaw rate which in turn impacts the yaw angle. Note that z' and $\dot{\psi}$ are not outputs but would otherwise be included in the dependencies.

Tuning the feedback matrix is easier when the dependencies are known, this is because specific poles can be moved by varying the gain for each dependency. An example of this is shown below, where the feedback matrix is built such that the roll and y-position are controlled. The input is an impulsive torque around x at $t = T/4$. When trying to control the roll and y position the control input of interest is the torque around x.

In Figure 10.12 the feedback for the torque around x contains a gain for the roll rate only. It is clear that the response is dampened and the roll rate returns to its initial state, however this not the case for the other outputs.

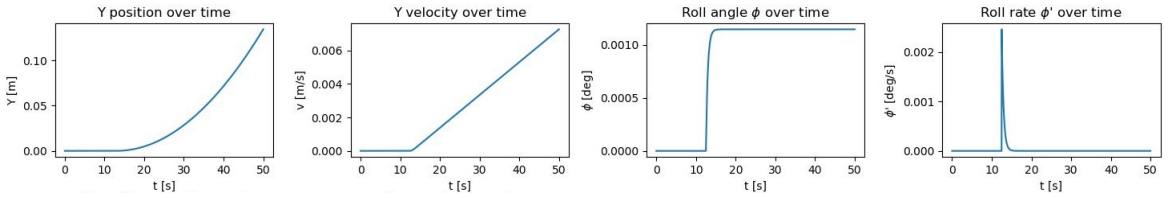

Figure 10.12: Roll response with feedback for roll rate only

In Figure 10.13 a feedback gain is given for the roll rate and roll angle. The response is still dampened but now two of the states return to their initial state.

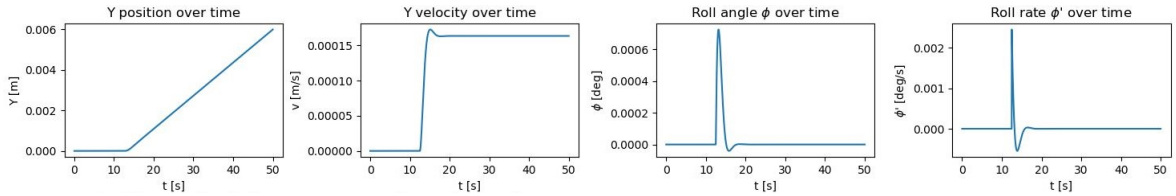

Figure 10.13: Roll response with feedback for roll rate and roll angle

In Figure 10.14 a feedback gain is given for all relevant outputs. By adding the correct feedback gain for each dependency the response can be fully dampened and all states return to their initial state.

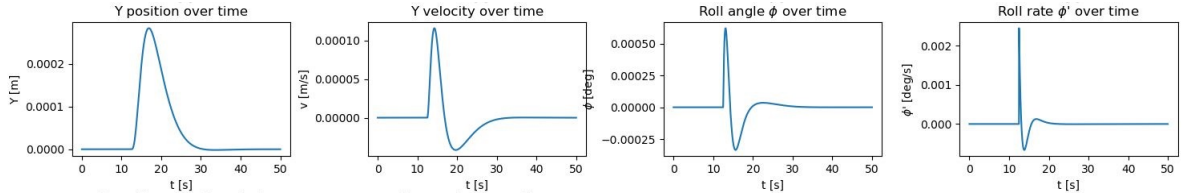

Figure 10.14: Roll response with feedback for all dependent states

This example shows that the states can be controlled by correcting the corresponding control input through a gain matrix. The aim is to dampen the response in a short time interval with a low oscillatory response frequency. This can be achieved by having large negative real parts of the poles and small imaginary parts. Note that the wind disturbances are not control inputs and therefore the gain matrix is zero for the disturbances. The proposed feedback matrix is shown below. The first subscript determines which control input is controlled by the gains and the second subscript determines which output is the gain applied to. For example $K_{\tau_{x_y}}$ refers to the gain that controls the engine torque around x due to the y-position.

$$\begin{bmatrix} e_1 \\ e_2 \\ e_3 \\ e_4 \\ e_5 \\ e_6 \\ e_7 \\ e_8 \\ e_9 \\ e_{10} \end{bmatrix} = \begin{bmatrix} f_z \\ f_{wx} \\ f_{wy} \\ f_{wz} \\ \tau_x \\ \tau_y \\ \tau_z \\ \tau_{wx} \\ \tau_{wy} \\ \tau_{wz} \end{bmatrix} - \begin{bmatrix} 0 & 0 & K_{f_{z_z}} & 0 & 0 & 0 & 0 & 0 & 0 & 0 \\ 0 & 0 & 0 & 0 & 0 & 0 & 0 & 0 & 0 & 0 \\ 0 & 0 & 0 & 0 & 0 & 0 & 0 & 0 & 0 & 0 \\ 0 & 0 & 0 & 0 & 0 & 0 & 0 & 0 & 0 & 0 \\ 0 & K_{\tau_{x_y}} & 0 & K_{\tau_{x_\phi}} & 0 & 0 & 0 & K_{\tau_{x_{\dot{y}}}} & K_{\tau_{x_{\dot{\phi}}}} & 0 \\ K_{\tau_{y_x}} & 0 & 0 & 0 & K_{\tau_{y_\theta}} & 0 & K_{\tau_{y_{\dot{x}}}} & 0 & 0 & K_{\tau_{y_{\dot{\theta}}}} \\ 0 & 0 & 0 & 0 & 0 & K_{\tau_{z_\psi}} & 0 & 0 & 0 & 0 \\ 0 & 0 & 0 & 0 & 0 & 0 & 0 & 0 & 0 & 0 \\ 0 & 0 & 0 & 0 & 0 & 0 & 0 & 0 & 0 & 0 \\ 0 & 0 & 0 & 0 & 0 & 0 & 0 & 0 & 0 & 0 \end{bmatrix} \begin{bmatrix} x \\ y \\ z \\ \phi \\ \theta \\ \psi \\ x' \\ y' \\ \dot{\phi} \\ \dot{\theta} \end{bmatrix} \tag{10.27}$$

For clarity the gains have been included in a separate table (See Table 10.4).

Table 10.4: Feedback matrix gains

Parameter	$K_{f_{z_z}}$	$K_{\tau_{x_y}}$	$K_{\tau_{x_\phi}}$	$K_{\tau_{x_{\dot{y}}}}$	$K_{\tau_{x_{\dot{\phi}}}}$	$K_{\tau_{y_x}}$	$K_{\tau_{y_\theta}}$	$K_{\tau_{y_{\dot{x}}}}$	$K_{\tau_{y_{\dot{\theta}}}}$	$K_{\tau_{z_\psi}}$
Gain	-1e4	2.5e5	7.5e5	3e5	7e4	-2.5e5	7.5e5	-3e5	7e4	5e3

The gains were chosen in such a way that all poles lie on the negative real axis or have no real parts, furthermore the oscillatory frequency (imaginary) part was minimised such that the response is dampened quickly with low oscillation. The pole-zero map of the controlled and uncontrolled system can be seen in Figure 10.15.

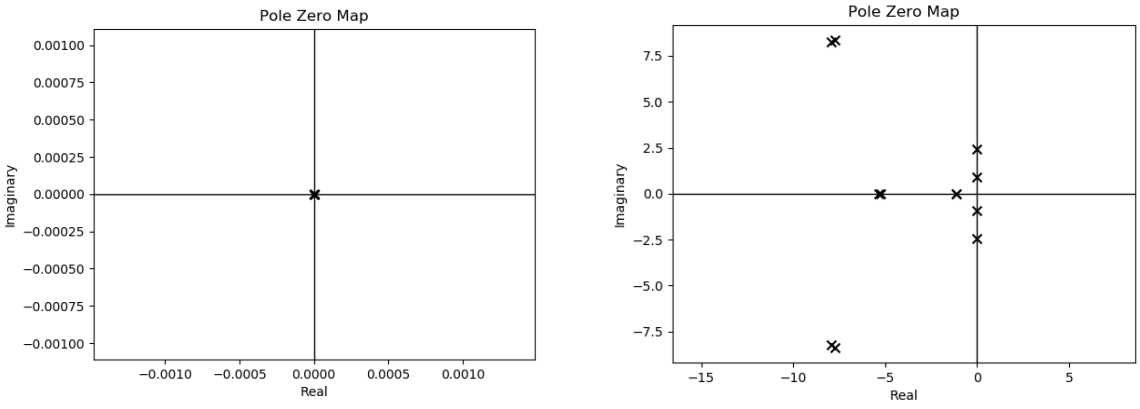

(a) Pole-zero map of uncontrolled system

(b) Pole-zero map of controlled system

Figure 10.15: Pole-zero map of the controlled and uncontrolled state space model

From Figure 10.15a it is clear that the uncontrolled system is marginally stable, the poles do not have an imaginary or real part which leads to unbounded outputs. A small disturbance leads to an uncontrolled output. Figure 10.15b shows the revised pole zero map, it is now clear that 2 poles and their complex conjugate are still marginally stable but all other poles have a negative real part and therefore dampen the response over time. By changing the imaginary part of the stable poles the oscillations during the response can be altered. Various combinations of gains are evaluated until the response is controlled in a rapid and smooth manner. At this stage the controlled system's response to various disturbances can be evaluated, this will be the subject of the next subsection.

10.9. Control of Quadcopter

After deriving the feedback gain matrix the state space model can be controlled, this is done by adding a feedback loop to the system. In order to test the system's response to various disturbances multiple case studies will be considered. The case studies of interest will be: the system's response due to non-zero initial conditions, the system's response due to non-zero disturbances, the system's response due to non-zero initial control inputs. Note that these case studies are the same as for the analysis of the system stability.

The first case study is shown in Figure 10.16 where the system response is evaluated for non-zero initial conditions, for this case the initial conditions were set to 1 for all states.

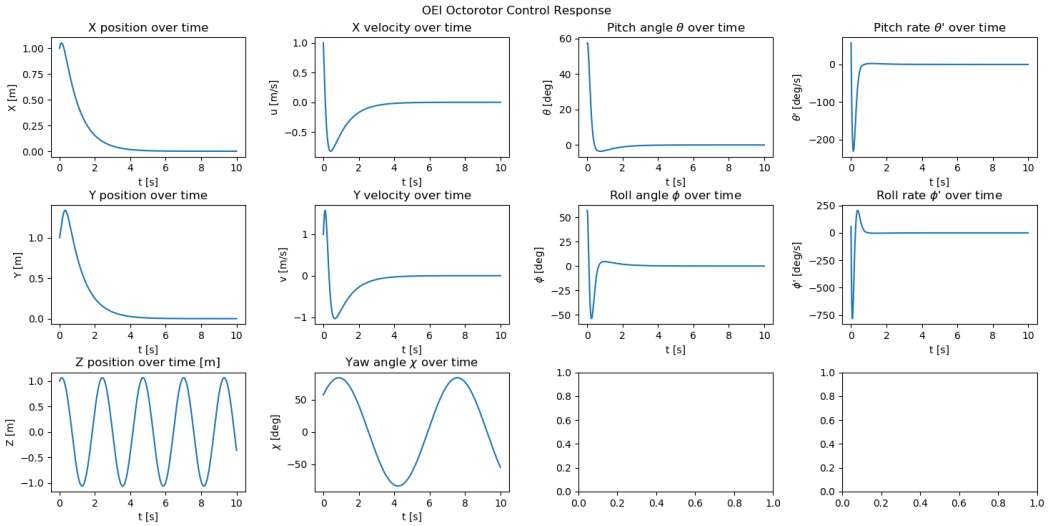

Figure 10.16: Controlled quadcopter response to non zero initial conditions

In Figure 10.17 the system response is shown for an impulsive disturbance input, all the disturbances are set to be 1 at $t = T/4$.

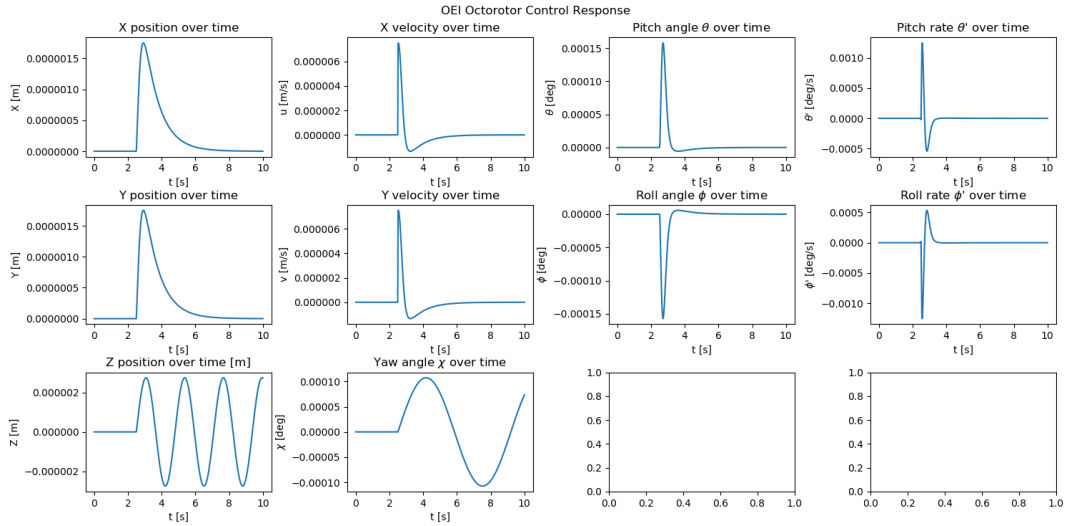

Figure 10.17: Controlled quadcopter response to impulsive disturbance inputs

Finally, in Figure 10.18 the system response is shown for an impulsive control input. In this case the control inputs are set to 1 at $t = T/4$.

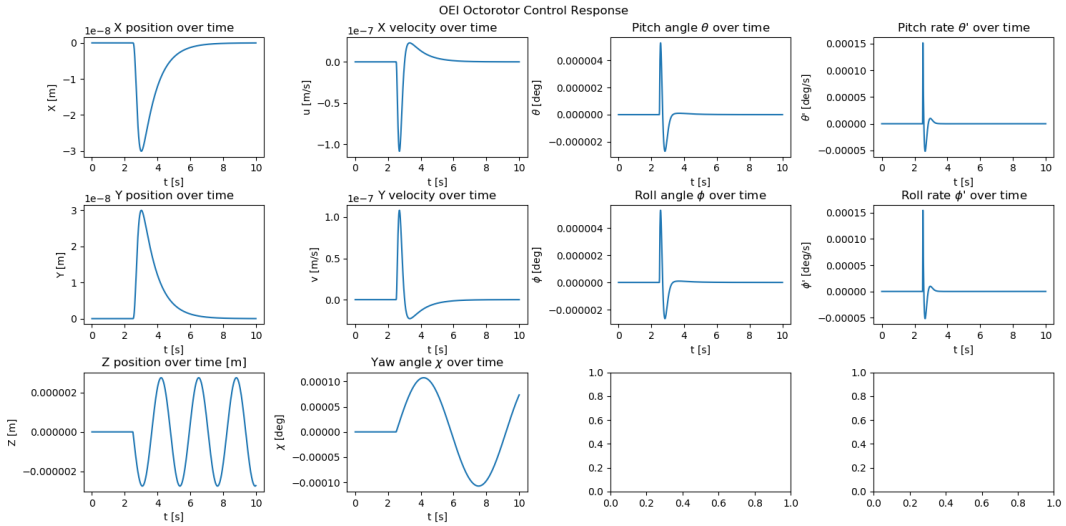

Figure 10.18: Controlled quadcopter response to impulsive control inputs

From the three aforementioned case studies it is clear that the system is partially stable. The roll-axis is stable as a disturbance in y-direction or around the x-axis leads to a dampened response where the states go back to their initial state. This is also applies to the pitch axis. The system is only partially stable as in the vertical axis (yaw angle and z-position) the states oscillate around their initial state after a disturbance, this corresponds to the poles with no real parts. The system can be considered stable as all states tend to their initial state after a disturbance, the oscillations in or around the z-axis are only marginally stable.

The system's response was evaluated for impulsive inputs, this is not the only loading scenario that the craft needs to handle. Therefore, the system's response due to a step disturbance input is also evaluated. Figure 10.19 shows the response due to a step disturbance input where the disturbance is equal to 1 for $t \geq T/4$.

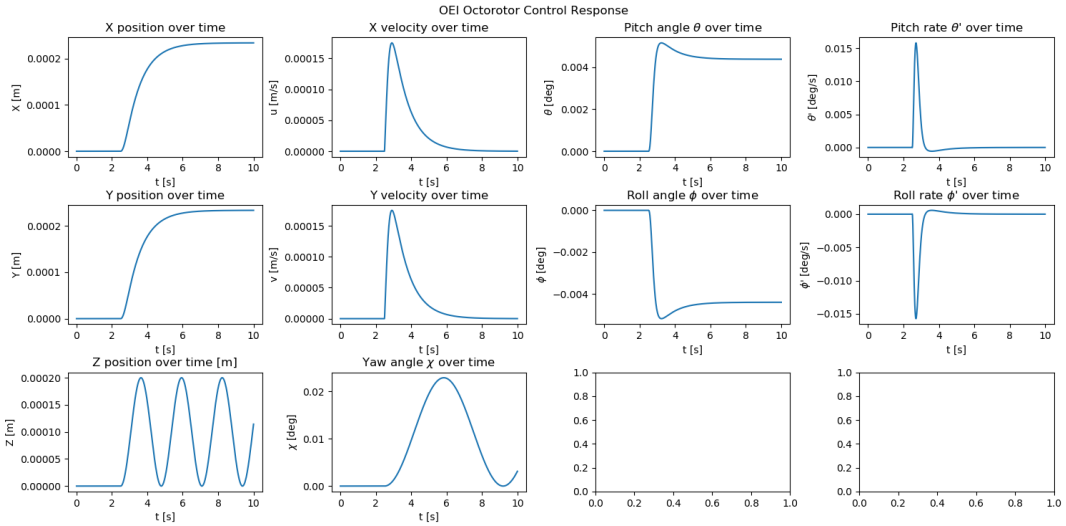

Figure 10.19: Controlled quadcopter response to step disturbance inputs

It is clear that the system is able to stabilise under a step disturbance input, the velocity, angle and angular rate return to their initial state. However, the system is unable to return to its initial position in x and y. This is because there is a continuous disturbance input so the craft must counter-act the disturbance continuously which prevents the craft from returning to its initial position. This is because

the craft must stay at a constant angle to counter act the disturbance. Once again the vertical axis is marginally stable.

This shows that the system is controlled and its stability has been addressed, the next step is to study the system's response to the disturbances identified in Section 10.3

10.10. Controlled Response to Operational Disturbances

In order to characterise the performance of the controlled state space model the system response to the operational disturbances will be analysed. The magnitude and time-evolution of the disturbances was derived in Section 10.3.

10.10.1. Controlled response to gust disturbances

In order to evaluate the system response to a gust disturbance the gust load and torque are input to the system in all directions. The gust disturbance inputs in each axis are shown in Figure 10.20. The gust disturbance was generated using the gust model.

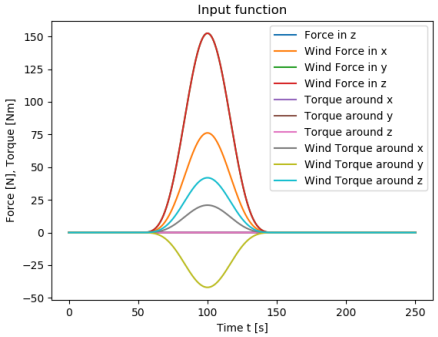

Figure 10.20: Quadcopter disturbance certification inputs

Using the given disturbance inputs the system response to the maximum gust loading can be evaluated. The system's response is shown in Figure 10.21.

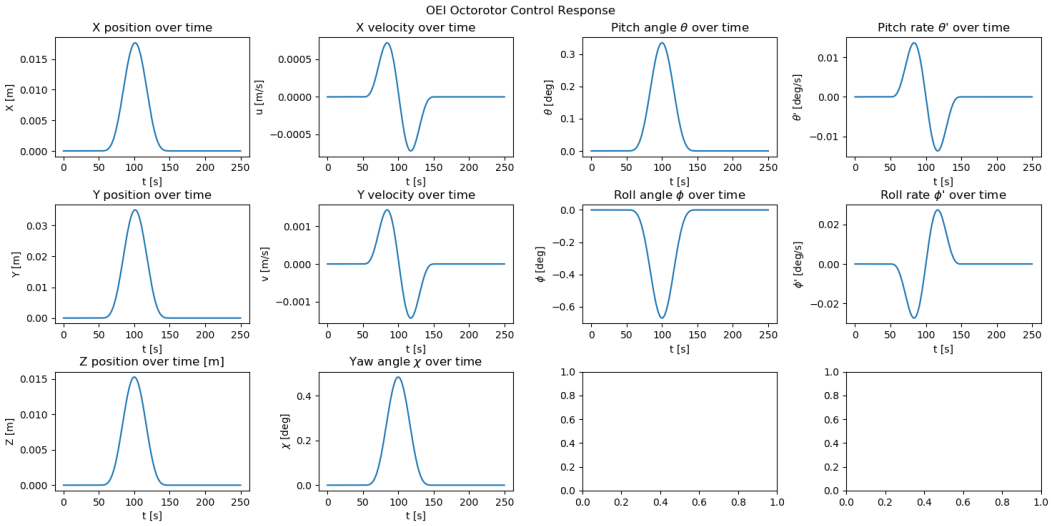

Figure 10.21: Controlled quadcopter response to operational disturbance inputs

From Figure 10.21 it is clear that the gust disturbance is controlled and the system is able to stabilise. Furthermore, the response is dampened quickly with little oscillations. Note that the z-position and yaw

angle look stable, this is due to the smooth input, in reality both states are marginally stable and will oscillate around their initial state. The craft only displaces by a total of 3 *cm* in x- and y-direction due to the maximum gust loading, on top of that the craft's change in angle is less than 1 *deg*, which is good for payload safety and comfort.

Due to the smooth nature of the input function the response is also very smooth, this means that the system's shall be analysed for discontinuous input functions as well. For the discontinuous input case study a square wave of equal magnitude and length to the maximum gust load will be applied, the response is shown in Figure 10.22.

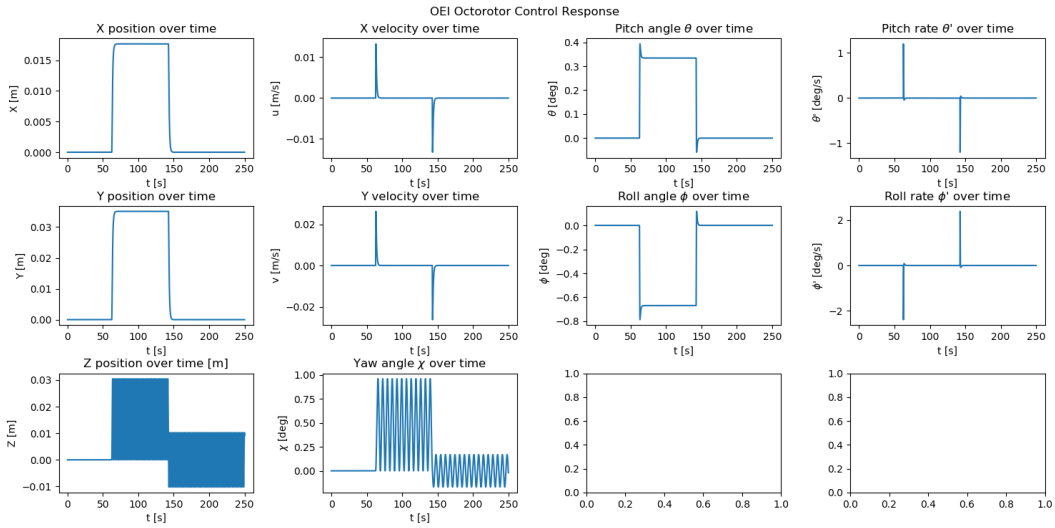

Figure 10.22: Controlled quadcopter response square wave gust disturbance input

Once again the system is able to stabilise the disturbance. Here the z-position and yaw angle exhibit their marginally stable behaviour unlike in Figure 10.21, this is because the function is discontinuous. This shows that the control system's behaviour not only depends on the magnitude of the disturbance but also its shape. For discontinuous inputs the system tends to oscillate more.

The control system is able to control the craft and return to its initial position due to gust disturbances. Using the CS25 certification method it can be said that the craft is able to resist gust disturbances. This ensures the payload is safe during nominal flight conditions. Next the system's response to changes in centre of gravity will be analysed.

10.10.2. Controlled response to CG shifts

When boarding the payload there will be instants in time where the CG is unbalanced (See Section 10.3. This happens when the payload is boarding asymmetrically and leads to a torque unbalance around the x- and y-axis. In order to simulate the torque applied due to a shift in CG assumption A5 will be used. Assumption A5 assumes that the payload boards instantaneously, this means that the torque is applied instantaneously and is constant in magnitude for a certain amount of time. In order to account for the worst case scenario the torque around x and y due to CG shift will be applied as a square wave for half the estimated boarding time. The corresponding input functions can be seen in Figure 10.23.

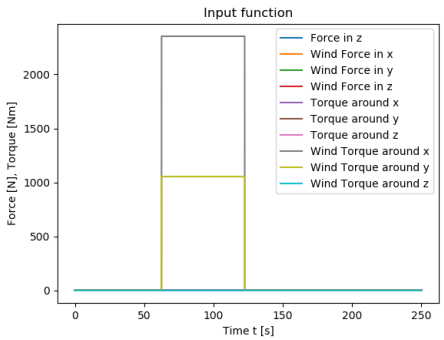

Figure 10.23: Quadcopter CG imbalance disturbance inputs

Moreover, the system response due to a disturbance input corresponding to the maximum CG imbalance in both x and y direction can be seen in Figure 10.24.

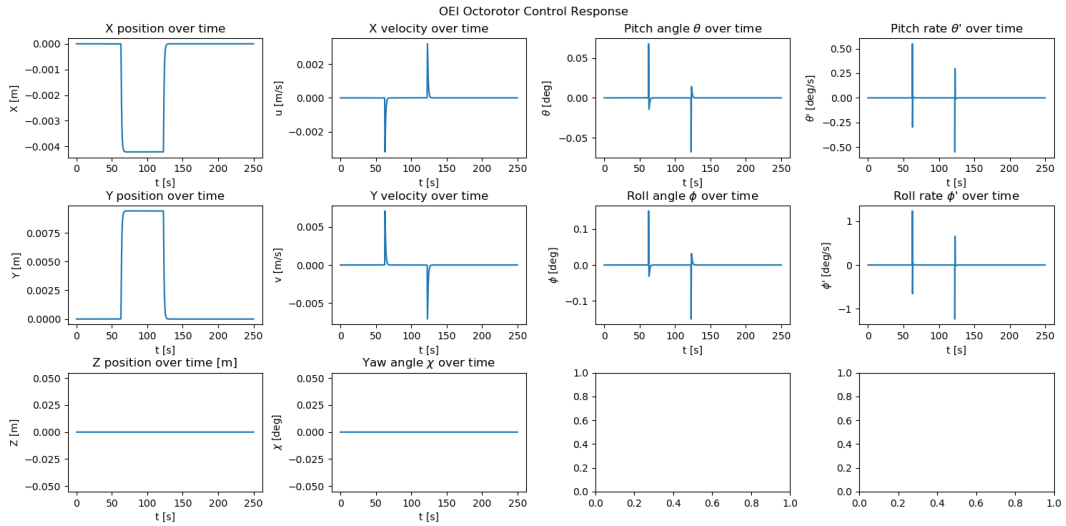

Figure 10.24: Controlled quadcopter response square wave CG disturbance input

When taking a look at Figure 10.24 it is clear that the system is able to control the disturbances due to a CG imbalance. The response is dampened quickly and the oscillations are kept to a minimum. Furthermore, the maximum displacement due to a CG imbalance is less than 1 *cm*. This is deemed safe for passenger boarding and transport.

This concludes the analysis of system response due to various operational disturbances. The system is able to stabilise and return to its initial state for a range of disturbances. The last step is to study the case for One Engine Arm Inoperative (OEAI), which will be done analytically in order to verify the robustness of the state space model.

10.11. One Engine Arm Inoperative Control

To have all the critical conditions inspected, the OEAI has to be analysed in full detail. The case where a single engine fails is neglected and only a failure of a full arm is analysed due its importance as discussed previously. Due the absence of sophisticated simulation tools designed explicitly for the analysis of critical loading scenarios, several assumptions are made in order to simplify the manoeuvre. These assumptions can be seen in the list below.

- A8 : Zero net torque on the system during OEAI
- A9 : Propeller thrust is constant in time

- A10 : Motion controlled if the final velocity and angle return to their initial state

First, the yaw in OEAI case can be neglected if other counter-spinning engines are equal in torque due the symmetry of the craft. Lack of yaw implies that the roll and pitch induction characteristics of the craft due yaw oscillations are mitigated, which leads to OEAI being pure rolling and rolling caused translation. As second, the acceleration of the motors is assumed to be constant for which the drag of the propellers is assumed to be negligible. The constant acceleration implies that external disturbances such as gusts are neglected for the analysis, as these are implemented with the help of the state-space (SS) model. Lastly, the motion is assumed to be complete if the end velocity and the roll angle returns to equilibrium. The position can be deviating from the null with respect to initial conditions, as else the manoeuvre becomes too unsafe to be executed. The calculations performed for OEAI case are performed analytically. This derivation is also used to verify the state-space model. The verification consists of feed-forwarding the programs intermediate outputs into the state-space model and comparing the end results. The program is based on numerical integration with a time step of 0.01 in which all accelerations are assumed to be constant. This is the same time discretisation as for the state-space model.

To define the initial conditions of the case, the failure mode of the craft has to be designed. There are two main failure methods, namely an electronics/software issue such as a short-circuit or a bug and debris critically damaging the craft. Assuming that a debris' impact is so severe, that the initial moment caused by the collision cannot be counteracted in time by reversing the engines, only the electronics failure mode will be discussed further. For electronics to fail both engines at the same time, the HV battery has to terminate the power line to the motors. Assuming such a scenario, one can conclude that the failed motors will not stop immediately, thus there will be marginal thrust generated. It is assumed that initially the engines are 80% operational and then gradually reduce to 40% in systems response time, which is defined as the time in which the gyroscopes notice the disturbance. The total response time was estimated to be 0.2 *s*. During the response, the accelerations in all directions are assumed to be varying with the angle as given in Equation 10.28.

$$a_{x_i} = \frac{T_i sin\theta_{x_i}}{M_{tot}} \tag{10.28}$$

In Equation 10.28 T_i is defined as total thrust at a particular time instant i, θ_{x_i} is defined as the roll angle and M_{tot} is the total mass of the craft taken to be at full payload as critical case. For acceleration in y-axis the pitch angle replaces the roll angle, while for the z-axis acceleration the sine becomes a cosine and the weight has to be taken into account. The velocity and position can be computed by integrating Equation 10.28 assuming a constant acceleration. The angular acceleration can be computed using Newtonian physics for rotation as described by Equation 10.29:

$$\alpha_{x_i} = \frac{M_x}{I_{yy}} \qquad\qquad M_x = dT_i \cdot D_{arm} \tag{10.29}$$

where M_x is the moment around x-axis, I_{yy} is the moment of inertia around y-axis, dT_i is the thrust difference between the diagonal engines and D_{arm} is the arm between the diagonal engines divided by two. The angular velocity can be acquired assuming constant α and integrating it once, while the rotational angle requires two integrations. After the response time the autopilot will take control and stop the engines located diagonally from the failed motors. During this time, it is assumed that the failed engines will reach stand still at exactly the same time as the manually stopped motors. The motion characteristic parameters can be computed using the same formulae as for the response time. Additionally, while the engines are stopped, the four complementary engines' rotational speed are increased until they reaches 1.9 times the initial thrust value ($T_i nit$ give $\frac{T}{W}$), such that the crash landing can be survived by the evacuees. The reversal of engines opposite to the failed ones follows as the next step in the manoeuvre, where the throttle is set for thrust levels of -0.5 of the initial thrust value and the time of application is equal to 0.95 *s*. The time defined does not include the engine re-acceleration as it is implemented separately just like the engine stop time. When the counter rotation has been performed, the engines are stopped again and accelerated to 0.25 original thrust and run for 1.62 *s*.

Lastly, the final acceleration to level the craft is -0.1 thrust over weight ratio applied for 1.43 *s*. The total manoeuvre envelope can be seen in Figure 10.25. It can be noticed that the final roll and pitch angles and the velocities in lateral direction reach equilibrium stage, however, the position does not return to zero. The position is not forced to reach initial conditions as doing so with manual programming is inefficient due the more sophisticated tools as the SS model which has gain feedback loop.

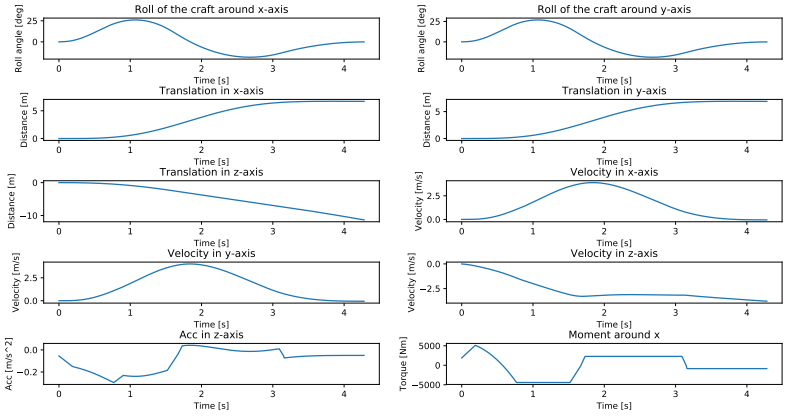

Figure 10.25: OEAI manoeuvre envelope

10.11.1. State-space model verification using analytical OEAI model

The state-space model derived earlier will be the primary model used for control. Before the state space model can be used it must first be verified and validated. This can be done using different methods, the chosen method is to use the analytical OEAI control derivation to verify the consistency of the state space model.

When studying OEAI an analytical derivation using the equations for translational and rotational motion was performed. The result of the analysis is the craft's position, angle, velocity and angular rate for a given thrust and torque input. In order to validate the uncontrolled state-space model, the calculated thrust and torque input from the analytical derivation will be input to the state-space system. The system response due to the control inputs from the OEAI derivation can be seen in Figure 10.26. Note that the feedback matrix is a null matrix as the analytical derivation for OEAI does not include a controller.

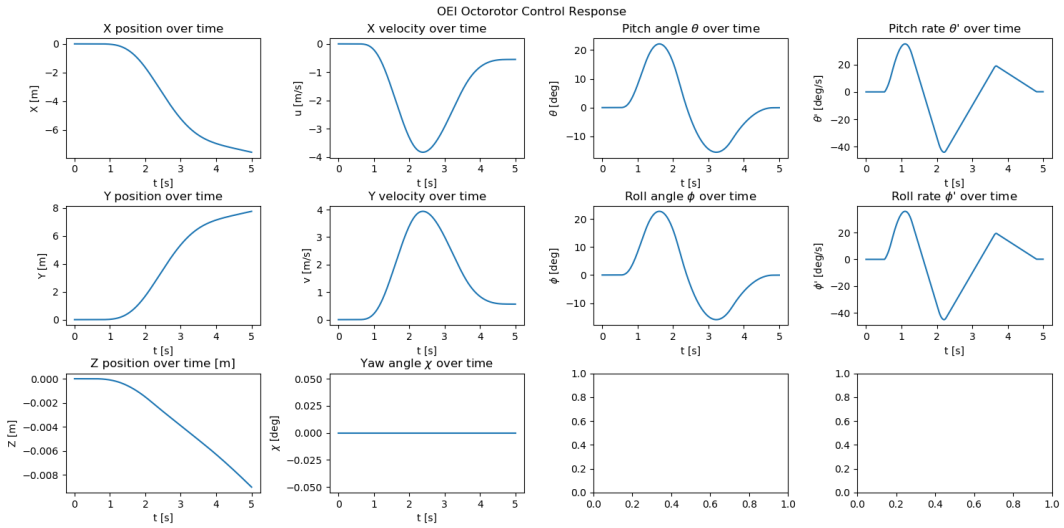

Figure 10.26: Uncontrolled quadcopter response to analytical OEAI control inputs

There is a clear match between Figure 10.25 and 10.26, the states behave in the same way for both the uncontrolled state-space model and the analytical derivation used for the OEAI manoeuvre. This validates the results of the state-space model and the OEAI case. It should be noted that the controlled system is better at controlling the OEAI condition than the analytical derivation. Overall, the craft behaves in the same way for both the analytical and state-space model. Note that for a longer simulation time the craft's states tend to infinity due to its inherent instability. This concludes the analysis of the stability and control characteristics of the system, the results of the analysis will be discussed in the next section.

10.12. Results

The system is able to control the craft throughout operations to a large extent. The results of the control analysis will be discussed here.

First, it should be noted that the uncontrolled system is inherently unstable and the proposed control method is able to partially stabilise all the states. Furthermore the control system exceeds all control system and subsystem requirements. Finally the required control torque for the maximum disturbance scenario (See Figure 10.27) can be achieved by the rotors with the available power at the power required for ascent (maximum power scenario).

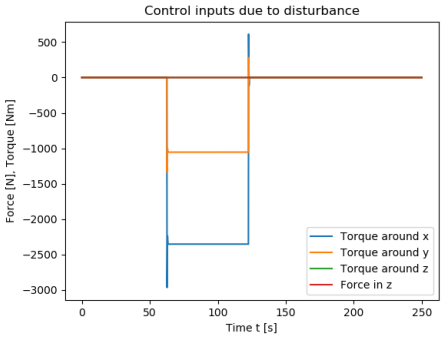

Figure 10.27: Required control torque to counter-act disturbance

The maximum required control torque is 2966 *Nm*, assuming that the minimum distance to the centre of gravity is the radius of the propeller (in reality it will be more) this means an additional 355 *N* of thrust per arm is necessary for the maximum disturbance scenario. This fits within the thrust budget of the craft. An overview of all relevant stability and control characteristics is shown in Table 10.5.

Table 10.5: Stability and control characteristics of controlled system.

Parameter	x-axis	y-axis	z-axis
Gust disturbance force [N]	96.60	193.2	193.2
Gust disturbance torque [Nm]	20.9	41.9	41.9
Gust SS response max. displacement [mm]	17.6	35.0	30.5
Gust SS response max. rotation [deg]	0.786	0.393	0.961
CG max. differential thrust [N]	409	996	0
CG disturbance torque [Nm]	1054	2353	0
CG SS response max. displacement [mm]	4.21	9.41	0
CG SS response max. rotation [deg]	0.151	0.0678	0

The control system's performance is very robust as the maximum displacement due to any disturbance is 35 *mm*, this accounts for the absolute worst case scenario disturbance which is unlikely to happen. In order to put this into perspective this corresponds to three 100 *kg* passengers jumping on the left

most side of the craft uninterruptedly for 60 *s*. This is leads to a very large moment and yet the system only displaces by a total of 3.5cm before it returns to its initial position. Furthermore the disturbance is counteracted in less than 2 *s*. This demonstrates the robustness and efficiency of the control system which is able to fully stabilize the craft due to any disturbance in a manner that is barely noticeable for the evacuees. Next, the limitations of the control model and approach will be discussed and some recommendations will be proposed.

10.13. Limitations & Recommendations

Overall, the control system is able to partially stabilise the craft and return to its initial state after a disturbance. Furthermore, the system performance exceeds the relevant requirements, however it also has some clear limitations.

The first limitation of the system is that the system is only marginally stable in z-direction and around the yaw-axis, this is because there is only one term in the feedback loop for the respective control inputs. This is due to the nature of the output vector, it only contains the z-position and the yaw angle, this was chosen since it is preferable to have a square C matrix. Furthermore, the impact of marginal stability (in z- and yaw-axis) on the system performance is deemed not critical. In order to stabilise the z- and yaw-axis the system should also output the z-velocity and yaw rate, given that those are states this can be implemented without changing the state equation. By outputting the velocity and angular rate as well an extra term can be added to the feedback loop for the force in z and the torque around z, this make the real part of the poles non-zero and would lead to a dampening effect. Due to time-constraints this was not implemented but will be at a future stage in the project.

Another limitation of the system is that its control inputs are the force in z-direction, and the torque around each axis. It would be preferred to have the individual rotor thrusts as inputs. This means that an extra layer of computing and control must be applied to convert the individual thrust of the rotors to the chosen control inputs. In order to convert the individual rotor thrusts to the control inputs the distance from the rotor to the craft centre of gravity must be known at all times and converted to a torque around the relevant axis. Given that the system has a movable rotor system the distance to the centre of gravity changes throughout operations. This limitation can also be an advantage as the distance to the centre of gravity is not part of the equations of motions for a 6 DOF state space model unlike the 3 DOF model [35]. This means that the matrices inside the state equation stay constant by having a separate computing unit that converts the rotor thrusts into the respective control inputs. This is preferable as the pole-zero map will be constant throughout operations.

The control approach also has some limitations. The feedback matrix that is proposed does not generate a perfectly smooth response, the angular rates and angle oscillate slightly. This was chosen in order to have a responsive and reactive system that can maintain its position in space. In order to mitigate this the feedback matrix could be further refined to be smooth for all states, this would lead to a lower dampening factor. Alternatively, multiple gain matrices can be used for different flight scenarios during approach, docking, boarding and landing the propose feedback matrix can be used. For a smoother hovering, ascent and descent a feedback matrix that leads to a smoother response can be used as larger variations in position are acceptable during those phases.

Finally, the system does not take into account the time needed to increase or decrease the rotor thrust. This means that the control system is able to vary the torque around each axis very quickly, in reality there will be a delay which might lead to larger magnitude in the response. This can be overcome by inputting the motor velocity as the control inputs. This would require an extra layer of computing again where the motor velocity is converted to motor thrust and finally to the current control inputs. This way the motor speed limitations can be taken into account.

10.14. Conclusion

Overall, the current craft configuration is not stable but controlled in such a way that operations can be performed efficiently and safely. The systems stability is extremely robust and barely reacts due to all potential disturbances. This was proven through a stability and control analysis by means of state-space model for a quadcopter configuration. The analysis started by identifying the critical operational phases which were hovering, landing and docking approach. Then the operational disturbances were

identified and modeled. The dynamic model of the quadcopter concept was derived, linearised and used to construct a state space model. The next step was to investigate the natural stability of the craft which demonstrated that the craft was inherently unstable. A control approach was chosen and the process of gain tuning was performed in order to control the unstable craft. Using the chosen feedback matrix the craft's controllability was evaluated and several responses were analyzed. As a final verification step the controlled craft model was tested against the worst case scenario disturbances. The results of the analysis were evaluated and some limitations and recommendations of the control system were given. In the future, the control system will be improved such that all states are stabilised, this will require increasing the amount of outputs and changing the gain matrix. Next the structural characteristics of the craft will be detailed.

11. Structural Characteristics

In order to satisfy the mission requirements, safely housing the evacuees throughout, it is necessary to provide the vehicle of a structure that bears the loads it is subjected to. The design and analysis of this structure is the topic of this chapter, with the goal of satisfying the system requirements as described in [2]. This is done by first analysing the system as a whole, and then subdividing it into components that can be analysed and designed separately.

The design of each component starts by assuming one more geometries, or by choosing readily available components. The stresses in these geometries are then determined analytically, or sized for directly using modelling and analysis software. When solved analytically, the geometry is optimized for minimum mass using Python scripts. This geometry is then verified using validated software analysis software. For the modelling and analysis of components, the software CATIA is used.

Due to the time constraints and scope of the project, the structural design is limited to the main components of the system. Secondary structures such as equipment or electronics supports, along with joining methods, holes and cutouts are not considered. These non-critical components must be designed and analysed in the post-DSE phase.

11.1. Global Analysis

To design and produce an analysis on the system's components, it is necessary to first study the system as a whole and identify the loads it must withstand. In doing this, it is necessary to make some simplifications and assumptions in order to make the design problem solvable within the time constraints of the project. At a global level, the following assumptions are made about external forces:

- **ASUM-SYS-1**: Aerodynamic forces other than propeller thrust are negligible
- **ASUM-SYS-2**: The vehicle lands perfectly upright
- **ASUM-SYS-3**: Friction force with ground negligible

The first is considered valid since the system operates at relatively low free-stream velocities. For the second, this is considered valid since high system controllability is possible as demonstrated in Chapter 10, meaning that precise upright landing should always be possible. This means only forces normal to the ground are introduced during landing. In reality, more aggressive landings may occur for the sake of higher rescue rate. This should be investigated further in post-DSE, but for the current stage the model is deemed sufficient. Once these assumptions are made, it is possible to analyse the system as a whole to identify relevant loads. Based on the preliminary configuration in the mid-term report [2], a Free Body Diagram (FBD) of the system as a whole can be made, shown in Figure 11.1.

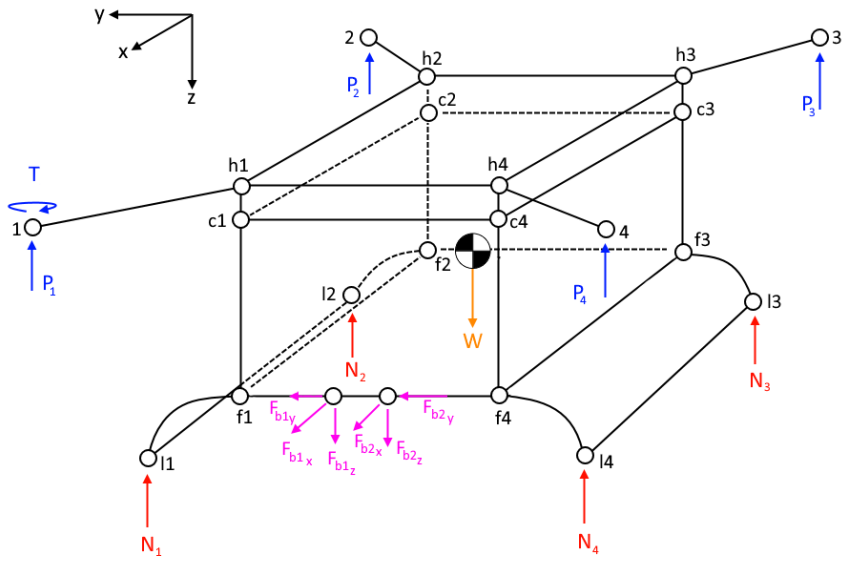

Figure 11.1: Global FBD of vehicle

The loads which enter the structure through the environment are:

- Force due to propeller lift: This force is caused by the propeller and corresponds to anywhere between 0 and 6365 *[N]* depending on the loading condition. This force points in the negative z-direction relative to the vehicle centred body axis.
- Torque due to one engine inoperative: This torque corresponds to the torque produced by one engine. This torque is equal to 542 *[Nm]* This load is introduced into the structure in the case when one engine fails, and the torque produced by the other is no longer balanced.
- Weight: This force is caused by the mass of the vehicle, and consists of a vector pointing down in the earth centred axis
- Bridge force: This force is caused by the interaction of the tip of the bridge and the building. It consists of a vector that can take any orientation relative to the vehicle centred body axis. This force only appears in loading conditions where the vehicle is in the docking phase.
- Bridge moment: This moment is introduced at the tip of the bridge from interactions with the building, analogous to the bridge force.
- Landing gear force: This force is caused by the normal force exerted from the ground onto the landing gear. This force only appears in loading conditions where the vehicle is landed.

After having identified all relevant forces, it is possible to further simplify the problem by performing cuts on the structure and identifying individual structural components of interest. It was consequently decided to split the vehicle into six main sub assemblies. These are the following:

1. Rotor arm
2. Hinge
3. Drone Centrepiece
4. Cabin
5. Bridge
6. Landing gear

These are these all visible below in Figure 11.2

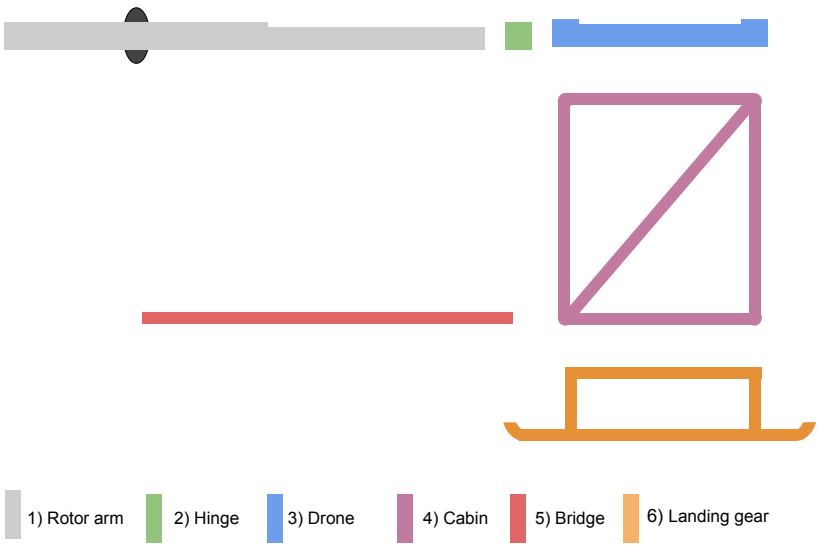

Figure 11.2: Craft subdivisions

The goal with this is to first perform an analysis on the parts of the system that receive loads from the external environment, and work towards the cabin. This is because if the analysis follows the paths of the loads, each time that a piece is analysed, the relevant reaction forces on the next component will be calculated as they are equal to the internal forces at the end of the component.

At this point the materials for the analysis are also chosen. It is determined that those components for which standard parts are not available or commonplace will be sized using common aerospace materials. This was done to ensure the ability to source materials for production. The materials initially being put under scrutiny were aluminium alloys, steel alloys and titanium alloys. It was decided not to consider anisotropic materials such as composites as these have significantly less predictable failure methods, and therefore would have rendered the analysis too complex. Furthermore composites are generally much more expensive than metal alloys. The information taken on these materials was compiled from [36] [37] [31] [32] [33] [34] [35]. The data is shown below in Table 11.1.

Table 11.1: Materials for structural analysis

Material	E [GPa]	G [GPa]	σ_y [MPa]	τ_y [MPa]	ρ [kg/m^3]	Cost [USD/kg]
Aluminium 7075-T651	71.7	27.5	501	331	2700	1.8
Aluminium 2024-T4	73.1	28.0	324	283	2770	2
Aluminium 6061-T6[36]	68.9	26.0	276	207	2700	2.4
Titanium 6Al4V	100	40	910	550	4500	16.25
Steel, high strength 4340	210	76	1240	620	7800	0.25
Steel, mild 1020	210	76	200	100	7800	0.25

[31] URL https://web.mit.edu/course/3/3.11/www/modules/props.pdf [cited 10 June 2021]
[32] URL https://www.thomasnet.com/articles/metals-metal-products/2024-aluminum/ [cited 10 June 2021]
[33] URL https://yctsteel.en.made-in-china.com/product/fXIElKYDhvrB/China-Factory-Alloy-Alu-Sheet-T651-7075-6061-T6-Aluminum-Price-Per-Kg.html [cited 15 June 2021]
[34] URL https://onlinelibrary.wiley.com/doi/epdf/10.1002/adem.200310095 [cited 12 June 2021]
[35] URL https://kyocera-sgstool.co.uk/titanium-resources/titanium-information-everything-you-need-to-know/ti-6al-4v-grade-5-titanium-alloy-data-sheet/ [cited 12 June 2021]
[36] URL http://www.matweb.com/ [cited 19 June 2021]

In order to aid with the design, it was deemed necessary to use and in some cases create different tools for structural analysis of specific parts of the vehicle. It was noted that some of the components could be analysed as beams under loading, as the case for the rotor arm and bridge, some as truss structures, as is the case for the cabin, and some could be sized based on existing components, such as the landing gear. These methods are covered in the subsequent sections.

11.2. Rotor Arm Analysis & Design

The rotor arm is the structural component which connects the propeller to the drone's hinges. This component was selected as first for the analysis as it lies at the edge of the craft, and therefore, by performing a first analysis on it, some relevant loads into the drone centrepiece may be found. Furthermore, all four rotor arms are identical, and therefore only one is necessary to analyse under all loading conditions.

The rotor arm must carry the load induced by the lift of the engine as well as the torque induced by the one engine inoperative condition. It is determined that the combination of these two external loads cause the critical loading condition. Thrust will not be nominal in the case where one engine is inoperative, however, at the instant where one of the propellers stops producing torque, it is still rotating at velocity, and therefore generating lift. Because of this, there is an instant where both propellers on one arm are producing full lift, but only one is producing a torque. This is therefore the maximum loading the arm will experience in operation and therefore the one under analysis.

There are additional geometric constraints to add to the design to limit its size. The first of these is the length, which is determined from the stowage arrangement during transport of the propellers in Chapter 7. The length used is the minimum one which can satisfy this condition, which is 1.7119 *m*, rounded up to 1.72. This value is also shown in Table 11.2. Another requirement is that the rotor arm may not occupy a volume of more than 0.315x0.315x1.72 [m]. This follows from the height requirement of the centrepiece Section 11.5 times an additional factor of 1.05 which is estimated form the distance of the hinge. The rotor arm is also expected to have a vertical deflection less than 0.02 *m*. This value is taken from the need to remain within the small angle approximation to assume vertical lift Section 8.2.

To analyse this component an additional assumption was introduced:

- **ASUM-ROTORARM-1**: The rotor arm can be modelled by a beam clamped at one side. While the arm is attached to a hinge, this hinge is ultimately controlled by actuators and can be kept fixed. Because of this, the condition for which the loading will be more critical is when induced moments are allowed to pass through the hinge. This yields a loading condition similar to that of a beam clamped to one side, and consequently this assumption was determined to be valid for this case.

By analysing the rotor arm as a beam with all aforementioned assumptions, it is possible to create a free body diagram of the rotor arm as shown below in Figure 11.3.

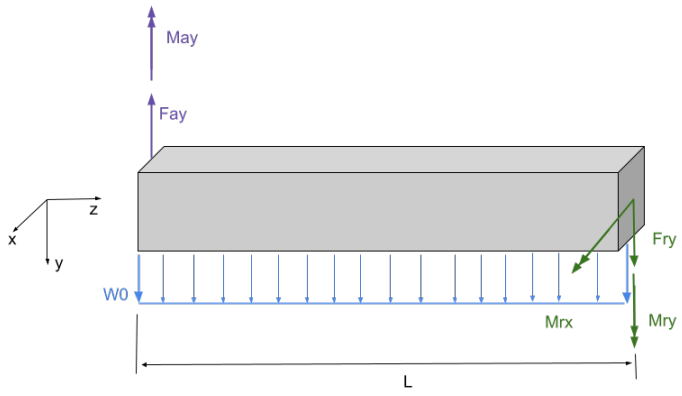

Figure 11.3: Rotor arm free body diagram

This simplified component can now be straightforwardly analysed and an internal loading diagram may be produced. Furthermore the value of the force and torque acting on the beam may be seen below in Table 11.2.The value used for the maximum force F_{ay} is computed from the maximum weight, multiplied by the maximum thrust to weight ratio and divided by the number of arms. Given the repeated loading of this component within it's lifetime, and the danger in case of it's failure, an additional factor of 2 was imposed on the thrust force. M_{ay} is determined straightforwardly from the maximum torque one engine can exert.

Table 11.2: Rotor beam computation inputs

Variable	F_{ay} [N]	M_{ay} [Nm]	$L_{rotorarm}$ [m]
Value	12740	542	1.72

It is now possible to determine the internal loadings and deflections. The internal ladings are produced from a script which uses the method of cuts with Malacauy functions [38] to determine the internal reactions at every point in the beam. Computing deflections, instead, is done through the use of Euler Bernoulli beam theory [38] and the formula below, Equation 11.1.

$$M = -EI\frac{d^2v}{dz^2} \tag{11.1}$$

This is done by integrating the moment function twice and applying the boundary constraints to solve for the constants of integration. The results of this are then plotted and the maximum value of deflection is returned.

The use of this formula introduces an additional assumption:

- **ASUM-EULER-1**: Euler Bernoulli Beam theory is an adequate representation of beam deflection for this purpose.

Having done this, it is now possible to analyse the internal loading and deflection of the beam.

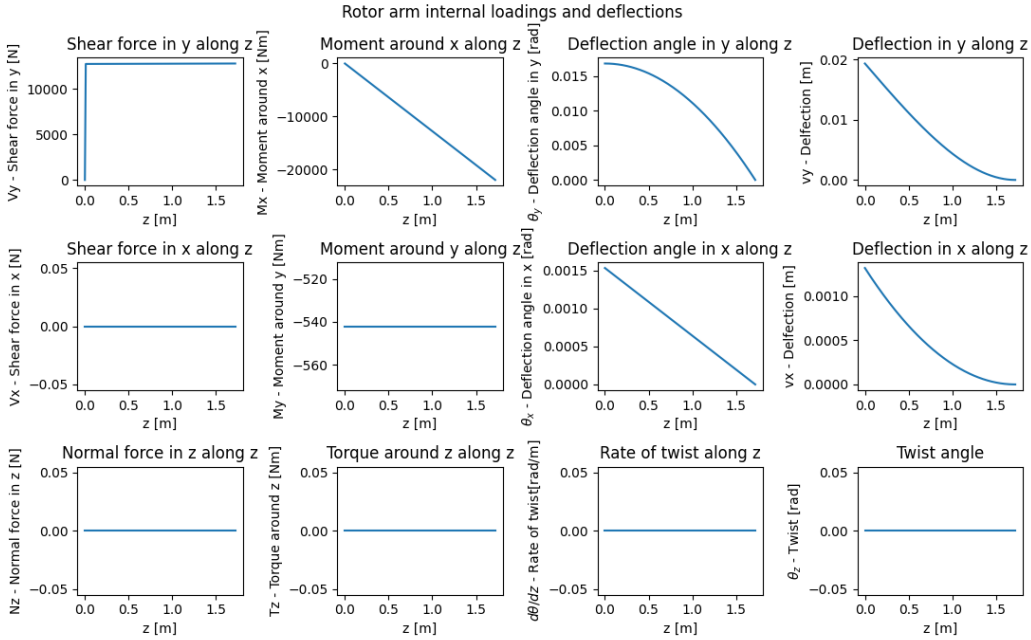

Figure 11.4: Internal loading and deflections of the rotor arm

It is important to note that the results are computed with the use of one iteration of cross section corresponding to Aluminum 7075 T651. Therefore the deflections are iteration specific and are not general to all the beams. It can additionally be confirmed that the deflections of the beam in both the x- and y-axis lie between the imposed bounds.

The maximum loading position can now be identified as being the centrepiece side of the beam. These internal loads are shown below in Table 11.3

Table 11.3: Rotor beam maximum internal loads

Internal load	F_{ry} [N]	M_{ry} [Nm]	M_{rx} [Nm]
Value	-12788	-542	21953

It is now possible to test different cross sections to these loads and optimize for mass. It was decided to only test closed section symmetric beams. The reasons for this was that closed cross sections have superior properties against torsion. Additionally, a closed interior may provide housing for electronics and additional subsystems.

The analysis was only limited to two types of cross sections, these were a circular and parallelogram thin walled cross sections. With this decision the thin walled assumptions are introduced in the problem.

- **ASUM-TOOL-1**: Thin walled assumption [39].

It was decided at a later point to only treat cross sections with a constant thickness due to the difficulty of accounting for stress concentrations caused by variations in thickness. The cross sections tested were all those sections in the ranges from 0 to the maximum height, width, and skin thickness, with in total 20^3 iterations per material.

Now a safety factor can also be imposed on the stress constraints. This was chosen to be 1.5 [40]. From this result, the normal stress distribution at every point on the cross section can be computed using Equation 11.2 in the point of maximum loading.

$$\sigma = \frac{M_x \times y}{I_{xx}} + \frac{M_y \times x}{I_{yy}} + \frac{N_z}{A} \tag{11.2}$$

[41]

Additionally, the shear distribution may also be computed through Equation 11.3 and Equation 11.4.

$$\tau = -\frac{S_x \times I_{xx} - S_y \times I_{xy}}{I_{xx} \times I_{yy} - I_{xy}^2} \int_0^s s \; ds \; - \frac{S_y \times I_{yy} - S_x \times I_{xy}}{I_{yy} \times I_{xx} - I_{xy}^2} \int_0^s s \; ds \tag{11.3}$$

[39]

$$\tau = \frac{2T_z}{2 \times A_m} \tag{11.4}$$

[39]

The normal force is computed directly from the xy position of the cross section component. The shear is instead computed though the method of cuts. Cuts are applied through the cross section at the points of application of forces, and the shear flow is integrated throughout the cross section. This is done for shear in both axes, and shear flow due to torque is also computed. The results are then added to produce the total shear flow distribution. These results can then be plotted along the cross section and visualized as shown below in Figure 11.5 for the normal stresses, and Figure 11.6 for shear stresses. Note that the shear stress distribution is plotted along the unfolded perimeter of the cross section, starting from the top centre plate.

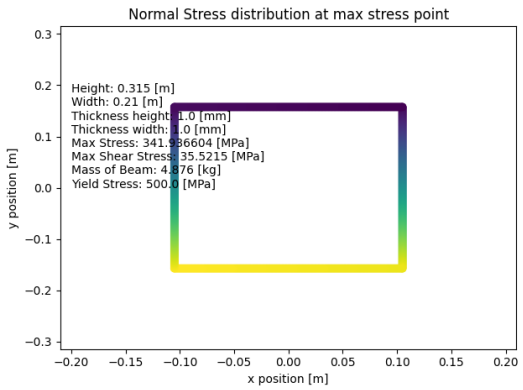

Figure 11.5: Internal normal stress distribution of rotor arm

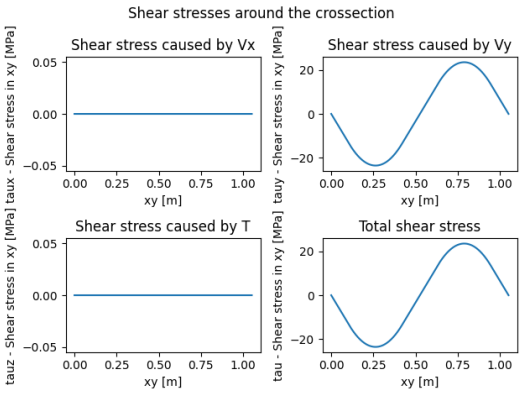

Figure 11.6: Internal shear stress distribution of rotor arm

The results are as expected, as the beam has maximum internal normal force in the bottom and top flanges as is clear in Figure 11.5. Additionally, the normal force distribution is slightly skewed to the left as a result of the one engine inoperative torque. This operation is done for each cross section type and material. For each of these, a set of combinations of parameters for the cross section of interest is computed, and the section with the lowest mass is returned. An upper bound for the maximum von Mises stress [42] is also used in the computation to exclude non valid sections. The formula for this is Equation 11.5

$$\sigma_{vM} = \sqrt{\sigma^2 + 3\tau^2} < \sigma_{yield} \tag{11.5}$$

The maximum numerical results are represented below in Table 11.4.

Table 11.4: Rotor beam maximum internal stresses and deflections

Type	σ [MPa]	τ [MPa]	v_x [m]	v_y [m]
Value	228	23.7	0.00132	0.0193

Please note that these values in the table are less than the limit condition shown on Figure 11.5, as individual stresses in the diagram are multiplied by the safety factor of the analysis.

The results of this analysis for the materials in Table 11.1 are shown below in Table 11.5.

Table 11.5: Rotor beam iteration results

Material	Type	Dimensions ([t,h,w] or [t,r]) [m]	Weight [kg]	Cost [USD]	Deflection in x [m]	Deflection in y [m]
Aluminium 7075-T651	Square	[0.001 , 0.315 , 0.21]	4.88	8.78	0.00132	0.0193
Aluminium 7075-T651	Circle	[0.00125 , 0.158]	5.74	10.3	0.00073	0.0197
Aluminium 2024-T4	Square	[0.001 , 0.3 , 0.255]	5.29	10.6	0.000876	0.0185
Aluminium 2024-T4	Circle	[0.0015 , 0.15]	6.74	13.5	0.000690	0.0186
Titanium 6Al4V	Square	[0.001 , 0.315, 0.09]	6.27	102	0.00503	0.0196
Titanium 6Al4V	Circle	[0.001 , 0.15]	7.29	119	0.000663	0.0179
Steel, high strength 4340	Square	[0.001 , 0.255, 0.075]	8.85	2.21	0.00485	0.0198
Steel, high strength 4340	Circle	[0.001, 0.12]	10.1	2.53	0.000703	0.0190
Steel, mild 1020	Square	[0.001, 0.315, 0.225]	25.4	12.7	0.000221	0.00362
Steel, mild 1020	Circle	[0.00225, 0.158]	29.9	14.9	0.000138	0.00376

It was noted that the results show that the optimisation algorithm tends to favour low thicknesses. This is due to the fact that the computation neglects local buckling and therefore aims at increasing moment of inertia while minimizing mass by making the perimeter longer and thinner.

With these resultant designs it is possible to conduct a trade-off. The criteria chosen for this trade-off are:

- Weight: Weight is of the highest importance, as it will have a trickle down effect on the mass of all other subsystems. As a result, it receives a weight of 0.5
- Deflection: Deflection is an extremely relevant parameter as it gives an indication of the stiffness of the member. In this case however, since the stiffness requirement has already been met, higher stiffness is desirable but not necessary, so it receives a weight of 0.1.
- Cost: Cost is a parameter for interest for the production of the system, however, it is of less relevance to success than weight properties. Therefore it receives a weight of 0.4.

Weight and cost were taken straightforwardly from Table 11.5, while the deflection parameter was taken as total deflection in xy. All these values were normalised on the difference between the best performing and worst performing candidate in each category.

Table 11.6: Trade-off table for rotor arm

Weights	0.5	0.4	0.1	
Component	**Weight**	**Cost**	**Resitance to Deflection**	**Result**
Aluminium 7075-T651 Square	5	4.72	0.289	4.42
Aluminium 7075-T651 Circle	4.83	4.65	0.20	4.29
Aluminium 2024-T4 Square	4.90	4.64	0.518	4.36
Aluminium 2024-T4 Circle	4.63	4.52	0.53	4.17
Titanium 6Al4V Square	4.66	0.728	0.042	2.63
Titanium 6Al4V Circle	4.51	0	0.738	2.33
Steel, high strength 4340	4.03	5	0	4.02
Steel, high strength 4340	3.96	4.99	0.41	4.01
Steel, mild 1020	0	4.55	4.65	2.29
Steel, mild 1020	0	4.46	4.96	2.28

The result of the trade-off suggested the circular Based on these results the first design making use of Aluminium 7075-T651 and a rectangular cross section with 315 *mm* in height , 210 *mm* in width and 0.001 *mm* skin thickness was selected as it had the most appealing properties. The weight of the steel makes it unsuitable and the cost of the titanium make it an attractive but too expensive option.

With the cross section stresses calculated, the next step is analysing the additional failure mode. Since a thin walled structure was chosen, the most prevalent mode is buckling. An analysis on shear buckling of the web plates is carried out for the internal stresses given in Table 11.4. The equation for shear buckling in a flat plate is given by Equation 11.6 [43].

$$\tau_{cr} = K_s E \left(\frac{t}{b}\right)^2 \tag{11.6}$$

A safety factor of 1.5 [40] is applied to account for uncertainty in the edge conditions of the plate. This condition is used to determine the value of K_s from Figure 11.7. It is found to be 6.4.

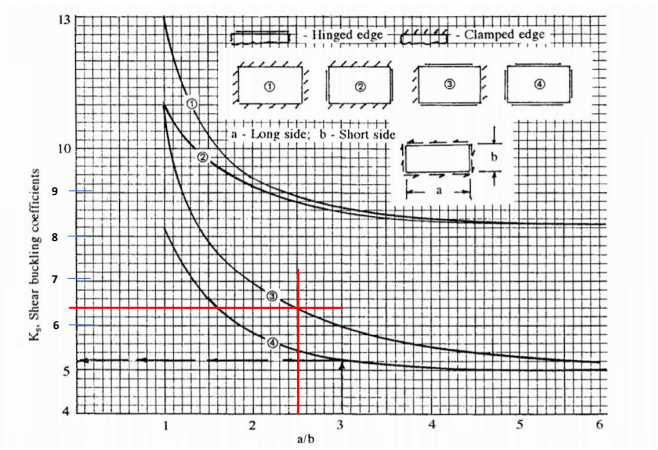

Figure 11.7: Shear buckling coefficient for a flat plate with different support cases at the edge [43]

The aim of this analysis is to determine what the required stringer spacing on the web plate is and what the dimensions of the stringer should be to prevent shear buckling and stringer column buckling. To simplify the analysis, the stringer will be a T-section with equal width and height. The thickness and width/height have to be such that the stringer is rigid relative to the web plate. Therefore the thickness was set to 2 *mm* and the width/height to 15 *mm* giving the stringer cross section a flexural ridigity of 98.4 Nmm^2. This is 8 times stiffer then the plate alone. At a later stage the stringer geometry can be further optimised to decrease the weight but for this stage of the design process this estimate is deemed appropriate. With the stringer geometry taken care of, the stringer pitch was determined by solving for b in Equation 11.6. The result is that the minimum stringer spacing is 14.9 *cm* or 14 stringers evenly spaced along the length. Since the stringers will be made from aluminium, the added structural weight of the stringers can be estimated by calculating the volume of one specimen and multiplying by the density. In total the added weight of the stringers is 3.63 *kg*.

Thus, the total weight of this component is 8.51 *kg*, and since four are needed, this adds a weight of 34.04 *kg* to the craft.

11.3. Bridge Analysis

The bridge is the component connecting the door of the cabin to the building during operation. This is another component which introduces significant loads into the cabin from external disturbances, and therefore was the second part of interest in the analysis.

This component is subject to many disturbance forces at the tip, as well as the loads induced due to people using the bridge. This introduces an axial force at the tip of the bridge in x-, y- and z-directions. Additionally, interactions between the tip of the bridge and the facade of the building may introduce torques into the structure. Because of this, three torques are applied at the tip of the beam. The weight of the bridge is another load of interest into the structure. In this case, the forces induced by the payload loading are parallel to the weight, and will consequently cause increased stresses in the component. Three point loads are additionally introduced by the payload boarding. These are shown applied at the extremes of the bridge and at the middle. The decision to size the bridge for three people loading at the same time against the firefighter's instructions was done to account for possible panic and disorderly boarding. Consequently, the additional assumptions introduced for this component are listed below:

- **ASUM-BRIDGE-1**: The interaction between the bridge and the facade of the building can be modelled as a sum of forces and moments at the tip of the bridge.
- **ASUM-BRIDGE-2**: The loads caused by the weight of the payload loading can be modelled as point loads along the length of the bridge.
- **ASUM-BRIDGE-3**: The weight of the bridge can be modelled by a constant distributed load along the length of the bridge.

- **ASUM-BRIDGE-4**: The passengers do not introduce loads along the z- and y-axis while walking across the bridge
- **ASUM-BRIDGE-5**: The passengers walk on the centre of the bridge

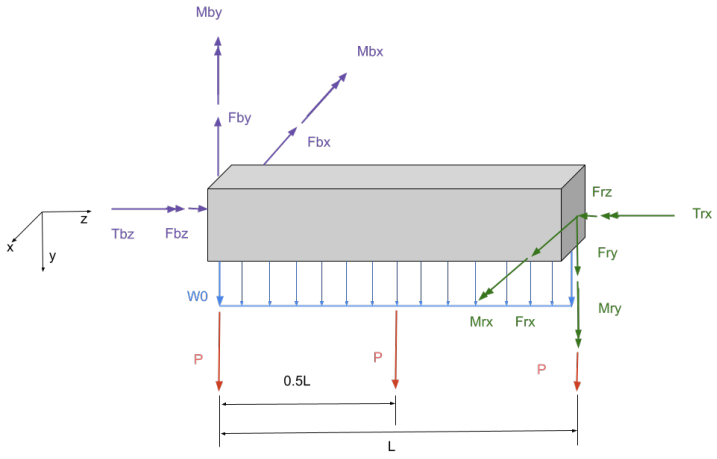

Figure 11.8: Bridge free body diagram

It is necessary to determine the bounds of the analysis under which to size the bridge. It was determined that the optimal positioning for the bridge would be under the cabin in Chapter 7. This limited the size of the bridge by the maximum rectangular volume which could be attributed to the space between the aerodynamic skin and the bottom side of the cabin. It was found that this distance was constrained to 14 *cm* in height to provide abundant space for guiding rails, and 1.3 *m* in width. The width of the bridge was also set at a minimum of 0.75 *m* as this is the average width of one passenger taken from Chapter 7. The shape of the cross section was constrained to rectangular as the circular cross section would be impractical as bridge.

In order to determine the length of the bridge, both operational and stability constraints were taken into account. It was determined in Chapter 7 that the maximum depth of facade considered would be 0.5 *m*. From this, a constraint from the wall is imposed on the length of the bridge. A safety factor of 1.5 was used to account for possible variations in this size and the presence of obstructions that may increase the local wall thickness. It was then determined from Chapter 10 that the maximum movement caused by gust loads would be 4 *cm* in every axis. In order to account for possible horizontal motion of the sliding bridge, 10 *cm* plus a safety factor of 1.5 were considered as additional bridge length to the wall constraint. This corresponds to the amount the bridge may move forwards or backwards while at full operational extension. It was then determined that an additional 0.9 *m* would be required to overcome the frontal distance of the rotors, and consequnetly the total length of the bridge was set at 1.8*m*. Furthermore, it was determined that since boarding is a critical phase of the mission, where the payload is at the highest risk, it is vital that the bridge is sufficiently stiff as to not cause cause bending while loading. This is important both for the safety of successful boarding as the negative psychological effect of boarding on a non stiff bridge. Alternate sources discussed in Chapter 7 recommend at most 5% deflection for comfortable boarding, but in this case this would be almost 9 *cm* which was deemed to much. As such, it was determined that a safe bound for this deflection would be 1 *cm*. It is recommended in future phases of the analysis to further determine the necessity of this stiffness requirement, as its reduction might lead to a reduction in weight. It was additionally determined that the minimum thickness chosen for this analysis would be 2 *mm*. This was done to somewhat limit the effect of buckling before the addition of stiffening elements and reduce the potential perceived deformation of the bridge under the passengers.

It is now possible to use the same method of analysis as the rotor arm by placing the following inputs for limit forces and torques the bridge is expected to experience as detailed in Table 11.7

Table 11.7: Bridge input loads

Internal load	F_{bz} [N]	F_{bx} [N]	F_{by} [N]	T_{bz} [Nm]	M_{bx} [Nm]	M_{by} [Nm]	P [N]
Value	203	203	203	56	56	56	981

Once again, the results are specific to each iteration, so only one of these will be shown. This iteration is that of high strength steel 4340.

This yields the internal loading shown in Figure 11.9. Once again this is computed through Equation 11.1.

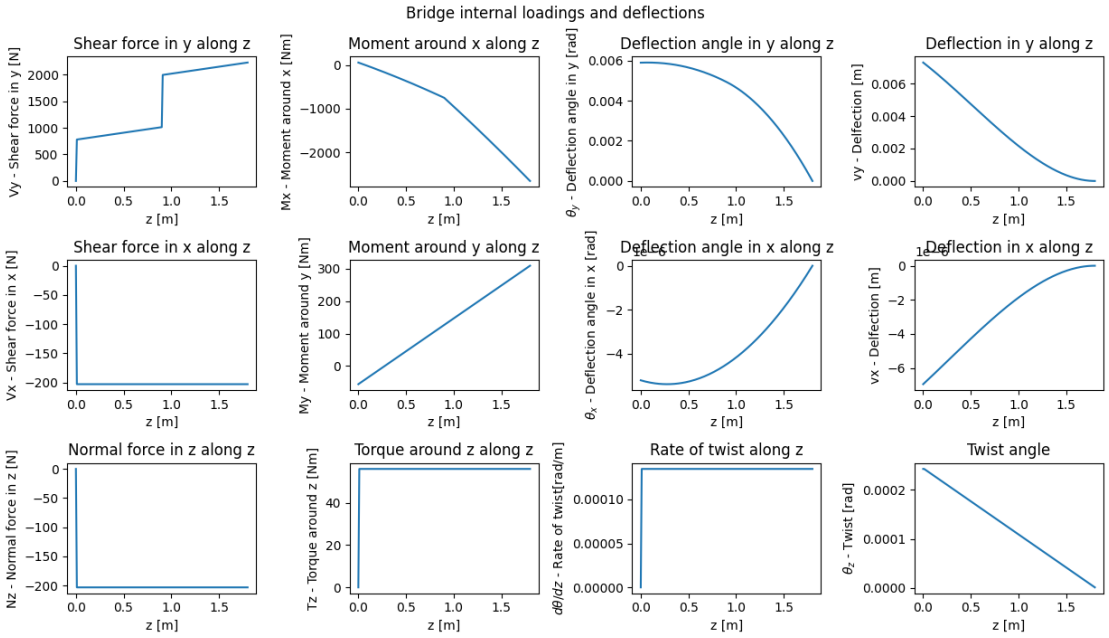

Figure 11.9: Internal loading of the bridge

The condition of maximum internal loading is therefore the one shown in Table 11.8

Table 11.8: Bridge maximum internal loads

Internal load	F_{rz} [N]	F_{rx} [N]	F_{ry} [N]	T_{rz} [Nm]	M_{rx} [Nm]	M_{ry} [Nm]
Value	-203	-203	1922	56.0	-2374	309

Once these loads are obtained it is possible to cycle different rectangular sections to result in the lowest mass one which conforms to all requirements. The internal normal and shear forces are shown below in Figure 11.10 and the shear forces are depicted in Figure 11.11. Once again these are computed through the use of Equation 11.3, Equation 11.4 and Equation 11.2.

The maximum internal stresses are shown below in Table 11.9.

Table 11.9: Bridge beam maximum internal stresses and deflections

Type	σ [MPa]	τ [MPa]	v_x [m]	v_y [m]
Value	24.8	8.40	2.03e-05	0.00953

It is now possible to iterate this process for all the materials under scrutiny. Once this was done, the results were collected and are shown below in Table 11.10.

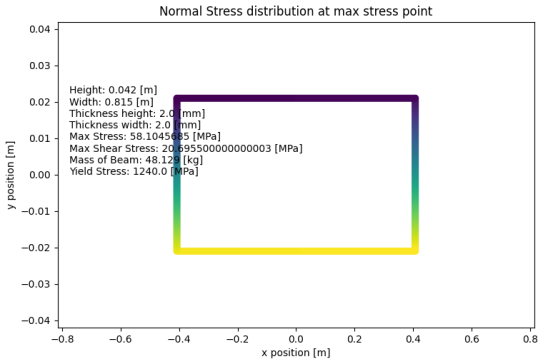

Figure 11.10: Internal normal stresses of the bridge

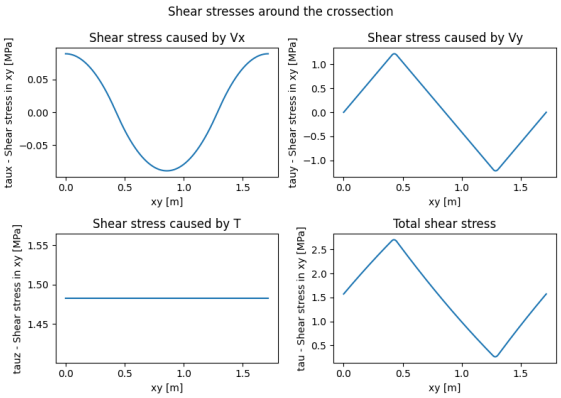

Figure 11.11: Internal shear stresses of the bridge

Table 11.10: Bridge iteration results

Material	Type	Dimensions ([t,h,w] or [t,r]) [m]	Weight [g]	Cost [USD]	Deflection in x [m]	Deflection in y [m]
Aluminium 7075-T651	Rectangular	[0.002,0.06,0.8]	16.7	30.1	1.87e-5	0.00834
Aluminium 2024-T4	Rectangular	[0.002,0.063 , 0.815]	17.5	35.0	1.87e-5	0.00834
Titanium 6Al4v	Rectangular	[0.002, 0.049 , 0.815]	28.0	455	1.25e-5	0.00922
Steel, high strength 4340	Rectangular	[0.002 , 0.042 , 0.815]	48.1	12.0	6.05e-6	0.00730
Steel, mild 1020	Rectangular	[0.002, 0.042 , 0.815]	48.1	24.1	6.95e-6	0.0072 30

Having obtained these results, it was possible to conduct a trade-off to determine the most optimal material and cross section for this application. As a result, three criteria were once again selected for the trade-off of the bridge. These are the same criteria as previously determined, but their weights have been altered. These are described below:

- Weight: It was deemed vital that the weight of this system be contained, as it will increase MMOI when deployed which will make the craft less controllable. As a result, the weight is the most important parameter, with a criterion weight of 0.6.
- Cost: Cost is a parameter of importance in this situation, as it will affect the final cost of the vehicle. It is however of less importance than weight and therefore receives a score of 0.3.
- Deflection: Deflection is an important parameter, however, since the requirement on maximum deflection is quite tight, the additional benefit of deflecting less than 1 mm was judged to be of low importance. Consequently, this criterion has a weight of 0.1.

Table 11.11: Trade-off table for Bridge

Weights	0.6	0.3	0.1	
Component	**Weight**	**Cost**	**Stiff-ness**	**Result**
Aluminium 7075-T651	5	4.80	2.29	4.66
Aluminium 2024-T4	4.87	4.74	2.29	4.57
Titanium 6Al4V	3.20	0	0	1.92
Steel high strength 4340	0	5	5	2
Steel, mild 1020	0	4.86	5	1.96

Consequently, the chosen section was the one with the highest score, being the Aluminium 7075-T651 section. This section has so far not been analysed for buckling loads.

Since the bridge is a thin walled structure, just like the rotor arm as described in Section 11.2, buckling is possibly the first failure mode to occur under the aforementioned stress state. The maximum shear stress in the cross section is 8.4 *MPa*, more than 35 times lower than the yield strength of the aluminium alloys and 20 times lower than the steel alloys in Table 11.1. It was therefore decided that adding stringers to the panel was not necessary. However, since the bridge's height is only 6 *cm*, this allows for the possibility to reinforce the bridge with a honeycomb structure. This will make the structure significantly more rigid, thereby increasing passenger comfort. It also eliminates the problem of compression and shear buckling in the web plates since the honeycomb will carry the shear loads and reduce the local section size of the compression panel[44]. Note that the bridge requires wiring for the clamp to operate. This is provided by two channels running lengthwise through the bridge. The shear stress in the analysis is so low that the channels can be there without reinforcement.

Thus, the weight added by the bridge consists of 16.7 kg.

11.4. Landing Gear Analysis

The landing gear supports the craft during landing and on ground, and serves as the load path for ground normal forces to keep the aircraft upright. It was determined that given the high saturation of the market for such components for similar craft hat this component would be selected from existing designs and therefore outsourced.

Consequently, existing landing gear types were identified and a trade-off was conducted between these. Given the use of vertical takeoff and landing capabilities in the craft, only those landing gears used in vehicles with vertical landing and take-off methods were chosen for the analysis. Due to time constraints, it was further deemed necessary to reduce the number of considered landing gear types to the most commonly used, being skids and wheels [45, 46].

The criteria on which these are evaluated are the following:

- Weight: This is of high relevance for our vehicle, as the landing system is deployed for only a very small part of the mission. A small increase in system weight may negatively impact all other systems, so it is of high importance to minimise the component weight. Consequently, the weight given to this criterion is 4.
- Cost: This is parameter of interest, as cost is to be minimised. However, it is not of particular relevance compared to other criteria such as weight or safety, and therefore the weight given to this criterion is 2.
- Complexity: This parameter is of importance due to the possible increase in the number of failure mechanisms with the increased number of components. However this parameter is judged of less relevance than cost and especially weight, and therefore receives a score of 1.

In order to determine the most optimal design type literature and current market designs were considered.

It was found that landing skids weigh consistently less than wheel designs for same sized crafts, but that wheel designs had a large range in weights[37]. Consequently the skids received the highest score in this category and the wheels received a three given their higher variability in weight. Similarly, cost is also higher for skids than wheels but the discrepancy is smaller and therefore the two scores are closer. In complexity on the other hand, the skids are by far superior to the wheels, utilising a lack of moving components and receiving the highest score.

Table 11.12: Trade-off table for Landing Legs

Weights	0.6	0.3	0.1	
Component Type	**Weight**	**Cost**	**Complexity**	**Results**
Skids	5	4	5	4.7
Wheels	2	3	1	2.2

Consequently from the trade-off, skids are selected as the most attractive landing gear design type. The landing gear selected should be rated to withstand the design load consisting of the weight of the craft, as well as having dimensions to allow proper fastening of the cabin during production.

Unfortunately it was found that most companies producing these products are unwilling to share technical information on their products to private entities. Because the project is so far not affiliated with a company it was therefore not possible to accurately compare the specifications of different designs. It is therefore recommended to perform a more in depth selection on this component in the post-DSE phase when the project responsible bureaucratic entity is created. Because of this, it was necessary to look at craft of comparable weight to identify landing gear designs which can support the required maximum load of the craft of 26400 *kg* as follows from Section 4.4 .

It was found that the skids employed in the Bell 407 would be appropriate for this purpose as the craft has a maximum gross weight of 2722 *kg* [38].

By sourcing individual components of this landing gear, it was possible to obtain a list of all the necessary components to assemble it and evaluate their cost and weight [39] as can be seen in Table 11.13.

Table 11.13: High skid gear data

Assembly	Product tag	Weight [kg]	Cost [USD]
High Skid Gear	206-321-404	27.19	22601

It was noted that since all the individual component part costs were taken from the sale of spares and individual components, and therefore serve as an upper bound for the cost of this component. Furthermore the individual fasteners (such as nuts and bolts) have not included in the total cost.

It is considered that this cost may be lowered dramatically through an accord with the production company, so it is recommended to contact the producer company and receive quotes for the cost of the landing gear if bought in bulk with an exclusive contract. Otherwise, if this cost proves excessive to bear for the project, it may be necessary to vertically integrate landing gear production and therefore perform an additional sizing analysis on this part in the post DSE phase.

[37] URL `https://savback.com/whats-the-best-landing-gear-wheels-or-skids/` [cited 20 June 2021]

[38] URL `https://www.bellflight.com/products/bell-407` [cited 18 June 2021]

[39] URL `https://www.aero-access.com/products/bell-407-high-skid-gear-components-replacement.html` [cited 15 June 2021]

11.5. Centrepiece & Hinge Design

The design of the drone centrepiece starts at the selection of the connectors that attach the cabin to the centrepiece. The connectors are assumed to be pin connections, with x-, y- and z- positions fixed but all rotations free. While these types of connectors may in reality not be very practical or the most reliable, involving ball joints or multiple rotating elements, they simplify the design problem as the contributions to moments from the cabin can be neglected. In post-DSE stage the possibility and effect of changing the connector types must be evaluated.

Given the general subdivision of Figure 11.2, some top-level design options were considered:

1. A truss structure, with rods connecting the top and bottom parts of the hinges together and additional members for shear
2. Beams, connecting the hinges in a square shape
3. Beams, connecting the hinges in a cross shape
4. A box with load-bearing skin
5. A topology optimised structure

Due to the time constraints of the project it was not possible to evaluate all five options, instead it was decided to evaluate only one in detail. A topology optimisation program would have to be written from scratch or purchased, which was deemed impractical and was therefore discarded. A closed box was deemed too complex to analyse by hand under the difficult 3D loading and constraining problem, and was therefore also discarded. The cross-shaped beam was also discarded, since it was deemed impractical when the centrepiece has to enclose large volumes of equipment such as batteries. Both the truss and beams in square shape solutions seemed equally practical. It was decided to opt for beams, since their webs already partially enclose the structure, removing the necessity for additional covers, and due to the simplicity of their analysis.

Given the top-level structure, a free body diagram (FBD) was created, which is depicted in Figure 11.12. In the creation of this FBD, several assumptions are made:

- **ASUM-CENTREPIECE-1** Equipment such as batteries are carried by secondary structures and are thus not part of the analysis
- **ASUM-CENTREPIECE-2** Actuators can be represented by rigid connections between rotor arm and hinge
- **ASUM-CENTREPIECE-3** Rotor arm hinges coincide with cabin connectors
- **ASUM-CENTREPIECE-4** Weight of structural components negligible

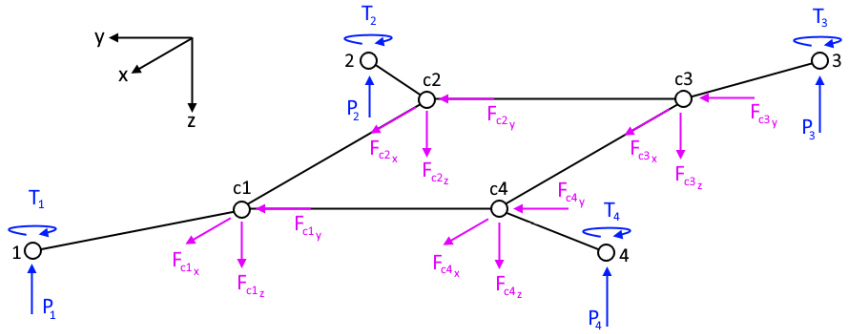

Figure 11.12: Centrepiece free body diagram

The nodes c1, c2, c3 and c4 represent both the hinges and the pin connections to the cabin. Note that the arms are connected rigidly to the centrepiece beams. To calculate the external loads on the

centrepiece beams, the problem can be split up into the moments along the x- and y-axes, and the moments along the z-axis, then added according to the principle of superposition. The bending problem in x- and y-axes becomes simple when the torsional stiffness is neglected. This decouples each beam, and is valid since generally for tall beams the bending stiffness is much larger than the torsional stiffness. This is confirmed later in this chapter. The bending problem around the z-axis is statically indeterminate, since all four beams are connected to each other rigidly via the hinges. The problem can be solved by dividing is as shown in Figure 11.13. It is assumed that the deflection in the length of the beam is zero. This is considered valid since the longitudinal stiffness of beams is generally much larger than their bending stiffness. Forces in x- and y-direction coming from the arms are also neglected. This comes from the assumption that the motor thrust acts perfectly along the z-axis. To summarise, the assumptions made are:

- **ASUM-CENTREPIECE-5** Torsional stiffness of beams negligible compared to bending stiffness
- **ASUM-CENTREPIECE-6** Longitudinal deflection of beams negligible
- **ASUM-CENTREPIECE-7** Motor thrust acts perfectly along z-direction

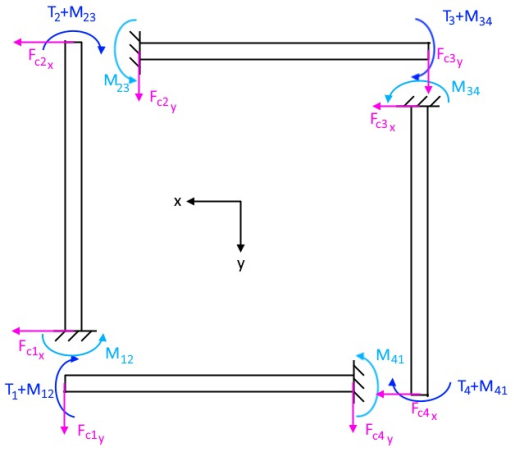

Figure 11.13: Free body diagram of subdivided centrepiece

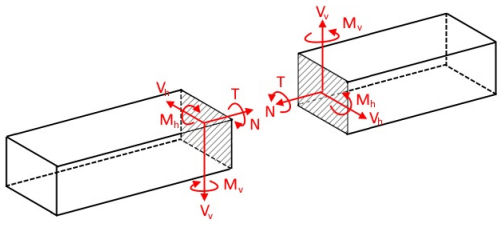

Figure 11.14: Internal loads definitions

The problem can be solved by setting two constraints. The first is that the bending deflection at the end of each beam is zero, due to the pin connection at either end. The second is that the deflection gradient at the start of each beam equals the deflection angle at the end of the beam it is rigidly connected to. Together with the force and moment equilibria of each beam, this results in 16 equations and 16 unknowns. For a given cross-section geometry, these are put into a matrix and solved using python's `scipy.linalg.solve()` function.

With the external forces known, the internal loads can be calculated by via force and moment equilibria, using the axis definitions depicted in Figure 11.14. The normal stresses are calculated simply according to Equation 11.2, where x and y are local cross-section coordinates with y positive for the top half of the beam and x is positive for the right half, resulting in a positive stress (tension) in the first quadrant. Note that the subscripts v and h are used to avoid confusion with the global x- and y-axes. The internal loading of the beam connecting points 1 and 2, in the configuration shown in Figure 11.15, can be seen in Figure 11.16.

To calculate the shear flows, the cross-section geometry must be defined. The internal loads are predominantly high horizontal axis moments and vertical shear forces and, per assumption, no torsion. Due to their widespread use in structural solutions, a simple I-profile was deemed most appropriate. To calculate the shear stresses, the cross-section is assumed to be thin-walled. This is confirmed later in this chapter. As a result, the web is assumed to have no contribution to the shear resistance in x'-direction. The resulting shear distributions in the flange and web are calculated from Equation 11.7 and Equation 11.8 respectively.

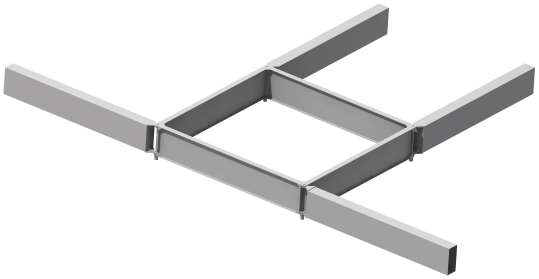

Figure 11.15: Internal loads configuration

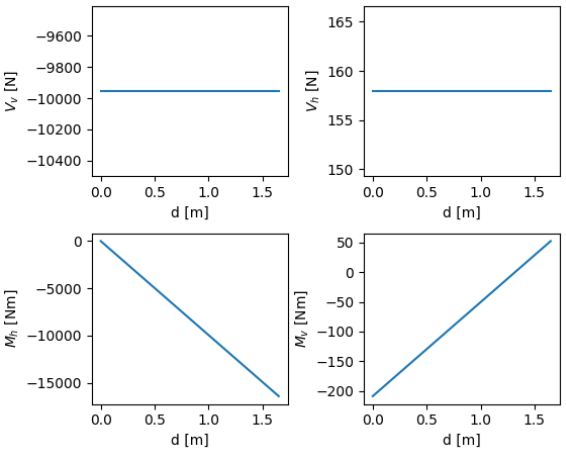

Figure 11.16: Internal loads of centerpiece beam 1-2

$$\tau_f = \frac{V_v(\frac{bht_f}{4} - \frac{ht_f}{2}x)}{I_{xx}t_f} + \frac{V_h(\frac{b^2t_f}{8} - \frac{t_f}{2}x^2)}{2I_{yy}t_f} \quad 0 \leq x \leq b/2 \tag{11.7}$$

$$\tau_w = \frac{V_v(\frac{hbt_f}{2} + \frac{h^2t_w}{8} - \frac{t_w}{2}y^2)}{I_{xx}t_w} \quad 0 \leq y \leq h/2 \tag{11.8}$$

Where b, h, t_f and t_w are the profile width, height, flange thickness and web thickness respectively. To determine whether a given geometry fails under the loading, the failure criteria must be defined. For the scope of the analysis, three failure criteria were used. First is the von Mises yield criterion, defined by Equation 11.5 [42]. Second is shear buckling of the web, defined by Equation 11.9 [43]. The coefficient K_s is taken for short edges clamped and long edges hinged, for an a/b of 5. This results in K_s = 5.2 from Fig. 11.3.5 of [43]. η_s, the plasticity factor, is taken equal to unity since the analysis is done in the elastic regime. The last failure criteria is column buckling of the top flange, defined by Equation 11.10 [43]. Note the negative sign for compression. The coefficient k_c is taken for a simply-supported edge with infinite length, resulting in k_c = 0.47. η_c is again taken as unity. Note that b is multiplied by 0.5 since in the analysis of flange buckling only one half of the flange is considered.

$$|\tau_w| < \tau_{s,cr} = K_s\eta_s E\left(\frac{t_w}{h}\right)^2 \tag{11.9}$$

$$\sigma_f > -\sigma_{c,cr} = -\frac{k_c\eta_c\pi^2 E}{12\,(1-\mu^2)}\left(\frac{t_f}{0.5b}\right)^2 \tag{11.10}$$

With these criteria, a factorial experiment tool was written in Python to optimise the values of b, t_w and t_f for the lowest resulting mass. The height h wad determined from an initial estimate of the volume that the centerpiece has to encapsulate. It was estimated that the LV batteries, electronics, cables and their respective supports and casings would sum up to a volume of roughly 550L. With a contingency of 50% this results in a minimum height of roughly 0.3 *m*.

The experiment ran at the limit load case, which was determined to be motor failure at full engine thrust, multiplied by a safety factor of 1.5. This means that at the moment of failure, the propeller of the inoperative motor is still generating thrust, but the driving torque of the motor is no longer present. In the final design iteration, this amounts to a net torque of $1.5 \cdot 278$ *Nm* at the end of the rotor arm. The maximum load is based on the maximum thrust-over-weight ratio of 1.95 determined later in Chapter 13. The safety factor is mandatory, and must be applied to the limit external loads on the vehicle [40]. The

limit load is then described by Equation 11.11. For the final iteration, a mass of 1331 *kg* was used. This load case was checked over a rotation range of arms 1 and 4 of $\pi/2$ radians. This was done with arms 2 and 3 angled at $\pi/2$ and $3/2\pi$ radians respectively, and with both arms at π radians, the latter depicted in Figure 11.15. The optimisation experiment was performed for the materials shown in Table 11.1. The results can be seen in Table 11.14.

$$P_1 = P_2 = P_3 = P_4 = 1.5 \cdot \frac{m_{mhw} \cdot 9.81}{4} \cdot \frac{T}{W} \tag{11.11}$$

Table 11.14: Beam profile optimizations for centrepiece (h=0.3 *m*)

Material	***b*** **[mm]**	t_w **[mm]**	t_f **[mm]**	**Mass [kg]**	**Material Cost [USD]**
Al 7075-T651	33.684	2.2526	2.6632	15.24	27.43
Al 2024-T4	52.632	2.2526	2.6632	17.48	34.96
Al 6061-T6	52.632	2.2526	3.0737	17.81	42.74
Ti 6Al-4V	24.211	2.2526	1.8421	22.72	369.2
HS Steel 4340	24.211	1.8421	1.4316	32.02	8.005

Note that these results confirm the thin-walled assumption, since for all materials $b \gg t_f, t_w$. Furthermore the torsional stiffness is generally in the order of 0.02% of the bending stiffness, confirming the assumption that it can be neglected. Since the material costs are very low compared to the total cost requirement of the craft, their contribution to the trade-off is neglected. The choice of material is therefore solely based on the resulting mass, leading to Aluminium 7075-T651 being the best choice. It should be noted that other criteria such as hardness, corrosion resistance, thermal behaviour, machinability and workability in general are also important factors in material selection. Especially thermal behaviour should be heavily considered since the craft may experience high temperature fluctuations in the harsh rescue environment. The trade-off result may therefore change when these factors are included. However, for the scope of this design project, which in the long run is very preliminary, these factors are neglected.

To verify the results of the calculations, namely that the final, optimized cross-section for Aluminium 7075-T651 can carry the limit loads of the craft, and that the python model accurately calculates the von Mises stresses in the cross-section, a CATIA model of the beam profile was made. A simple hinge was also modelled as part of the centerpiece, which due to the complexity was based on trial-and-error design in CATIA. Bearing loads equivalent to the moments introduced by the arm were then imposed on the hinges. Note that the restraint is set in the middle of the hinge while in reality the connection to the cabin may differ. This effect must be investigated in post-DSE. The result can be seen in Figure 11.17. A close-up of the developed hinge can be seen in Figure 11.18.

At the centre of the top flange of beam 4-1, the CATIA analysis returns a von Mises stress of 243 *MPa*, as shown in Figure 11.17. At this same location, the analytical model in Python returns a von Mises stress of 268 *MPa*. Given the assumptions made, this 10% discrepancy, combined with the fact that the analytical estimate is conservative, is deemed small enough to verify the analytical model. Furthermore, no failure occurs in the cross-section of the beams, which confirms the design of the centerpiece given its constraints. Yield does however occur within the hinge bearings. The design of the hinge must therefore be revised in post-DSE. Interactions between the hinges and the beams must also be investigated in post-DSE, as they give rise to stress concentrations than may cause yield in the beams.

11.6. Cabin Analysis

The cabin is both the most involved and most difficult to analyse structural component of the craft. This is because it is located at the convergence of many loads, and their interactions may yield unfavourable stress concentrations. Additionally, the cabin must house the payload safely, so it may not be allowed to deflect excessively. Initially, it was necessary to choose the type of structure which the cabin should

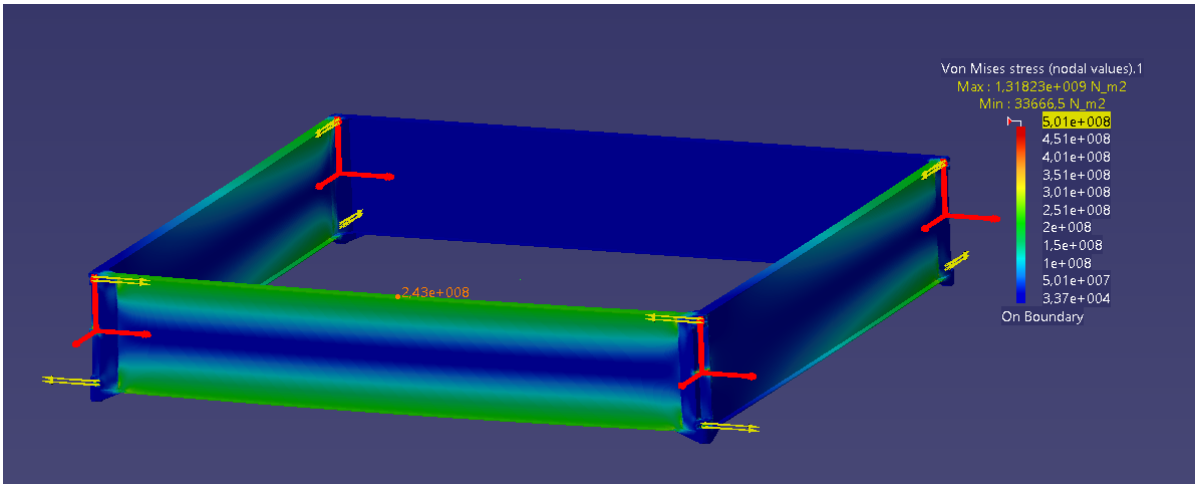

Figure 11.17: CATIA Finite Element Analysis of centerpiece

take. In order to do this, first, a free body diagram of the cabin under the loads introduced by the other subsystems is created. This can be seen in Figure 11.19.

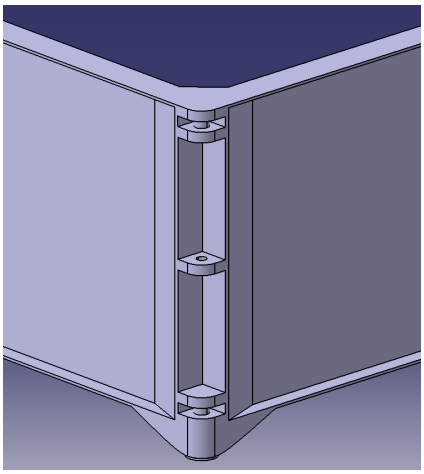

Figure 11.18: CATIA model of centerpiece hinge

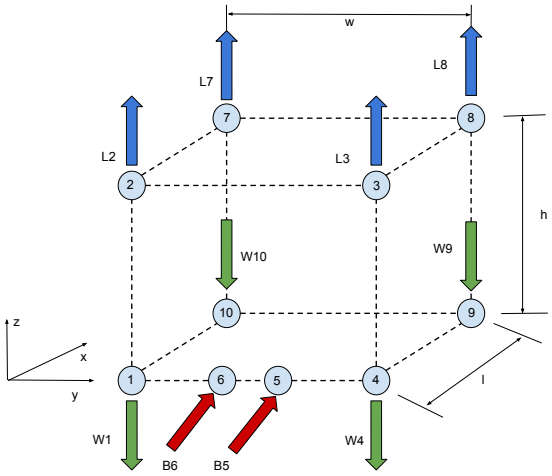

Figure 11.19: Cabin FBD

The additional assumptions made to simplify this problem to this level are the following:

- **ASUM-CABIN-1** The weight acts only in the z-axis irrespective of the orientation of the vehicle. It is decided as the vehicle will not have a high pitch angle.
- **ASUM-CABIN-2** The lift acts only in the z-axis irrespective of the orientation of the vehicle. This is once again consistent with with the low pitch angle of the vehicle.
- **ASUM-CABIN-3** The bridge forces and moments can be represented as forces acting on pins, which represent the hinge of the bridge with the craft.
- **ASUM-CABIN-4** It is assumed that the joints of the truss act like pin connections and do not transfer internal moments.
- **ASUM-CABIN-5** It is assumed that fixing the top nodes relative to each other is a reasonable assumption for the increased stiffness caused by the centrepiece.
- **ASUM-CABIN-6** It is assumed that during landing the bottom perimeter nodes may be considered fixes as deflections are constrained by the landing gear and ground.

By identifying all the locations at which loads are introduced a general representation of the cabin was able to be created. By now identifying the load paths it is possible to identify different representations for the structure, and later selecting the most optimal for the given application. As can be seen in Figure 11.19 all the points of application of loads have had a node numbered and placed at that location. The weight of most craft components acts on the bottom four nodes of the structure, and the bridge at the top four nodes of the cabin.

Several different top level designs were considered to represent the cabin structure. The first of these was representing the cabin as a system of perpendicular rods and thin panels between them, to make use of shear diffusion properties to maintain rigidity. This is shown as type a in Figure 11.20. The second design theorized was the use of a solid thin walled structure which would essentially be a hollow cube with cut outs due to the presence of the door, which is shown as type b. The last design under interest was the use of a truss structure.

It was determined in Chapter 5 that the minimum dimension of each side of the cabin needed to contain the payload would be 1.65 m. It was therefore decided that the structure of the cabin would contain a volume of 1.65 x 1.65 x 1.65 m.

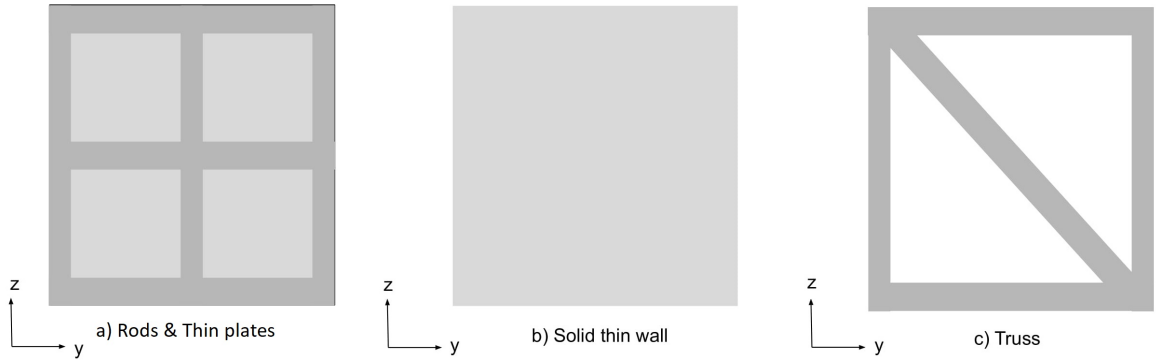

Figure 11.20: Cabin structure types

It was initially determined that the most effective representation of the cabin would be the rods and thin plates. As such, a method of analysis was under development for this representation of the cabin. However, it was determined in Chapter 7 that windows may be necessary to conform to the requirements on safety and to improve the passenger experience. Due to this, and the decision made in Chapter 8 to use an external skin for aerodynamics, it was determined that both the rod and thin plates representation and the thin walled wall representation would lead to a design where this would be more difficult to implement, due to stress concentrations from introducing the window. It was also hypothesized that the external aerodynamic skin structure may also improve the torsional stiffness of the cabin, lowering the need for the presence of skin panels in the cabin structure. It was consequently decided to use a truss structure for the cabin. It is noted that due to time constraints it was not possible to conduct a full trade-off on this choice. It is recommended to perform such a trade-off to verify or disprove the claim that this is the most optimal cabin representation and to further refine the weight estimates.

It was decided to use a truss structure with a separate floor laying on the outermost bottom connections of the truss.

This structure would be formed of beams with 10 intersection points. Nodes were placed at the source of external forces, and different combinations of structural members were to be tested to evaluate the combination with best general performance.

It was decided to perform a qualitative analysis of possible truss solutions and then identify a working model to later verify in CATIA. This was because alternative solutions like creating a script to model the system or making use of scripts like trusspy was deemed too time consuming. Despite being taken into consideration, these were ultimately not used in the analysis. It is therefore recommended to conduct additional research into this truss arrangement in the post-DSE phase.

Having chosen the preferred method to analyse the cabin, it is now possible to generate the trusses to analyse, and the load cases to input. It was determined that there would be three different cases of analysis. These would be the following:

- The landed case, where it is assumed that all four bottom perimeter nodes of the structure are fixed, and a force is exerted at the top.
- The flying case, where the opposite was done, and the cabin was considered to be firmly clamped to the centrepiece, and the weight of most craft elements hangs on the bottom four nodes.
- The clamped case, where the bridge is constrained and both forces and weight act on the structure.

Out of these, the most critical loading case was identified. This was chosen to be the scenario when the craft is at full operational weight, while the bridge is secured to the wall, and three additional people are trying to enter the craft against the firefighter's instructions. This leads to a situation where all the loads located in Section 11.3 in Table 11.8 are applied onto the structure as well as the full weight of the payload and other subsystems.

The cabin would have to carry the weight of everything secured to it, including the bridge, batteries, payload and floor.

The total loading was therefore a result of these weights and the following two assumptions:

- **ASUM-CABIN-7** The moments in x and z can be considered to act as forces along the nodes 6 and 5.
- **ASUM-CABIN-8** The moments in y can be considered to diffuse through the floor and act as forces on nodes 1, 4, 10 and 9.

The forces are described in Table 11.15

Table 11.15: Cabin input loads

Loads	$B6_x$ [N]	$B6_y$ [N]	$B6_z$ [N]	$B5_x$ [N]	$B5_y$ [N]	$B5_z$ [N]	W_1 [N] & W_4 [N]	W_{10} [N] & W_9 [N]
Value	101.5	-891	488	101.5	-1031	-285	3299	1851

First, beams were placed in order to form a cube in which to order the truss. It was then decided that in order to distribute the loads induced by the bridge into the structure four beams would connect nodes 5 and 6 diagonally across the structure.

Despite the fact that trusspy was ultimately not used for the analysis, it was noted that during the development of the script the deformation pattern of unsymmetrical trusses often resulted in torsion of the truss. This pattern was later also observed in the later CATIA modeling of the truss, which led to the decision to add two reinforcing rods in the back. These, despite not being as heavily loaded as the front ones, are important for maintaining rigidity of the assembly. The most loaded members are the vertical rods in the front section. Because of this, one of these rods was chosen to size all other rods.

It was decided to use Aluminum 7075 T651 for it's excellent strength to weight properties which had been selected for the trade-off in Section 11.3. The cross section selected would be a circular section with outer diameter $50\ [mm]$ and an inner section of $45\ [mm]$. Unfortunately a proper trade-off could not be conducted on this due to the inability to apply the optimization program, It is therefore recommended to further investigate this in the post DSE phase.

An FEM analysis of the cabin is shown below in Figure 11.21. As can be seen, the stresses experienced in the analysis are all below the yield stress of the material. The highest stress experienced is 22 MPa, which is judged to be comfortably lower than the yield stress, and no alarming stress concentrations are noticed on the model. It is noted that the presence of weld lines may exasperate the stress concentrations and it is recommended to perform additional analysis on the effects of this. Another possible issue is that the fastening mechanism of the vertical columns to the floor is not included, which may introduce stress concentrations to be analysed in the post DSE phase.

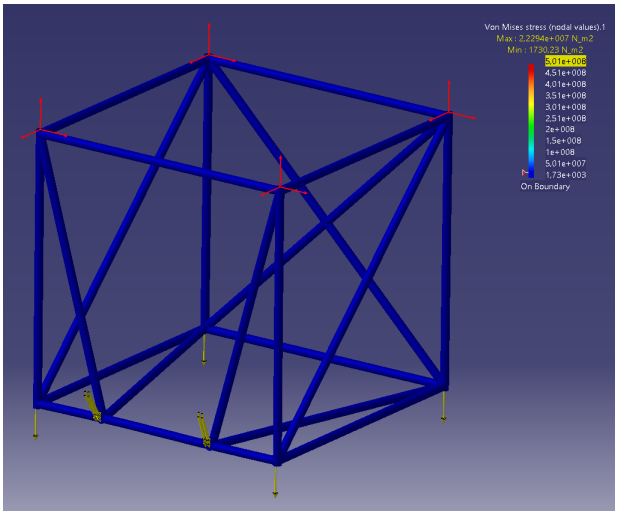

Figure 11.21: Cabin FEA

Once this had been done it was necessary to consider a solution for the floor of the cabin. This would have to be a stiff and lightweight. By reviewing literature, it was determined that the best performing material for this application would be a honeycomb composite structure [44]. However, given the extremely high cost of this material, it was decided to use a thin plate with stiffener reinforcement.

The vertical clamps proposed in Chapter 7 would then be attached to the holes at the top of the truss and the clamps would then transfer the load to the vertical beams. The landing skids would then be attached to the bottom holes of the truss with an additional securing mechanism, also to be discussed in the post DSE phase.

Overall, the total weight of the cabin truss without the flooring or attachment mechanisms is 35.07 kg. It is noted that the floor will add a significant contribution to this weight, as well the mechanism to fasten batteries. Both these will be under scrutiny in the post DSE phase. At this time, a factor of 1.2 will be used to account for the presence of these additional elements, bringing the weight of the cabin truss to around 42 *kg*.

11.7. Conclusions & Recommendations

Overall, the structural analysis was able to include most of the main components of the craft and size them for operation. The masses of these bodies and the internal stresses are found and evaluated to identify the most optimal design. This yields most of the structural mass, but neglects connection mechanisms and secondary non critical load bearing structures. For example, suspension springs, fasteners, bolts, nuts, thin paneled floors and walls are all neglected in this analysis. Because of this, it is expected that the mass of the structural subsystem will increase in the post-DSE phase.

It is recommended in future design phases to also account for weld lines and other soldering mechanisms between standard components (see Section 11.6). Another recommendation is to use the same method of analysis for all components. In this case, different analyses were performed due to time and resource constraints.

12. Information Handling

Now that the main characteristics of the system have been determined, the information handling system of the craft has to be designed to ensure that the craft can be controlled by the pilot at all times. As a fully electric concept was opted for, the main components for controllability insurance are electronics and communication components. The electronics do additionally support the data acquisition and handling due integrated circuit implementation. As first, the electronic devices and their interface with electrics components of the craft are discussed in Section 12.1. The software block diagram is given

in Section 12.2. As next, the communication of the craft both internally and externally is described in Section 12.3. Lastly, the data handling capabilities of the system are provided in Section 12.4.

12.1. Electrical & Electronics Block Diagram

To have a complete overview of electrical components in the system and their interfaces, an electrical & electronics block diagram is created. As the design has come into the final stage of the DSE, the diagram depicted in Figure 12.1 is tailored specifically to the current design of the craft, including the amount of instances (redundancies included) and connections for each device. It has to be noted that the hardware of the system consists only from electrical devices, thus, to provide a concise and clear overview of the system's components, only a single diagram is provided in the analysis, engulfing the electrics, electronics, communications and the data handling concepts.

To indicate repeatedly occurring interfaces, colour indication is used such that clear overview is achieved. Inspecting the figure it can be noted that the system is split into two parts electrically - controller and craft - as required by the SYS-OPS-06. Additionally, a legend in the right top corner has been added to clarify the notation used. At first, the general layout of the block diagram and its core division are discussed. As next, most of the components not discussed anywhere else in the report are scrutinized in detail. Lastly, the electrics and electronics system redundancies are discussed.

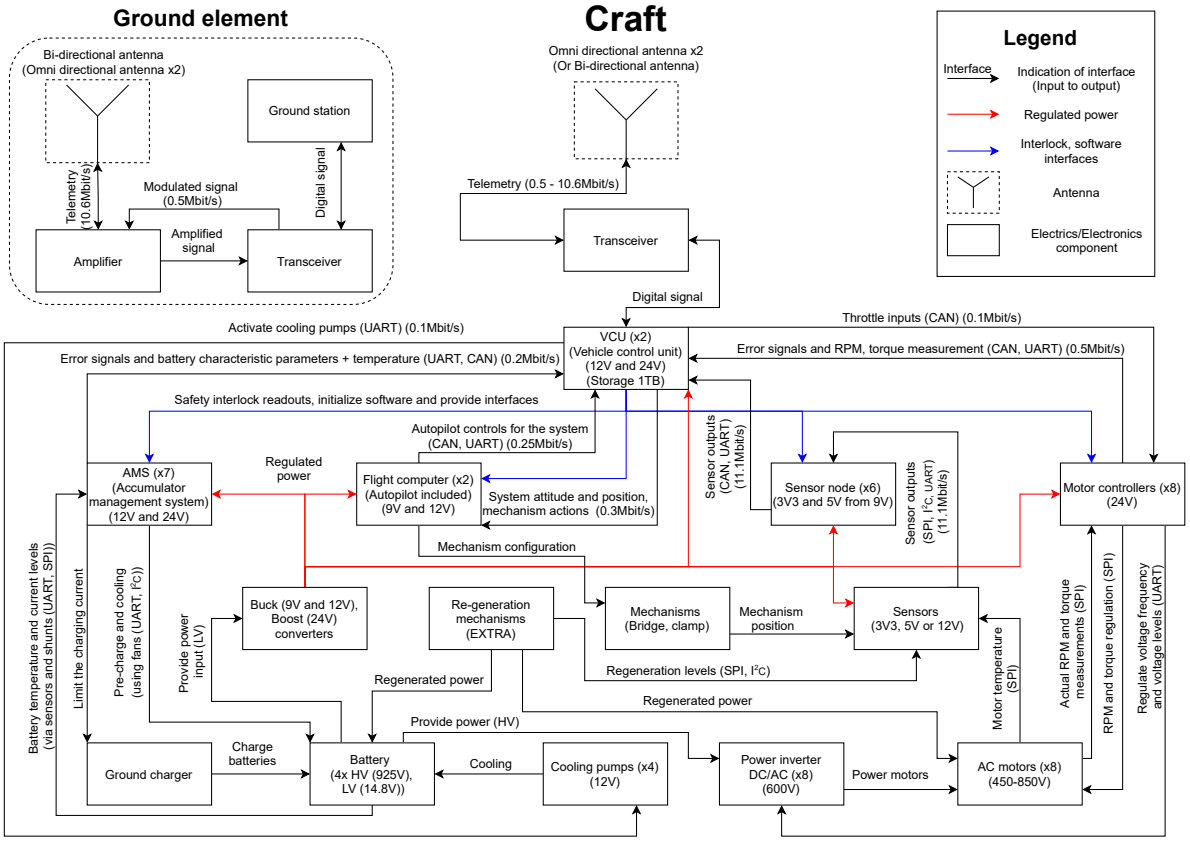

Figure 12.1: Electrical block diagram including electronics

12.1.1. Base division

The remote controller of the craft consist from three main components: antenna and the ground station. A more elaborate discussion of the antenna and the transceiver can be found in Section 12.3.1. Due the focus being mainly shifted towards the craft, the remote controller is not designed in detail. Nevertheless, one has to note that the ground station can be an intricate system of electronic devices, such as, displays, signal amplifiers and PCBs which receive, process and send data for further use. Given the fact that the bi-directional antenna of the ground station cannot be mounted on a hand-held con-

troller according to Section 12.3.1, a transportable ground station has to be established for the controls. Nevertheless, as the ground station is not consuming the crafts power for operations, the station is not defined at any stage of the project due its uselessness in the analysis without a sophisticated design.

The craft on the other hand is designed to a greater detail, as can be seen in Figure 12.1. In the craft itself, electrical and electronics components can be distinguished, where the bottom two rows correspond to electrical components and the rest belongs to electronics, with the exception of antenna and the transceiver. The electric and electronic components differ with the fact that electronics have data processing abilities while the electrical devices only convert electrical power into other types of energy. Regarding the electric devices, the most important for the design of the craft are set to be the batteries and the motors, with the converters and inverters being the secondary equipment. Moreover, regeneration mechanisms are added as an extra that can be implemented in the system at the final stage of the design, which is not covered during the DSE. A description of the regeneration mechanisms applicable to the particular mission can be found Midterm report of Group 13 [2].

12.1.2. Electrics

Before delving deeper into the realm of electronics, the more simple components of Figure 12.1 are discussed, which include devices not exhibiting any processing capabilities. It has to be noted that the wiring mass was not done separately, thus, its total mass was estimated to be around 10 *kg*.

Motors, Inverters, Mechanisms, Cooling pumps and Ground Charger

An in depth description of the motors can be found in Chapter 9 and inverters are discussed in Section 9.5, where all the characteristic parameters of the motor used in the design are mentioned. The cooling pump sizing can be found in Section 14.1. The ground charger is assumed to be the generator located on the firefighter truck. However, if the power required exceeds the available power at any point in the mission, a new generator has to be selected and transported together with the system.

The release mechanism will require a command from the flight computer to perform the release and attachments of the cabin. The mechanism will provide a feedback to let the VCU know whether the process has been successful. Likewise, a command from the flight computer is required for the bridge extending mechanism for actuators to respond and act accordingly. Once again, a feedback is sent to VCU. A further elaboration of the electrical mechanisms can be found in Chapter 7.

Batteries

A discussion o batteries in great detail can be found in Chapter 9, however, the cell layout and the total voltage of the batteries is yet to be discussed. Knowing that the chosen battery (according to Section 9.3) cell voltage nominally is 3.7 *V*, the total nominal voltage of the batteries can be determined. As the cell mass is not defined, it is assumed that their size is small, so that large quantities can be put in series to acquire necessary voltages. For HV applications it is assumed that 250 cells are connected in series, such that a battery nominal voltage of 925 *V* is acquired. The level of the voltage is chosen to ensure that the inverter defined in Section 9.5 operates on high efficiency ratings. As for the low voltage battery, the nominal voltage is set to be 14.8 *V* which is in between the electronics main operational voltages (9V - 24V). The selected layout of the cells ensures the highest efficiency of the converters due the lowest possible voltage variance applied in the range.

Converters

As for the converters, it was decided to have only the general voltage regulation (9, 12, 24 *V*) and PCB specific voltages are regulated on the boards themselves. Having two required voltages below the LV battery nominal voltage, it is clear that two buck type converters and a single boost type converter are needed. The buck converter is defined as a voltage altering device, which lowers the output voltage with respect to the input one, while the boost converter is based on the opposite principle. In order to have accurate sizing of the batteries, the converter efficiency has to be determined. It has to be noted that it was opted not to select converter circuitry available in the market currently, as the input voltage is too specific to find an exact match, leading to reduction in efficiency. For the initial sizing, the converters are assumed to be simple circuitry, consisting from only five main components as can be seen in Figure 12.2[40]. It has to be noted that the switch is replaced by a MOSFET (metal-oxide-semiconductor field effect transistors) in the particular application.

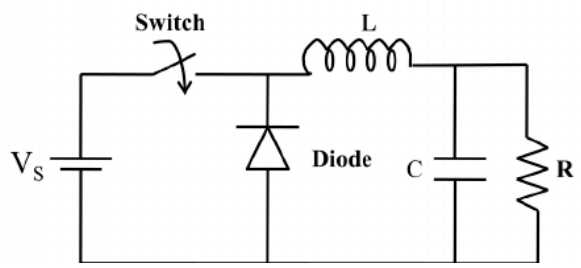

Figure 12.2: Simple converter

In order to size each component of the circuitry, first, parameters influencing the overall performance of the converters have to be defined. To achieve the highest efficiency and fastest transient response, it is assumed that the converters operate on the verge of discontinuous conduction mode (DCM), meaning that the inductor output current is equal to zero for for a slight portion of a switching interval. The continuous conduction mode (CCM) was not chosen as it offers lower efficiency than DCM [41]. The switching frequency (f_s) - the inverse switching time (T_s) - of the transistor is selected to be 600 *kHz*[42]. The last parameter influencing the entire system is the duty cycle (D) of the system, which represents the fraction of the time interval for which the switch is conducting. To determine it, a DCM current relationship has to be be used, which implies that the maximum current flowing through an inductor is at least twice as large as the average output current. Thereafter, first, the power consumption for the buck converters have to be defined. Referring back to Figure 12.1 where the voltage levels for the PCBs are defined and the power definitions provided in Section 9.4 it can be concluded that majority of power is going to be dissipated on 12 *V* line. Thereafter, it is assumed that the PCBs on the 9 *V* grid consume a total of 217 *W* of power while the dissipation at the end of the 12 *V* circuitry reaches 1406 *W*. The output current of the converters can be found by dividing the power outputs with their respective voltages. To approximate the maximum current on the inductor, the relation provided in Equation 12.1 can be used [47].

$$\Delta I_L = \frac{(V_{In} - V_{Out})DT_s}{L} \tag{12.1}$$

In Equation 12.1, the L is defined as inductance and V with their corresponding subscripts are the voltages. The duty cycle for a buck converter in a DCM can be computed as shown in the following equation:

$$D = \sqrt{\frac{2LP_{Out}}{V_{In}\left(V_{In} - V_{Out}\right)T_s}} \tag{12.2}$$

Combining Equation 12.1 with Equation 12.2 and using the aforementioned DCM limitations, it is acquired that the inductance of the buck converters cannot be more than 122 *nH* for 9 *V* and 16 *nH* for 12 *V*. The values used in further computations are assumed to be 110 and 15 *nH* to avoid over-current of the circuitry, as lower inductance implies higher inductor currents according to Equation 12.1. Before the efficiency of the converters can be defined, the time it takes for the inductor current to reach zero from the maximum has to be determined by Equation 12.3, such that power losses on all components can be determined.

$$\Delta_L = D\left(\frac{V_{In}}{V_{Out}} - 1\right) \tag{12.3}$$

[40] URL `https://www.researchgate.net/figure/Schematic-diagram-of-the-buck-converter_fig1_270122337` [cited 17 June 2021]

[41] URL `https://www.monolithicpower.com/en/the-difference-between-ccm-and-dcm-explained` [cited 17 June 2021]

[42] URL `https://www.sunpower-uk.com/glossary/what-is-switching-frequency/` [cited 17 June 2021]

Knowing the characteristics of the entire switching cycle of the converter, the root-mean-square (RMS) currents of all the components can be found as follows:

$$I_{C_{RMS}} = \sqrt{\left(I_{L_{RMS}}^2 - (D+\Delta_L)\,\Delta I_L I_{Out} + I_{Out}^2\right)} = \sqrt{\left(I_{S_{RMS}}^2 + I_{D_{RMS}}^2 - (D+\Delta_L)\,\Delta I_L I_{Out} + I_{Out}^2\right)}$$
$$= \sqrt{(D+\Delta_L)\left(\frac{\Delta I_L^2}{3} - \Delta I_L I_o\right) + I_{Out}^2}$$

To determine the final power losses, the approximate resistances of the components have to be determined. For simplicity, it is assumed that the components are the same for all the converters. To acquire a more accurate estimation on the power losses, a test is required where the input power has to be compared with the output power. The estimated values for the resistance are: 5 *m*Ω for inductor and the switch, 3 *m*Ω for the diode and 25 *m*Ω [47]. Applying Ohm's law the total power dissipation across the buck converters is acquired, which if divided by the output power provides the efficiency. The efficiency for the buck converters were determined to be 91% for 9 *V* and 77% for 12 *V*. Additionally, the turn-on power loss of the diode was accounted for, which can be computed by multiplying the forward voltage is multiplied by the average diode current, which is equal to half the current ripple ΔI_L multiplied with Δ_L. The efficiency values are accepted as preliminary estimations as the determined numbers are sufficiently high, thus no reiterations are performed. The analysis for the boost converter has similar analogy, however, this time the maximum inductor current has to be at least twice as high as the input current, which can be determined by Equation 12.4.

$$I_{In_{avg}} = \frac{P_{Out}}{V_{In}} = \frac{(D+\Delta_L)\Delta I_L}{2} \tag{12.4}$$

The output power of the boost converter was assumed to be equal to 732 *W* distributed across the MCs, AMS and the VCU. To determine all the parameters, the highest inductance has to be found once more. In order to find the L, the constraint on the DCM currents have to be applied and the two equations given below have to be combined by by plugging the D inside the equation for current ripple ΔI_L:

$$\Delta I_L = \frac{V_{In} D T_s}{L} \qquad\qquad D = \sqrt{\frac{2P_{Out}L}{V_{Out}V_{In}^2 T_s}\,(V_{Out} - V_{In})}$$

The maximum applicable inductance is found to be 95.6 *nH*. For further calculations the inductance is taken to be 85 *nH*. As next, the Δ_L has to be found, which can be expressed as provided in Equation 12.5

$$\Delta_L = \frac{2I_{Out}L}{V_{In}DT_s} \tag{12.5}$$

Lastly, to find the efficiency, the RMS current flowing through the components has to be determined. The currents can be found by plugging the determined parameters in equations below:

$$I_{L_{RMS}} = \sqrt{I_{S_{RMS}}^2 + I_{D_{RMS}}^2} = \sqrt{(D+\Delta_L)\,\frac{\Delta I_L^2}{3}} \qquad I_{C_{RMS}} = \sqrt{\Delta I_L^2\left(\frac{\Delta_L}{3} - \frac{\Delta_L^2}{4}\right)}$$

Applying the Ohm's law ans summing up all the powers returns an efficiency of 85% for the boost converter. A discussion of the combined efficiency of the converters can be found in Section 9.4

Sensors
All the sensors present on the craft are summarized under a single block to increase the ability to comprehend Figure 12.1. The sensors located on the craft are namely: cameras, altimeter, proximity (Time-of-flight), Global positioning system (GPS), temperature, RMS, mass flow sensors, gyroscope and accelerometer.

On the craft there are four 180° regular cameras used for video feed to the pilot. The cameras are located on each side of the craft, except the top and bottom to ensure full visibility during operations. The visibility of the regular cameras in dim conditions is aided by the use of projectors, one on each side of the craft. The total power consumption of a projector plus the camera is 72 *W* where 12 *W* are required by the cameras [43]. Moreover, night vision cameras might be implemented in a future design with the purpose of people location in the building, however, future tests are required to verify the feasibility of the idea [44].

An altimeter is used to determine the altitude of the craft. The altimeter module can measure the altitude up to a height of 8000 *m*[45]. The power consumption of the altimeter module is 0.042 *W* which is almost neglegible when computing the LV battery weight.

The time-of-flight sensors are used for obstacle avoidance, pilot aid and automated flight in case of communication failure. The sensor group consists of two ”towers” out of 8 sensors each, covering 360°, and two single sensors at the bottom of the craft for close proximity altitude measuring. The range of each sensor is 60 *m*, and peak power consumption is 1.65 *W*. The proximity sensors are elaborated in detail in Section 14.2.

The GPS sensor measures the longitudinal and latitudinal position of the craft as well as the altitude with an accuracy of 2.5 meters. The GPS sensor consumes 0.0594 *W* of power[46]. The RMS sensors are used to measure the angular velocity of the motors, thus, their count is set to be eight. Each RMS sensor is estimated to consume around 0.48 *W* of power [47]. Even though the chosen sensor is specifically designed for cars, it is assumed that a similar size and power consumption device can be manufactured for the particular design.

To measure the temperature at different locations of the craft, ten temperature sensors are taken excluding the thermistors and battery temperature sensors attached to the AMS. The temperature sensors consume as little as 10 μA per instance[48]. The mass flow sensors are applied to measure the flow rate of the cooling pipes. Four mass flow rate sensors are required to match the number of cooling systems as is discussed in Section 14.1. Each sensor is estimated to consume 0.6 *W* of power which sums up to a total of 2.4 *W*[49].

On the craft, there are three electric rate gyroscopes used to sense the rotation around all three axis with a limitation of 300°/*s* [50]. The total power consumption of the gyros does not exceed 0.075 *W*. Lastly, there are three accelerometer used on the craft to measure up to 50g's of acceleration [51] in each direction. To ensure redundancy, the accelerometers are put in a triangle configuration and their respective outputs are normalised. The power required for all accelerometers to work is mere 0.1 *W*. It has to be noted that the sensor list is not permanent at the current stage of the design and more sensors could be added if the project is to be continued.

[43] URL https://security.panasonic.com/training_support/support/technical_information/power_consumption_info/ [cited 21 June 2021]
[44] URL https://www.dronivo.de/FLIR-Vue-TZ20-Dual-Waermebildzoom_1 [cited 21 June 2021]
[45] URL https://www.banggood.com/FlySky-FS-CAT01-Altitude-Sensor-I_bus-Data-Port-Compatible-FS-i6-FS-i8-FS-i10-Transmitter-p-1661314.html [cited 21 June 2021]
[46] URL https://docs.rs-online.com/74ea/0900766b8147dbe2.pdf [cited 20 June 2021]
[47] URL https://www.omniinstruments.co.uk/displacement-position-sensors/optical-and-proximity-type-rpm-sensors/hall-effect-gear-tooth-sensor.html [cited 18 June 2021]
[48] URL https://www.embedded.com/tiny-temperature-sensor-features-low-power-consumption/ [cited 18 June 2021]
[49] URL https://www.ifm.com/img/sv-brochure.pdf [cited 18 June 2021]
[50] URL https://www.gyroscope.com/d.asp?product=PIEZO#changecurrency [cited 21 June 2021]
[51] URLhttps://www.te.com/commerce/DocumentDelivery/DDEController?Action=srchrtrv&DocNm=3038_Accelerometer&DocType=DS&DocLang=English [cited 21 June 2021]

12.1.3. Electronics

The electronics discussed in the subsequent subsections are only preliminary, as the project is done by aerospace engineers with little to no knowledge in the field of electronics. Designing version zero (V0) of a single PCB would require immense amount of full time work, measurable in length of the whole DSE. Nevertheless, full effort is given to acquire the highest design of the processing units. The analysis is began with the PCBs which design is at its earliest stages and progressively continued with the more developed concepts.

Sensor nodes

The sensor nodes are the smallest PCBs on the craft, as their main purpose is to acquire data from the sensors and transfer it to the vehicle control unit (VCU). The sensor nodes can vary in the design, however, for the project at hand, it is assumed that the sensor node circuitry consist of a 16-64 pin micro-controller unit (MCU) which supports at least two distinct I^2C and SPI lines and at least one UART connection and such that multiple sensors can be attached to one sensor node. To allow for external sensor connection, connectors with variable pin count are used. In Section 12.3.2 the communication protocols mentioned are discussed in more detail. Additionally, two linear voltage regulators are implemented in the circuitry, such that 5 V and 3V3 (3.3 V) voltage can be supplied to the small scale sensors. Moreover, clock circuitry is required, as majority of the sensors require clock tick counting, which is equivalent to taking time in digital systems[52]. A sensor located on the node itself is a thermistor, which is needed to indicate the temperature of the PCB. If wiring is performed correctly, the sensor node is a universal PCB applicable to read data from almost all types of sensors and their respective arrays. Lastly, an USB plug needs to be added to the circuitry to ensure availability for testing and CAN protocol established to allow for communications with VCU. It has to be noted, that USB, CAN protocol circuitry, internal temperature sensor and the connectors are part of every single PCB, thus they are not mentioned in subsequent paragraphs if no further clarification is required. Moreover, one has to keep in mind that the passive components as resistors, capacitors and inductors are neglected as their exact count and location in the circuitry cannot be determined at the current stage.

Motor controllers

The motor controllers in the particular design are rather small PCBs as the inverter is designed separately. Thereafter, the MCs are mainly responsible for pulse width modulation [48] to vary the voltage amplitude and frequency of the motor input signal [49], which implies that the majority of the circuitry is made up from comparators and logic gates used to drive the inverters circuitry. The microcontroller does not have to be too powerful, a 64 pin processor should be sufficient. Lastly, the motor controllers are responsible for start up and the direction controls of the motors. To prevent short circuits when changing the motor rotation, additional buffers to the circuitry have to be added which ensure that the signals are passed on when the motor has stopped.

Flight computer

The flight computer (FC) is a larger scale PCB, which has at least one powerful micro-controlling unit consisting of more than 64 pins, such that it can support the autopilot. For the autopilot, countless logic gates (or transistor relays) and comparators would be required in addition to the micro controller, to ensure that the right connections are selected every time, and one does not have to depend only on the correctness of the software. Lastly, a safety relay or a buffer which permits only one of the flight computers to be active at the time has to be implemented. The second flight computer is added as redundancy as discussed in Section 12.1.4. A possibility which was deemed unnecessary at the current design phase of the processing units is the establishment of direct communication between the sensor nodes and the FC to reduce the data travel time and the decisions on the response can be performed as rapidly as possible.

Vehicle control unit

The vehicle control unit (VCU) is both the ”brains” and the ”black-box” of the craft as it has to process and distribute the largest amount of data in the craft and store an immense amount of information for back-tracking. Thereafter, its processor could scale up to 144 pins or more, such that all the required responses can be performed. To reduce the size of the MCU, one could opt for two processors running

[52] URL `https://chortle.ccsu.edu/java5/Notes/chap02/ch02_11.html` [cited 17 June 2021]

in tandem, however, in such a case, the reliability of the system would be slightly lower. For data storing, a secure digital (SD) card can be used, which could potentially store all the information recorded in a single mission. After the mission, however, the data has to be transferred to an external device if necessary to prevent over-writing[53]. Another functionality of the VCU is initialization of the system and it also has to allow for software flashing (discussed in Section 12.3.2) if CAN bus(-es) are supported by it. The initialisation of the system includes the error checks and interlock readouts - verifying if the main communication is sequential rather than parallel[54]. Moreover, the VCU is responsible for the communications with the ground station, meaning that the required circuitry and connectors which support a transceiver have to be established. Lastly, the VCU has to be able to establish variety of small scale communication protocols between PCBs, mainly a multitude of UART connections. The communication has to be stable, thus, passive component filtering (RLC circuitry).

Accumulator management system
The accumulator management system or accumulator master switch (AMS) is responsible for continuously checking the status of the battery - temperature, depletion stage and power drawn. Additionally, the AMS has to establish even voltage distribution of the battery cells to avoid differential depletion and rapid degradation of cells. It is determined that a single AMS PCB is not sufficient for the particular design as the total power consumption of the PCB would lead to overheating. Thus, a master-slave configuration is used. The master is mainly designed to provide the clock inputs for the slaves and to process the incoming data. Therefore, the master would require a powerful micro controller, having around 144 pins, large capacity SD card and several I^2C or SPI communication protocol circuitry. The master also has to control the connections between the batteries and the external power supplies or consumers, such that no short circuitry is caused. For the control purpose either MCU controlled MOSFETs or logic gates can be used. As for the slaves, shunt (low series resistance) resistors are needed to get in- or out-flow current values, such that an approximate depletion of the batteries can be determined. To measure the temperature of the batteries, a simple thermistor can be used. To ensure the same voltage level on all the battery cells, passive cell balancing [50] can be applied. The circuitry required consists of MOSFETs and passive components as capacitors and resistors. It has to be noted that active cell balancing is a more efficient way of attaining equal voltage across the cells, however, implementation of the active balancing requires more sophisticated circuitry which is neglected for the time being [51].

12.1.4. Redundancies

To have a complete design of the electrical system, the required redundancies of the components need to be implemented. It has to be noted that the amount of extra components is designed for a single mission cycle with the conditions of a single component failure. From the constraint it can be concluded that the broken PCBs have to be changed right after the mission, implying that spare processing units always have to be kept at the maintenance station. Do keep in mind that the current estimations on the redundant electrical devices is temporary - more sophisticated analysis and testing has to be performed to acquire the actual reliability of the system.

The electric components having redundant device are the converters only. As the converters are responsible for power provision to the processing units, thus, directly influencing the craft's controls, it was decided to have a fail-safe system, since without LV grid enabled the craft would be destined to crash. Having redundant motors or batteries would lead to highly over-designed system, thus their reliability has to achieve values close to unity. The inverters are light weight, however, not knowing which of the inverters would fail implies that each of them needs a back-up. Doubling the amount of the DC/AC converters does lead to significant increase in the total mass, thus, it is assumed that no redundancies are used. The regeneration mechanisms themselves are considered an extra, thus no redundant components are required.

For the electronic components, it was decided to take a single extra PCB for each type of processing unit, except the MCs and sensor nodes. Neglecting the extra motor controller inclusion is analogous to the reasoning behind not including extra inverters. As the sensor communication is distributed across several PCBs, failure of a single sensor node is deemed not to be critical. The AMS requires a single

[53] URL https://wtop.com/tech/2018/02/an-explanation-of-sd-camera-cards/ [cited 17 June 2021]
[54] URL https://www.oxfordreference.com/view/10.1093/oi/authority.20110803100006950 [cited 18 June 2021]

extra PCB which can take up both, the masters and the slaves functions if either of the two fails. Thus, the AMS idle PCB would be of a larger size than the operational ones. As for the FC and VCU extra copies, a buffer relay is required to prevent the idle PCBs from activating, else a miscommunication might occur leading to craft being uncontrollable. To find the exact configuration, tests are required. With the last redundancies defined, the communication between the electronics components of the system can be discussed, as is done in Section 12.3.

12.2. S/W Diagram

The software block diagram is displayed in Figure 12.3. In the software block diagram, the functions of the craft electrical and electronics components are depicted, together with the inputs and outputs. The two tasks that are of great importance are the data collection and data processing which is done mainly by the VCU. After the data is processed, it is distributed among the components requiring the data for operations - mainly the flight computer and motor controllers. As the components do include the processing units and logical gates on them, the information is further processed on each of the devices. In the case of the flight computer, the data is used to reconfigure the autopilot such that stability during flight is retained. The motor controller will receive data on what thrust setting is required and will adjust the voltage of the inverter to vary the RPM and torque to achieve thrust. As bridge actuator and the centrepiece clamps are electric components, they will only execute commands provided to them by the flight computer. Additionally all the sensor contributions - attitude, temperature, video can be found in the diagram. The green and red arrows show the order of functions that are performed for the uplink and downlink respectively.

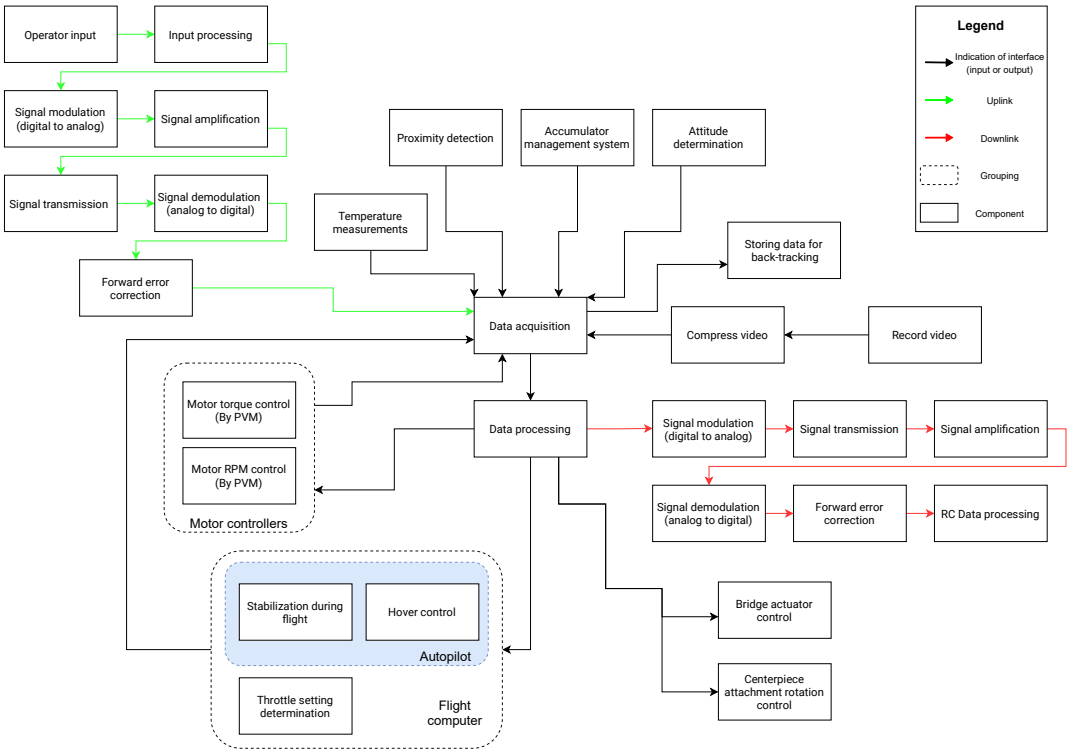

Figure 12.3: Software block diagram

12.3. Communications

The communication flow diagram is a tool used to depict the most important data links of the systems components. In order to generate such a diagram, the links between the devices have to be investigated on both internal and external scale. For external communication an antenna system is used for which the link budget is performed in Section 12.3.1 while the on craft communication is elaborated in Section 12.3.2. It has to be noted that there is no independent figure for communication flow as

it was opted to fuse all the communication and data link specifications with the Figure 12.1 for figure optimization as mentioned at the beginning of the chapter.

12.3.1. Link budget

For the communication purposes, a complete link budget has to be analysed to determine whether a reliable communication link can be established. A good link is characterised by signal to ratio (SNR) above 25 *dB*[55] margin, which is set to be the bare minimum for the analysis to follow. The SNR is used to compute a noisy communication link maximum channel capacity which is further used to determine whether the data of the system can be transferred across the system.

As first, the channel capacity based on Shannon-Hartley theorem is defined [52]:

$$C = B \cdot \log_2(1 + \frac{S}{N}) \tag{12.6}$$

For Equation 12.6, the channel bandwidth, *B*, and the signal to noise ratio, $\frac{S}{N}$, are needed. The channel bandwidth can be determined from antenna specifications. From literature, it is found that aviation air-to-ground communication is done on very high frequency (VHF) which ranges from 30-300 *MHz*[56]. Thereafter, it is decided to look for on-the-market antennas which operate in VHF range. In addition, a decision to use the MLB3001 antenna[57] for the craft has been made. The antenna has an operating frequency of 30-54 *MHz* which provides a bandwidth of 24 *MHz*. The ground antenna is chosen to be parabolic antenna with an initial diameter estimate of 1.5 *m*. It has to be noted that to receive the highest efficiency the parabolic antennas are commonly applied for ultra high frequency (UHF) range [52]. Nonetheless, it was opted to use a dish antenna due its attachments flexibility for pointing and the sizing simplicity. The highest attainable pointing accuracy is desired to mitigate the signal losses and to establish a strong connection between the craft and the ground.

Other than the antenna's, the communication system also makes use of transceivers and amplifiers. A transceiver is present on both the craft and the remote control whereas amplifiers are only present on the remote control. The transceivers takes digital signal from the remote control and VCU and put them on an analog carrier wave which is sent by the antennas. The amplifiers enhance the complete signal received by the ground antenna. The specifications of the antennas, transceiver, amplifiers and cables can be found in Table 12.1. Since the loss factor is dependent on how long the cable is, a parameter L has been introduced which is the length of the cable. Moreover, the gain of the cable is the inverse of the loss factor of the cable.

Table 12.1: Communication components

Module	Gain [dB]	Noise figure/ loss factor [dB]
Craft antenna[58]	2.14	-
Ground antenna	0.092	-
Amplifier[59]	20	5.7
Transceiver[60]	-	1.6
Cable	$\frac{1}{Loss factor}$	$0.5904 \cdot L$

System noise

The noise of the system components is one of the key parameters to be mitigated in order to reduce the overall noise interfering with the signal. One has to keep in mind that noise temperature in this concept

[55] URL https://resources.pcb.cadence.com/blog/2020-what-is-signal-to-noise-ratio-and-how-to-calculate-it [cited 14 June 2021]

[58] URL https://shop.rfwel.com/30-54-mhz-lowband-full-length-quarter-wave-antenna/ [cited 14 June 14 2021]

[56] URL https://terasense.com/terahertz-technology/radio-frequency-bands/ [cited 14 June 2021]

[57] URL https://shop.rfwel.com/30-54-mhz-lowband-full-length-quarter-wave-antenna// [cited 14 June 14 2021]

[60] URL https://www.isispace.nl/product/vhf-uhf-ground-station-transceiver/ [cited 14 June 14 2021]

[59] URL https://www.ti.com/lit/ds/symlink/ths7001.pdf [cited 14 June 14 2021]

is not a physical, measurable parameter, but rather an engineering approximation.[61] To calculate the system noise power density Equation 12.7 can be used, where k is the Boltzmann constant and T_{sys} the noise temperature of the system.

$$N_0 = k \cdot T_{sys} \tag{12.7}$$

Before the noise temperature of the system can be found, the individual noise temperatures of the communication components have to be calculated. The noise of the antenna is usually a value between 700-750 *K* [53]. Assuming the worst case scenario, the noise temperature value for the antenna is taken to be 750 *K*. The noise figures of the amplifier and receiver are as stated in Table 12.1. Thus, Equation 12.8 can be applied, taking a value of 290 *K* for T_0. The cable noise temperatures can be calculated using Equation 12.9, making use of the loss factor of the cable.

$$T = T_0 \cdot (F - 1) \tag{12.8}$$

$$T = T_0 \cdot (L - 1) \tag{12.9}$$

To find the noise temperature of the whole system, the system first needs to be described. Data flow of the system can be described as depicted in Figure 12.4. Exploiting the fact that the SNR at any point on the receiving end is the same, as both the signal and the noise get amplified due a gain in the system, the total system noise is computed just at the receiving antenna. Equation 12.10 and Equation 12.11 are set up using Figure 12.4 and the sound to noise ratio characteristics. These equations are the system noise temperature for the downlink and uplink respectively. Do note that all variables in the equations below are expressed in non-decibel units and must hence be first converted from decibels. With the temperature computed, the total noise power ath receiver of the downlink is acquired to be -196.3 *dB*.

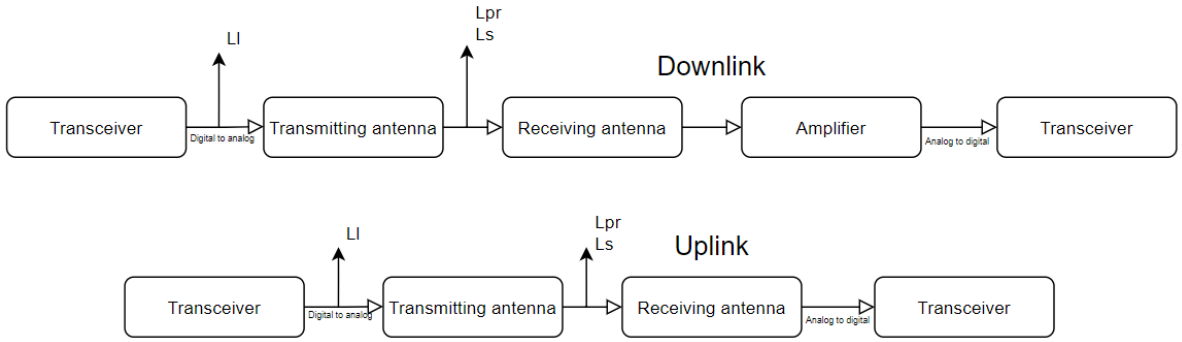

Figure 12.4: Antenna communication flow

$$T_{sys} = T_{antenna} + T_{cable1} + \frac{T_{amplifier}}{G_{cable1}} + \frac{T_{cable2}}{G_{cable1} + G_{amplifier}} + \frac{T_{receiver}}{G_{cable1} + G_{amplifier} + G_{cable2}} \tag{12.10}$$

$$T_{sys} = T_{antenna} + T_{cable1} + \frac{T_{receiver}}{G_{cable1}} \tag{12.11}$$

[61] URL `https://glossary.ametsoc.org/wiki/Noise_temperature` [cited 16 June 2021]

Signal
The next step is to find the signal power. The general equation for the power received by the receiving antenna is shown in Equation 12.12.

$$P_{rec} = P_t \cdot L_l \cdot G_t \cdot G_r \cdot L_s \cdot L_{pr} \cdot L_r \tag{12.12}$$

This equation contains the power sent by the transmitting antenna, P_t, the gain of the transmitting and receiving antenna as well as several loss factors, where the individual loss factors are evaluated in the following paragraphs.

Firstly, L_l is evaluated, which takes into account the loss of power before it is sent by the transmitting antenna. L_l is assumed to be consisting only from the loss of the cable connecting the amplifier to the antenna. Secondly, L_s is the free space loss which is the loss due to the environment in which the signal is travelling. The Equation 12.13 is used to determine the L_s [54]. Since the craft operates in an urban environment, alpha is taken to be 3.6 [55]. Moreover, d is the distance that the signal has to travel. By assuming a maximum angle of 60 *deg* between the receiver and antenna, a maximum signal distance of 800 *m* is obtained, as maximum operational altitude is 400 *m*.

$$L_s = -10\alpha \log_{10}(\frac{4\pi d}{\lambda}) \tag{12.13}$$

L_{pr} is the loss of signal due to pointing errors. The pointing loss error can easily be calculated using Equation 12.14 [52]. The two missing variables are the pointing offset, e_t, and the antenna half power beamwidth (HPBW),$\alpha_{1/2}$. The pointing offset is assumed to be 10° as the ground station has some pointing capabilities. The HPBW can be found using Equation 12.15 for the parabolic antenna, making use of the wavelength,λ and the antenna diameter, D [56]. For the monopole antenna on the craft a HPBW of 45 *deg*[62] is taken The last loss factor is L_r which approximates all the losses which cannot been determined directly. In the particular case, the L_r loss is set to zero due the absence of testing and similar missions.

$$L_{pr} = -12 \cdot \left(\frac{e_t}{\alpha_{1/2}}\right)^2 \tag{12.14}$$

$$\alpha_{1/2} = 58.4\frac{\lambda}{D} \tag{12.15}$$

The gains from both the transmitting and receiving antenna are given in Table 12.1. The maximum power that the craft antenna's can provide are 250 *W*. Since the ground antenna is big and connected to a power supply on the ground the maximum power is estimated to be 500 *W*. With all the parameters known, the received power can be calculated for both uplink and downlink. To obtain the received energy, the received power needs to be multiplied by duration of a bit, which is assumed to be equal to the inverse of bitrate. The bitrate is defined as the data in bits sent per second. The bitrate of the system is adapted accordingly to the analysis performed in Section 12.4. In Table 12.2, the received energy, system noise, signal-to-noise ratio, and channel capacity are displayed. As can be seen by these results, the assumed diameter of the ground antenna suffices to establish a stable communication link. Another option to estimate the SNR is to find the total noise power by determining the equivalent noise bandwidth and multiplying it with the noise power density. Then the received power can straight forwardly be divided by the signal noise power. Nevertheless, the equivalent noise bandwidth estimations require testing, thus, the methodology was omitted from the analysis. Lastly, the delay of the signal can be estimated to be the maximum communication distance taken equal to 800 *m* divided by the speed of waves traveling which can be approximated to be $3{\cdot}10^8$ *m/s* which returns 2.67 μ*s*.

[62] URL `https://www.ahsystems.com/articles/Understanding-antenna-gain-beamwidth-directivity.php` [cited 16 June 2021]

Table 12.2: Calculation results

Parameter	Downlink	Uplink
Received energy [J]	1.23E-10	2.46E-20
System noise [J]	2.34E-20	1.3E-10
Signal-to-noise ratio [dB]	26.8	62.8
Channel capacity [Mbit/s]	213.5	500.5

12.3.2. Internal communication protocols

To complete the overview of the communication links established for the whole system, the internal protocols have to be investigated. The internal communication is characterized as the data line connections between inter-dependant electronics components, where the communication can be established with electronics and/or software.[63] The protocols can be split into two main groups - inter and intra system[64]- where former implies communication between two devices, for instance a testing computer added to any PCB while the latter considers internal communication of PCB components, for example, a light emitting diode (LED) strip or a sensor is attached to the micro-controlling unit.

The inter communication links can be further split into two commonly used links, namely Universal Serial Bus (USB) and Universal Asynchronous Receiver/Transmitter (UART). The USB protocol is mainly used for testing or software programming purposes of the processing units where the device used for the testing is the master - all controls are inputted through it - and the test subject (PCB) is the slave which fulfils all the commands.

The USB link is used on almost every PCB as it ensures rapid and simple connection usable for software updates and flashing[65] and the USB connector is generally universal, meaning that any PCB containing MCU does support the use of USB. Additionally, a single USB port can be used to support large magnitude of different devices, making it a powerful testing tool. Nevertheless, the issues with using the USB protocol are the necessity for sophisticated drivers which can enable the functionalities of the device and the requirement for powerful master, as it commonly serves as a power source while the connection is intact. Thereafter, the internal communication using USB is omitted as much as possible.

The UART on the other hand is less of a communication protocol but rather a circuitry which exploits the principles of converting serial data - sending data along one line - to parallel data - sending split data along multiple lines simultaneously[66]- and vice versa so that the signal can be sent from the transmitter to the receiver along one wire. The refactoring of the information leads to a more cost effective solution of data transmission and makes the clock signaling obsolete, however, the time it takes for the data transfer is increased when compared to an USB connection. Moreover, the UART establishes the connection between one master and one slave only. The UART is commonly used when linking the AMS to VCU or flight computer to the VCU to reduce the transmission losses as large quantities of data are sent to and back between the processing units.

As for intra communication systems there are three main protocols in use for PCBs: serial peripheral interface (SPI), inter integrated circuit (I^2C) and controller area network (CAN). The SPI protocol is based on master slave relationship, where the slave takes instructions form the master. The slaves are usually smaller scale devices as drivers, memory cards or sensors, while the master is commonly selected to be MCU. The master can control several slaves, meaning that sensors of similar type located at different locations of the craft can be run by a single PCB. Additionally, using SPI, the information can be communicated in both directions simultaneously with relatively high data rate. Nevertheless, the potential flaws of using SPI communication protocol are the rapid increase of complexity and wiring

[63] URL https://www.seeedstudio.com/blog/2019/07/03/basic-electronics-wired-communication-protocols-in-embedded-design/ [cited 15 June 2021]

[64] URL https://www.elprocus.com/communication-protocols/ [cited 15 June 2021]

[65] URL https://jolla.zendesk.com/hc/en-us/articles/203533993-Software-flashing-vs-Software-updating [cited 15 June 2021]

[66] URL https://www.quantil.com/content-delivery-insights/content-acceleration/data-transmission/ [cited 15 June 2021]

if multiple slaves are implemented due the inter-dependencies of the clock signal (used to count the ticks passing) and the slave selection circuitry. The multiple slave protocol is mainly used by the sensor nodes and AMS to which a multitude of sensors are attaching.

The I^2C protocol is differing from SPI with the fact that for the inter integration it is possible to not only attach single master to multiple slaves but also magnitude masters to a single slave or multitude of slaves. The entirety of the data is transmitted along two lines just as done for the UART, meaning that the wiring and the complexity of the circuitry is reduced with respect to the SPI protocol. Nonetheless, the potential problems with using the I^2C protocol are the limitations for the communication speed caused by the use of single line for communication in both directions and the maximum of 9 bit information which can be transferred. The I^2C in the current configuration is used to integrate the redundant PCB circuitry, such that if a single component fails, the master can be replaced almost instantly.

Possibly the most important communication protocol on the craft is CAN, which is used for data transmission between different PCBs connected in a single network. Knowing that there is comparatively small number of large scale PCBs (masters) used in the craft at the current stage, a single CAN bus can be assigned to cope with the data loads of all the processing units simultaneously. Thereafter, the main advantages of using the CAN in the particular design of the craft is the reduced weight of the wiring as all the communication is performed on a twisted two line link and the high-speed reliable connection, which is important for flawless execution of crafts controls. It has to be noted that the protocol is relatively complex, thus external software experts would be required to fully develop a working CAN drive. As the sensors on the craft, communication protocols and links have been determined, the data rate and how to handle it can be determined.

12.4. Data Handling

A good data handling structure is crucial for the intended mission as the data links between the subsystems of the craft have to have sufficient capacity at all times, such that the total information is continuously communicated. Else, the system could reach overflow and the data could get irreversibly damaged, leading to loss of control. Thereafter, the data rate of the system is analysed, and the necessary components that have to handle the data are sized. One has to note that the data handling components (memory size, internal communications and bitrate) are included in Figure 12.1, however, the processor specifications are kept in the text not to overfill the diagram.

The bitrate that is required for the downlink is significantly higher than the one required for uplink due the large difference in the amount of data needed to be sent to the pilot versus to the craft. For the downlink, the data that will take up most of the bitrate is the feed of each camera. There are four cameras on-board for which the video is continuously communicated to the remote control at the same time. The selected resolution of the cameras is 1280x720 pixels with the frame rate of 30 frames per second. Assuming a colour depth of 24 bits per pixel, the video feed will require a bitrate of 663 *Mbit/s* per camera, which can be computed by multiplying all the given numbers together. The video is compressed before sending to significantly reduce the continuous data rate. The compression rate is taken to be 250 which allows for a total bitrate of 10.6 *Mbit/s* for all four cameras[57]. The only other modules that will be sending data are the GPS module, temperature sensors and the time-of-flight sensors discussed previously. The GPS module will send 8 bits of data at a rate of 5 *Hz*[67]. The ten temperature sensors each contribute 16 bits at a rate of 4 *Hz*[68]. Lastly, the ten time-of-flight sensors provide a total bitrate of 0.48 *Mbit/s*[69]. All of the bitrates add up to a total bitrate of 11.1 *Mbit/s*. From the electronics components, it is estimated that the FC and AMS will be accountable for the most bitrate generated as autopilot control sequence and internal not yet defined sensors are going to be present. Nonetheless, the data from the PCB traveling through the system shall not exceed the total amount of information generated by the time-of-flight sensors. The only processor sized at the current phase of the project is the VCU's micro-controller as it has to handle the most data. It is assumed that technically all the other processing units can have exactly the same MCU, such that the data handling requirements are met.

The total data rate processed by VCU's processor has to be estimated. It is known, that the camera feedback is sent to the pilot only, as the video feed is not useful for the autopilot controls, meaning that the data from cameras is not handled by the MCU on the VCU. Nevertheless, one has to note that the video compression circuitry is located on the VCU. Summing up the rest of the contributions, it is

acquired, that the bitrate through the VCU is approximately 1 *Mbit/s*. To be certain that the data rate is enough at all times, a safety factor of 1.5 is taken into account. The processor chosen is STM32F446xC with LQFP144 pinout to have all the necessary connection possibilities[70]. The MCU's maximum bit rate for a single CAN is 1*Mbit/s*, thus meaning that two CAN might be required. Nevertheless, it has to be kept in mind that the communications might occur through different links, which bitrate is higher. The static random access memory (SRAM) of the VCU would reach 132 *KB* which is equivalent to approximately 1 *Mbit* which is most certainly sufficient enough to access the necessary data momentarily as the incoming data is mostly sequential rather than parallel. The combination of UART and SPI connections support a total of 50 *Mbit/s* which is sufficiently more than the total data rate required. The MCU selected is currently too powerful for the application, however, it could happen that a stronger MCU is needed in the future when a more detailed design is achieved.

For data storage on the VCU an SD card is selected as mentioned previously. To make sure that the data can continuously be stored on the VCU, the limitations to the back-tracking of data are set. Assuming that the data is recorded for the whole duration of the mission, the total data amount on SD card is required to be 26 *GB* if 20 cycles each of 15 minutes. The maximum writing and reading rate of 1.45 *MB/s* which can be easily achieved by the modern SD cards [71]. If one opts to not extract data from the SD card until a technical issue occurs during a mission, a data overwriting software has to be implemented, which has to start its operations in the 39th cycle, if a 1 *TB* card is used. It has to be noted, that all the data was assumed to be stored on the VCU only, nevertheless, minor data might get stored on a small capacity SD card on the AMS.

12.5. Conclusion

In this chapter, all electronics necessary for the craft to function properly, have been determined. A detailed electrical block diagram has been created to display the interfaces between the components and how the data is handled. Moreover, a communication link is set up between the remote control and the craft to allow for clear and stable data transfer.

The vehicle was designed to be fail-safe however an emergency might occur. Thus an analysis needs to be performed on how to keep everyone safe if an emergency were to happen. The next chapter will outline the analysis and design the craft for safety during an emergency crash landing.

13. Crash Landing Analysis

The system is designed with safety in mind and the fail-safe methodology is applied, however there is still a chance that an emergency might occur. In that case, the vehicle should still be able to land while delivering the payload, thus the evacuees and the firefighter, safely to the ground.

The aim of this chapter is to outline the analysis and design of the craft for safety during an emergency crash landing.

Since the craft is required to safely land after an engine failure as defined by SYS-SAFE-03, the propulsion system and structural components should be designed with this in mind. in Section 9.3 it was mentioned that the expected likelihood of an engine failure will be once in the product life cycle. To maximise safety during an engine failure, the propulsion system could be designed to have so much excess thrust that the craft can hover with one rotor arm completely shut. This requires the design thrust to be at least twice the craft maximal weight. That is too much energy to have a feasible electric propulsion system so instead it is opted to analyse a crash landing where the thrust is used to decrease the ground contact speed as much as possible. The landing gear will then be used as a failure by de-

[67] URL https://docs.rs-online.com/74ea/0900766b8147dbe2.pdf [cited 16 June 2021]

[68] URL https://ams.com/documents/20143/36005/AS621x_DS000677_2-00.pdf/a90b32a5-d1f8-e6df-5327-bec856e093dd [cited 16 June 2021]

[69] URL https://terabee.b-cdn.net/wp-content/uploads/2021/02/User-Manual-for-TeraRanger-Evo-single-point-distance-sensors-and-backboards.pdf [cited 16 June 2021]

[70] URL https://eu.mouser.com/datasheet/2/389/stm32f446ve-1839298.pdf [cited 18 June 2021]

[71] URL https://tweakers.net/pricewatch/1375144/sandisk-1tb-microsdxc-uhs-i/specificaties/ [cited 22 June 2021]

sign crush zone to stretch the deceleration over a distance of 65 *cm*. Since the detail design of the landing gear will happen in the post DSE phase as mentioned in Section 11.4, this is a preliminary value. The limiting factor in a crash landing is the G tolerance of the evacuees. The maximal acceleration on the human body is dependent on the axis of application and is summarised in Figure 13.3 for a vertical application of the load. The lateral and axial Eiband curves are omitted from this report. The coordinate system used is given in Figure 13.1.

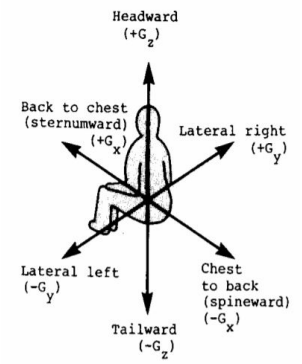

Figure 13.1: Human coordinate system for crash acceleration [58]

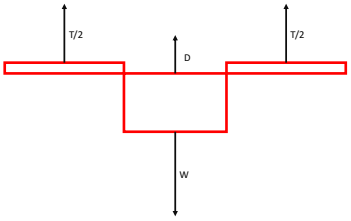

Figure 13.2: Free body diagram of craft during descent with engine failure

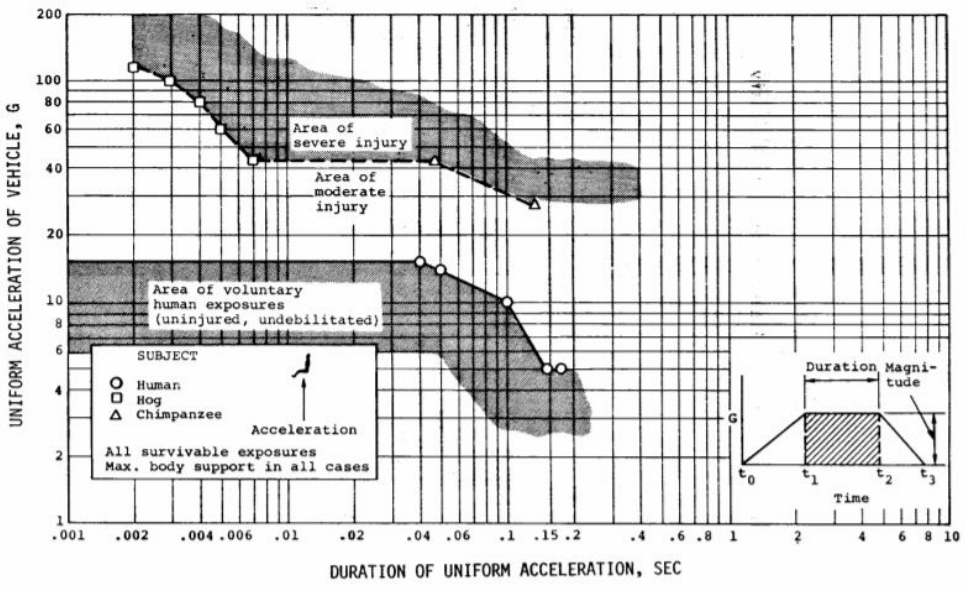

Figure 13.3: Eiband curve for vertical acceleration G_z [58]

To then calculate the accelerations of the craft during a ground impact, a triangular model for the acceleration as described in [59]. This is also the model recommended in [58]. Equation 13.1 gives the peak acceleration for this model. The average acceleration is half of that.

$$a_{peak} = \frac{2\Delta V}{T} \tag{13.1}$$

Where $\Delta V = V_i$ is the ground contact speed since the craft will decelerate all the way to a complete stop. T is the impact duration which is related to the mutual crush of the craft and the ground by Equation 13.2. Since urban areas have concrete undergrounds, the mutual crush is actually just the crush of the vehicle.

$$T = \frac{\Delta S}{2V_i} \tag{13.2}$$

Now to complete the analysis of the crash landing, a model for the fall of the craft is needed. It was opted to use a model of a vertical fall with a constant thrust setting and air resistance which is described by Equation 13.3. The expression is the equations of motion derived from the Free Body Diagram in Figure 13.2

$$m\frac{dV}{dt} = W - T - D \tag{13.3}$$

By rearranging and letting $D = C_D \frac{1}{2}\rho V^2 S$ Equation 13.4 is obtained.

$$\frac{dV}{dt} = (1 - \frac{T}{W})g - \frac{C_D \rho V^2 S}{2m} \tag{13.4}$$

This is a non-linear first order separable differential equation which was solved with forward Euler numerical time integration. The solution was verified with the analytical expression for the terminal velocity which is obtained by letting $\frac{dV}{dt}$ = 0 Equation 13.5

$$V_{term} = \sqrt{\frac{2m}{C_D \rho S}(1 - \frac{T}{W})g} \tag{13.5}$$

The result of solving Equation 13.4 numerically is shown in figure Figure 13.4. The most important results are the ground impact velocity and the time it takes to reach the ground. Note that all plots are obtained at a density of 0.92 kg/m^3. which is the density at the limit altitude of 3000 *m*.

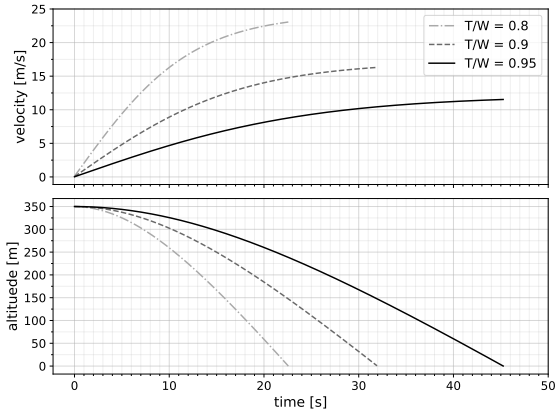

Figure 13.4: Solution of (13.4) for different values of $\frac{T}{W}$ at an altitude of 3000 *m*

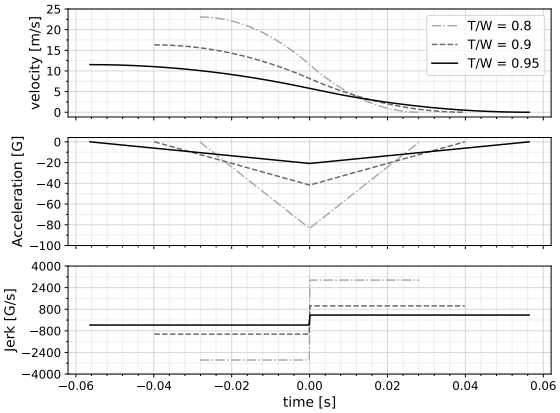

Figure 13.5: Model of ground impact for different values of $\frac{T}{W}$ at an altitude of 3000 *m*

It can be seen that for $\frac{T}{W}$ = 0.8 the peak acceleration is in the lethal range for hogs and the average acceleration is in the region of moderate to serious injury. For $\frac{T}{W}$ = 0.9, the peak acceleration and average acceleration lie both in the region of moderate to serious injury. Only for $\frac{T}{W}$ > 0.95 is the average G in the region of voluntary exposure. The peak acceleration for this case is 21 *G*. Note that the Eiband curves were derived from experiments performed by Colonel John Stapp on himself, his coworkers and volunteers. Colonel John Stapp was a US Air Force pilot and his demographic of volunteers was mostly healthy young men. Therefore an appropriate safety margin should be implemented to make the design compliant with SHR-U-09 which states that the craft should be save for evacuees of all physical abilities. It was decided to apply a safety factor of 1.5 on the maximum vertical acceleration (G_z) resulting in a maximum average acceleration of 14 *G*.

Some exotic design options for crash landing include having an emergency parachute on board, having an actuator tilt the seat before impact to allow a more favourable load application, or fitting the craft with an airbag. To slow down the cabin to 8.3 *m/s* the parachute with a drag coefficient of 1.75 [72] would need to have a diameter of almost 17 *m*. When looking at Google Maps, in urban environments the distance between two high rise buildings which are across the street from each other is usually around 30 *m*. Using a parachute of the size mentioned before might seem doable at first but when opening a parachute, the descent is not in a straight line, it tends to swing a bit so the parachute can get stuck to something easily in an urban environment especially with that size. It was thus deemed unfit. Since the craft is expected to have only one engine failure in its operational life, it is not desirable to have six heavy actuators permanently under the seats adding complexity and weight. A crash airbag can still be implemented but if so it will be an internal system like in a car as the added complexity of an external crash airbag is undesirable. Also the landing gear is in the way of an external airbag so it would have to be discarded before hitting the ground. Therefore it is deemed acceptable to just let it fail by design during a crash landing.

From this analysis it can be determined that the thrust to weight ratio during an engine failure should be at least 0.95 to have a safe crash landing. With the current rotor design, the motor is powerful enough to deliver a maximum thrust of 1.95 times the craft maximum weight. This equates to 6.37 *kN* of thrust per rotor arm. Given that during an engine failure only 2 rotors will carry the weight of the craft, that means that the OEI thrust to weight ratio is 0.975. Since the G tolerance is met at a Thrust to weight ratio of 0.95, the craft is capable of surviving from an engine failure followed by a crash landing.

It should be noted that this is a safe procedure during an emergency. However, a landing at this lower thrust to weight ratio cannot be performed every landing to save energy. This is because such a rough landing is survivable and safe if a person endures it once. However, the firefighter that will be in the cabin accompanying the evacuees must endure the landing several times when an emergency happens. Therefore a rougher landing is not an option as the firefighter will endure multiple of these landings in a short amount of time.

14. Aircraft System Characteristics

The main systems of the vehicle have now been analysed and sized. However, several important subsystems that are specific to the system have not yet been sized, while they do add significant complexity, mass or power requirements to the system.

In this chapter, relevant supplementary subsystems and their characteristics are sized and presented. Firstly, the thermal management will be explained in Section 14.1 before detailing the obstacle avoidance sensors that the vehicle will contain in Section 14.2.

14.1. Thermal Management

The primary concern of the thermal management system is the excessive heating of the high voltage battery. Normally, designing a cooling system able to properly mitigate the heating issues requires a detailed numerical model. However, due to time and resource limitations of the project, only preliminary sizing was done, thus only the governing system parameters are determined.

In order to cool down a surface that dissipates heat with a fluid, Equation 14.1 is used [73].

$$P_{loss} = \dot{m} \cdot \Delta T \cdot C_p \cdot Eff \tag{14.1}$$

Where P_{loss} is the heat dissipated, $\dot{m}$ is the mass flow of the fluid, ΔT is the temperature rise of the fluid, C_p is the specific heat of the fluid, and Eff is the efficiency factor. For liquid cooling, it is applied due to the brass/copper presence and the fluid friction with the pipes, and taken as 0.7.

In order to determine the theoretical temperature increase of the batteries per second, heat loss on the batteries has to be found. The heat can be approximated as the product between the power dissipation and the time of application, where time is set to be one second. The heat dissipation per second of a

[72] URL `https://www.grc.nasa.gov/www/k-12/VirtualAero/BottleRocket/airplane/rktvrecv.html`[cited 17 June 2021]

single high voltage battery can be found by multiplying the total available power with a factor of $1 - \eta_{bat}$ and dividing by the number of the HV battery. To acquire the temperature increase of the battery, the equation Equation 14.2 can be used.

$$\Delta T = \frac{P_{loss}}{C_{bat} M_{bat}} \tag{14.2}$$

In Equation 14.2 C_{bat} is defined as the specific heat capacity of the battery. The battery consists of three main components, namely anode, cathode and electrolyte, for which the sum of the individual specific heat capacities can be averaged and assumed to make up the total one. The anode and cathode are set to be made of lithium metal and vanadium oxide while the electrolyte is assumed to be solid polymer, more specific epoxy resin [60]. The mass fractions between the battery components are 1/6, 1/6 and 2/3 where the largest portion is taken up by the electrolyte. Finding that the specific heat capacities are 1110 *J/kg·K* [74] for the cured epoxy, 490 *J/kg·K* [75] for the vanadium oxide (assumed to be the same as vanadium) and 3600 *J/kg·K* [76] for lithium metal. Thus, the estimated specific heat capacity of the battery is 1421 *J/kg·K* and thus the temperature increase of approximately 0.18 *K* per second. It is assumed that all this heat is taken out from the batteries almost instantaneously, and thereafter, the battery temperature is assumed to be in the range of 35 $\pm$ 15 °*C* for safe and efficient operations. Having determined the heat that has to be continuously extracted from the batteries, the required cooling system can be sized.

The approach is to first check whether it is possible to use air cooling, which is the lightest and most simple solution. However, when large amount of heat needs to be transferred, air may require unfeasible mass flow supply. This was one of these cases, as when C_p of air is substituted, the required mass flow becomes 2,05 *kg/s*, which is equivalent to about 1.67 m^3/s with ISA air density. Therefore, a more efficient thermal management system is needed. Liquid cooling is a widely used system in various kinds of vehicles, and so it will be sized next. Using the same parameters in the formula, but changing C_p to 4186 *J/kg·K* of water, the mass flow now becomes just 0.49 *kg/s*, which is manageable.

Conventional liquid cooling system generally consists of pipes with the fluid, radiator cooler, tank or some storage for reserve fluid, and liquid pump. Cold plates can be used for heat exchange with heat source. The surfaces to be cooled are the all ”shared” walls of the patches, and all bottom surfaces - i.e. all instances where patch surface is in physical contact with another surface. All of the components need sizing.

After for the conventional system with cold plates was done, the system turned out to be extraordinarily heavy for a UAV, reaching almost 300 *kg* of mass. The primary problem were the aluminium cold plates, which made up about 2/3 of the total mass. Some re-design considerations have been done, specifically: the cold plates were removed altogether, leaving the cooling to be done directly by the pipes; the pipes themselves have been changed from circular to rectangular shape to increase contact are with the surface, ***without*** changing the cross-section or material percentage surrounding the flow. This almost did not affect the computation procedure, which is described further.

Pipes

Having a mass flow requirement, and a set flow velocity of 4.6 *m/s* to have only partial turbulence within pipes, it is possible to calculate the necessary cross-sectional area, using water density and a 1.1 factor for the extension in each of the two dimensions to coat the flow with a material, presented in Equation 14.3. For the pipes, Copper-Nickel 70/30 material was used. Then, it was assumed that the width of the rectangular cross-section is 4 times its height. As height times width equals the computed cross-section, a simple system of 2 equation and two unknowns allows to compute both of them. It is

[73] URL http://www.nessengr.com/technical-data/water-cooling/ [cited 11 June 2021]

[74] URL https://www.engineeringtoolbox.com/specific-heat-polymers-d_1862.html [cited 10 June 2021]

[75] URL https://www.nuclear-power.net/vanadium-specific-heat-latent-heat-vaporization-fusion/ [cited 10 June 2021]

[76] URL https://www.nuclear-power.net/lithium-specific-heat-latent-heat-vaporization-fusion/ [cited 10 June 2021]

assumed that the pipes cover 80% of the surface area that has to be cooled.

$$A_{pipe} = \frac{\dot{m}}{\rho_{water} \cdot V_{flow} \cdot 1.1^2} \tag{14.3}$$

$$W_{pipe} = \sqrt{4 \cdot A_{pipe}}$$
$$H_{pipe} = 4/W_{pipe}$$

Radiator

Moving on to the radiator, made of aluminium. Under these conditions, it has a heat transfer coefficient h = 350. The required flat plate area to dissipate energy is found by dividing power loss P_{loss} by a product of h and temperature difference. By stacking small plates on top of each other to achieve the necessary area, and assuming a plate thickness of 0.35 *mm*, a gap between plates twice the thickness - 0.7 *mm*, length of each plate $L_{radiator}$ of 0.4 *m* and a width ("depth" of radiator) $W_{radiator}$ of 0.08 *m*, radiator height can be calculated as in Equation 14.5, while the estimated volume of the radiator can be simply calculated by multiplying its area by plate thickness. The cooling pipes within the radiator are assumed to have a diameter of 80% of the radiator "depth", thus equal to 0.06667 *m*. Their respective area of the material part (only this part is needed for sizing) is then just full area with material factor 1.1^2 minus shallow area for the fluid, giving material cross-sectional area of 0.00162 m^2. The length of the pipes within radiator is calculated as in Equation 14.7. Finally, the volume of the pipe material $V_{cool-pipes}$ is just length times material cross-sectional area, and the mass is the result times density of aluminium material.

$$A_{radiator} = P_{loss}/(h \cdot \Delta T) \tag{14.4}$$

$$H_{radiator} = \frac{A_{radiator}}{W_{radiator} \cdot L_{radiator}} \cdot (0.00035 + 0.0007) \tag{14.5}$$

$$V_{radiator} = A_{radiator} \cdot 0.00035 \tag{14.6}$$

$$L_{rad-pipe} = \frac{H_{radiator} \cdot L_{radiator}}{(D_{rad-pipe} \cdot 2)} \tag{14.7}$$

Pump

The pump characteristics were estimated based on existing pumps for cooling systems in cars. The necessary performance parameter was the mass flow, 0.49 *kg/s*. This is equivalent to 29.4 *kg/min*, and in case of water, 29.4 *l/min*. The pump was searched to satisfy this mass flow. Attributes such as mass and power consumption have been considered in the choice. Therefore, the pump's characteristics are based on a universal car electric water pump [77]. It has a capability of 80 *l/min*, has a mass of 0.9 *kg*, and a power consumption of 112 *W*. The pump is chosen too powerful on purpose as the required cooling is expected to increase when the design reaches a more detailed design.

System parameters

Finally, it is possible to estimate general characteristics of the cooling system. Again, material cross-section A_{m-pipe} of the main pipes is determined by subtracting necessary flow area from the total pipe area. It is taken by qualitative judgement that the pipes would cover 80% of the cooled area surface. With placement of 8 battery patches next to each other, the surface to be cooled consists of 7 patch walls in-between, and the complete battery floor surface, and all times 1.05 factor. Equation 14.8 gives a cooling surface from this calculation. The volume to be cooled is then that total surface area times the pipe height. From that, it is possible to calculate the mass of the water needed for the system by taking the volume of it running in each surface for all 7 wall + 1 floor cooled surfaces, then adding 3 extra metres e_m of pipes to connect the system together and adding the water running through the radiator. Calculation is presented in Equation 14.10, where 1.1^2 is material coverage of pipes, N_{bat} is the number of batteries and ρ_w is the water density. Mass of the pipes is estimated in the same manner, but only

[77] URL `https://races-shop.com/water-pumps/88340-universal-electric-water-pump-80l-min-75a.html` [cited 22 June 2021]

considering the pipes themselves without water and radiator, calculated in Equation 14.13. Lastly, the mass of the radiator is the previously calculated volume of radiator times aluminium density with addition of radiator pipes mass, with 1.1 factor to account for structural coating around plates. Finally, the total system mass is computed by a sum of all individual masses in Equation 14.15. The sizing is summarized in Table 14.1.

$$A_{cooling} = 1.05 \cdot (7 \cdot H_{bat} \cdot W_{bat} + 1 \cdot L_{bat} \cdot W_{bat}) \tag{14.8}$$

$$V_{cooling} = A_{cooling} \cdot H_{pipe} \tag{14.9}$$

$$M_{water} = (\frac{V_{cooling} \cdot 0.8}{1.1^2} + \frac{A_{pipe} \cdot e_m}{1.1^2} + \frac{V_{rad-pipe}}{1.1^2}) \cdot N_{bat} \cdot \rho_w \tag{14.10}$$

$$A_{m-pipe} = A_{pipe} - \frac{A_{pipe}}{1.1^2} \tag{14.11}$$

$$L_{pipes} = \frac{V_{cooling} \cdot 0.8}{A_{pipe}} + e_m \tag{14.12}$$

$$M_{pipes} = A_{m-pipe} \cdot L_{pipe} \cdot N_{bat} \cdot \rho_{pipe} \tag{14.13}$$

$$M_{radiator} = (V_{radiator} \cdot \rho_{al} + D_{rad-pipe} \cdot L_{rad-pipe} \cdot \rho_{al}) \cdot 1.1 \tag{14.14}$$

$$M_{total} = M_{pipes} + M_{water} + (M_{radiator} + M_{pump}) \cdot N_{bat} \tag{14.15}$$

Table 14.1: Summary of battery thermal management system main characteristics

Parameter	Symbol	Value
Mass flow [kg/s]	$\dot{m}$	0.49
Flow speed [m/s]	v_w	4.6
Pipe X-sectional area [mm^2]	A_{pipe}	129
Pipes length [m]	L_{pipes}	5.56
Pipes mass [kg]	M_{pipes}	4.33
Radiator area [cm^2]	$A_{radiator}$	590
Single Radiator mass [kg]	$M_{radiator}$	6.39
Single pump mass [kg]	M_{pump}	0.9
Water mass in system [kg]	M_{water}	9.91
Total mass of cooling system [kg]	M_{total}	43.4

14.2. Obstacle Avoidance Sensors

For additional drone control assistance, obstacle avoidance system shall embedded. There are multiple types of sensors available on the market that measure distances to the objects. There are sonic sensors, which rely on sound waves propagation, there are those that use lasers, there is infrared triangulation method, relying on angles , and then there is time-of-flight (ToF) sensors. The latter ones are those that are going to be used for the current design. They are light-weight and compact, allow for long-range and high frequency measurements, and are eye-safe. Sonic sensors are also small and light, but are not as efficient in distance measuring. Also, sonic sensors have a drawback when working against large flat surfaces, which the buildings can be. Lasers have good performance, but they are lose on weight and size criteria, and also pose some danger to the human eyes.

Time-of-flight sensors emit light as a short beam and measure the time it takes for it to reflect from the surface ahead and travel back to the receiver. They can be direct or indirect. Indirect ToF send out short pulses of light of variable length and distinguish them when read back. Direct sensors send a continuous beam of light and calculate distance based on phase change of the received light.

As a reference for the preliminary design, TeraRanger Evo 60m and Terabee TeraRanger Tower Evo 60m x 8 have been used. Essentially, the latter is a module that consists of the former. Evo 60m is a ToF sensor with a range of 60m designed for outdoor use and drone obstacle avoidance and

altitude control are among is design applications. The tower version is 8 of those sensors combined in a module to provide full all-around observation. Again, these sensors are going to be used as an assistance to the pilot, and potentially for a function similar to DJI's ”Return home”, where a drone uses similar sensors to return to the landing area on its own in case of loss of signal with control unit. Therefore, it is not necessary to implement a complex and expensive LIDAR system used on automated cars that can picture complete area around the vehicle. As of now, two Tower Evo modules are going to be used at the craft's geometrical centre on the roof. Two separately dedicated Evo 60m sensors will be used for altitude control to always have control over ground clearance. The reason both are paired is for redundancy. The complete specifications for both the Evo 60m and the Tower are provided in Table 14.2.

Table 14.2: Specifications of TeraRanger Evo 60m and its Tower version

Parameter	**Value**	**Value**
Name	TeraRanger Evo 60m	TeraRanger Tower Evo 60m x8
Detection principle	Infrared Time-of-Flight	Infrared Time-of-Flight
Range	0.5 - (10-60) *m*	0.5 - (10-60) *m*
Update rate	up to 240 *Hz*	up to 120 *Hz* per sensor
Accuracy	+/- 4 *cm* below 14 *m*, 1.5% above 14 *m*	+/- 4 *cm* below 14 *m*, 1.5% above 14 *m*
FoV	2°	2° per sensor, 45° between sensor axes
Supply voltage	5*V* DC	12*V* to 24*V* DC
Supply current	90 - 330 *mA*	1.1 *A*
Dimensions	29x29x22 *mm*	120x42 *mm*
Mass	12 *g*	135 *g*
Cost	99 *Euro*	599 *Euro*

During later design stages, it is possible to add additional ToF sensors if more precision is needed during certain operations (e.g. one at the front for docking).

Conclusion
This chapter was focused on the remaining subsystems that had to be sized. The thermal management system of the battery was sized first, to fit the specifics of the battery itself and ensure its proper operation. Then, the sensors for the obstacle avoidance system have been determined, with chosen type that would function best in the expected operational environment. With that, it is now possible to move to the next stage in the design process and determine the placement of the subsystems on the craft.

15. Configuration

Once all relevant subsystems had been sized, it was possible to determine the relative placement of these and the overall configuration of the craft. The external configuration is visible in Figure 15.1. The skin was applied around the truss with connection points at the top four and bottom four ends of the truss. The landing skid assembly then is also secured to the bottom four nodes of the truss. The electric hinges connecting the centerpiece and the cabin lie on the top four nodes of the truss. The arms are then hinged onto the centerpiece and are moved with actuators. Radiators are located at the extremity of the arms under the propellers.

Most of the electrics with the exception of the HV batteries (gold in Figure 15.2) are then contained within the centerpiece, and are carried from one cabin to another with the drone. These include the LV batteries, gyroscopes and accellerometers as well as other electronics detailed Section 12.1.

The sensors are split in location between the cabin and the centerpiece, although the specific location has not yet been determined as it is very sensitive to final craft geometry and orientation.

The internals and the seating arrangement are visible in Figure 15.2. The seats are laid out with three in parallel per side (in blue on Figure 15.2). The firefighting equipment is also stored within the walls, between the truss and the outward skin. This is done to limit the encumbrance inside the small cabin and prevent accidents while the payload is entering the craft.

Figure 15.1: External configuration of craft

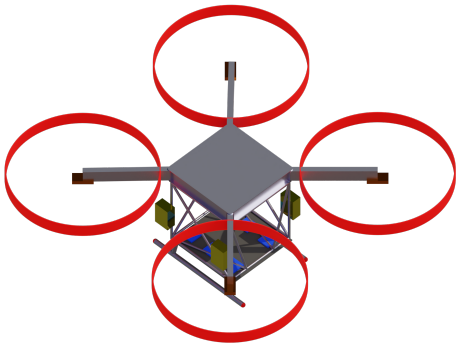

Figure 15.2: Internal configuration of craft

15.0.1. Sensitivity Analysis

To determine how quickly the design characteristics converge when a parameter change has been applied, a sensitivity analysis has to be performed. To have a full coverage of the systems response, all the parameters of the system are varied by first multiplying and then dividing the standard value by a factor of two. Knowing that parameters as processing units have negligible mass, their contributions are added under a larger subsystem mentioned further to limit the amount of components which specifications have to be varied.

For the mass variations, five large subsystems are set up: LV grid, which includes all the sensors, electronics and low voltage battery; HV grid, which is made from the HV batteries an inverters; the propulsion, which includes the motors and the propellers; structures which consists of all the structural elements and lastly the payload. Knowing that the payload is the heaviest group, it can be concluded, that its variations leaves the greatest impact on both the power required and the total mass of the craft, as all the subsystems except the LV grid are deemed to become heavier or lighter depending on the factor chosen. An increase in HV grid mass would have the smallest impact on the power requirement, as having additional energy on board reduces the depletion rate of the batteries, thus expanding their lifetime. It might turn out, however, that the engines would have to become more powerful to be able to carry the updated mass. Reducing the HV battery mass leads to a large drop in the payload mass to be carried, which in turn scales down the structures and propulsion subsystem masses. The subsystem which is not influenced by a change in other system mass is the LV grid, as the electronics and communications do not have a direct link with other subsystems. Nonetheless, increasing the LV grid mass increases the mass of all the other systems (except the payload) comparingly little, thus, can be assumed to be the least influential subsystem.

All in all, it can be concluded that the system is most sensitive to the changes in payload mass and reduction in HV battery mass.

16. Verification, Validation & Compliance

In this chapter the verification & validation plan will be presented as well as a compliance matrix to check whether the design has met its requirements. First of all, the verification and validation of the numerical models used for the sizing of the craft are shown in Section 16.1. After that, the verification and validation methods of the final craft are elaborated on. The former will be combined with a compliance matrix in Section 16.2 and the latter will be discussed in Section 16.3.

16.1. Model Verification & Validation

In this section the model verification and validation is discussed. Different models have been created for the purpose of sizing subsystems. These models are verified and validated for the Structures, Stability & Control, Aerodynamics, Power & Propulsion and Data Handling departments.

16.1.1. Structures

The structures department has created a model which is able to calculate the deflections, twists and stresses when a certain geometry is exposed to a particular loading. This model is complicated and requires a lot of computations and inputs. Three methods are applied to verify and validate this model. First of all, to see whether the magnitude of the calculated forces are correct, an external program called Matrix Frame is used. This program requires a geometry and input loads. The program outputs the final loading on the geometry. The results of the program are then compared to the results of the self-made model.

The next method that is applied is the use of Catia. First a geometry is created and the loading is introduced. Catia is then able to perform a stress analysis on the geometry. It outputs the internal stresses of the geometry which can then be compared to the stresses that resulted from the self-made model. The results are displayed in Table 16.1.

Table 16.1: Comparison of Model and Catia results

Part	Method	Max von Mises Stress [MPa]	Max Deflection [m]
Rotor	Model	228	0.0193
-	CATIA	251.2	0.021
Bridge	Model	28.7	0.00953
-	CATIA	32.1	0.013

From the results in Table 16.1 it can be said that the model is verified. As can be seen the model tends to slightly underestimate both stress and deflection. However, it is visible, that in both cases, the maximum internal Von-Mises stress is far below yield, and therefore the component will not fail at the design load. The results of this are also visually in Figure 16.1 and Figure 16.2.

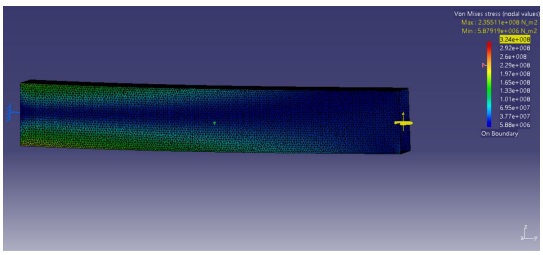

Figure 16.1: Rotor Arm FEM analysis

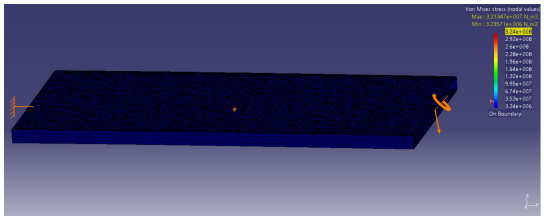

Figure 16.2: Drawbridge FEM analysis

Some unit tests have also performed throughout the model to verify the results outputs of the model. These include analytical tests on the generation of cross sections and their respective moments of inertia, and testing for some known loads to evaluate the resultant stresses. This includes testing for the maximum shear stress in a predefined section with an alternate formula. This was tested for the circular cross section and the result was in the order of 2% of difference for a range of inputs. It is recommended to conduct several additional tests to the script in the post DSE phase to further confirm the validity of these results. These can include but are not limited to:

- Unit testing of the normal force produced by bending on beam element.
- Unit testing of deflection produced by moment on beam element.
- Integration testing of the individual contributions to shear stress.

- Integration testing of addition of normal and shear stress in von Mises stress computation

In order to validate the results, a test campaign is proposed in the post-DSE phase with the goal of performing the following tests:

- Non destructive testing of individual structural elements to loading.
- Cyclic loading testing of the rotor beams, bridge and truss structure to analyse creep behaviour and fatigue crack propagation.
- Destructive buckling test on the rotor beam and cabin elements

With these results it will be possible to validate or disprove the results and gain additional information on the long term structural performance of the craft.

16.1.2. Stability & control

The stability & control department has created a state space model for the stabilitiy of the craft during flight. An analytical model has been developed next to the state space which has been used to verify that state space model. More details and the results of the verification is found in Section 10.11.1.

16.1.3. Aerodynamics

The aerodynamics department has created a crash landing model and used a python model for propeller blade analysis. The propeller analysis makes use of blade element momentum theory. It has been opted to make use of an external python program instead of creating an own python model. This python program has been validated thoroughly[78]. Thus it can be assumed that this program will return accurate results.

Furthermore, a crash landing model has been made which is able to calculate the speed of impact in case the craft crashes. This model is verified in two ways. First of all, the model has been designed such that the craft still produces an amount of thrust while crashing. The model can be validated by setting the thrust to zero and comparing it to a result coming from the equation for terminal velocity.

Moreover, verification tests have been performed. One example is setting the thrust to weight ratio in the program to be a value of 1. This will mean that the craft does not move at all.

16.1.4. Power & prop

For the power & propulsion department, a model has been made for the battery and motor sizing. Unit tests have been performed on this model as well as an inspection of the code. To validate that the energy consumption of the craft during descend and ascend is correct, the equation for potential energy is used. By comparing the result of this equation to the energy required to ascend the model can be validated. Of course, the inefficiencies of the propeller and motors must be taken into account when performing this validation.

Throughout the models, unit verification tests are performed. First of all, the battery sizing model is verified. The first unit test is to double the acceleration. This should result in an end velocity which is twice as high and a doubled total distance travelled. Moreover, the thrust required should also be twice as big compared to the normal value. Furthermore, the application of the efficiencies can be verified by setting the value of each of them to zero. The power required should then go to infinity. The power itself can also be doubled to verify the calculations of the battery as the weight of the battery should also double. The amount of motors can be halved to see whether each motor will require double the thrust compared to normal values.

The low voltage battery sizing model is also verified. The first verification test that is applied is doubling the amount of flight cycles and the battery mass should therefore double as well. In addition, the power of each individual component making use of the low voltage battery is doubled. This will always result in an increase in battery mass. Another test is to double the cable lengths which will result in a power loss double the size of the original value. Moreover, since the computations are not complex and do not require iterations, the model is also verified by performing hand calculations.

Lastly, the smaller models which are the inverter sizing and the thermal management system sizing models are verified. Since these models are rather small in size and do not require complex calculations,

these models are verified by performing hand calculations and comparing them to the results of the model.

Additionally, the thermal management system sizing for the battery has been verified in largely the same manner. The sizing has been done with a written program, so code inspection and a number of unit tests have been implemented to verify it. Because the program generally consists of step-by-step interdependent calculations, it is relatively easy to check whether reduction/increase of a base parameter leads to a logical shift in final system characteristics. Thus, reducing the amount of battery coverage by water pipes by a factor of 2 results in significant reduction in water mass in the system, but a small reduction in the overall system mass. Doubling the battery temperature upper bound leads to an almost half the size of the whole cooling system, which makes sense as less cooling needs to be performed. More tests have been done involving shifts in cooling efficiency, battery size, heat dissipation from battery, etc., all resulting in logical outcomes for the system characteristics.

16.1.5. Data handling

For the data handling a model is created to calculate parameters for the communication. This is a simple model which only requires parameters from the communication elements and will output the parameters such as signal-to-noise ratio and channel width. Unit tests and sanity checks have been applied to the model as well as an inspection of the code.

The first unit test is seeing whether the power received equation is correct. This is done by looking at all the parameters and adjusting them. Each loss is increased by a factor of two and the power received by the antenna should be halved. Likewise, the power can be increased by a factor of two and the power received should be doubled.

The same approach is taken for testing the noise equation. A decrease in the loss factors should result into a decrease in noise, whereas a decrease in gain should increase the noise. Moreover, since these are simple calculations the power received and noise can be verified by hand calculations.

16.2. Product Verification & Compliance Matrix

The product verification and compliance matrix were combined into one as can be seen in Table 16.2 - Table 16.4. This way it is immediately clear how it was proven that the system complies with a certain requirement. Note: The second part of the requirement ID indicates the origin of the requirement. GEN stands for general, LAW for laws and regulations, STRUC for structural, PAYL for payload, SAFE for safety, OPS for operational, COM for communication and DEV for development. The light cyan coloured requirements are driving requirements and the coral coloured ones are killer requirements. Requirement SYS-GEN-04 has been crossed out in the compliance matrix for the same reasons discussed in Section 4.4.

Table 16.2: Product verification and compliance matrix part 1/3

Requirement	Verification method	Compliance
SYS-LAW-01: The system operational noise shall not exceed 110 *dB*[79].	Demonstration	Yes, see Figure 8.5
SYS-LAW-02: The system shall comply with local emission regulations.	Demonstration	Yes, see Chapter 6
SYS-LAW-03: The system shall be flight-certifiable by local authorities.	Demonstration	Uncertain, see Chapter 19
SYS-LAW-04: The system shall not exceed 2.55 *m* in width when in stowed configuration[80].	Inspection	Yes, see Section 7.5
SYS-LAW-05: The system shall not exceed 4 metres in height from the road when in stowed configuration on the transport vehicle.	Inspection	Yes, see Section 7.5

Table 16.3: Product verification and compliance matrix part 2/3

Requirement	Verification method	Compliance
SYS-LAW-06: The system shall not exceed 12 *m* in length when in stowed configuration including the transport vehicle.	Inspection	Yes, see Section 7.5
SYS-LAW-07: The system including the transport vehicle shall not weigh more than 18 tons.	Demonstration	Yes, see Chapter 18
SYS-STRUC-01: The system shall be operable on at least 95% of high-rise buildings [5].	Analysis	Uncertain, see Section 7.5
SYS-STRUC-02: The system shall be operable in at least 90% of high-rise disaster conditions/environments [5].	Analysis	Yes, see Section 7.5
SYS-STRUC-03:The system shall provide position securing mechanisms for payload.	Inspection, demonstration	Yes, see Section 7.5
SYS-STRUC-04: The system shall provide a minimum of 3.6 m^3 of payload volume.	Inspection	Yes, see Section 11.6
SYS-STRUC-05: The system structure shall provide interfaces to integrate other subsystems.	Test	Yes, see Section 11.6
SYS-STRUC-06: The system shall be equipped with means of providing ground support for a minimum load bearing capability of 2640 *kg* which derives from the first estimate of maximum craft landing weight of 2200 *kg* with a safety factor of 1.2	Analysis	Yes, see Section 11.4
SYS-STRUC-07.1: The system shall be able to deliver the payload to the ground intact after a ground impact with a peak acceleration of 26 *G*	Analysis, test	Yes, see Chapter 13
SYS-STRUC-8: The system shall provide structural means of keeping the payload safe from the hazardous environment	Test, demonstration	Yes, see Section 7.5 & 11
SYS-PAYL-01: The system shall be able to carry a payload of at least 100 *kg* during ascent [5].	Analysis, demonstration	Yes, see Section 9.3
SYS-PAYL-02: The system shall be able to carry a payload of at least 600 *kg* during descent [5].	Analysis, demonstration	Yes, Section 9.3
SYS-PAYL-03: The system shall accommodate 20 *kg* of firefighter equipment.	Analysis, demonstration	Yes, see Table 9.2
SYS-GEN-01: The system shall provide transportation means to individuals trapped in high-rise disaster situations.	Testing, analysis	Yes, see Section 7.5
SYS-GEN-02: The system shall be reusable.	Demonstration	Yes, see Section 9.3
SYS-GEN-03: The system shall be operable on buildings with a height of at least 1000 *m*.	Analysis, demonstration	Yes, see Chapter 13
SYS-GEN-05: The system shall be able to land and take-off in 0 *m* distance.	Demonstration	Yes, see Chapter 5
SYS-GEN-06: The system shall require no more than one firefighter to provide evacuation means to the evacuees.	Demonstration	Yes, see Section 7.5
SYS-GEN-07: The system shall remain stable and controllable when there are external disturbances present	Analysis, demonstration	Yes, see Section 10.14
SYS-GEN-08: The system shall provide control assist in case of external disturbances.	Analysis, demonstration	Yes, see Table 10.5
SYS-GEN-09: System shall be equipped with mechanically deployable mechanisms for a semi-safe landing in case of a full system shutdown.	Analysis, demonstration	No, see Chapter 13

Table 16.4: Product verification and compliance matrix part 2/3

Requirement	Verification method	Compliance
SYS-SAFE-01: The system shall safely transport the evacuees.	Demonstration	Yes, see Section 7.5
SYS-SAFE-02: The system shall safely transport the operators.	Demonstration	Yes, see Section 7.5
SYS-SAFE-03: The system shall be fail safe.	Analysis	Yes, see Chapter 13
SYS-SAFE-04: The system shall have a reliability of at least 95% for 5 years of operation [5].	Analysis	Uncertain, see Section 18.2
SYS-OPS-01: The system shall have a turn around time of at most 120 *s* [5].	Demonstration	Uncertain, see Section 7.2
SYS-OPS-02: The system shall have an availability of at least 95% for 5 years [5].	Analysis	Uncertain, see Section 18.2
SYS-OPS-03: The system shall be able to perform evacuation within 10 minutes after fire department arrival to the scene [5].	Test	Uncertain, see Chapter 7
SYS-OPS-04: The system shall be maintainable within one day (8 hours) per week [5].	Test	Uncertain, see Section 18.2
SYS-OPS-05: The mobile segment of the system shall be transportable by a fire department truck [5].	Demonstration	Yes, see Section 7.5
SYS-OPS-06: The craft shall be remotely operated.	Demonstration	Yes, see Section 12.3
SYS-OPS-07: The system shall not damage the infrastructure outside of the operational area in the course of regular operation.	Analysis	Yes, see Section 7.5
SYS-OPS-08: The system shall not damage structural integrity of the building when docking.	Analysis	Yes, see Section 7.5
SYS-OPS-09: The system shall not damage structural integrity of pavement within landing area during normal operation.	Test	Yes, see Section 7.5
SYS-COM-01: The system shall communicate all state variables necessary for operations.	Demonstration	Yes, see Section 12.3.2
SYS-COM-02.2: The system shall have Signal-to-Noise ratio of at least 25 *dB*.	Analysis, test	Yes, see Section 12.3.1
SYS-COM-04: The system shall have a maximum delay of 0.1 *s* from the control input.	Test, demonstration	Yes, see Section 12.3.1
SYS-COM-06: The system shall operate in a synchronized manner without non-intended delays.	Test, demonstration	Uncertain, see Section 12.4
SYS-DEV-01: The system cost shall be less than 500,000 *USD* [5].	Analysis	No, see Chapter 4
SYS-DEV-02: The system end of life waste shall be less than 20% [5].	Analysis, inspection	Uncertain, see Chapter 6
SYS-DEV-03: A single craft shall be manufactured and assembled in no more than <TBD> days.	Demonstration	Uncertain, see Section 4.4
SYS-DEV-04: The system controls shall be teachable to a full-time firefighter in 1 months time [5].	Test, demonstration	Uncertain, see Section 4.4
SYS-DEV-05: The system shall support software updates/patches for all of the subsystems even after being sold.	Demonstration	Yes, see Section 12.3.2

Separate remark: The **SYS-DEV-04** requirement is impossible to check until the product is ready. Its uncertain status is determined from a fire department interview, where information was shared that it takes 3 months for a firefighter to learn how to use a ladder truck, while the vehicle to be designed is aerial type and is expected to require more training than conventional ladder fire truck. On the other hand, no certain proof can be presented that the expectations will be justified.

16.3. Product Validation

The product needs to be validated before it can be sold on the market. The validation checks whether product has been properly designed such that it can carry out the mission for which it was designed. The product is exposed to multiple validation tests.

- **Ground test**: First of all, A ground test with stand-in evacuees can be performed to validate the bridge's structural integrity. Furthermore, other elements of the evacuation such as the accessibility for incapacitated people and the speed of evacuation can be validated.
- **Software test**: Since the system consists of multiple subsystem software, the complete system software must be validated. This is done by linking all the subsystem software together and giving inputs to this system. Each subsystem software should then interact with each other to produce a fitting output. This is how the system software is validated.
- **Windtunnel test**: The craft's hover stability can be validated in a windtunnel test. The windtunnel can simulate the gusts at different speeds to which the craft must react to stay stable during hover. This test can further validate the findings of the aerodynamic properties of the cabin and craft.
- **Impact test**: An impact test is done using test dummies in the cabin with accelerometers and force sensors. With these sensors the result of a crash impact on a person can be measured. With these results the surviveability of a crash can be validated. Moreover, the structural integrity of the product as a result of an impact can be validated.
- **Communication test**: The communication system can be validated by performing a test on the ground using the same equipment as the product. The test should be performed in an urban environment at the maximum distance between antenna's which is 800 m. By measuring whether all inputs and outputs are sent and received the communication system is validated.
- **Test ride**: To validate the transportability of the system, a test ride can be done. The test ride is divided up in multiple parts. Firstly, the mounting of the system is tested by loading the system onto a truck . Secondly, the transportability through traffic is tested by driving with the truck through an urban area. Lastly, the unloading of the system is tested. During the last two part of the test, the required time to perform these parts should be timed to validate the deployment time as required by SYS-OPS-03. This is how the transportability of the product is validated.
- **Simulated flight test**: A simulated flight test is performed to reenact real life application of the craft. All systems are tested during this flight test except for the transport of the system. The most important part of the product to be validated during this test flight is its ability to deploy its bridge into a building while hovering.

With these tests the system all together is validated. Each individual test validates an element or function of the system. With these tests, all different element and functions should be covered.

16.4. Conclusion

In conclusion, all models used for the sizing of the craft have been verified. Where possible, model validations have been applied using mostly external software. Through the compliance matrix the

[0] *URL* https://www.govinfo.gov/content/pkg/FR-2014-08-08/pdf/2014-18738.pdf [cited 17 May 2021]
[0] *URL* https://www.nfpa.org/~/media/Files/forms%20and%20premiums/nfpa72emergencycomm.pdf [cited 17 May 2021]
[0] *URL* https://www.itf-oecd.org/sites/default/files/docs/dimensions-2019.pdf [cited 17 May 2021]
[0] *URL* https://eur-lex.europa.eu/legal-content/EN/TXT/PDF/?uri=CELEX:32015L0719&from=EN [cited 17 May 2021]
[79] *URL* https://www.nfpa.org/~/media/Files/forms%20and%20premiums/nfpa72emergencycomm.pdf [cited 17 May 2021]
[80] *URL* https://www.itf-oecd.org/sites/default/files/docs/dimensions-2019.pdf [cited 17 May 2021]

product verification has been and tests have been set up to validate the product.

17. Market Analysis

When designing a new product, it is important to look at the existing market. This is done to identify the competitive products and determine their quantity and cost. It is essential to find out what the added value of the new product will be to the market as this might influence the design of the product and more importantly, the number of systems to be built. All of this will influence the cost of the system as well and subsequently the profit that can be made.

This chapter aims to analyse the market and the accompanying costs it brings to the production of the system. This will be done through analysing the return on investment and operational profit in Section 17.1. Afterwards a general analysis is done in Section 17.2.

17.1. Return on Investment & Operational Profit

During the development of a project which aims at delivering a specific product a detailed analysis of the project costs and potential returns must be done. The product and project will have a certain total cost, by studying different market and product aspects a quantitative estimate of the Return on Investment (RoI) can be derived. The RoI is defined as the difference between the revenues and costs divided by the total cost. In order to study the RoI first the total volume of potential products must be evaluated. A detailed study of the market share gives information on the potential returns. Then the total system costs must be determined, this is broken down in three distinct categories development, production and operational costs. Finally, a product market price must be determined such that the RoI can be evaluated.

17.1.1. Market volume

The project is unique given it is an emergency rescue vehicle, this means that there is no clear market to study. This is because the system is only useful for a small set of rescue services, furthermore the vehicle will only be purchased if deemed necessary. An estimate that can be done for the total market volume is to study the amount of emergency vehicles currently available for rescue services and the frequency at which new emergency vehicles are purchased.

Given that the project is unique, a detailed analysis of emergency vehicle -particularly fire truck- market will be performed. For the purpose of this report only fire rescue services will be considered. Worldwide the amount of emergency service vehicle market share for residential rescue is more than 50% of the total market, the rest is split over company and military rescue. Furthermore, in 2020 the total fire truck market exceeded 4.5 billion *USD* and has been steadily increasing over time and this market value is predicted to reach 6.5 billion *USD* in 2026 [81]. Note that the total fire rescue equipment market value is well beyond 40 billion *USD*. When looking at the number of urban areas worldwide there are a total of around 4037 cities with more than 100,000 inhabitants [82].

Using this information an estimate for the total market volume can be derived. In order to derive the total market volume some assumptions are made, first of the 4037 cities with a population of over 100,000 only a fraction of them will have them resources to purchase the system. This is due to the GDP and investment capability of the country where the city is located. The second assumption is that the fire departments in each city that will buy the system will only want a single system, this system will be replaced when it fails. Note that in reality larger cities will own multiple systems and smaller cities might not buy the system. It is expected that the average amount of units sold will approach one craft per city.

By assuming that only developing countries with a high GDP per capita will purchase the system, the total amount of dense cities that will potentially purchase the system reduces to 3000. This is because a lot of high density urban centers are in Brazil and India, however both countries have a high rate of poverty and their ability to purchase the system is low.

The conclusion is that the potential market volume is around 3000 units of the system. Note that the demand is not periodic, the fire rescue services will purchase one system and maintain it until failure,

this means that there will be a maximum of 3000 operational systems worldwide at the same time. Furthermore this market volume does not take into account the price versus demand relationship and the market volume will go down with total cost of the system. For an expensive system the number of units sold will be under 3000 and the opposite will also be true for a cheap system.

17.1.2. Development cost of the product

The development cost of the product has a significant impact on the RoI however it is not a periodic cost and only incurs prior to the production of the first product. In a standard project setting the main development costs can be broken down into: engineering costs, certification costs and labour cost. Fortunately for this project there are no development labour costs up to the final design review. Furthermore, the engineering costs are very low since the TU Delft offers a wide variety of tools and models to develop engineering projects. The certification costs for this project will be very high, this is because the product is unique and its certification will require a lot of steps. The system performance and safety must be validated through a certification process which is very costly for aerospace systems. Finally the current system exceeds current UAV certification requirements in terms of maximum take-off weight (MTOW) and maximum operating altitude. This complicates the certification process further and will increase the development costs. A lower estimate for the development costs would be in the order 1 million *USD* however due to the issues with current UAV regulations the development cost is expected to be 5 million *USD* [83].

17.1.3. Production costs

The next step in the RoI analysis is to determine the total production costs of a single unit. For the purpose of this analysis the production costs will include the material, machining and labour costs. For a clearer overview of the production steps and processes required for a single unit refer to Section 19.4. The total production cost breakdown of a single unit is in Table 17.1. This includes the cost of two cabins with two separate communication, battery and electronic subsystems.

Table 17.1: Production costs for a single unit of the system

Subsystem	Component	Cost [USD]	Contingency
Data Handling	Communications	50,000	5,000
-	Ground controller	10,000	5,000
Aerodynamics	Propeller	800	200
-	Cabin shell	15,000	1,000
Power and Propulsion	Battery	170,000	17,000
-	Motors	80,000	20,000
Stability and Control	Controller	100	10
Structures	Rotor arms	1,000	100
-	Center piece	3,000	1,000
-	Cabin truss	1,000	100
-	Drawbridge	15,000	2,000
-	Landing skids	44,000	5,000
Electronics	Cooling	1,500	100
-	Electronics	5,000	500
Total	-	396,400	57,660

The contingency details the predicated variation from the estimated cost, those can be positive or negative variations. This leads to an upper and lower bound for the total system cost, the maximum

[81] URL https://www.gminsights.com/industry-analysis/fire-truck-market[cited 22 June 2021]

[82] URL https://brilliantmaps.com/4037-100000-person-cities/[cited 22 June 2021]

[83] URL https://www.aveva.com/content/dam/aveva/documents/perspectives/success-stories/SuccessStory_AVEVA_AirbusHelicopter_03-20.pdf.coredownload.inline.pdf [cited 22 June 2021]

cost is 454,060 *USD* and the minimum cost is 338,740 *USD*[84].

17.1.4. Operational costs

For the proposed system the operational costs will be relatively low. This is because the system is sold to a third-party service (fire department) and they will operate the craft using their labour and equipment. The operational costs are limited to system maintenance and recharge. By looking at the requirements it can be said that the maximum maintenance time is 8 hours a week, this translates to 416 working hours a year. The average aerospace technician earns 20 *USD* an hour, assuming two technicians are required for maintenance this translates to a yearly maintenance labour cost of 17,000 *USD*. An additional 5,000 *USD* of replacement components is expected to incur yearly. Finally the recharge cost of the craft is approximately 42 *USD*, assuming 50 recharge cycles a year this leads to a total yearly operational cost of 24,100 *USD* a year. For a five year life cycle the operation costs amount to 120,500 *USD* total.

17.1.5. Product market price

After having determined the total project costs the product market price must be chosen. Due to the nature of the design the aim of the project is not to make a significant profit. The goal of the project is to provide a vehicle that can rescue people in high rise situation hence the business model will be non-profit. This means that the product price will be determined in such a way that overtime the total revenues match the total costs such that the RoI is 0. The equation used for RoI can be seen in Equation 17.1.

$$RoI = \frac{PP \cdot n - [(PC + OPC) \cdot n + DC]}{(PC + OPC) \cdot n + DC} \tag{17.1}$$

Where PP is product price, n number of units, PC is product cost, OPC is operational cost over life cycle, and DC is the product development cost.

Using the costs detailed below and the relationship for RoI the minimum required product price such that the project breaks-even is 460,900 *USD*. The maximum required product price is 576,200 *USD*. By taking the average of these values an estimate for the product price can be given, this is equal to 518,566 *USD*.

17.2. General Analysis

All in all, the fact that the market remains completely unsaturated gives a lot of freedom in the entrance to it. The product would be first of its kind, and thus, at first period of time, full market share is to be expected. For this same reason, final product characteristics do not pose any significant changes to the preliminary market analysis done earlier [1]. However, the estimated cost is now known, as well as main design aspects and characteristics. Thus, it is possible to reflect them on the market analysis for a better prediction of product performance in the market.

Current vehicle design satisfies the SWOT analysis introduced earlier. It assesses the product's strengths and weaknesses from internal and external perspectives, and has not changed from preliminary analysis [1].

As of now, the determined system price is within a price range of a modern fire truck [85], which varies between 300,000-700,000 *USD*. The more extreme versions can cost as high as 1,000,000 *USD* [86]. This is a positive note, as that means that most fire departments in developed countries can afford the proposed aerial vehicle. It would simply be similar to buying another fire truck, cost-wise. It is also expected that the craft will be have similar operational life conditions - normally, due to high vehicle cost, the fire departments utilise their trucks up until the moment when maintenance costs overcome the cost of a new vehicle. Since estimated operational costs for first 5 years of the craft are about a quarter of its price, it is expected the product will be in use for a 10-15 year period at least.

[84] URL `https://www.aero-access.com/products/bell-206a-b-low-skid-gear-components-replacement.html` [22 June 2021]

[85] URL `https://kleinfiredept.com/faqs/2-how-much-does-a-fire-truck-cost` [cited 22 June 2021]

[86] URL `https://www.firerescue1.com/fire-products/fire-apparatus/articles/1-million-dollars-for-a-fire-t`

As for the Porter's Five Forces analysis, it is now possible to reflect the market appeal onto the current design. This is heavily based on the preliminary analysis done before [1]. The market is analysed on five aspects: rivalry among competitors, bargaining power of suppliers, bargaining power of buyers, threat of new entrants, and threat of substitutes.

Rivalry among competitors - low. This is because there are essentially no competitors, and in fact, the current vehicle will open a new separate market segment - small air mobility vehicles used for evacuation of people in urban areas. Switching costs for the users are high for the reasons described earlier. Furthermore, fire departments normally exploit a vehicle until the cost of maintenance becomes higher that the cost of the product. In Section 17.1.4 it has been assessed that the operational costs in a five-year period do not make up even a quarter of a new product cost. Therefore, it takes a significant time period before preferable switching capability, while keeping in mind all of the maintenance and training procedures updates for a potential competitor.

Bargaining power of suppliers - high. Significant portion of technology implemented in the vehicle is not custom, but rather a separately made product. While the sensors and the cameras are available in large varieties, components such as motors are very specific, and as of now only one company produces the ones required for vehicle operation - therefore heaving a strong pull to their side. The aforementioned reasons make the switching costs of the supplier high for many components, while forward integration is problematic for complex technology.

Bargaining power of buyers - low. The quantity of buyers relatively large, as assessed in Section 17.1.1. However, the product differentiation overcomes the problem, as the vehicle is unique in its essence.

Threat of new entrants - low. Technology is new and heavily untested. During the design process, an interview with a Dutch fire department showed that they are interested in the potential of the vehicle, but are also rather sceptical about its practicality and especially safety. This shows that new entrants would have to overcome this problem again, and not just the certifications to be trustworthy. The time and cost of entry remain high, meaning that by the time the operational life cycle of the product expires, which is 10-15 years, product loyalty is to be expected from users, while the potential new entrant would have to prove itself to be competitive first.

Threat of substitutes - low. All the substitutes discussed previously [1], which utilise evacuation from outside of the building structure, are not implemented practically. Meanwhile, their costs remain unknown, while the current vehicle to come has a price of a fire truck. It is deemed practical to utilise reusable equipment which is brought on sight, otherwise each building would have contained the expensive firefighting equipment, which is not the case. I.e. it is expected that the price of the product is lower than that of the discussed substitutes. Therefore, until better solutions are invented, the current substitutes do not pose a significant threat to the product.

17.2.1. Alternative use-cases

Throughout the market analysis the market was analyzed from the perspective of a high-rise fire evacuation vehicle. Given that this design aims at demonstrating the technological feasibility of a large UAV for rescue services, this means that by adapting the design slightly its use-case can be broadened. In this case an important market that the design can enter is the mountain rescue market. An example of this would be evacuation from ski lift or avalanche rescue. Another important use case of the design would be cargo hauling for construction projects. Instead of building and moving large cranes every time a construction project starts, the system can be used to bring materials to the top of a construction site as well as ferry passengers safely. Given that the system was designed to operate on high-rise buildings this would be particularly relevant for high-rise construction projects.

During the post -DSE phase an in-depth analysis of potential use cases and their impact on the cost and revenue of the project will be performed, this section serves to demonstrate the modularity of the system and the potential increase in market volume. It is expected that potential the market volume will grow significantly (by at least one order of magnitude) if the design is modified such that it can be

ruck-yup-and-heres-why-miZF81kYVmcMxoZ0/ [cited 22 June 2021]

used for multiple case scenarios.

18. Final Design Analysis

First, the mass and power budget will be given in Section 18.1. Lastly, a RAMS and risk analysis performed on the system in Section 18.2 and Section 18.3.

18.1. Resource & Budget Allocation

To ensure the performance requirements are still met even if in the post-DSE phase the craft gains weight or requires more power then sized for in this report, a resource allocation & budget breakdown is performed. This is outlined for both the weight of the craft as well as the energy/power in the batteries. It must be noted that the batteries are one of the main constituents of the craft total weight and therefore these budget breakdowns are very much correlated.

Mass & power budget

In Figure 18.1 the craft weight is divided over the different subsystems with their associated margins. A comparison is made between the baseline values from the conceptual design stage and the current mass budget. Note that the total variance in the craft weight estimation has come down from 25.5 % in the baseline report [1] to 8.9 % at the current design stage. It is expected that the margins will further decrease when detailed parts design is performed in the post DSE phase.

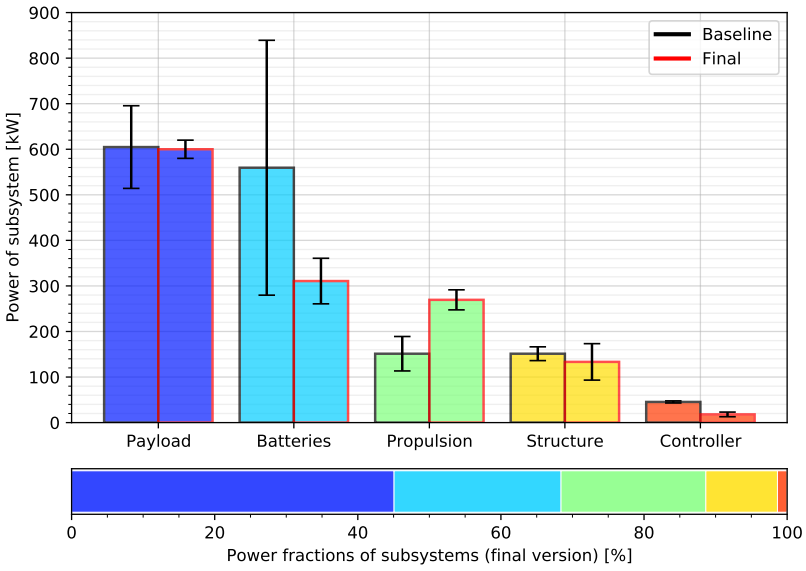

Figure 18.1: Distribution of craft total weight over the subsystems

From the figure it becomes apparent that all subsystem have a lower uncertainty in the mass budget. Also it can be seen that the structures, batteries and controller turned out lighter then expected. The propulsion system however gained weight. The total mass budget is now 1685 ±150 *kg*.

Energy & Power budget

Note that it was decided in Chapter 9 to have both a low voltage battery and a high voltage battery on the craft. In order to have a meaningful comparison with the baseline report, they are combined in this analysis. Figure 18.2 displays the breakdown of the power budget. Note that the battery efficiency is not taken into account in this section, so the battery does not consume power. The battery efficiency is calculated in Chapter 9.

It can be noted from the figure that the propulsion system takes up almost all of the power. The total

power reduced from 560 ±257 *kW* at baseline to 260.7 ±37 *kW* at the current design stage.

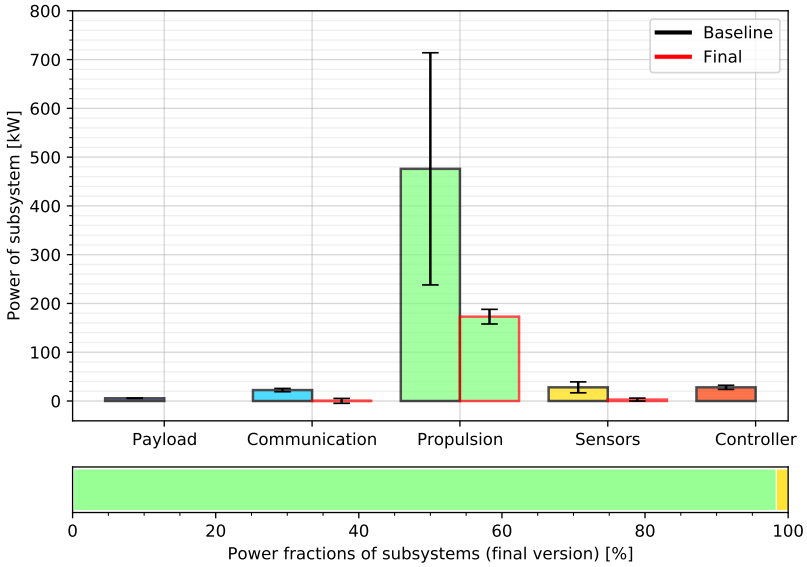

Figure 18.2: Distribution of the power budget over the subsystems

18.2. RAMS

For each product or design a Reliability, Availability, Maintainability and Safety (RAMS) analysis should be done. This defines each of the four characteristics. It determines the expected reliability and availability as well as sketches out the maintainability. Lastly, it focuses on all critical safety characteristics. The four characteristics are discussed below in the same order.

Reliability

Reliability is a probability that a failure will not occur in a specified time. It does not have to mean that the failure will occur in reality, but can also indicate that it will fail during the time period without proper maintenance. Failure can also concern both individual subsystems and the system as a whole, and when a subsystem fails it does not have to lead to a system failure. However, it is important to analyse individual subsystems first, and then discuss reliability of their combinations (whole system).

Most main components of the craft are based on freshly developed technology. Although this may have a positive effect on efficiency, there is limited technical information available on reliability and safety of those components. Therefore, the analysis was done mostly qualitatively, with some numerical data.

- **Battery** The battery is the most significant component affecting reliability of an EV [61]. The chosen cells are lithium-metal, being widely considered the next generation battery due to its superior characteristics including energy density. However, the reason it has not yet been implemented on a large scale lies in its flaw - non-uniform electrode position of lithium. The non-uniform deposits are referred to as dendrites, and their formation causes short-circuit in the battery. This is a significant issue, highly researched in the field for solutions, as this is the main barrier in using this new perspective battery type. As of now, this flaw makes the Li-metal battery unreliable for usage, while conventional certified Li-ion have failure rates 1 in a million to 1 in 10 million. It is expected that either Li-metal reaches reliability rates that prove to be safe and certifiable, or it may be the case where the main battery will have to be switched to a different, more reliable type. Now, the use of Li-metal battery highly depends on current research to solve its short-circuit problem.

  Additionally, a thermal management system has been preliminary sized and will be implemented to maintain the cells within operational temperatures. It is a simple and very conventional liquid cooling system with consisting of radiator, pump, cooling liquid, and pipes that ”wrap” the battery

packs around. This will ensure proper operation of the battery and prevention of its degradation over life time. The cooling system itself is expected to be highly reliable, due to its simplicity, and even in case of failure, it does not affect the instantaneous operation of the craft.

- **Propulsion** Propulsion unit essentially consists of an electric drive motor and an ESC (motor controller). The currently chosen motors are not yet used commercially, but have been developed specifically for CityAirbus manned UAV. The motor SP200d is freshly developed, and very limited information is available on it. Unfortunately, little can be said about its reliability directly. However, its use in manned UAV program from an aerospace giant company leads to an assumption that it has sufficient reliability and is thus safe to be used. As for the ESCs used in CityAirbus, even less information is available, and none in regards to the RAMS analysis. Furthermore, due to technical reasons, the ESCs had to be designed on their own to fit the motors, meaning no information on their reliability can be stated at this point in time. Additionally, a separate research [62] showed that in an electric drive unit, ESC is much more prone to failures than the drive motor itself, which means special attention has to be paid to their operational use. It has been found that over 30,000 operational minutes for an average electric motor unit, failure probability of an ESC is 4 times larger than of the drive motor [62]. Nevertheless, it safer to apply additional measures to keep propulsion system within the reliability limits. The propulsion system has been designed with redundancy in mind, and with the current aircraft parameters, it is possible to remain operational in case of a motor unit failure. It is also possible to avoid complete system failure even when a pair of motors fail (complete loss of thrust on one arm), and land safely. This is achieved by placing a pair of counter-rotating motors on each arm, and having reserve excess thrust in each (the craft is designed to operate below maximum engine thrust levels). This of course has a positive effect on reliability of propulsion system.
- **Communication system** A custom communication system had to be designed to fit the operational conditions. As of now, with regards to its reliability, it is known that the system is designed to withstand a data rate twice the size of the required one for vehicle operation, minimising data overload possibility. Meanwhile, its signal-to-noise ratio is 25, as described in Section 12.3.1. This ensures a confident signal between the craft and the control unit in noisy environment, such as large city centers. Additionally, further software development will ensure that the vehicle will maintain its position in case of a total communication loss, the vehicle will remain on standby for a specified amount of time in case communication is restored, warning the passengers about its autonomous operation. When the time period has passed, it will return to the landing zone on its own, using obstacle avoidance.
- **Vision sensors** Vision sensors are essential for the vehicle operation as they provide necessary information to the pilot to operate it. All cameras and range sensors are therefore chosen to be high quality and are placed with redundancy. In case of a sensor failure, there will still be vision in its direction ensured by a spare one, ensuring reliability of a sensor system.
- **General** As a separate note, a research by Talukdar, B.K. and Deka, B.C [61] looks into RAM analysis of a plug-in electric vehicle (PEV). In their studies, they analysed reliability of an electric vehicle mainly focusing on the ”battery, motor-drive, controllers, energy management systems, etc.”, which are attributes of the UAV designed in this paper. It is therefore sensible to take their research as a basis for this RAMS analysis. It should be noted that the battery in the PEV system studied was lithium-ion, while for the UAV lithium-metal is used. For reliability, it has been found in their paper that it decreases exponentially with time. Reliability starts at a value of 1, and then decays to 0.488 after 5 years, 0.2382 after 10 years, and 0.1162 after 15 years. This is theoretical reliability of the system if there was no maintenance performed. However, with regular maintenance, the *availability* (operational state) of the system stagnates at a level of 0.8396.

Availability

Availability is considered as a measure of proportion of time that the system is available to use, and integrates reliability and maintainability [61]; the latter is discussed in the next subsection. For the current design, there is a requirement `SYS-OPS-04`: ”The system shall be maintainable within one working day (8 hours) per week.”, i.e. the system shall be available the remaining 160 hours a week. Different characteristics influence the availability of the system positively or negatively. Several of these properties are discussed below.

1. Modular design: An advantage of an electrical based system is that the components are simply attached to each other, and can be disconnected easily. This means that in case of a component failure, it can be swapped with a new one, which is sometimes much quicker than fixing the component directly on the main structure. This way, it is more likely that the system shall meet the availability requirement, while the flawed component can be fixed in ”background hours”. This modular design involves an easier motor replacement, especially when compared to a heavy and complex IC engine, potentially ESC units, depending on their final placement. Of course, the cabin is detachable, too, as the concept is mainly based around this feature, so multiple cabins should be available. The cabin is by far not the most expensive component, so it is possible to have a spare one. This would provide redundancy in case a cabin gets damaged or is in maintenance and thus improve the availability.
2. Battery powered: Since the vehicle will be battery powered it is important that the batteries are fully charged when the vehicle is needed. This will improve its availability, instead of having to recharge batteries each time the system has to be operated. Therefore batteries should be able to stay fully charged for at least 160 hours, until the next scheduled maintenance takes place and they can be recharged.
3. Transportablity: SHR-U-13 states ”The mobile segment of the system shall be transportable by a fire department truck”. This means that the system will be available at any place the fire department truck can reach. This is an important requirement to meet, as this will make sure the vehicle will be present where it needs to be and is able to get there. To meet this requirement, certain restrictions are put on the size and weight of the vehicle. This ensures transportability on a fire department truck over conventional roads.
4. Design for environment: The vehicle is designed to operate in night time with night vision cameras and range sensors to avoid obstacles, and under severe weather conditions. It is able to withstand rain, as all water-vulnerable components will be sealed. The fog is avoided with range sensors for obstacle avoidance. The craft is designed to withstand gusts of at least 20 [m/s]. High temperatures are avoided using cooling system for all main components that heat up. As for now, low temperatures where the battery cannot heat itself up enough cannot be overcome, but they may be by implementing a heater in the thermal management system later on. This allows the vehicle to be available for operation regardless of the environmental conditions outside.

With all of these parameters considered, it is expected that the vehicle will meet the availability requirement SYS-OPS-04. However, further insight is needed for confidence, with potential experimental tests.

Maintainability

Maintainability concerns how likely it is that a failed system is restored to its operational condition within a given time frame. Requirement SYS-OPS-04 ”The system shall be maintainable within one day (8 hours) per week.” specifies how long maintenance is allowed to take. One should look at what maintenance needs to happen and how to do this within the time frame. Two types of maintenance can occur:

1. Scheduled maintenance: It is important to schedule regular maintenance so the fire department is aware of when the system will be unavailable and can take that into account. Scheduled maintenance will include visual inspection of the system and its subsystems: checking for cracks, fluid leakage from batteries, rust etc. Maintaining batteries does require some caution because it can be a hazardous task so proper measures, like wearing safety gear, need to be taken. Other maintenance checks will include running the engines, checking if the attachment/detachment mechanism functions properly and testing the winch system and the harness. The tilting mechanism of the rotor arms also needs to be inspected and checked during maintenance.
2. Non-scheduled maintenance: After the system has been used in operations, a checkup needs to be performed to make sure everything is okay for the next operation. This includes: checking the seat belts and head protection, cleaning the vehicle from any debris, recharging the batteries and a visual inspection. The fire department cannot prepare for the unavailability of the system during non-scheduled maintenance.

Regular monitoring of the system is very important as it gives an indication of the condition of the different parts and how long they will last before they need to be swapped improving both maintainability and availability and decreasing the chance that failure occurs. The older the vehicle is, the higher the chance of failure thus the higher its maintenance rate needs to become in order to increase the availability. With experience comes knowledge so after some time it becomes easier to predict when a certain part needs maintenance and how long it will take to repair or swap a part, which increases the maintainability.

High voltage batteries need to be replaced every 1500 cycles and low voltage batteries every 3000 cycles. To swap the batteries, they first need to be removed from their casing which is inside the cabin. When adhering to the proper safety measures switching one battery is estimated to take 30-60 minutes. As five high voltage batteries and one low voltage battery are present, this will take at most six hours. As just switching the engines takes 75% of the time maintenance is allowed to take per week, it is vital to know when to change out the batteries to not waste more time than needed. Charging the batteries on the other hand does not take a long time: around 12 minutes. For engine maintenance, the propellers will need to be removed first but since the engines themselves are small they are more maintainable compared to, for example, an engine of a jet plane.

To increase maintainability it is important to have spare parts available. Mainly the parts that are vital for the vehicle, can degrade in quality quickly and are specifically designed for the vehicle. This would include spare batteries, spare electrical wiring, spare clamps, spare landing gear and spare rotor blades.

Safety

Safety is a top priority for any product. As this rescue vehicle will be operating at large heights this is of even larger importance. Therefore it is important to identify the biggest safety risks and find a way to mitigate them. This is largely done in Section 18.3. However, several of the largest safety risks and the mitigation approach will be discussed here.

Firstly, the boarding of the craft by the evacuees is a dangerous operation. They will have to board the craft and exit the building at very large heights. To make sure the evacuees cannot fall from this height the control system of the vehicle is optimised in such a way that the cabin will not be heavily disturbed by wind gusts. In Section 10.12 it was determined that the cabin will at most move 35 *mm*. This means that no large gap will present itself between the building and the cabin and thus the risk of falling is reduced. Next to that, the bridge over which the evacuees will board the cabin will be rigidly attached to the building with clamps. This means that even if there is a gust, no gap at all will be present. Both of these measures together create redundancy and thus increase the safety. In addition to this, the bridge will have railings on the sides and anti-slip material on the floor to prevent falling or stumbling.

Next to that, the propellers will pose a danger for the evacuees. They will be rotating at high speeds and thus evacuees should not be able to bump into them. This is one of the reasons why there will be ducted fans, this not only provides clearance between the rotor blades and the evacuees, but also between the rotor blades and possible obstacles like a building which could cause damage to the fans and make it unable to fly as a result.

Lastly, evacuees may panic and as result injure themselves or others. This is a risk when they are already inside the cabin. Therefore lights will be provided in the cabin so that there is clear sight. Next to this, the cabin walls will contain windows so that it is clear what is happening around the cabin and any unexpected dangers from outside can be seen by the firefighter and the evacuees themselves. If evacuees are injured due to the fire or another emergency they can receive immediate first aid from the firefighter as there will be a first aid kit on board. After they land evacuees can be helped out of the cabin quickly and their injuries can be treated.

Now that the biggest safety risks have been touched upon, the overall safety strategy can be discussed. The two most important approaches for safety are the redundancy philosophy and the fail safe approach. Both of these approaches must be applied everywhere to ensure safety. Finally, it is important that the product is completely verified and validated and that it complies with all requirements as this will ensure proper functioning.

18.3. Risk Analysis

In the earlier design stages, an extensive risk analysis was performed [1, 2]. During those analyses, 30 technical risks, 7 development risks and 14 operational risks were identified and mitigated. In this stage of the design, there are still technical risks and development risks and many of the risks from the previous reports still apply. The newly identified risks are listed in Table 18.1. Technical risks are denoted with TN-RSK-##, operational risks have the identifier TN-OP-RSK-## and development risks have TN-DEV-RSK-## as an ID. In this table also the likelihood scores and consequence scores are given. These scores are given based on the same score assignment as in the baseline and midterm report. [1] [2]

Table 18.1: Newly identified risks

ID	Risk description	Likelihood score	Consequence score
TN-OP-RSK-15	Point of attachment to centerpiece loses structural integrity	2	4
TN-OP-RSK-16	Extendable part of bridge fails	2	3
TN-OP-RSK-17	Folding mechanism of propulsion part fails	2	1
TN-OP-RSK-18	Firefighter winch system fails	1	2
TN-OP-RSK-19	Railings on bridge do not unfold fully	1	3
TN-OP-RSK-20	Mission duration is longer then estimated	2	3
TN-DEV-RSK-08	A critical bug or mistake is found late in the design process	4	3
TN-DEV-RSK-09	Lithium metal batteries are not at an acceptable technology readiness level in time to be implemented in the craft	2	4

Requirements TN-RSK-15 up to TN-RSK-76 have been given a likelihood score of 2 as these components are designed not to fail, however due to their frequent use they might still fail. Whereas TN-RSK-17 has almost no consequence to the mission at hand, TN-RSK-15 and TN-RSK-16 do play a significant part in the mission and without them the mission cannot continue or can only be done using one cabin. TN-RSK-18 and TN-RSK-19 are likely not to happen due to the simplicity of the system and their consequence are also not as severe. However, with TN-RSK-19 only one of the cabins can be used if this risk occurs.

A likelihood score of 2 has been assigned to TN-OP-RSK-20 because a lot of safety margins have been applied to the time assignment of each mission phase, hence such a low likelihood. Moreover, in the battery design safety margins have been added such that there is enough energy. The first development risk is likely to happen due to the nature of this project, hence delay will most likely occur but depending on the significance of the bug, will most likely be solvable within time. Lithium metal batteries have already been applied in EV's hence it is likely the will be available in the near future. However, if they are not, the battery and propulsion system needs to be redesigned.

18.4. Risk Mitigation

Since some of the risks have a high combined likelihood and consequence, some risk mitigations are applied to lower the risk.

The technical risks TN-RSK-15 up to TN-RSK-19 have been mitigated with safety factors in the structural design. Also to minimise manufacturing related malfunctions, there will be rigorous product quality control and only very skilled technicians will be employed to manufacture the craft.

The technical development risks TN-DEV-RSK-08 and 09 summarise the riskiest aspects of the project

at the current stage. Both have the potential to render the entire product infeasible until the craft is redesigned. Note that TN-DEV-RSK-09 was intentionally taken as current batteries on the market would not come close to the performance determined in Chapter 9. TN-DEV-RSK-08 can be partially mitigated by performing unit tests whilst developing the models. This will both reduce the likelihood and consequence if done frequently. TN-DEV-RSK-09 can however not be mitigated as the batteries development is out of control of the project.

In Figure 18.3 a post mitigation risk map is displayed. This risk map gives an overview of all the added risks and their consequence and likelihood post mitigation.

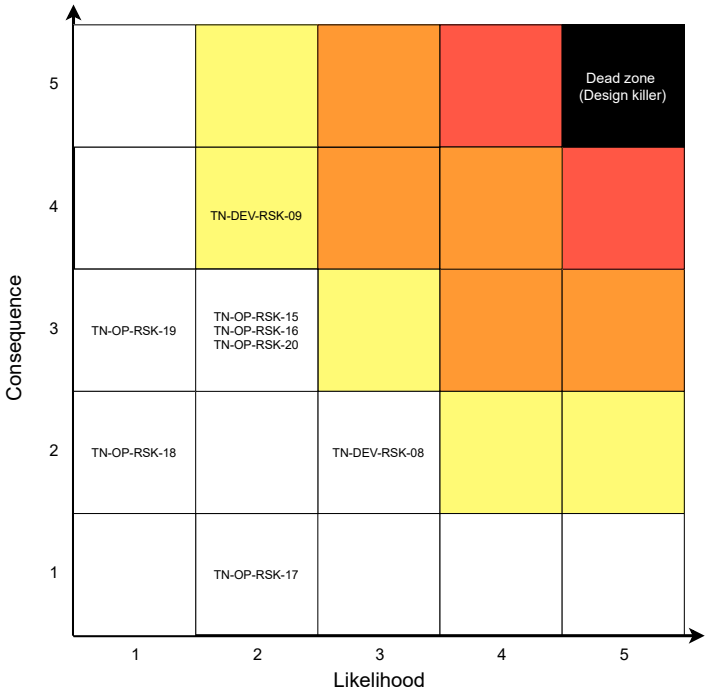

Figure 18.3: Post mitigation risk map at final report

19. Post Planned Project Phase

In this chapter the post DSE activities are discussed. These are the activities that are not dealt with or cannot be fully completed during the DSE. Firstly, the Project Design & Development Logic is presented in Figure 19.1. A post DSE project Gantt chart is made and elaborated on in Section 19.2. In Section 19.3, the cost breakdown structure is explained. Finally, the production plan is shown in Section 19.4.

19.1. Project Design & Development Logic

This section will outline the future of the product within a diagram, namely Figure 19.1. This diagram has been setup according to the current needs however which cannot be completed in the current project schedule.

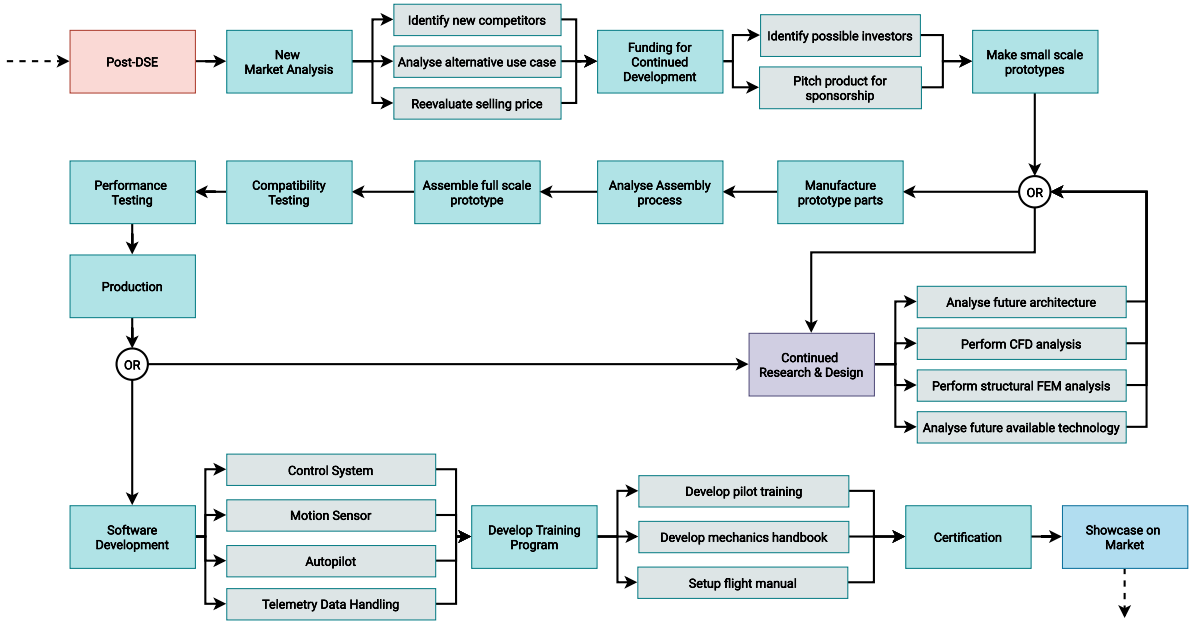

Figure 19.1: Project Design & Development Logic diagram

The major stages that have been established as critical are, in chronological order, as follows. A new market analysis has to be made which includes, but is not limited to, identifying new competitors according to the current form and function of the product, analysing possible alternative use cases for the product, and reevaluating. After these have been established possible sponsorships can be sought for by pitching the product to probable interested parties. Next a small-scale prototype can be produced from which one can choose to continue further research and design by conducting new tests, or reevaluating previously done experiments. Or the other path that can be chosen is to start manufacturing parts and assembling the product in question.

When the full-scale prototype has been assembled compatibility tests and performance tests can be conducted. When these tests yield unfavourable results it can be chosen to at this point go back to the drawing board. When the compatibility and performance tests do yield favourable results the software for the product can be developed. This stage entails, but is once again not limited to, the development of an autopilot system, motion sensing system, and telemetry data handling system.

Following are the final stages of the product. The product has to be certified for flight by local authorities after which a handling training program can be developed. This program consists of a pilot training program as well as a flight manual and maintenance handbook.

Finally the product has to be sold to the global market. With a clear overview of the Project Design & Development Logic (PDDL) a Gantt chart can be made for the post-DSE phase of the project.

19.2. Project Gantt Chart

Using the PPDL diagram a list of tasks and sub-tasks can be created. This details the activities that must be performed by the group in order to finish the product. For the gantt chart a team of 10 people working 8 hours a day for 5 days a week is assumed. Given that the team will not continue after the DSE the tasks have no assignees. This allows a future team to organize themselves and get an estimate of the time required for each task. The gantt chart can be seen in Figure 19.3, 19.4 and 19.5. The figures should be read from left to right and then top to bottom, for clarity the sub tasks are colored blue. Finally, note that at this stage the post-DSE activities are only known at a macro level.

19.3. Cost Breakdown Structure

Having determined the future project phases it is now possible to define the cost elements of the future phases. Since the design will not be finished by the end of the DSE it is preferable to identify the cost elements in the future such that another team can finish the project. This gives an estimate of the cost elements in the future as well as the amount of initial capital necessary to finish the project. One of the ways to show this information is via a Cost-Breakdown-Structure (CBS) the CBS for this report is shown Figure 19.2.

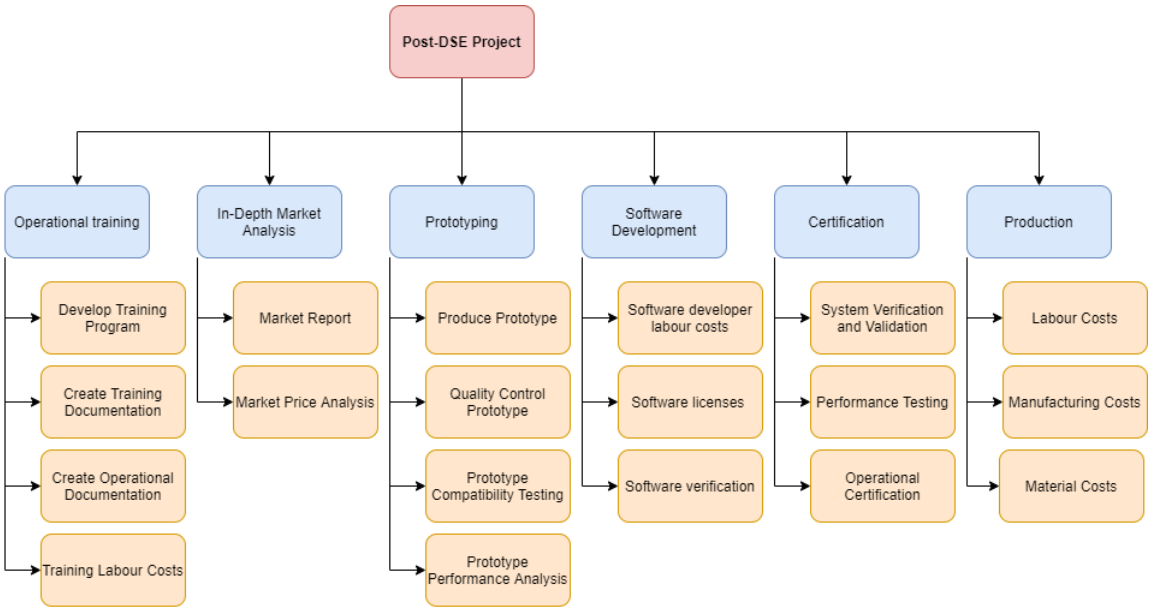

Figure 19.2: Cost-Breakdown-Structure

The main cost elements correspond to the boxes, those represent the main activities of the post-DSE phases. It is expected that certification and production will the largest cost elements in the CBS. Note that from the post-DSE phase onward the labour costs become a major cast factor.

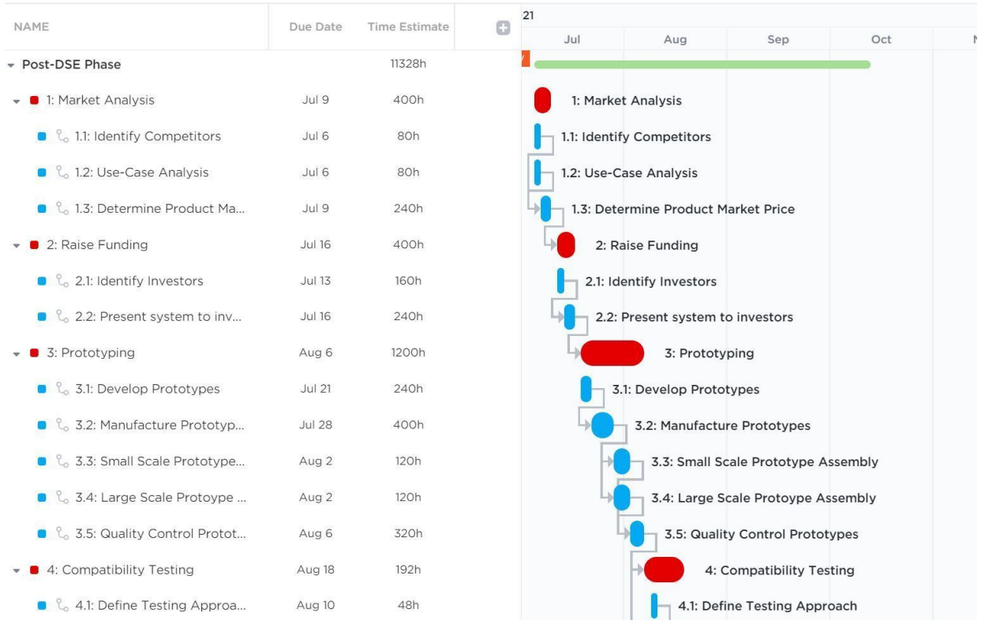

Figure 19.3: Project Gantt chart first section

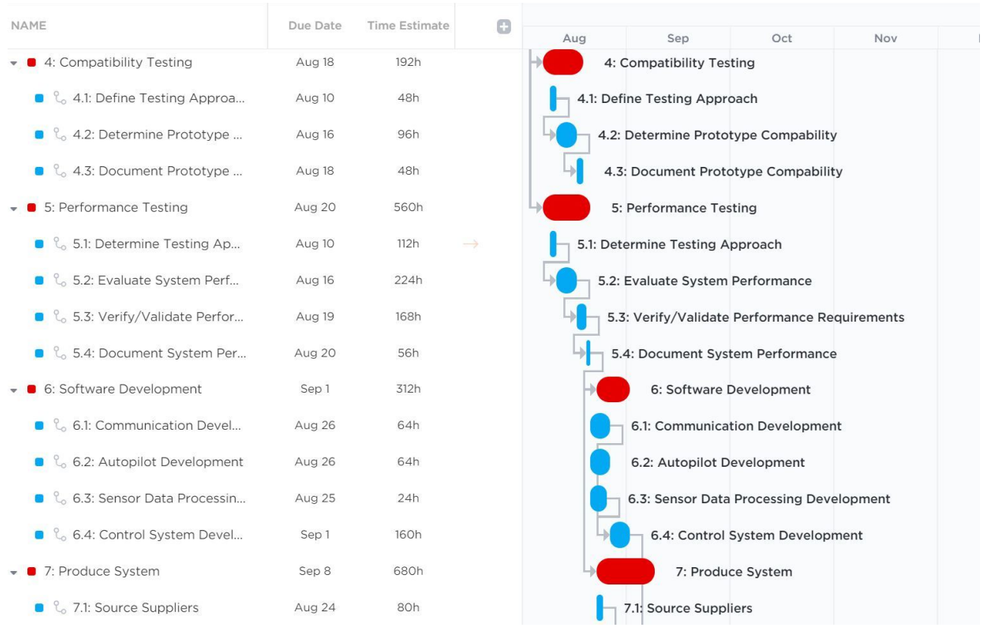

Figure 19.4: Project Gantt chart second section

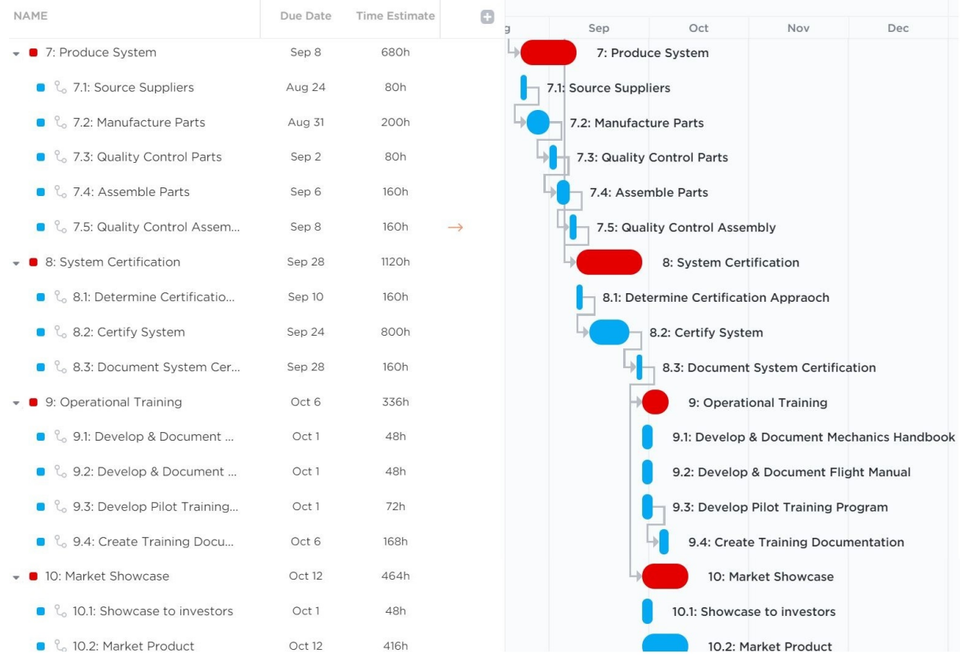

Figure 19.5: Project Gantt chart third section

19.4. Production Plan

A production plan is developed to set up how the manufacturing and assembly of a product will be carried out. This should be detailed in advance such that all aspects can be accounted for. The manufacturing of the vehicle will be done in line production. This means that there will be several stations for different tasks of the production, which will be carried out by the same crew every time. This is an appropriate method of manufacturing and assembly as the number built is relatively small at 3000. Before and while assembly takes place all components need to be made available. Part of the components will be bought from external parties, another part will be manufactured specifically for product. This division can be seen in Figure 19.6. This diagram depicts the flow of the manufacturing and assembly line, do note that the distance between subsequent steps does not signify anything. During this assembly the principal of lean manufacturing will be taken into account, which ensures that all waste will be minimised. This encompasses material waste, but also waste of budget resources and time.

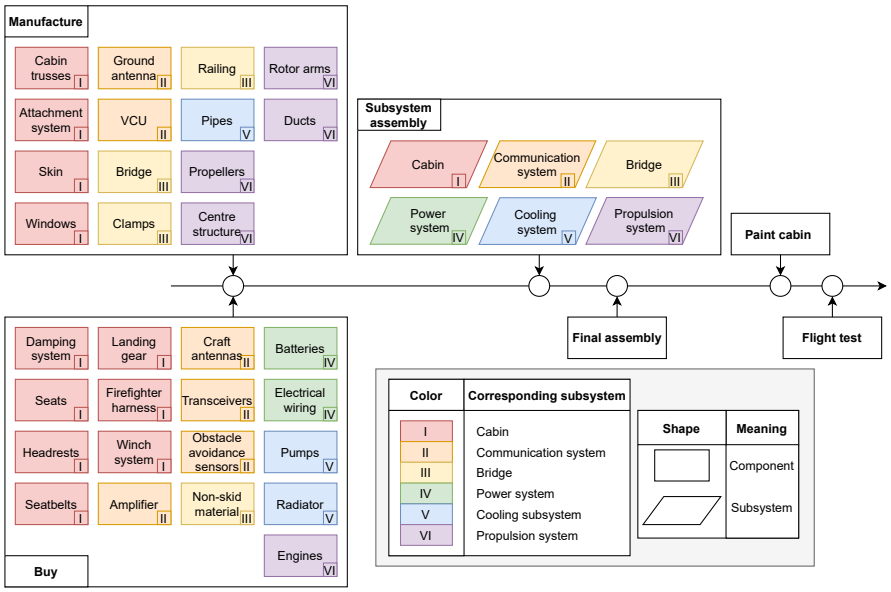

Figure 19.6: Production plan diagram

In total six subsystems need to be produced. Due to the way the system works everything but the following needs to be produced twice: propulsion system, the ground transceiver (part of 'Transceivers'), the ground antenna and the amplifier. Some of the main components will be made out of a metal: the cabin skin will be made out of a metal sheet material formed by roll bending, the bridge and rotor arms will be made out of ALU 7075 T651. The rotor arms will have a thin walled rectangular cross section and will be reinforced with stiffeners. These stiffeners are produced through rubber forming. The bridge will have a thin walled, rectangular cross section with internal honeycomb. This aluminium honeycomb is made through the process of corrugation, where corrugated sheets are made by pressing the sheet of aluminium between toothed rollers. After this the sheets are either brazed, bonded or resistance welded to form the honeycomb structure [44]. The pipes are made out of Copper Nickel 70/30. The pipes are preferred to be seamless as that will make them more resistant to corrosion. A seamless pipe is manufactured using extrusion where the billet contains a mandrel to create a hole. The windows will be made out of acrylic[87] as this is lighter but much stronger than glass. It can be used over a wide temperature range and it will shatter rather than break under high impact. If it does break, it breaks into large dull pieces.

An estimate on how long it will take to produce one system can be seen in the gantt chart in Section 19.2. It has to be noted that this is a preliminary estimate. Quite some parts have to be ordered thus there is

a heavy reliance on how fast other companies can produce and transport the ordered parts.

20. Conclusion

The goal of this DSE project is investigate the feasibility of designing and operating an airborne vehicle to provide a solution for evacuating people from high rise buildings. The aim of this report, the final report, is thus to present the final design of the system and demonstrate the feasibility of the project.

Firstly, the general description of system can be given. The cabin will be a cube with sides of 1.65 *m*. This cube will be surrounded by an aerodynamic skin in the shape of a pill. The seating configuration will be two rows of three people shoulder by shoulder facing each other. Thrust will be provided by eight electrical motors in four pairs placed above the cabin. Two cabins will be present in addition to one propulsion system which switches cabins to decrease the turnaround time on the ground. A twist and lock system will be used to attach and detach the propulsion system to and from the cabin.

The total mass of the system, one cabin with the propulsion system on top, is 731 *kg*. The mission consists of four phases: ascent, hover, descent and turnaround. One mission duration will take 778 *s* or approximately 13 *min* of which 11 *min* is in the air. This includes: ascent, hover, descent and turnaround time. On average, for normal operations, the required power is 86.25 *kW*.

A set of requirements was set up for the system. Of all 48 requirements 96% are met by the current design. However 18.6% of the 48 requirements are still uncertain they will later be validated from extensive testing of a prototype, it is expected that they will be exceeded. The remaining 4% are the two requirements that are not met. This includes the only killer requirement, namely a requirement on the total cost of the system to be below 500,000 *USD*.

Given that a large part of the requirements are met the design has very few shortcomings. However, some can still be present. The main shortcoming of the design was identified, this comes from the external structure of high-rise buildings and not the design itself. High-Rise building architects need to design special entry points in the buildings outer structure where destructive entry is a possibility. Otherwise people can only be evacuated from buildings with load bearing glass if there is an existing entry point or if they can be evacuated through the internal structure to the ground. This shortcoming only applies to a fraction of high-rise buildings and is not always encountered.

As becomes clear from this, steps still need to be taken to create a final design that is ready for production. Therefore it is recommend to take several actions to further refine the design. First, all requirements of which compliance is at this stage uncertain should be analysed and verified. Second, an in depth sizing of the remaining non-critical subsystems must be performed. Given that the aim of the report was to prove the feasibility of such a system all critical operational elements have been designed and verified. The remaining design elements that need to be designed are considered non-critical and do not contribute to demonstrating the feasibility of the project. Therefore, it is advised to continue with the post-DSE phase and raise funding for manufacturing a protoype. This should then be tested and validated before production of the actual product can begin.

[87] URL https://www.acmeplastics.com/content/advantages-acrylic/[cited 18 June 2021]

References

[1] M.C.B. van den Berg et al. “DSE Group 13 Baseline Report: Flying Carpet for Fire Departments”. Delft, the Netherlands, 2021.

[2] M.C.B. van den Berg et al. “DSE Group 13 Midterm Report: Flying Carpet for Fire Departments”. Delft, the Netherlands, 2021.

[3] D. Curia. “High Rise Firefighting Strategies for the Durham Fire Department”. In: (2007).

[4] J. Aldred. “Burj Khalifa – a New High for High-performance Concrete”. In: *Proceedings of the Institution of Civil Engineers - Civil Engineering* 163.2 (2010), pp. 66–73. DOI: 10.1680/cien.2010.163.2.66. URL: https://doi.org/10.1680/cien.2010.163.2.66.

[5] R. van Gent. “Project Guide Design Synthesis Exercise: Flying Carpet for Fire Departments”. Delft, the Netherlands, 2021.

[6] K.D. Goepel. “Implementation of an Online Software Tool for the Analytic Hierarchy Process (AHP-OS)”. In: *International Journal of the Analytic Hierarchy Process* 10 (2018), p. 5. DOI: https://doi.org/10.13033/ijahp.v10i3.590.

[7] A. Chan et al. “Recycling of Aircraft: State of the Art in 2011”. In: *Journal of Industrial Engineering* 2013 (2013), p. 8. ISSN: 2314-4882. DOI: https://doi.org/10.1155/2013/960581. URL: https://www.hindawi.com/journals/jie/2013/960581/.

[8] N. Jesuarockiam, M. Jawaid, and N. Saba. “Sustainable bio composites for aircraft components”. In: Jan. 2018, pp. 109–123. ISBN: 9780081021316. DOI: 10.1016/B978-0-08-102131-6.00006-2.

[9] C. Yuan et al. “Manufacturing energy analysis of lithium ion battery pack for electric vehicles”. In: *CIRP Annals* 66.1 (2017), pp. 53–56. ISSN: 0007-8506. DOI: https://doi.org/10.1016/j.cirp.2017.04.109.. URL: https://www.sciencedirect.com/science/article/pii/S0007850617301099.

[10] J. Kilpatrick. “Lean principles”. In: *Utah Manufacturing Extension Partnership* 68.1 (2003), pp. 1–5.

[11] J.P Womack and D.T. Jones. *Lean Thinking: Banish Waste and Create Wealth in Your Corporation*. 1st ed. New York: Simon & Schuster, 2003.

[12] T. Omori et al. “Superelastic Effect in Polycrystalline Ferrous Alloys”. In: *Science* 333.6038 (2011), pp. 68–71. ISSN: 0036-8075. DOI: 10.1126/science.1202232. eprint: https://science.sciencemag.org/content/333/6038/68.full.pdf. URL: https://science.sciencemag.org/content/333/6038/68.

[13] Wilfried Laufs and Andreas Luible. “Introduction on use of glass in modern buildings”. In: (Apr. 2003).

[14] M. Martín et al. “Polymeric interlayer materials for laminated glass: A review”. In: *Construction and Building Materials* 230 (2020).

[15] G. Castori and E. Speranzini. “Structural analysis of failure behavior of laminated glass”. In: *Composites Part B: Engineering* 125 (2017), pp. 89–99.

[16] B.M. Novac et al. “Cockpit Canopy Shattering Using Exploding Wire Techniques”. In: Oct. 2005, pp. 20/1–20/4. ISBN: 0-86341-558-X. DOI: 10.1049/ic:20050045.

[17] Samuel L Venneri and Ahmed Khairy Noor. *Future aeronautical and space systems / edited by Ahmed K. Noor, Samuel L. Venneri.* eng. Progress in astronautics and aeronautics; v. 172. Reston, Va.: American Institute of Aeronautics and Astronautics, 1997. ISBN: 1563471884.

[18] M.O.L. Hansen. *Aerodynamics of Wind Turbines*. 2nd ed. James & James, 2008, pp. 27–62.

[19] G.J.J. Ruijgrok. *Elements of Airplane Performance*. 2nd ed. Delft Academic Press, 2009.

[20] Dick. G. Simons. *Introduction to Aircraft Noise*. 2019, pp. 206–209.

[21] F Anton and AG Siemens. “eAircraft: Hybrid-elektrische Antriebe für Luftfahrzeuge”. In: *14. Tag der Deutschen Luft-und Raumfahrtregionen* (2019).

[22] John Raymond Hall. *High-rise building fires*. The Association, 2013.

[23] B. Liu, J. Zhang, and W. Xu. “Advancing lithium metal batteries”. In: *Joule* 2.5 (2018), pp. 833–845.

[24] H Yoon et al. “Fast charge/discharge of Li metal batteries using an ionic liquid electrolyte”. In: *Journal of the Electrochemical Society* 160.10 (2013), A1629.

[25] J. Lang et al. “High performance lithium metal anode: progress and prospects”. In: *Energy Storage Materials* 7 (2017), pp. 115–129.

[26] R. Wang et al. “Lithium metal anodes: Present and future”. In: *Journal of Energy Chemistry* 48 (2020), pp. 145–159.

[27] Y. Mikhaylik et al. “Sion Power’s Licerion® Batteries”. In: *ECS Meeting Abstracts*. 3. IOP Publishing. 2018, p. 302.

[28] B. Xu et al. “Modeling of lithium-ion battery degradation for cell life assessment”. In: *IEEE Transactions on Smart Grid* 9.2 (2016), pp. 1131–1140.

[29] Y. Liu et al. “Strategy of enhancing the volumetric energy density for lithium–sulfur batteries”. In: *Advanced Materials* 33.8 (2021), p. 2003955.

[30] M. Filipenko. “HTS-Technology for hybrid electric aircraft”. In: *European Cryogenic Days 2017, Karlsruhe, Germany, 13th-15th September 2017*. 2017.

[31] C. Blake and C. Bull. “IGBT or MOSFET: choose wisely”. In: *International Rectifier* (2001), pp. 1–5.

[32] M. Schweizer, T. Friedli, and J.W. Kolar. “Comparative evaluation of advanced three-phase three-level inverter/converter topologies against two-level systems”. In: *IEEE Transactions on industrial electronics* 60.12 (2012), pp. 5515–5527.

[33] G. Lakkas. “MOSFET power losses and how they affect power-supply efficiency”. In: *Analog Appl* 10.2016 (2016), pp. 22–26.

[34] W.A. Timmer and van Elsloo S.J. *Project Reader - Aircraft - WP4-5*. TU Delft, Nov. 2020.

[35] Zaid Tahir. *State Space System Modelling of a Quad Copter UAV*. URL: https://arxiv.org/ftp/arxiv/papers/1908/1908.07401.pdf.

[36] *Modules in Mechanics of Materials*. URL: https://web.mit.edu/course/3/3.11/www/module_list.html.

[37] T. Zhao and Y. Jiang. “Fatigue of 7075-T651 aluminum alloy”. In: *International Journal of Fatigue* 30.5 (2008), pp. 834–849. DOI: 10.1016/j.ijfatigue.2007.07.005. URL: https://www.researchgate.net/publication/223427277_Fatigue_of_7075-T651_aluminum_alloy.

[38] Calvin Rans. *Lecture 12 examples - Macaulay step function and superposition*. 2020. URL: https://brightspace.tudelft.nl/d2l/le/content/140498/viewContent/1063678/View.

[39] Calvin Rans. *Lecture 8 - Shear flow in thin walled beams*. 2020. URL: https://brightspace.tudelft.nl/d2l/le/content/140498/viewContent/1063674/View.

[40] United States. Federal Aviation Administration. *Certification of Transport Airplane Structure*. U.S. Department of Transportation, Federal Aviation Administration, 1999.

[41] Calvin Rans. *Lecture 6 Examples - Bending stresses in beams Download*. 2020. URL: https://brightspace.tudelft.nl/d2l/le/content/140498/viewContent/1063672/View.

[42] S.J. van Elsloo, J.M.J.F. van Campen, and W. van der Wal. *Description of the developer model used in the AE3212-II Project*.

[43] M.C.Y. Niu. *Airframe Stress Analysis and Sizing*. 2nd ed. Hong Kong: Hong Kong Conmilit Press LTD, 1999.

[44] S. Upreti et al. “Modelling and analysis of honeycomb sandwich structure using finite element method”. In: *Materials Today: Proceedings* 25 (2020). 2nd International Conference on Computational and Experimental Methods in Mechanical Engineering, pp. 620–625. ISSN: 2214-7853. DOI: https://doi.org/10.1016/j.matpr.2019.07.377. URL: https://www.sciencedirect.com/science/article/pii/S2214785319325568.

[45] D. Christ and L.H. Seymes. 1981, pp. 1–194. URL: https://apps.dtic.mil/sti/pdfs/ADA105512.pdf.

[46] *What’s the Best Landing Gear: Wheels or Skids?* Sept. 2019. URL: https://savback.com/whats-the-best-landing-gear-wheels-or-skids/.

[47] *EE3125TU - Advanced Electronics for Robotics PE Lecture 1-3*. URL: https://brightspace.tudelft.nl/d2l/le/content/299751/viewContent/2016240/View.

[48] J. Holtz. “Pulsewidth modulation for electronic power conversion”. In: *Proceedings of the IEEE* 82.8 (1994), pp. 1194–1214.

[49] D.G. Holmes and T.A. Lipo. *Pulse width modulation for power converters: principles and practice*. Vol. 18. John Wiley & Sons, 2003.

[50] N. Samaddar, N.S Kumar, and R. Jayapragash. “Passive Cell Balancing of Li-Ion batteries used for Automotive Applications”. In: *Journal of Physics: Conference Series*. Vol. 1716. 1. IOP Publishing. 2020, p. 012005.

[51] W.C. Lee, D. Drury, and P. Mellor. “Comparison of passive cell balancing and active cell balancing for automotive batteries”. In: *2011 IEEE Vehicle Power and Propulsion Conference*. IEEE. 2011, pp. 1–7.

[52] *AE2111-II Lecture S3 Telecommunications*. URL: https://brightspace.tudelft.nl/d2l/le/content/292970/viewContent/1905842/View.

[53] R.C Moore. “Satellite RF Communications and Onboard Processing”. In: *Encyclopedia of Physical Science and Technology*. Elsevier, 2003, pp. 439–455. DOI: 10.1016/b0-12-227410-5/00884-x. URL: https://doi.org/10.1016/b0-12-227410-5/00884-x.

[54] *Digital Communication Systems (EE3115TU)*. URL: https://brightspace.tudelft.nl/d2l/le/content/299747/viewContent/1921442/View.

[55] M. Suchanski et al. “Prediction of VHF and UHF wave attenuation in urban environment”. In: 1 (May 2012). DOI: 10.1109/MIKON.2012.6233496.

[56] Daniel Minoli. *Satellite Systems Engineering in an IPv6 Environment*. 2009. URL: https://books.google.nl/books?id=4yJi1UQDPp8C&amp.

[57] O. Rippel et al. “Learned Video Compression”. In: Oct. 2019, pp. 3453–3462. DOI: 10.1109/ICCV.2019.00355.

[58] D.F. Shanahan. “Human Tolerance and Crash Survivability”. In: *NATO RT Organisation* 1 (2004). DOI: 10.14339/RTO-EN-HFM-113. URL: https://www.sto.nato.int/publications/STO%5C%20Educational%5C%20Notes/RTO-EN-HFM-113/EN-HFM-113-06.pdf.

[59] M.S. Varat and S.E. Husher. “Crash Pulse Modeling for Vehicle Safety Research”. In: *Proceedings of the 18th International technical conference on the enhanced safety of vehicles* 1 (2003). URL: https://trid.trb.org/view/750814.

[60] P. Van den Bossche, J. Matheys, and J. Van Mierlo. “Battery environmental analysis”. In: *Electric and Hybrid Vehicles: Power Sources, Models, Sustainability, Infrastructure and the Market* (2010), p. 347.

[61] B.K. Talukdar and B.C. Deka. “An Approach to Reliability, Availability and Maintainability Analysis of a Plug-In Electric Vehicle”. In: *World Electric Vehicle Journal* (2021), p. 17.

[62] X. Shu et al. “A Detailed Reliability Study of the Motor System in Pure Electric Vans by the Approach of Fault Tree Analysis”. In: *IEEE Access* (2019). DOI: 10.1109/ACCESS.2019.2963197.